Preparation and Properties of Isolated Z-disks

Thesis by

Mara Camelia Rusu

Submitted in accordance with the requirements for the degree of

Doctor of Philosophy

The University of Leeds

Faculty of Biological Sciences

School of Molecular and Cellular Biology

August 2014

The candidate confirms that the work submitted is her own and that appropriate credit has been given where reference has been made to the work of others.

This copy has been supplied on the understanding that it is copyright material and that no quotation from the thesis may be published without proper acknowledgement.

Acknowledgements

I would like to thank my supervisor, Professor John Trinick, for the unique opportunity to work on this exciting and challenging project. Throughout the four years his advice, patience and enthusiasm proved to be invaluable resources, especially during stressful periods. I would like to thank my co-supervisor, Dr Larissa Tskhovrebova, for her contributions to this project.

My thanks to all the members of the MUZIC consortium with which I have spent great moments during our meetings, workshops and conferences. Lucian Barbu-Tudoran has sparked my interested in electron microscopy and I would like to thank him and Dr. Peiyi Wang, Dr. Stephen Muench, Martin Fuller, Dr. Kyle Dent and Rebecca Thompson for the technical help and discussion, especially during the steep learning curve of cryo-electron microscopy.

I would like to extend my sincere gratitude to Dr. Sonja Welsch, Dr. Sacha de Carlo (FEI), Dr. Shaoxia Chen, Dr. Greg McMullan and Dr. Cristos Savva (MRC LMB) for their help with data collection on the Titan Krios. I am truly grateful to Dr. Kenneth Taylor for tomogram reconstruction and subtomogram averaging and to Dr. Peiyi Wang for the 2D crystal unbending. My thanks to Dr. Kathryn White for her help with fluorescence microscopy and to Dr. Marcin Wolny for his assistance during protein purification.

Also I would like to thank the members of the Molecular Contractility Group at Leeds University. I am grateful to my good friends Emanuel Fertig, Marcin Wolny, Sarika Khasnis, Ania Wroblewska-Wolna, Kasia Makowska, Marta and Marcin Kurzawa, Kat White, Kieran Lee, Fran Parker, Ruth Hughes, Ada Klyszejko-Kupinska, Adam Kupinski, Matt Batchelor, Derek Revill, Anna Lopata and Charlie Green for the moral support they have given me throughout my stay in Leeds and for making me feel right at home. My deepest gratitude extends to my friends and family who have supported me emotionally during this time of learning Ovidiu Hosu, Ioana Mihalache, Georgiana Delea, Ioana Cilean, Sabin Bogdan, Cristian Iacob, Lorena Popa and Eugen Gheorghiasa.

I am truly grateful to my mother who raised me to be the person I am today. Her strength during times of adversity motivates me to become better each day. My late

father fueled my passion in biology and my parents were always supportive and understood my interest in science, encouraging me every step of the way.

The work presented has been funded by the European Seventh Framework Programme through the Marie Curie Initial training Network – MUZIC. I am truly grateful for the funding and support given by the network and the European Research Council.

Abstract

Z-disks form the boundaries of the sarcomeres, the basic contractile units of muscle cells. Within the Z-line thin filaments containing mainly actin interdigitate and are crosslinked by α-actinin. Ends of the giant proteins titin and nebulin are also anchored in the Z-disk. The Z-line was originally thought to have the purely mechanical function of transmitting contractile force along the myofibrils. However, more recently, the Z-disk has emerged as a highly dynamic structure involved in stress sensing and important signaling pathways that govern muscle homeostasis. In order to fully understand how the Z-disk functions a detailed description of its molecular organization is essential. Even though the structure the structure of the Z-disk has been studied by electron microscopy techniques its molecular organization is known only in outline to a resolution of about 5 nm, whereas at least 3 nm is required to begin distinguishing protein shapes and to accurately dock crystal structure.

Reports describing the isolation of intact Z-disks from insect indirect flight muscle date from 30-40 years ago, but these preparations have not been subjected to modern electron microscopy techniques. We improved the existing methods for the isolation of the Z-disk from honeybee flight muscle and investigated its structure using cryo-electron tomography and subtomogram averaging. The preliminary data indicate that the resolution was improved when compared with past studies of plastic sectioned muscle. We have also investigated the protein composition of the preparations to monitor the components that are washed away during preparation.

Methods for the isolation of intact Z-disks from vertebrate muscle are not available. We explored strategies for isolating Z-disks from skeletal and cardiac muscle. Even though such a preparation has not been achieved we present promising approaches that, with optimization, should enable isolation of Z-disks from vertebrate muscle.

Table of Contents

List of Figures

Chapter 1

Chapter 3

Chapter 4

Chapter 5

List of Tables

List of Abbreviations

Units

Å	Ångstrom (10^{-10} m)
°C	Degrees Celsius
Da	Dalton(s)
× g	Acceleration of gravity
kDa	10^{3} Daltons
MDa	10^{6} Daltons
kV	10^{3} volts
mA	10^{-3} ampere
mbar	10^{-3} bar
ml	10^{-3} litre(s)
mm	10^{-3} meter(s)
mM	10^{-3} molar
µl	10^{-6} litre(s)
µm	10^{-6} meter(s)
µM	10^{-6} molar
nm	10^{-9} meter(s)
nM	10^{-9} molar
pN	10^{-12} newtons
rpm	Revolutions per minute

Other

2D	Two dimensional
3D	Three dimensional
ABD	Actin binding domain
ACTN	Actinin
ADP	Adenosine diphosphate
Amp	Ampicillin
APS	Ammonium persulfate
ATP	Adenosine-5'-triphosphate
BLAST	Basic Local Alignment Search Tool
C-	Carboxyl-
CaM	Calmodulin
CapZ	Capping protein Z
CARP	Cardiac ankyrin repeat protein
C_C	Chromatic aberration
CCD	Charged coupled device
CCP	Cambridge Centre for Proteomics
CEMOVIS	Cryo-electron microscopy of vitreous sections

CLEM	Correlative light and electron microscopy
C_S	Spherical aberration
DCM	Dilated cardiomyopathy
DEAE	Diethylaminoethanol
DED	Direct electron detector
DNA	Deoxyribonucleic acid
DTT	Dithiothreitol
e^-	Electron
EDTA	Ethylenediaminetetraacetic acid
EGTA	Ethylene glycol tetraacetic acid
EM	Electron microscopy
ET	Electron tomography
FEG	Field emission gun
FFT	Fast Fourier Transform
FIB	Focused ion beam
FITC	Fluorescein isothiocyanate
Fn	Fibronectin
FS	Freeze sustitution

FSC	Fourier Shell Correlation
h	Planck constant
HEPES	4-(2-Hydroxyethyl)piperazine-1-ethanesulfonic acid
HIV	Human Immunodeficiency Virus
HPF	High pressure freezing
HT	High tension
IFM	Insect flight muscle
Ig	Immunoglobulin
IPTG	Isopropyl β-D-1-thiogalactopyranoside
LB	Luria Broth
LGMD	Limb girdle muscular dystrophy
LMB	Laboratory for Molecular Biology
MDA	Multivariate data analysis
MES	2-(N-morpholino)ethanesulfonic acid
MFM	Myofibrillar myopathies
MLP	Muscle LIM protein
MOPS	3-(N-morpholino)propanesulfonic acid
MS	Mass spectrometry

MuRF	Muscle specific ring finger protein
MW	Molecular weight
MWCO	Molecular weight cutoff
N-	Amino-
NAD(H)	Nicotinamide adenine dinucleotide
NEB	Nebulin
NEBL	Nebulette
NFAT	Nuclear factor of activated T-cells
OD	Optical density (absorbance)
p	Particle momentum
PBS	Protein buffer saline
PDB	Protein Data Base
PFA	Para formaldehyde
pH	Decimal logarithm of hydrogen ion activity
Pi	Inorganic phosphate
PiP_2	Phosphatidylinositol 4,5-bisphosphate
PIPES	Piperazine-N,N′-bis(2-ethanesulfonic acid)
PKC	Protein kinase C

PMMA	Poly(methyl methacrylate) (PMMA)
PMSF	Phenylmethanesulfonylfluoride or phenylmethylsulfonyl fluoride
ppi	Pixels per inch
PS	Pixel size
RELION	REgularized LIkelihood Optimization
RCT	Random conical tilt
S.D.	Standard deviation
SDS-PAGE	Sodium Dodecyl Sulphate Polyacrylamide Gel Electrophoresis
SNR	Signal to noise ratio
SP	Sulphopropyl
TCA	Trichloro acetic acid
TCap	Telethonin
TEM	Transmission electron microscopy
TEMED	N,N,N′,N′- Tetramethylethane-1,2-diamine
TES	2-[[1,3-dihydroxy-2-(hydroxymethyl) propan-2-yl]amino]ethanesulfonic acid
TMR	tetramethyl-rhodamine-5-maleimide
UNIPROT	Universal Protein Resource
UV	Ultraviolet

Zasp	Z-band alternatively spliced PDZ motif protein

List of Movies

–

Movie 1	Aligned tilt series of a negatively stained (1% phosphotungstic acid) isolated Z-disk. Data was recorded at 9900x, on CCD (2k x 2k) on the FEI T12 TEM. Fiducialess alignment was performed in IMOD.
Movie 2	Reconstructed tomogram of a negatively stained (1% phosphotungstic acid) isolated Z-disk. Reconstruction was carried out using IMOD.
Movie 3	Aligned cryo-electron tomography tilt-series. Data was recorded at MRC LMB Cambridge.
Movie 4	Fourier transforms of the aligned tilt series in Movie 4, showing loss of lattice regularity due to radiation damage.
Movie 5	Preliminary 3D structure of the honeybee Z-disk obtained from cryo-ET. Data was processed by Dr. Kenneth Taylor and Zhonjun Hu (Florida State University)

1. Introduction

1.1 Striated muscle: structure and function

Muscle cells are highly specialized to undergo contraction. In vertebrates there are three types of muscle: smooth, skeletal and cardiac. Morphologically two types can be distinguished: smooth and striated. Skeletal and cardiac muscle represent the striated variety due to the characteristic cross-striated pattern resulting from the in-register organization of filaments of exact length into sarcomeres (Campbell and Reece 2005). Smooth muscle forms the walls of internal organs and blood vessels and consists of spindle shaped cells that contract involuntarily. Smooth muscle cells is not organized in sarcomeres and lacks cross-striations (Somlyo and Somlyo 1994).

Skeletal muscles attached to bones via tendons are responsible for voluntary movement, locomotion and posture, and are under the control of the somatic nervous system (Campbell and Reece 2005). Skeletal muscle cells, or myotubes, are elongated, multinucleated cells that result from the fusing of mononucleated myoblasts during myotube genesis (Bismuth and Relaix 2010). Skeletal muscles are composed of different fiber types: energy conserving slow fibers (type I) that are adapted to undergo prolonged contraction, and fast fibers (type II a and II b/x) that are associated with shorter and highly energy consuming contractions (Schiaffino 2010; Westerblad et al. 2010).

Cardiac muscle forms the bulk of the heart and it is capable of contracting involuntarily at a roughly constant rate (in humans 70-90 beats/minute), which can rise to >150 beats/minute during exertion. Cardiac muscle cells are branched, usually have a single nucleus, although sometimes two nuclei can be observed, and are rich in mitochondria (Fawcett and McNutt 1969; Ono 2010). Embryonic cardiomyocytes can undergo mitosis while the heart is exerting its pumping activity. It was shown *in vitro*

that cell division is accompanied by the disassembly of myofibrils, with the Z-disk being dissembled before the M-line. After the completion of mitosis the myofibrils are reassembled (Ahuja et al. 2004). Cardiac myocytes are mechanically and electrically coupled *via* intercalated disks, which are specialized structures composed of several cell-cell junctions including gap and adherens junctions and desmosomes (Vreeker et al. 2014).

In invertebrates there are three muscle types: striated, smooth and obliquely striated. Two forms of transverse striated muscle can be distinguished: with continuous and discontinuous Z-lines. Insect flight muscle (IFM) is striated and has a similar organization and protein make-up to that of vertebrate striated muscle (Royuela et al. 2000). Physiologically, depending on the correlation between nerve input and wingbeat, there are two types of IFM: synchronous and asynchronous. In synchronous flight muscle each contraction is initiated by nerve input. Asynchronous muscles are specialized for high-speed oscillation with the frequency of contraction being much higher than the frequency of nerve impulses. Oscillation is caused not only by calcium input, but also by stretch activation of the muscle. Also, the sarcomeres of asynchronous flight muscles are characterized by crystal-like arrangement of the myofilaments with the regularity being preserved across the entire myofibril (Peckham et al. 1992; Josephson et al. 2000; Holmes 2011; Iwamoto and Yagi 2013; Iwamoto et al. 2006).

1.1.1 Overview of vertebrate muscle structure

The contractile proteins of striated muscle cells are organized in specialized structures called myofibrils that occupy the bulk of the cytoplasm. Myofibrils are cylindrical, having a diameter of 1 - 3 μm (Craig and Padron 2004), and consist of repeating contractile units known as sarcomeres. Sarcomeres consist of overlapping thin and thick filaments held in register by proteins in the Z-disk and the M-line, respectively. Filamentous actin and accessory proteins form thin filaments. The arrays of thin filaments from adjacent sarcomeres interdigitate and are anchored in the Z-disk, at the end of each sarcomere. The Z-disk appears as a thin dark structure in the middle of the light I-band, which appears isotropic in polarized light, hence the name I-band. In the center of the sarcomere thick filaments, consisting mainly of myosin II filaments and associated proteins, form the darker A-band, which appears anisotropic in polarized

light. Thin filaments protruding from the Z-disk extend towards the middle of the sarcomere, overlapping with thick filaments in the A-band. In relaxed muscle, within the dark A-band a lighter zone is observed, called the H-zone, where the thin and thick filaments do not overlap. Inside the H-zone is the M-line formed of cross-connecting cytoskeletal elements and where thick filaments reverse polarity. During contraction, as the sarcomere shortens, the H-zone disappears (Craig and Padrón 2004) (**Figure 1.1**).

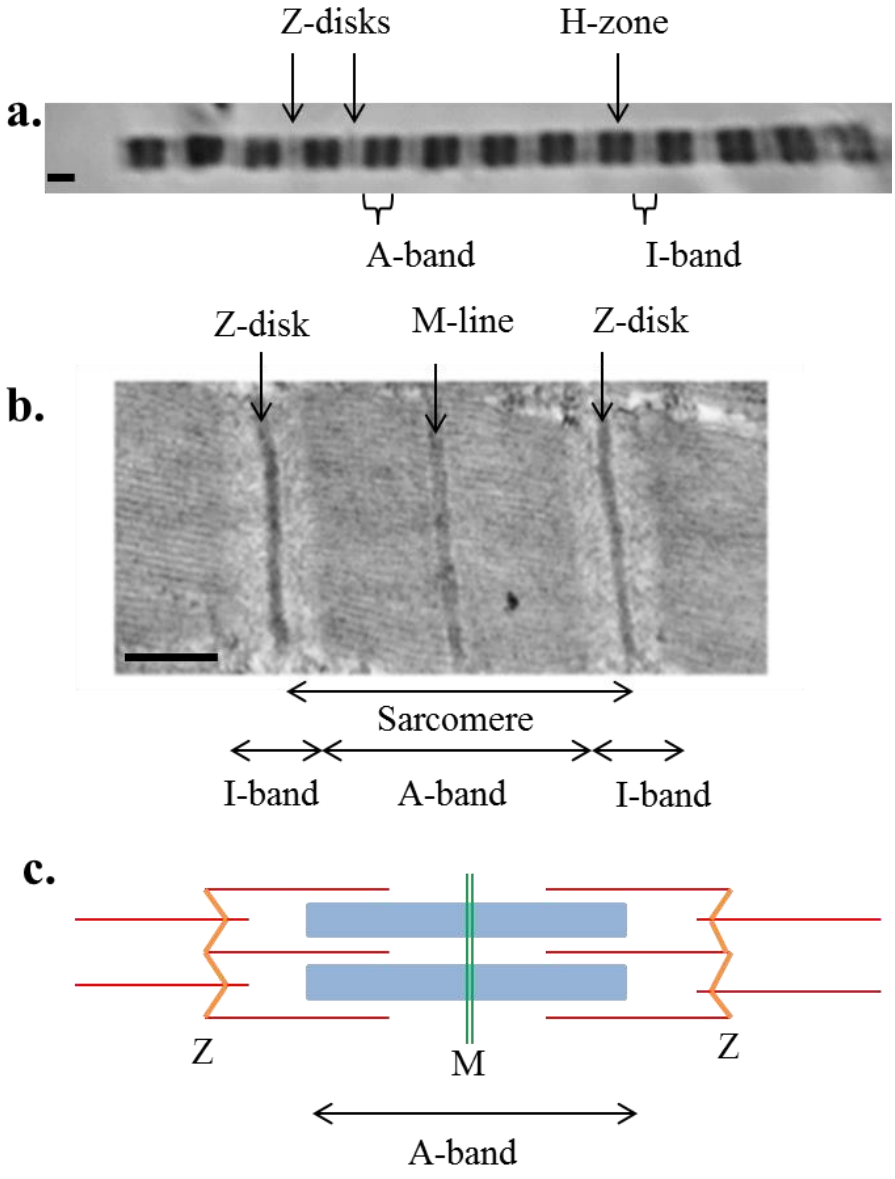

Figure 1.1 – Overall organization the sarcomere.

(a) Phase contrast light microscopy image of a rabbit psoas myofibril showing the distinct zones of the sarcomere: the I-band, the Z-disk, the A-band and the H-zone. Scale bar represents 1 μm.

(b) Plastic section electron micrograph of a rabbit psoas myofibril showing the distinct zones of the sarcomere. The specimen was stained with lead citrate and uranyl acetate. Data was collected on film on the Phillips CM 10 TEM. Scale bar represents 0.5 μm.

(c) Diagram representing filament arrangement in the sarcomere. Red lines show thin filaments which interdigitate in the Z-disk and are crosslinked by α-actinin (orange). Blue rectangles are thick filaments in the A-band, held in register at the M-line (green).

Peripheral myofibrils are coupled with the muscle cell membrane (sarcolemma) through a subsarcolemmal assembly of proteins known as the costamere. Costameres lie in register with the Z-disks of peripheral myofibrils. The costameric protein assembly helps transmit the contractile forces laterally to neighboring myocytes (Ervasti 2003).

During contraction myofibrils deform elastically. Longitudinal elasticity is related to titin, a flexible protein which establishes elastic connections between the Z-disk and thick filaments and ensures that force imbalances between the halves of thick filaments do not develop during contraction. During contraction the filament spacings with the thin and thick filament lattice increase due to lateral forces being developed, this requires transverse elasticity in both M-line and the Z-disk (Tskhovrebova and Trinick 2012).

The sarcomere is a beautifully ordered structure and it comprises a myriad of proteins; it is also a very dynamic structure capable of force generation while the proteins are constantly turned over. For example the exchange rate of myosin into the thick filament was measured to be 32.2 ± 2.5 minutes in isolated adult rat cardiomyocytes (Wolny et al. 2013). The turnover rate of myosin in beating hearts is much longer, measured in rat hearts to be approximately 15 days (Papageorgeopoulos et al. 2002). In order to fully understand how muscle works and how it is assembled, but also to be able to understand mechanisms of muscle disease, we must understand its structure. Progress has been made in the past decades towards understanding the mechanism of muscle contraction, muscle disease and the assembly of myofibrils (Sanger et al. 2010; Selcen 2011; Batters et al. 2014). However, while considerable progress has been made towards understanding the function and mechanisms of muscle,

the molecular architecture of all the major components (thick and thin filaments, M- and Z-line) is very incomplete and many processes remain to be understood.

1.1.1.1 Vertebrate A-band and M-line

The vertebrate A-band, 1.6 μm long, is located in the middle of the sarcomere and it consists mainly of thick myosin II filaments arranged in a hexagonal lattice (Craig and Padron 2004). Myosin II is a motor protein that binds actin reversibly and is capable of ATP hydrolysis in order to generate force. It consists of a tail and two heads and it self-assembles into bipolar thick filaments, with the tails forming most of the thick filament backbone. The heads or cross-bridges extend from the thick filament backbone and interact with actin (**1.1.1.3**) (Craig 2006). Several non-myosin proteins, which are thought to have roles in the regulation or stabilization of the thick filaments, are found in the A-band, including titin, obscurin, myomesin, M-protein, myosin binding protein C and H (Clark et al. 2002).

Thin and thick filaments overlap in the A-band region containing myosin heads, or cross-bridges. The part of the A-band containing only thick filaments is known as the H-zone, which varies in size with sarcomere length. In the centre of thick filaments is the bare zone, ~150 nm, where the myosin tails pack anti-parallel, and is so-called because there are no cross-bridges. At the centre of the bare zone lies the M-line, 75 nm, where thick filaments are aligned in register, stabilized and anchored by M-bridge cross-links (Craig and Padrón 2004). The M-line is connected to neighboring myofibrils as well as the sarcolemma and consists of 3 to 5 registers of M-bridges (Agarkova and Perriard 2005). M-bridges contain mainly M-protein and myomesin isoforms (Masaki and Takaiti 1971; Eppenberger et al. 1981). The M-line helps maintain registration between thick filaments during contraction, mainly through a transverse elastic network formed by myomesin antiparallel dimers (Schoenauer et al. 2005; Lange et al. 2005). It is thought that the M-line plays a role in the mechanism of stretch-sensing in muscle. Even though progress has been made towards understanding mechanical properties of different components of the M-band, the lack of a molecular detailed model hinders the understanding of how it behaves during contraction (Gautel 2011; Tskhovrebova and Trinick 2012).

The molecular architecture of the thick filament is better understood than that of the M-line. Cardiac thick filaments have been resolved from negative-stain EM to a resolution of 4 nm (Zoghbi et al. 2008) and to 2.8 nm respectively (Al-Khayat et al. 2013). These studies give insight in the assembly and function of thick filaments, but how the myosin tails are packed in the backbone of the filament is not known in detail, nor the detailed organization of the A-band including accessory proteins, which hinders understanding of their functions.

1.1.1.2 Vertebrate I-Band

Thin filaments in the I-band are composed mainly of filamentous actin (F-actin), a highly conserved protein in eukaryotes. Actin monomers (42 kDa) known as G-actin (globular actin) have two domains that are separated by a nucleotide binding site. Once ATP is bound in the cleft polymerization is initiated and G-actin polymerizes to form the helical polymer, F-actin. Filamentous actin that still has ADP-Pi bound is more stable than the actin-ADP complex (Murakami et al. 2010). Due to the characteristics of G-actin and the head-to-tail polymerization, the resulting filament has a structural and functional polarity. The polarity can be observed in electron micrographs by decorating the actin filaments with myosin heads, which will bind in a characteristic ‘’arrowhead’’ pattern; thus a ‘plus’ (‘barbed’) end and a ‘minus’ (‘pointed’) end can be distinguished. At the barbed-end the rate of association of G-actin is higher at the pointed-end of the filament (Au 2004; Alberts et al. 2008). F-actin associates with troponin and tropomyosin to form the thin filament. Tropomyosin is a double-stranded α-helical coiled-coil that binds to actin along each long-pitch strand of the filament. Three subunits form the troponin complex and bind to sites on tropomyosin and actin. Troponin binds calcium and, together with tropomyosin, regulates contraction (**1.1.1.3**) (Craig and Padrón 2004). Antiparallel thin filaments from adjacent sarcomeres interdigitate and are cross-linked in the Z-disk (**1.1.2**). The plus end is stabilized in the Z-disk by actin capping protein (CapZ) in the Z-line, while the minus end interacts with tropomodulin (Au 2004).

In the I-band of vertebrate skeletal muscle the giant modular protein nebulin runs along the actin filament interacting, amongst other proteins, with the plus and minus end capping proteins (Labeit et al. 2011). In cardiac muscle a shorter protein, nebulette,

which has a similar structure to that of nebulin is expressed (Kazmierski et al. 2003). It is thought that nebulin plays an important role in thin filament assembly and length regulation due to its ability to bind both tropomodulin (McElhinny et al. 2001) and CapZ (Pappas et al. 2008). Also it has been shown that cells lacking nebulin have thin filaments of variable length and the modular structure of nebulin can be correlated to F-actin filament length (Labeit et al. 1991). Nebulin may therefore act as a molecular ruler regulating exact thin filaments length in skeletal muscle, although this is not proven (Tskhovrebova and Trinick, 2012).

The atomic structure of uncomplexed G-actin in its ADP state has been determined crystallographically to a resolution of 1.54 Å (**Figure 1.2 a**). For that particular study tetramethyl-rhodamine-5-maleimide (TMR) was used to inhibit the polymerization of actin (Otterbein et al. 2001). The atomic structure of F-actin has not been determined crystallographically due to the innate flexibility of the filament, but also because actin filaments do not crystallize (Craig and Padrón 2004). The structure of reconstituted thin filaments in the presence of phosphate, from purified rabbit actin, was determined to a resolution of 0.5 nm by cryo-electron microscopy (**Figure 1.2 b**). In the cryo-EM 3D reconstruction it was found that the outer domain is rotated in a swing-door manner by 16º relative to the inner domain. The new structures also gives insight into the mechanism of ATP release (Murakami et al. 2010), which will not be discussed here.

X-ray crystallography and EM data has revealed the overall organization of the thin filament and the regulatory movements of tropomysin on F-actin. One such reconstruction of rabbit reconstituted F-actin decorated with gizzard tropomyosin resolved the structure to a resolution of 0.8 nm. The structure revealed the tropomyosin in its closed state and provides insight into the mechanism of transion from the closed to the open state, with the authors proposing two possible mechanisms (Sousa et al. 2013). The structure of the actin filament decorated by tropomyosin has been resolved by cryo-EM to a resolution of 0.37 nm for F-actin and 0.65 nm for tropomyosin. The determination of the structure to such a high resolution by cryo-EM was aided be the use of direct electron detectors and improved helical reconstruction methods (Raunser et al. 2014).

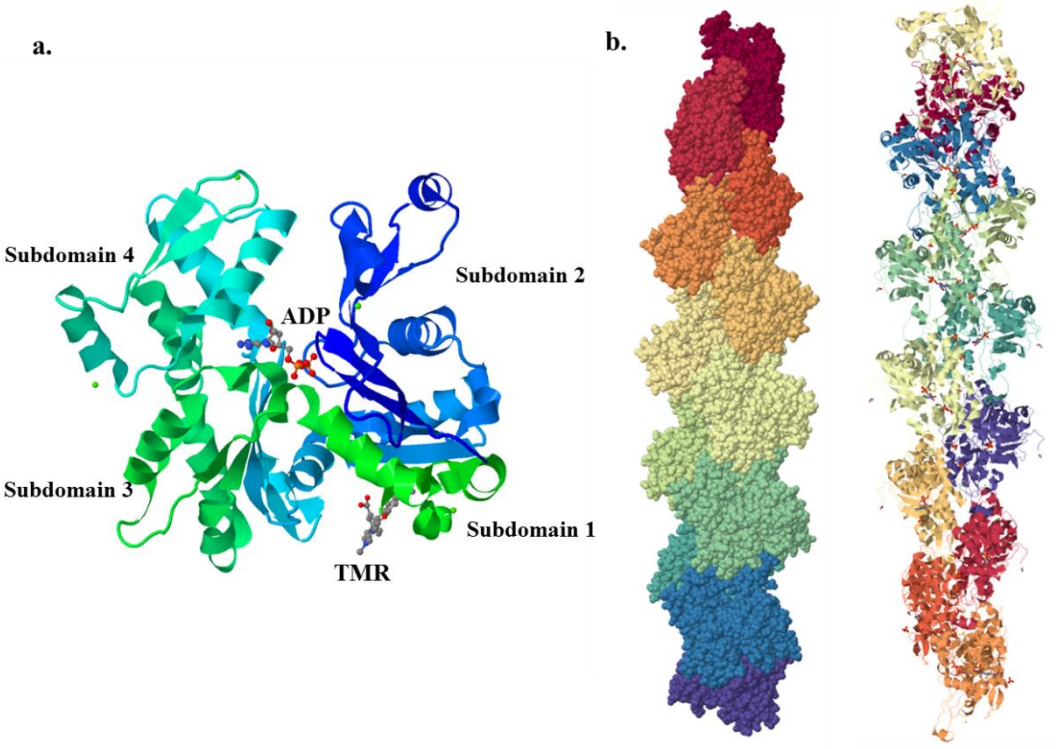

Figure 1.2 – Crystal structure of G-actin in its ADP state (a) and cryo-EM structure of F-actin (b). PDB accession codes: G-actin (IJ6Z), F-actin (3G37)

The 3D reconstruction of thin filaments showing the location of troponin has been hampered by the plasticity of the filament, and the flexibility of the troponin complex. Recently the structure of native cardiac thin filaments in the relaxed state has been resolved to a resolution of 2.5 nm using negative stain EM and single particle image processing. This reconstruction reveals the troponin position on the filament and the sufficiently high resolution allows for accurate docking of the crystal structure in the EM density map (Yang et al. 2014). To date, 3D reconstructions of the I-band showing the structure of thin filaments interacting with nebulin and tropomodulin that will enable us to fully understand how the I-band is assembled and functions are not available.

1.1.2 Overview of insect flight muscle (IFM) structure

Insect flight muscle (IFM) has a similar organization and protein make-up to that of vertebrate striated muscle, but with some differences. Sarcomere length is variable in insects with reported lengths as short as 1.7 μm in *Coccinella* and as long as 3.2 μm in *Drosophila* (Peckham et al. 1992).

1.1.2.1 IFM A-band

Thick filaments in the A-band of insect asynchronous flight muscle form a very well ordered lattice that is suitable for biophysical investigations such as fiber diffraction or low angle X-ray diffraction. Such approaches allow for the study of changes occurring in different states of muscle (Al-Khayat et al. 2003), but this is beyond the scope of this thesis.

Besides myosin, insect thick filaments contain paramyosin, the content of which can vary between 2 % and 18 %. It is thought that paramyosin has a mechanical role, contributing to the structural stability of the muscle and a physiological role, having an influence on ATPase activity of myosin (Beinbrech et al. 1992). Zeelins are proteins that have been found in the A-band of *Lethocerus* flight muscles, where they might be involved in maintaining the structure of the thick filaments (Ferguson et al. 1994). Myofilin (20 kDa) is expressed in early stages of development, is found associated with the thick filament and it is needed for the correct assembly of the thick filament (Qiu et al. 2005). Flightin (20 kDa) is associated with the thick filament and it is crucial for its structural integrity and assembly in late stages of insect development (Contompasis et al. 2010).

Reconstructions from cryo-EM data of tarantula isolated thick filaments yielded a structure with a resolution of 2.5 nm, which is sufficient to accurately dock crystal structures of myosin heads. This is the most detailed structure of the thick filament to date (Zhao et al. 2005; Alamo et al. 2008).

1.1.2.2 IFM I-Band

The I-band of insect flight muscle is very short, only about 50 nm (Bullard et al. 2006). In some asynchronous insect flight muscles a mono-ubiquitinated form of actin, arthrin, is incorporated into thin filaments. The molar ratio of arthrin to actin is 1:6.

Electron microscopy reconstruction of arthrin filaments has identified ubiquitin (8.6 kDa) on the side of subdomain 1 of actin. Arthrin polymerizes into F-arthrin and interacts with the troponin-tropomyosin complex. No functional differences between actin and arthrin have been identified. Arthrin is not found in the asynchronous flight muscles in Hymenoptera species (honeybees, wasps, bumblebees) (Burgess et al. 2004a; Hooper and Thuma 2005).

1.1.3 Mechanism of contraction in all muscle types

During muscle contraction the thick and thin filaments slide past one another leading to sarcomere shortening while the filament lengths remain unchanged. The sliding filament model for muscle contraction was first proposed in 1950s by H. E. Huxley and J. Hanson and A. F, Huxley and R. Niederke (Huxley and Hanson 1954; Huxley and Niederke 1954) and was based on light microscopy of stretched and contracted myofibrils.

Contraction is fueled by ATP hydrolysis and the reaction scheme is known as the 'Lymn-Taylor cycle' (**Figure 1.3**) (Lymn and Taylor 1971). At the start of the cycle the myosin head is bound to actin in the rigor conformation ('down'); once myosin binds ATP the affinity towards actin is reduced, which results in the separation of the two proteins. Once ATP is hydrolyzed to ADP-Pi the myosin affinity for actin increases, the crossbridge returns to the 'up' position, and then myosin rebinds actin again, which causes release of Pi and ADP. The release is accompanied by a large conformational change in the myosin head that results in the thin filaments sliding past the thick filaments. After the release of ADP-Pi, myosin returns to the rigor conformation (Zeng et al. 2004).

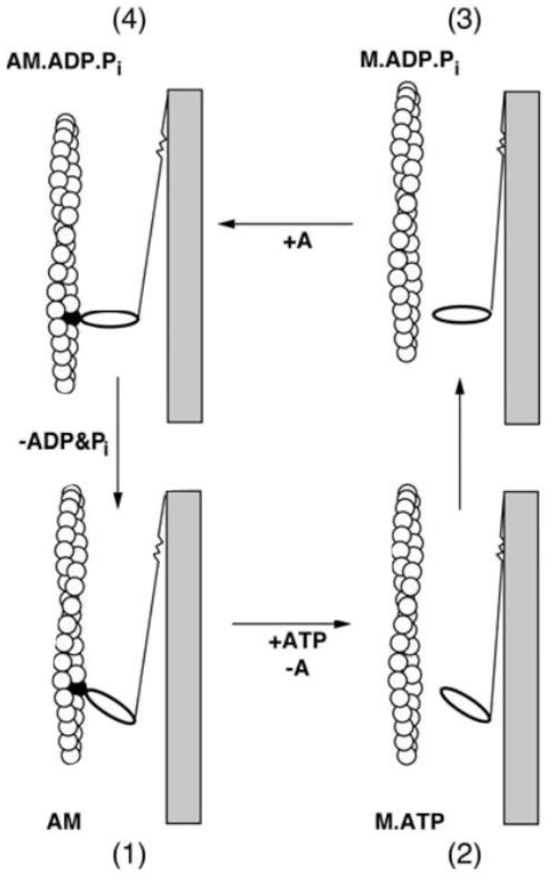

Figure 1.3 – The Lymn-Taylor cycle. The myosin (M) head is bound to actin (A) in the rigor conformation (1), ATP is rapidly bound which promotes myosin dissociation from actin (2). The ATP hydrolysis to ADP-Pi leads to an increase of myosin affinity towards actin (3), followed by rebinding (4) Release of ADP-Pi is accompanied by a conformational change.
Taken from Geeves and Holmes 1999.

Contraction is regulated by the troponin-tropomyosin complex (**1.1.1.2**) in response to calcium concentration. At low Ca^{2+} levels the interaction of actin and myosin is inhibited by tropomyosin, which covers the myosin binding sites on the surface of the thin filament (Barua et al. 2012). Once Ca^{2+} is released from the sarcoplasmic reticulum it binds to troponin, which in turn causes tropomyosin to slide across the filament, thus liberating the myosin binding sites (Filatov et al. 1999; Craig and Padrón 2004).

In insect flight the regulation of muscle contraction is similar, but Ca^{+2} influx alone is not sufficient to trigger contraction. Mechanical stretch is necessary to cause tropomyosin to move along the actin filament, liberating the myosin binding sites (Perz-Edwards et.al 2011).

1.1.4 The Z-disk

The Z-disks (or Z-lines) form the boundaries of sarcomeres and have an important structural role by tethering the ends of the antiparallel actin filaments (Craig and Padrón 2004). Connections between Z-disks from adjacent myofibrils are established by the intermediate filament protein desmin (53 kDa). This connection not only keeps the Z-disks, I-bands and A-bands in register in myocytes, but it allows for contraction to be finely coordinated between myofibrils. Desmin also interacts with mitochondria ensuring that the organelle is in the proximity of the sarcomere. Mutations in desmin lead to desmin-related myopathies (DRM) which are characterized by muscle weakness, accumulation of inclusion bodies and loss of the spatial organization of mitochondria (McLendon and Robbins 2011). Mammalian cardiac muscle has considerably more desmin (2 % of total protein) than skeletal muscle (0.35 %) (Paulin and Li 2004).

In the past the Z-disk has been viewed as having a merely structural role by tethering the ends of thin filaments, titin and nebulin. It was thought to be a passive structure being only involved in the transmission of force generated during contraction. This view of the Z-disk has changed with the discovery of many new proteins and the emergence of novel functions (Faulkner et al. 2001). Some of these proteins have the ability to translocate to different cellular compartments (e.g. the nucleus), being part of important signaling pathways involved in processes such as muscle growth and wasting (Clark et al. 2002; Pyle and Solaro 2004;).

1.1.2.1 Proteins in the Z-disk

The Z-disk interactome is refers to the macromolecular assembly comprising over 40 proteins, some of which have mainly structural roles; others are involved in signaling and some are associated with protein degradation (Frank et al. 2006). **Figure 1.4** is a diagram detailing the Z-disk interactome, comprising proteins within the disc and their binding partners which can be located in the nucleus, the costamere, intercalated disk or myotendinous junction.

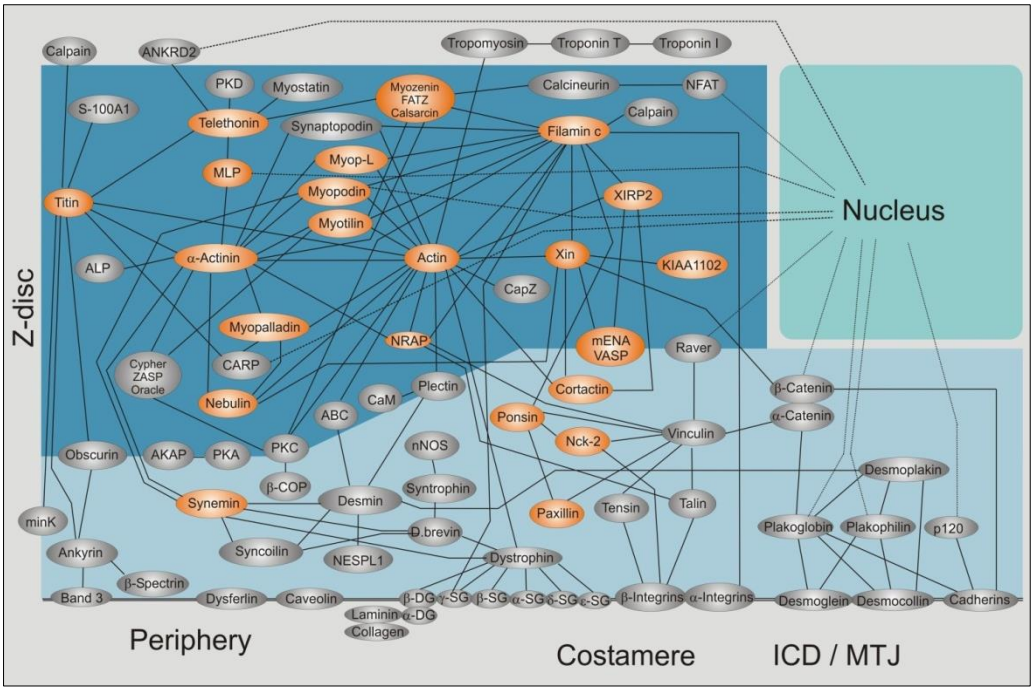

Figure 1.4 – Schematic showing the main protein components in the Z-disk and their interactions. Picture taken from http://www.proteopedia.org. ICD – Intercalated disk, MTJ – myotendinous junction.

α-Actinin

In the Z-disk the barbed ends of antiparallel thin filaments interdigitate and are cross-linked by α-actinin, a member of the spectrin superfamily. There are 4 isoforms of α-actinin in mammals: isoforms 1 and 4 are calcium sensitive and are expressed in non-muscle cells, while isoform 2 and 3 are muscle specific and calcium independent (Landon et al. 1985). In cardiac muscle only α-actinin 2 is expressed, while isoform 3 is found predominantly in fast muscle fibers. A null polymorphism for the actinin gene 3 (ACTN 3) affects around 16% humans worldwide and has been related to poorer sprint and power performance in athletes and general population (MacArthur et al. 2008; Berman and North 2010; Lek and North 2010).

The α-actinin molecule (**Figure 1.5**) is elongated with the N-terminal actin binding domain (ABD) composed of two calponin homology domains linked by a flexible neck region to spectrin repeats (4 in vertebrates). The C-terminus consists of a calmodulin (CaM) like domain. Functionally, α-actinin molecules form antiparallel homodimers,

giving the molecule a characteristic rod shape (Sjöblom et al. 2008; de Almeida Ribeiro et al. 2014). It is known that phophoinositides, mainly phophatidylinositol 4,5-bisphosphate (PiP_2), are implicated in α-actinin regulation. It has been shown that binding of PiP_2 increases α-actinin affinity for titin and actin (Young and Gautel 2000). Recently the structure of the α-actinin 2 homodimer (200 kDa) in its closed conformation was determined by X-ray crystallography (**Figure 1.5**) (de Almeida Ribeiro et al. 2014). The study of structure guided mutants, in which key contacts were disrupted in the neck region of the molecule so that the molecule adopted the open conformation, has revealed the structure of activated α-actinin and the basis of its activation. The conformational changes are modulated by the binding of PiP_2 and titin Z-repeat 7. Binding of PiP_2 is not sufficient to promote the transition of α-actinin from its closed conformation to the opened one, but it increases the affinity for titin Z-repeat 7, which binds the calmodulin domains. Upon binding of Z-repeat 7 α-actinin assumes the open conformation and binds actin (de Almeida Ribeiro et al. 2014). Electron microscopy of α-actinin-F-actin rafts showed binding to actin at a variety of angles, thus being a flexible linker, not a rigid spacer between thin filaments. It can also bind to actin filaments having the same polarity or to the same filament (Hampton et al. 2007).

α-actinin plays an important role in myofibrillogenesis, being present at very early stages in Z-bodies (Sanger et al. 2006). Because of the multitude of binding partners of α-actinin, the protein is regarded as a hub for protein interactions within the Z-disk. For example it has been shown that a substitution of the residue lysine 69 with arginine in α-actinin 2 caused a disrupted interaction with muscle LIM protein, and lead to a form of dilated cardiomyopathy (Mohapatra et al. 2003). It is thought that α-actinin can sequester proteins in the Z-line, preventing their transport to the nucleus, thus regulating signaling pathways (Lek and North 2010). For example α-actinin interacts with calsarcin, which modulates the calcineurin pro-hypertrophic signaling pathway. By sequestering calsarcin to the Z-disk α-actinin also inhibits calcineurin (Frey et al. 2004).

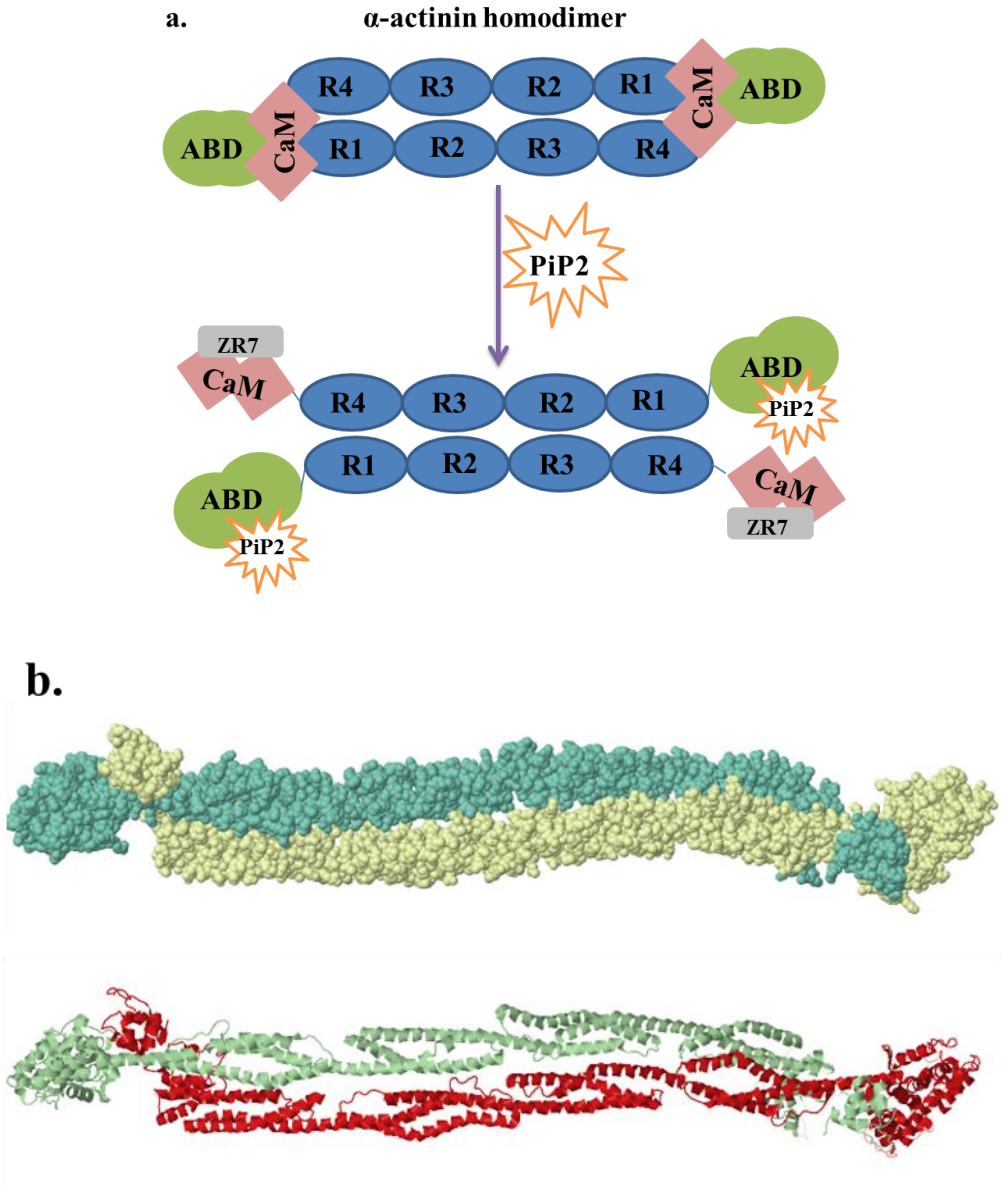

Figure 1.5 – Diagram of the α-actinin homodimer and its regulation (a). Crystal structure of α-actinin 2 homodimer (PDB accession code 4D1E). ABD – actin binding domain; R1, R2, R3, R4 – spectrin repeats; CaM – calmodulin; ZR7 – titin Z-repeat 7; PiP2 – phophatidylinositol 4,5-bisphosphate.

CapZ (actin capping protein)

CapZ is an actin binding protein expressed in all eukaryotic cells that caps the barbed end of the actin filament and prevents addition of monomeric G-actin. CapZ was shown to be a heterodimer with α and β subunits of 286 and 277 residues, respectively,

with two isoforms for each subunit. In cardiomyocytes the β1 isoform localizes in the Z-disk, while the β2 subunit is in the intercalated disk (Yamashita et al. 2003).

The crystal structure has been resolved to 2.1 Å resolution (**Figure 1.6 a**) (Yamashita et al. 2003), while the structure of the complex formed by F-actin and CapZ has been determined to a resolution of 2.3 nm by cryo-EM. Based on the model a mechanism for interaction was proposed: firstly CapZ interacts with the barbed-end of the filament electrostatically. Basic residues on the α subunit and acidic residues on the surface of actin seem to be involved in this interaction. Secondly the binding of the β subunit binds on the hydrophobic site on the filament and acts as a lock, thus reducing the off-rate of actin (**Figure 1.6 b**) (Narita et al. 2006).

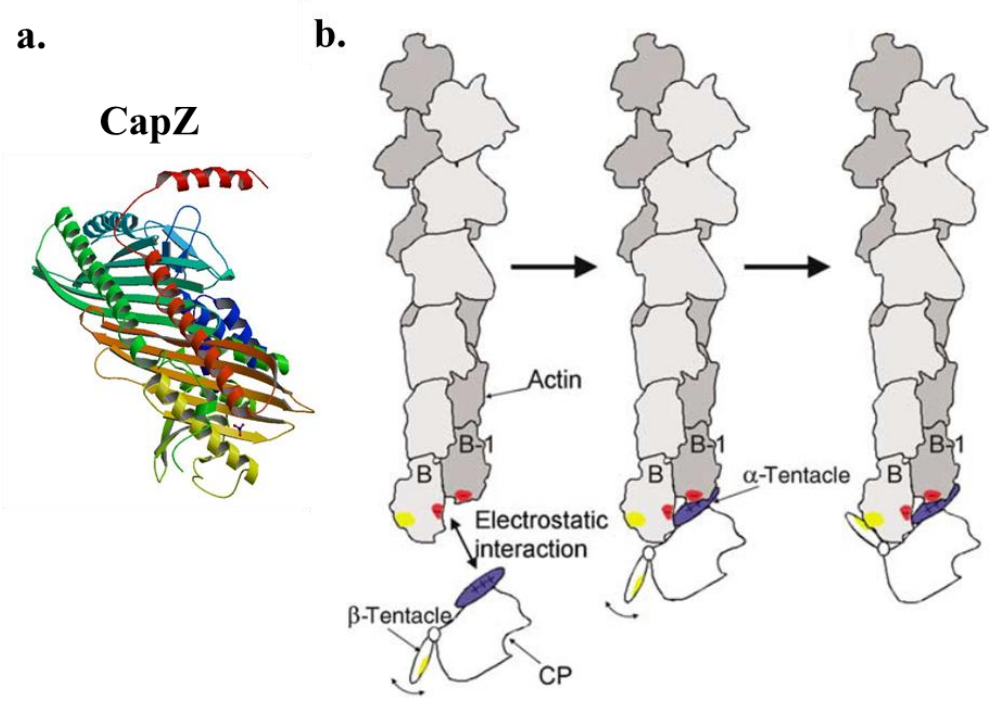

Figure 1.6 – a - Crystal structure of CapZ (PDB: 1IZN). b – Mechanism of actin capping (proposed by Narita et al. 2006). Firstly CapZ (CP) is attracted electrostatically to actin. Upon interaction of the α subunit, the β tentacle binds the hydrophobic regions of actin protomer B. Image was taken from Narita et al. 2006

CapZ interacts with nebulin and spectrin repeats of α-actinin helping with the tethering of thin filaments (Papa et al. 1999). CapZ has also been involved in signaling in the heart by regulating the binding of protein kinase C (PKC) to myofilaments. PKC is involved in the growth of heart muscle. In transgenic mice in CapZ was

downregulated in the myocardium, the function of PKC was abolished (Pyle et al. 2002).

Nebulin/nebulette

Nebulin is a giant modular filamentous protein (600 – 900 kDa, depending on the type of muscle) that associates with the thin filaments throughout their length (Wang and Williamson 1980). Nebulin is highly modular consisting of nebulin modules, which are short 35 aminoacid sequences specific to the nebulin family. Each module has an actin binding site and interacts with one actin monomer (Jin and Wang 1991)

The nebulin C terminal SH3 domain is in the Z-disk where it interacts with CapZ, α-actinin, desmin and myopalladin (Wright et al. 1993; Au 2004). Nebulin is predominantly expressed in skeletal muscle, though small amounts have been found in heart myofibrils (Kazmierski et al. 2003). Nebulin is crucial for proper Z-disk assembly: it is required for the localization of Cap Z to the Z-disk and lack of nebulin causes the loss of the regular arrangement of F-actin barbed ends (Pappas et al. 2008). It was proposed that nebulin acts as a molecular ruler regulating the lengths of thin filaments (Labeit et al. 1991; Littlefield and Fowler 2008).

Nebulette (107 kDa) is a shorter version that is expressed exclusively in cardiac muscle and localizes in the Z-disk (Moncman and Wang 1995). It was shown that targeted disruption of nebulette protein expression in cardiac cells alters the assembly and function of cardiac myofibrils (Moncman and Wang 2002). Mutations in the nebulette gene (NEBL) are correlated with cardiomyopathies and ultrastructural changes in intercalated disks from the cardiac walls (Maiellaro-Rafferty et al. 2013). Mutation A592E of the NEBL gene has been associated with a dilated cardiomaphy, in mice. The affected nebulette region is located in the Z-disk and it was shown that proteins such as α-actinin, ZASP and myopalladin were downregulated (Purevjav et al. 2010). The mutation G202R in the NEBL gene has also been associated with dilated cardiomyopathy in mice and it was found that troponin and tropomyosin were downregulated. Downregulation of filamin C was also reported in G202R mice (Purejav et al. 2002). Pathologically, mutations in the nebulin gene (NEB) are associated with nemaline rod myopathies that are characterized by muscle weakness and hypotonia and the presence of rod-like structures in skeletal muscle (Wallgren-Pettersson et al. 2011). In nebulin knock-out mice thin filaments were 15 % shorter, the Z-disks were abnormally wide and myopalladin was absent from the Z-disks (Witt et al. 2006).

Titin

Titin is the third most abundant protein in muscle, after actin and myosin, and the largest polypeptide found in nature, having a molecular weight up to ~ 4 MDa. Titin is constituted mainly of immunoglobulin (Ig) and fibronectin (Fn) domains. Its N-terminus is located in the Z-disk and the molecule spans half the sarcomere to the M-line (Tskhovrebova and Trinick 2003). In the I-band titin is a spring responsible for the passive of relaxed myofibrils (Linke 2008).

The first two Ig motifs (Z1 and Z2) are universally expressed, are located at the periphery of the Z-disk and interact with telethonin (Tcap) (Mues et al 1998). This interaction is necessary for myofibril architecture maintenance (Gregorio et al. 1998). The Z-disk region of titin contains Z-repeats, made up of 45 aminoacids. The number Z-repeats varies due to differential spilicing (Gautel et al. 1996). Titin Z-repeats interact with α-actinin and their number varies with muscle type (7 repeats in cardiac muscle and 2 or 4 repeat in fast muscles). It was thought that the number of Z-repeats are directly correlated with the ultrastructure of the Z-disk (Gautel et al. 1996, Atkinson et al. 2000). It was shown that the number of Z-repeats within the Z-disk does not correlate with the periodicities observed in the Z-disk, but there is a correlation between the actin filament cross-over and α-actinin crosslinks (Luther and Squire 2002). At the edge of the Z-disk titin attaches to the thin filament, but this interaction is poorly understood (Tskhovrebova and Trinick 2003).

Titin is not expressed in invertebrate muscles and the functions that titin has in vertebrates are fulfilled in IFM by two other classes of proteins: Sls (*Drosophila sallimus*) and projectins/twitchins. Several Sls proteins are encoded by the same gene and have their N-terminal in the Z-disk and extend across the I-band, to the edge of the A-band. Sls proteins have a highly modular structure, containing Ig repeats. Kettin (540 kDa) is the predominant isoform present in insect flight muscle (Bullard et al. 2006). Kettin binds actin, α-actinin and is essential to thin filament stability within the Z-disks and for maintaining passive tension in flight muscle (van Straaten et al. 1999; Kulke et al. 2001). Projectins and twitchins comprise Ig and Fn domains and are associated with the A-band and contact kettins in the I-band (Bullard et al. 2006).

Telethonin (Tcap)

Tcap is a small protein (19 kDa) interacts with titin (Gregorio et al. 1998), calsarcin and ankrd2 (Frey and olson 2002). It was shown that telethonin can translocate to the nucleus (Vainzof et al. 2002). Titin-Tcap interaction (**Figure 1.7**) is the strongest known to date and it is thought to be have a crucial role in maintaining Z-disk integrity. The rupture force of the complex was measured to be higher than 700 pN (Bertz et al. 2009). The crystal strcuture of the titin-Tcap complex has been solved (**Figure 1.7**) (Zou et al. 2006). The titin-telethonin interaction to be involved in mechano-sensing in striated muscle (Knöll and Buyandelger 2012). Mutations in Tcap are associated with limb girdle muscular dystrophy (LGMD) (Moreira et al 2000; Vainzof et al. 2002)

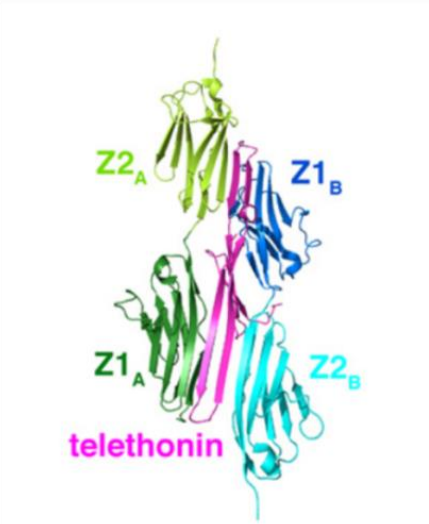

Figure 1.7 – Crystal structure of the titin-telethonin complex. $Z1_A$, $Z1_B$, $Z2_A$ and $Z2_B$ depict titin Z-repeats. PDB accession code: 1YA5. Annotated Image taken from Bertz et al 2009

Filamin C

Filamin is an actin binding homodimer which consists of two subunits of 290 kDa. Each subunit has an α-actinin like actin binding domain made up of two calponin homology domains. The rod regions contain 25 immunoglogulin like domains. The most C-terminal domain is necessary for the molecule to associate with itself and form the homodimer (Sethi et al. 2014).

Filamin C interacts with α-actinin, myotilin, calsarcin, sarcoglycans having roles in coupling thin filaments to the sarcolemma and acting as a scaffold for proteins involved in signaling (Faulkner et al. 2001; Gontier et al. 2005). Mutations in the dimerization domain have been shown to cause myofibrillar myopathies (MFM), which are characterized by myofibril destruction and aggregation of proteins in the cytoplasm (Vorgerd et al. 2005).

Myotilin

Myotilin (myofibrillar protein with titin-like immunoglobulin domains), 57 kDa, is composed of 2 Ig domains at its C-terminus and a unique serine-rich N-terminus. Myotilin form a homodimer interacts with α-actinin and filamin C and plays a role in sarcomere assembly (Shalaby et al. 2009). Mutations in the myotilin gene cause myotilinopathies such as LGMD and MFM, characterized by muscle weakness (Shalaby et al. 2009; Olivé et al. 2005).

Calsarcin (FATZ, myozenin)

Calsarcins (32 kDa) bind ZASP, Tcap, α-actinin, filamin C, myotilin, MuRF (Faulkner et al. 2000, Frey and Olson 2002). There are three isoforms of calsarcin (Faulkner et al. 2001). Calsarcins dephosphorylate NFAT transcription factors that translocate to the nucleus and activate the pro-hypertrophic gene program (Crabtree 2001; Michel and Dunn 2004). Mouse knock-out models for calsarcin 1 were characterized by an excess of slow muscle fibers and cardiomyopathy (Molkentin et al. 1998).

Myopalladin

Myopalladin (145 kDa) interacts with nebulin/nebullete and α-actinin possibly being involved in the tethering of nebulin in the Z-disk. It binds cardiac ankyrin repeat protein (CARP) which is involved in gene expression control (Bang et al. 2001).

Podin family

The podin family of proteins includes synaptopodin, tritopodin/CHAP and myopodin. Myopodin is a multiadapter protein that interact with filamin and α-actinin and can localize either in the Z-disk, or in the nucleus in a stress induced manner (e.g heat shock) (Weins et al. 2001; Linnenman et al. 2010). It was shown that inhibition of calcineurin in cardiac myocytes triggers the import of myopodin into the nucleus (Faul et al. 2007).

ZASP/Cypher/Oracle

ZASP/Cypher/Oracle interacts with the calmodulin region of α-actinin 2 (Klaavuniemi et al. 2004). There are many splicing variants of the protein: 31 kDa ZASP1 (Cypher2); 51 kDa ZASP 2; 67 kDa ZASP 3; 71 kDa Oracle 2 and the 76 kDa

Cypher 1 (Oracle 1). Its functions include embryonic Z-disk assembly and maintenance (Katzemich et al. 2013). The ablation of the protein in mice resulted in severe congenital myopathy (Zhou et al. 2001)

Muscle specific Ring Finger proteins (MuRF)

MuRFs are are ubiquitin ligases responsible for the targeting of Z-disk proteins to the ubiquitin proteasome (Bassel-Duby 2006). Hypertrophic cardiomyopathy and myopathy have been observed in MuRF knock-out mice, indicating an important role in muscle protein turnover (Frank and Frey 2011).

Muscle LIM Protein (MLP)

MLP comprises two LIM domains defined by a double zinc finger structure (Geier et al. 2003) and interacts with α-actinin and it is proposed to be a regulator of myocyte differentiation (Arber et al. 1994). Besides α-actinin MLP interacts with telethonin and calcineurin (Knöll et al. 2002). Mutations in the MLP gene have been associated with hypertrophic cardiomyopathy and dilated cardiomyopathy. At the molecular level the mutations caused decreased binding of MLP to α-actinin (Geier et al. 2003).

The description of Z-disk proteins provided in this introduction is not meant to be exhaustive, but to give the reader the context on which our work is based. The interactome is vast and has not been described in detail, but it is clear that the Z-disk is a dynamic structure that not only anchors the thin filaments, titin and nebulin, but is involved in many signaling pathways that govern muscle homeostasis. If we are to understand how healthy and diseased muscle works and the mechanisms of muscle ageing and death we need to visualize the molecular architecture of the Z-disk, to see in three dimensional space the proteins that make up the lattice and to be able to characterize all its protein-protein interactions. Structural data, integrated with molecular, biochemical and biophysical findings can help paint a more accurate picture of this most beautiful, complex and highly organized protein assembly.

1.1.2.2 Structure of the Z-disk

The three-dimensional structure of the Z-disk has mainly been studied in the past using electron microscopy of thin sections of muscle embedded in resin. In such electron micrographs, in longitudinal sections the Z-disk appears as an electron dense band in the middle of the I-band and has a characteristic zig-zag appearance in the most detailed pictures (Franzini-Armstrong 1973). The width of the Z-disk differs in various muscle types and is correlated with the degree of overlap of thin filaments and the number of α-actinin molecules: thus in fast muscle fibers the Z-disk is thin (30-50 nm) and wider in slow and cardiac muscles (100-140 nm) (Luther 2009). In insect flight muscle the Z-disk are wide, 120 nm (Cheng and Deatherage 1989). In the Z-line the antiparallel thin filaments are arranged in a tetragonal lattice in vertebrate muscle, while in IFM it is a hexagonal lattice (Saide and Ullrick 1974; Cheng and Deatherage 1989).

The structure of insect Z-disks

Asynchronous insect flight muscles are known for their particularly regular organization and can be considered quasi-crystals (Iwamoto et al. 2006). It was shown by direct 'end-on' X-ray diffraction of bumblebee indirect flight muscle fibers that the lattice order is well maintained over distances up to several millimeters of repeating 2.5 μm sarcomeres in neighbouring sarcomeres (Iwamoto et al. 2002).

The 3D structure of honeybee Z-disks has been solved to a resolution of 7 nm (Cheng and Deatherage 1989). Muscle fixed in glutaraldehyde was embedded in resin and accurately transverse sections were cut. The best preserved specimens prepared showed six orders of optical diffraction, to a resolution of 7 nm. For reconstruction, because transverse sections through the Z-disk can be considered crystalline, crystallographic methods were employed. Tilt series were collected (± 60°) around three tilt axes (with the approximate orientations of 0°, 45° and 90°) to ensure better sampling of the specimen. The Z-disk is 120 nm thick and the reconstruction showed that thin filaments overlap in the central region by 80 nm. The reported symmetry of the whole Z-disk was p312. P3 symmetry is characterized by the presence of three three-fold symmetry axes. In the case of the Z-disk, which exhibits p312 symmetry, the 3-fold axes are parallel to the axis of the myofibril and the 2-fold axes are in the transverse central plane and are perpendicular to the myofibril axis (Cheng and Deatherage 1989). It is interesting to note that Holmes et al. (1980) reported that the symmetry of giant water

bug (*Lethocerus cordofanus*) was p6, based on X-ray fiber diffraction. However, this is not exactly comparable with the bee data quoted here, as it was from the whole muscle and was a different species.

Data from the reconstruction obtained from tilted sections through the Z-disk was combined with three dimensional data obtained from oblique sections through the Z-disk, which give information regarding thin filament orientation throughout the lattice and their relationship with thick filaments in the A-band (Deatherage et al. 1989).

Connections (C1-C5) between thin filaments are solved in the 3D map and the relationship to the actin filament and each other can be investigated (**Figure. 1.8**). Connection C1, C2, C3 and C5 are seen crosslinking thin filaments of opposite polarity and C4 seems to be associated with filaments of the same polarity. The spacing between thin filaments was 170-240 Å. Considering the length of α-actinin and accounting for flexibility in the molecule, the authors proposed that the protein might be the main constituent of C1 and C2 connections. Another interesting feature observed was that C4 is a molecule with threefold symmetry that contacts three actin filaments of the same polarity, and its position in the Z-disk lattice is the same as the position of a thick filament from the neighboring sarcomere. This protein (C4) might be kettin, which is located in the Z-disk and connects it to thick filaments in the A-band. These observations are valuable but nonetheless speculative; due to the relatively low resolution (7 nm) of the map internal features cannot be solved and crystallographic data of known components of the lattice cannot be docked, thus the postion of α-actinin, kettin and other smaller components was not reliably determined.

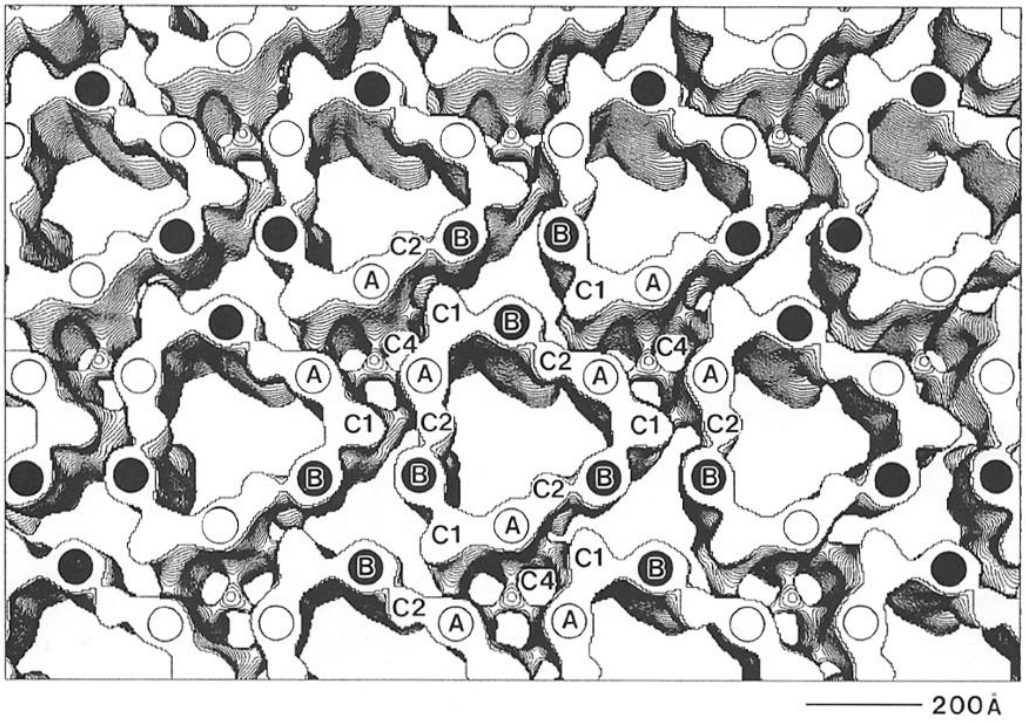

Figure 1.8 – Three dimensional reconstruction of the central region of the honeybee Z-disk. Actin filaments of opposite polarity are marked with circles and the letters A and B. The view of the map is from sarcomere A. Thin filaments of opposite polarity are connected by C1, C2, C3 and C5, while C4 contacts three thin filaments of the same polarity. Taken from Cheng and Deatherage (1989).

The structure of vertebrate Z-disks

The width of the vertebrate Z-disk also varies with muscle type, depending on the overlap of thin filaments and the layers of α-actinin present. In the Z-disk thin filaments from adjacent sarcomeres are displaced so that each filament is surrounded by four filaments of opposite polarity, giving the structure a tetragonal lattice (Luther 2000). The tetragonal lattice of vertebrate Z-disks changes appearance depending on the state of the muscle: thus in relaxed muscle the "small-square lattice" is present and in activated muscle it transitions to the "basketweave" appearance (**Figure. 1.9**) (Goldstein et al. 1987).

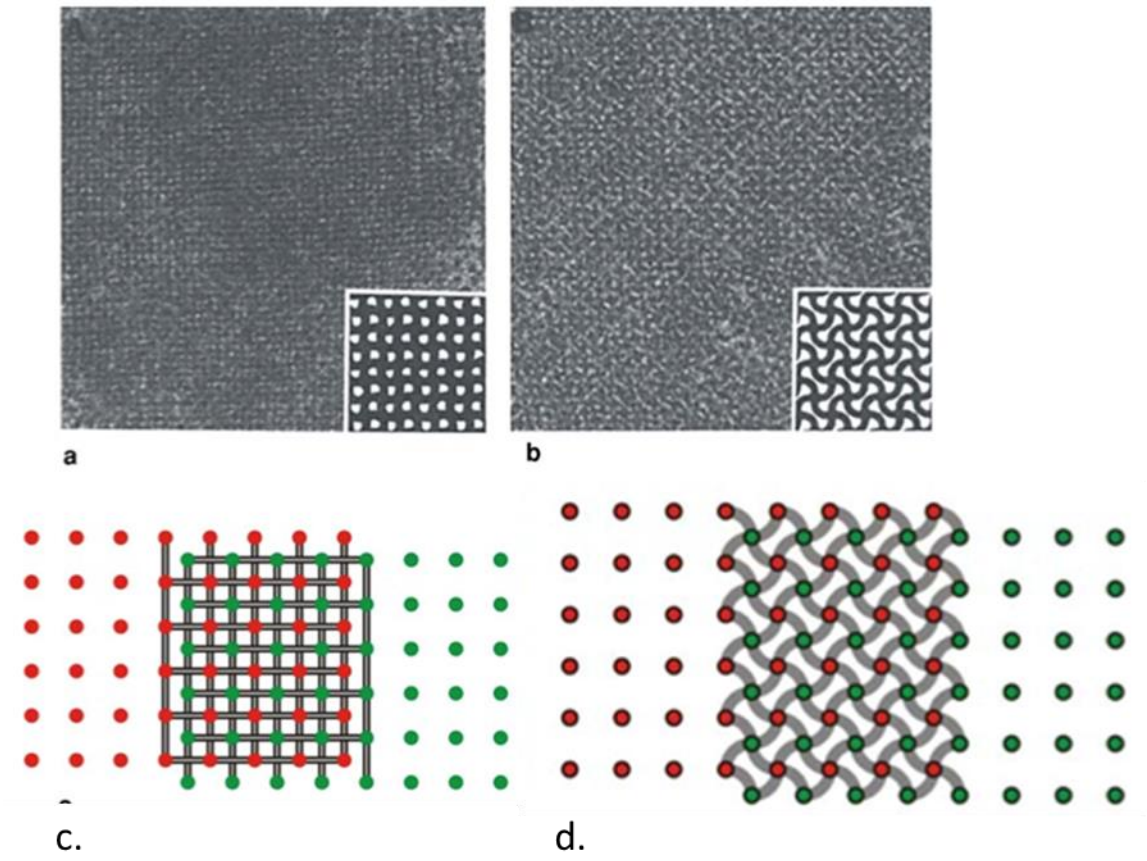

Figure 1.9 – Cross-section views of vertebrate Z-disks showing the small-square (a) and the basketweave lattices (b). The corresponding diagrams depict actin filaments of opposite polarity as red and green dots and Z-links as grey connectors. Taken from Luther, 2009.

It was shown that the two lattice appearances are not influenced by the activation state of the muscle, but that the transition can be triggered by temperature, osmotic pressure and ionic strength (Perz-Edwards and Reedy 2011). X-ray diffraction data of skinned psoas myofibrils has shown that the lattice appearance might be correlated with the position of tropomyosin on the thin filament. If tropomyosin adopts the open position the Z-disk lattice exhibits the basketweave conformation, while tropomyosin being in the closed or blocked position favors the small-square lattice. The transition of the lattice is accompanied by a 20% increase in lattice spacing (Perz-Edwards and Reedy 2011). Based on electron microscopy data (Morris et al. 1990; Luther et al. 2002); molecular dynamics simulations that postulate that α-actinin is characterized by rigidity in the central rod domain and flexibility in the peripheral domains (Golji et al. 2009) and X-ray fiber diffraction data (Perz-Edwards and Reedy 2011) the following

model of α-actinin binding was proposed. In the small-squared Z-disk the molecules adopt a sharp kink in the rod domain and associate forming a tetramer, while in the basketweave lattice the molecules are curved and are not associated.

Structural studies of vertebrate Z-disks carried out so far reveal the overall three-dimensional organization. Reconstruction of plaice fin muscle was carried out using crystallographic methods (Luther 2000). Thin filaments overlap by 25 nm and each filament is cross-linked to its four neighboring filaments by Z-links that are spaced at 15 nm. It was shown that appearances of longitudinal views are correlated with the number of Z-links present: thus if one investigates the symmetry of the Z-line one can determine if the number of Z-links is odd or even. For a simple Z-line, that comprises only a pair of Z-links, the symmetry axis is the center of the Z-disk, whereas in a 3-layer Z-disk the symmetry axis is diagonal to the unit cell (Luther 2000).

Tomographic reconstruction of the Z-disk from a vertebrate slow muscle revealed 6 layers of Z-links. Slow muscles and cardiac muscle have wider Z-disks (100 – 140 nm) with the thin filaments overlapping over 100 nm (±6 nm) and comprise more crosslinks between filaments, giving the rigidity necessary to withstand distortion that arises during muscle contraction (Luther et al. 2002).

1.1.3 The Z-disk as a stretch sensor

The sarcomere is a remarkable machine and the expression of the myriad of proteins that compose it is tightly regulated. Muscle performance directly correlates with the turnover of contractile proteins. A balance needs to be struck between protein synthesis and protein degradation so that ailments such as hypertrophy or atrophy will not impair muscle function. The existence of a stretch sensor in muscle has long been hypothesized. The Z-disk, situated in a place where it can sense the force developed during contraction, plays a role in passive force transmission and is mechanically coupled with the sarcolemma; thus it has been proposed that the Z-disk is involved in stretch sensing (Epstein and Davis 2003; Gautel 2011). This theory is supported by structural data (**1.1.2.2**) of the Z-disk or of its components: the degree of thin filaments overlap influences Z-disk rigidity (Luther and Barry 2002), the periodicity in the Z-line is correlated with the actin filament crossover (Luther and Squire 2002). Insect asynchronous flight muscles that undergo oscillatory contraction also have wide, rigid

Z-disks based on a hexagonal lattice (Deatherage et al. 1989). The tropomyosin positioning on the thin filament is involved in regulating lattice appearance (Perz-Edwards and Reedy 2011). The mechanism is not fully understood, but presumably titin and nebulin might play a role in this because both establish connections with thin filaments.

Within cardiac myofibrils the stretch sensor detects mechanical stress and hypertrophic gene programs are activated for muscle growth and development. The stretch sensor has not been fully identified, but the interaction between titin, Tcap and MLP plays an important role in stretch sensing (Knoll et al. 2002). Mutations withing the three proteins have been associated with hypertrophic cardiomyopathy (Bos et al. 2006) and dilated cardiomyopathy (Knoll et al. 2002). Tcap and MLP interaction is crucial for Z-disk integrity, the absence of MLP leads to mislocalization of Tcap on titin and the apparition of dilated cardiomyopathy (Knoll et al. 2002). MLP is not found exclusively in the Z-disk, but can localize in the cytoplasm as well as in the nucleus. It was proposed that the protein is bound to the Z-disk by α-actinin, and that it responds to mechanical stress by shuttling to the nucleus, where it triggers gene expression that will ultimately increase cell survival and prevent hypertrophic cardiomyopathy (Geier et al. 2008; Lek and North 2010). The interaction of MLP and Tcap was proposed to be tied to mechanosensing since Tcap binds titin; the titin/Tcap interaction is the strongest protein-protein interaction and can resist high forces *in vitro* (up to 700 pN) and seems to have a role in anchoring titin in the Z-disk, rather than mechanosensing (Bertz et al. 2009). The titin/Tcap/MLP/α-actinin interaction might play a role in mechano-sensing in cardiac cells, but this cannot be fully confirmed until data regarding the cellular localization of MLP or pathways triggered by mechanic signal is fully integrated in a three-dimensional map of the protein complex.

1.2 Electron microscopy and electron tomography of biological specimens

1.2.1 Development of electron microscopy

It was first thought that the main limitation to observing finer features using light microscopes was lens quality, but it became clear that the limitation stems not only from the resolving power of the lens, but from the properties of light. The spatial resolution of light microscopes is given by the Rayleigh criterion, which takes into

consideration the wavelength of light (λ) and the numerical aperture of the lens (NA); thus the smallest distance (d) that can be resolved by a microscope is given by the equation:

$$d = \frac{0.61\lambda}{NA} \tag{1.1}$$

For visible light the best resolution achievable using light microscopes is therefore around 200 nm. A revolution in the microscopy field was prompted in 1924 by Louis de Broglie, who hypothesized that particles such as electrons have wave-like properties according to the equation:

$$\lambda = \frac{h}{p} \tag{1.2}$$

Where λ represents wavelength, h is Planck's constant and p is the particle momentum. In 1927 de Broglie's hypothesis was confirmed by Davisson and Germer and Thomson and Reid by electron diffraction experiments. The first electron microscope was built by Ernst Ruska and Max Knoll in 1931 and transmission electron microscopes (TEM) were commercially available by 1936. For a 100 keV electron microscope the wavelength of the electrons is 0.04 Å. If we substitute this value into equation (1.1) we calculate that the resolution achievable with a TEM with a numerical aperture of 0.01 is around 0.2 nm. In reality electro-magnetic lenses used for TEM are far from perfect and limit resolution to few Angstroms (see **1.2.2**) (Williams and Carter 2009).

1.2.2 Overview of the transmission electron microscope

The principles behind TEM operation are similar to those of a light microscope with the exception that TEM uses electrons rather than photons to view the specimen (**Figure. 1.5**). The electrons are generated from a source (tungsten filament, lanthanum hexaboride crystals - LaB_6) by thermionic or field emission. In thermionic emission the tungsten filament or LaB_6 crystal is heated to 2000-3000°C, electrons are emitted and accelerated by an electric field. During field emission the electrons are generated from

an unheated source due to a strong potential gradient. The field emission gun (FEG) produces an electron beam that is brighter, smaller in diameter and more coherent than the beam generated by thermionic emission, and thus is used in high-performance TEM (Orlova and Saibil 2011).

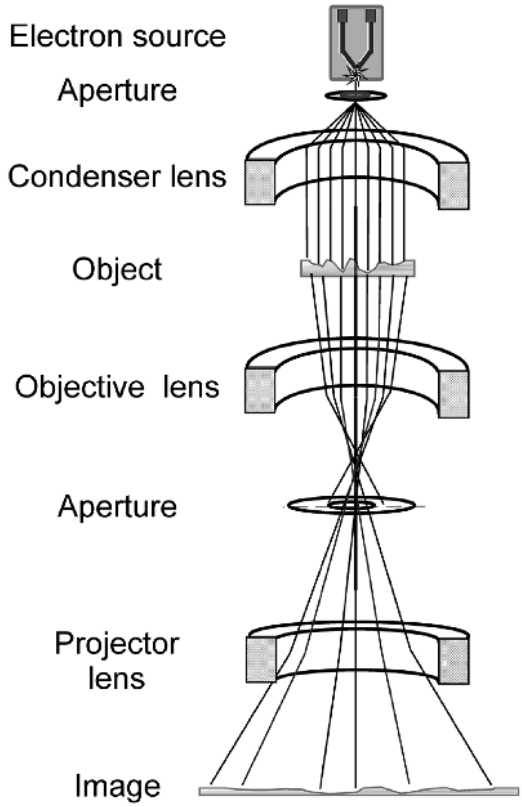

Figure 1.10 – Schematic of a transmission electron microscope. Electrons generated from an electron source are accelerated and travel in high vacuum down the column. The condenser lens collects the electrons and they illuminate the specimen. The objective lens is the primary magnifying lens. The projector lenses magnify the image further and will project the final image onto a viewing screen, typically a phospho-fluorescent surface. Image was taken from Orlova and Saibil, 2011.

The lenses of electron microscopes are coiled wire, electromagnetic and shape the electron beam as it travels through the high vacuum of the microscope column. The condenser system focuses the beam to illuminate the specimen. The objective lens is the primary source of magnification and is the most important optical element; aberrations of the objective lens ultimately influence and limit the resolution achievable by TEM. In

the back focal plane of the objective lens the diffraction pattern of the sample is formed, while the image is formed in the image plane. A system of projector lenses further magnifies the image before the electrons bombard the detector. Since electrons cannot be observed directly by eye the image is viewed on a phosphorus screen which emits light when bombarded (Williams and Carter 2009; Orlova and Saibil 2011). The images can be recorded using a variety of media, which will be discussed later in the chapter.

Electrons interact strongly with matter as they go through the specimen and cause radiation damage. Some electrons will not interact with the sample at all, while others can collide with the nucleus or be deflected by the outer electron shell or by the electrostatic field of the nucleus. If electrons interact with the sample without losing energy they are scattered elastically, while if they transfer some of their energy to the sample they suffer inelastic scattering. Apertures are inserted into the microscope column and their role is to limit the collection angle of the lens, in other words to eliminate peripheral electrons from the electron beam. The objective aperture prevents some scattered electrons to contribute to the final image, thus improving contrast (Hunter 1993).

As mentioned previously, subatomic resolution can theoretically be achieved using transmission electron microscopy, but in reality, due to lens aberrations, this is usually not possible. The aberrations of electromagnetic lenses are spherical and chromatic aberration, astigmatism, coma and curvature of the field. Spherical aberration (C_S) appears when rays are focused differentially depending on the distance from the optical axis; rays further away from the axis are refracted more strongly than the ones closer to the optical axis. Spherical aberration correctors are available commercially. Chromatic aberration (C_C) is an image distortion that appears due to the different wavelengths of the electrons; thus rays with longer wavelengths are focused more strongly and the plane of image formation is situated closer to the object, this results in halos appearing around the image. Chromatic aberration blurs fine details in the final image and arises due to a varying voltage in the electron source and due to the loss of energy during inelastic scattering events in the specimen. Chromatic aberration can be corrected by energy filtering. Astigmatism appears when the magnetic field is asymmetric and it is corrected by stigmator coils, which consist of eight electromagnetic lenses (Williams and Carter 2009; Orlova and Saibil 2011).

1.2.3 Image recording in transmission electron microscopy

Electron micrographs can be recorded using a variety of media: photographic film, charge-coupled devices (CCD) and, more recently, direct electron detectors (DED). Traditionally electron micrographs were recorded using photographic film which provides a large detection area and very good resolution. After exposure the negatives need to be developed and digitized using scanners (for example Imacon Flexlight or Zeiss SCAI); however, this introduces additional steps that are not compatible with the high-throughput of data acquisition, such as automated imaging. The implementation of automated data collection prompted the development of digital solutions for electron micrograph acquisition (Orlova and Saibil 2011).

Charge-coupled devices are effective and fast at recording electron micrographs, but they can be costly, have a poorer resolution and smaller area of detection when compared with photographic film. Nonetheless, due to the convenience of rapid image collection, CCDs are widely used. CCDs transform photon energy into an electronic signal. Because electrons are damaging a scintillator is used to convert the energy of the electron in photons, which can be transferred to the CCD chip without damaging it. The energy of the photon is converted into an electrical charge and then into an electronic signal that can be stored. The conversion of electrons into photons adds noise to the final image, but greatly increases the lifespan of the CCD (Faruqi and Subramaniam 2000). For cryo-electron microscopy the quality of the electron detector becomes increasingly important due images being recorded in low-dose regime (see **1.2.4**), thus CCDs do not provide the ideal solution for recording low-dose electron micrographs.

The recently introduced direct electron detectors do not have a scintillator to transform electrons into photons and have a faster read-out, improved sensitivity and better signal to noise ratio (SNR). Faster read-out allows for corrections of beam induced movement, which enhances contrast and reduces blurring (Ruskin et al. 2013). The improved DED, paired with better image processing techniques can potentially yield higher resolution structures of macromolecular assemblies from considerable smaller datasets. These detectors are giving a significant change in image quality, with further improvements in prospect. This is allowing larger molecular complexes (> 0.5 MDa) to be solved to atomic or near atomic resolution. It is likely that the DED will also impact tomography studies positively (Grigorieff 2013; Kühlbrandt 2014).

1.2.4 Sample preparation for biological electron microscopy

We discussed so far the limitations imposed by the hardware on the resolution achievable by TEM, but in biology the main factor limiting resolution is the specimen itself. Firstly, the main component of biological specimens is water and the sample preparation procedures need to prevent the material from collapsing in the high vacuum of the microscope. Secondly, the presence of mainly light atoms in biological samples makes them low-contrast objects, thus methods to improve the contrast need to be taken into consideration (Stahlberg and Walz 2008). Contrast increases with defocus and collecting micrographs at higher defocus will improve contrast, but this will have detrimental effects on resolution (Erickson and Klug 1971). Another issue is radiation damage that occurs when samples are bombarded with electrons. As a consequence micrographs are recorded under low-dose conditions, decreasing the SNR. Low-dose conditions are particularly important in cryo-EM (Stahlberg and Walz 2008).

Sample thickness has probably the greatest influence in electron microscopy. Electrons are absorbed easily by thick specimens and a sufficient number of particles need to go through the sample in order for significant information to be gathered by the electron detector. As mentioned previously, inelastically scattered electrons add noise to the image and damage the specimen, while elastically scattered electrons give contrast to the image, but only if they are scattered only once as they go through the sample. A thicker sample increases the possibility of multiple scattering events, thus lowering the contrast and attainable resolution (Koning and Koster 2009).

Electron microscopy can be carried out at room temperature or under cryo conditions. Room temperature EM requires the removal of water from the hydrated biological sample of interest. This is due to the fact that samples are to be visualized in high vacuum, which will promote water evaporation. The need to eliminate water prior to EM imaging and the need to stabilize the specimen has lead to the development of several methods that dehydrate and chemically fix the sample, such as negative staining, metal shadowing or plastic embedding (Hayat 2000). Water evaporation *in vacuo* can be prevented by cooling the specimen, but crystals that can occur will severely damage the sample. Fortunately if the cooling rate is fast enough (~10^6 °C/sec) water will not form crystals, but retains the high viscosity glassy or vitreous state. Rapidly frozen biological specimens are trapped in a near-native, frozen-hydrated state and show a high degree of structure preservation (Dubochet and Lepault 1984; Dubochet et al. 1985).

From frozen-hydrated catalase crystals the electron diffraction pattern extended to 0.35 nm, demonstrating that high resolution features were preserved during freezing (Taylor and Glaeser, 1974). Essentially the resolution attainable by cryo-EM is limited by radiation damage that occurs during data collection. The cryogenic transmission electron regime requires imaging under low-dose conditions; thus the SNR is very low because of the small number of electrons that can pass through the sample before damaging it (McMullan et al. 2009). Nevertheless, improvement in electron detector technology promises a continued resolution improvement in biological TEM, increasingly to atomic or near-atomic resolution.

1.2.4.1 Electron microscopy preparation of isolated particles

Negative staining

The simplest way to visualize isolated particles, such as proteins or viruses, is by negative staining, which is a convenient method that preserves the structure, somewhat prevents structure collapse and also minimizes radiation damage. Electron microscopy grids are coated with support films which can be colloidal in nature (e.g. Formvar) or carbon films, the latter being more stable in the electron beam (Hayat 2000). Carbon films can be made hydrophilic by plasma glow-discharge or by UV treatment. Usually a hydrophilic support film is desirable to obtain a thin layer of stain and an even particle spread (Burgess et al. 2004b). Once the sample is adsorbed onto the carbon film it is stained with heavy metal salts, which, after drying, encase the specimen and reveal its structure. The electron beam is strongly scattered by the stain, thus molecules are visualized because of the absence of stain and appear as white against a dark background, hence the term negative stain. An ideal negative stain is highly soluble in water, does not interact with the specimen, has a high boiling point and density and it is not susceptible to granulation under the electron beam (Hayat 2000).

Three dimensional reconstructions of negatively stained particles show that the molecules become flattened by the stain (Frank 2006), nonetheless negative staining is still considered a powerful technique that can provide useful structural information, especially for structures < ~0.5 MDa that are too small to align by image processing without staining. Negative stains commonly used are uranyl and tungsten salts, ammonium moybdate and aurothioglucose (Ohi et al. 2004). Uranyl salts are positively

charged and used in electron microscopy due to their high contrast and stability (Bremer et al. 1992). The working pH of uranyl acetate is 4.5, thus it is conceivable that proteins that are not stable in acidic conditions might unfold. It has been shown that uranyl acetate has a very rapid fixing effect on the actin and myosin, by preventing the dissambly of thick filaments from the end and does not influence the structure. This was carried out by comparing structures obtained from cryo-EM data sets (where proteins are a near-native state) and negative stain reconstructions, with no differences being observed. This indicated that changes reported in negative stain are not staining artifacts (Zhao and Craig 2003). Uranyl acetate has one of the smallest grain sizes which limits the resolution achievable to 2 nm (Ohi et al. 2004). Due to its acidity and positive charge uranyl acetate can rarely cause aggregation and precipitation of the sample. For high resolution EM uranyl formate is useful due to its small granularity after drying (Hayat 2000). Specimen preservation is good with aurothioglucose due to the glucose in its composition (Ohi et al. 2004), but the contrast of the stain is very low and it is radiation sensitive. It can also form gold crystallites upon electron irradiation (Bremer et al. 1992)

Ammonium molybdate and tungstate based stains are negatively charged and can be neutralized (Ohi et al. 2004). Potassium or sodium phosphotungstate have a slow specimen penetration, migrate less in the electron beam than uranyl acetate, but do not have a fixative effect on the specimen and long-term storage of EM grids is not possible (Hayat 2000). Potassium or sodium phosphotungstate stains produce high contrast positive staining which increases with the acidity of the solution and disrupt phospholipid membranes. Ammonium molybdate gives moderate contrast, it is relatively stable in the electron beam and it is suitable for staining fibrous proteins and membranes (Bremer et al. 1992). The downside is that the ‘shelf-life’ of EM grids stained with ammonium molybdate is limited to a few days (personal observation). Saturated ammonium molybdate (0.8 M) has been successfully used for cryo-negative staining, a method which allows the visualisation of biological samples in a vitrified thin layer of stain. This methods improves the SNR dramatically when compared with conventional cryo-EM and the resolution attainable is close to 10 Å (de Carlo and Harris 2011); however, this method has not been widely adopted.

Metal shadowing for transmission electron microscopy

Metal shadowing is a method that allows detection of small molecules that are not suitable for negative staining. The technique involves the adsorption of molecules onto the atomically flat, hydrophilic surface of freshly cleaved mica followed by metal deposition and carbon coating in high-vacuum. The dense metal (usually platinum) provides enhanced contrast, while the carbon layer stabilizes the replica. Prior to electron microscopy imaging the Pt-C replica is floated onto EM grids (Hall 1956). In the case of metal shadowing, sample buffers contain volatile constituents (typically ammonium acetate) to ensure the evaporation of the solution prior to drying *in vacuo*. Most often the buffer also contains glycerol, which has a protective effect. Proteins can be sprayed using a nebulizer or layered straight onto the mica surface (Tyler and Branton 1980; Mould et al. 1985; Trinick et al. 1984).

Plunge-freezing for cryo-electron microscopy

Plunge-freezing is a cryofixation method routinely used for suspensions containing isolated macromolecules and complexes. Typically the carbon films preferred for plunge-freezing are perforated, they can be either holey or lacey. The grids are made hydrophilic by glow-discharging and the sample is added. Buffer excess is removed by blotting, which can be done either manually or automatically, from one or both sides of the grid. Blotting ensure that a thin layer of suspension (100 - 200 nm) is formed. This layer can easily evaporate, thus it is recommended that the humidity of the surrounding area is high and freezing occurs soon after blotting. The grid is then plunged rapidly (~ 1m/s) into a cryogen. The cryogen is most often liquefied ethane cooled by a liquid nitrogen bath. Liquid ethane provides the fastest cooling rate, ensuring that the water is vitreous. Ideally the macromolecules of interest will become trapped over holes in vitreous ice. The samples can be stored in liquid nitrogen and imaged in the electron microscope using a cryo-holder cooled by liquid nitrogen. The size of the protein or assembly is what limits cryo-EM; structures below 100-200 kDa have a very low SNR and are currently regarded as difficult or impossible for structure determination by single particle methods. These proteins would be visible in tomographic reconstructions, provided that the resolution allows it (Iancu et al. 2006; Owen and Stokes 2007; Orlova and Saibil 2011). However, the new direct electron detectors may impact this limit.

1.2.4.2 Electron microscopy preparation of tissues and cells

Biological ultrastructural research using the transmission electron microscope is highly dependent on specimen thickness. For the study of tissues and intact cells methods that could produce a sufficiently thin specimen had to be developed. Sectioning (ultramicrotomy) is therefore widely used to obtain sufficiently thin specimens for study the ultrastructure of inherently thick specimens such as tissue and whole cells.

Room temperature ultramicrotomy

As discussed previously, biological specimens need to be fixed and dehydrated prior to analysis by TEM. In procedures for embedding and sectioning, samples are chemically fixed using aldehydes (commonly glutaraldehyde) followed by dehydration is a series of acetone or ethanol solutions. The dehydrated material can be contrasted using osmium tetraoxide, followed by embedding in an epoxy resin. The resin will slowly penetrate the sample and polymerization is triggered by heat or UV treatment. After polymerization the resin block is mounted in an ultramicrotome and sectioned using either glass or diamond knives. The sections are picked up using coated electron microscopy grids and contrasted. Often lead citrate and uranyl acetate are additional contrasting agents (Hayat 2000; Afzelius and Maunsbach 2004). Plastic sectioning is a powerful technique, but it has its limitations due to the poor preservation of high resolution features. Typically the best resolution of plastic sections does not surpass 7 nm , whereas ~2 nm is necessary to be able to recognize molecular shapes and to accurately dock resolved crystal structures (Sader et al. 2007). Well known fixation artifacts to be noted are: chemical fixation is somewhat slow and it is not selective (glutaraldehyde reacts with certain residues in proteins and does not provide fixation of sugars and nucleic acids); successive dehydration steps might lead to structure collapse and movements of molecules from their original positions; and contrasting might lead to the accumulation of lead or uranyl salts (McDonald and Auer 2006). The sectioning itself causes compression in the direction of cutting. It has been shown, in the case of muscle, that adding tannic acid to the sample preparation procedure will allow for better preservation of the fine structures, up to 5 nm resolution (Reedy et al. 1983a). Furthermore the changes occurring during sample preparation for plastic sectioning of glycerinated muscle were monitored by both EM and X-ray diffraction. These studies

are insightful in providing information on possible artifacts that may arise during sample preparation (Reedy et al. 1983b; Taylor et al. 1984). X-ray diffraction of embedded muscle fibers also showed that high resolution features up to 1.3 nm are preserved, whereas the best resolution obtained in the plastic sections was 5 nm (Sader et al. 2007), indicating that the preparation procedure is not as damaging as expected, but the loss of resolution appears to happen during the cutting process.

Compression occurs during the cutting process and it has detrimental effects on structure preservation. It was shown that using a low angle diamond knife reduces compression (Jésior 1985; Jésior 1986; Jésior 1989). Using an oscillating knife will essentially avoid compression of the sections, but no improvement of resolution was observed in sections cut with an oscillating knife in comparison with the ones cut without oscillation. This suggests that compression is not as detrimental (Sader et al. 2007).

High pressure freezing and freeze substitution

High pressure freezing (HPF) and freeze substitution have been developed as an answer to conventional room temperature sample preparation procedures that do not provide a satisfactory preservation suitable for structural studies of biological specimens. High pressure freezing is a form of rapid freezing that ensures specimen immobilization within a few milliseconds. During HPF the sample rests in an aluminum holder, rapid cooling is achieved by raising the pressure (to 2045 bar) and by jets of liquid nitrogen. This method ensures the vitrification of a 300 μm thick sample. Subsequent fixation occurs during the freeze substitution (FS) step, which involves the substitution of water with organic solvents such as methanol or acetone. FS takes place at -78° to -90°C. Depending on the sample osmium tetraoxide and glutaraldehyde may be added to the organic solvent. FS is followed by embedding in epoxy resin at room temperature (for structural studies) or in methacrylate resins at low temperature (for immunolabelling studies) (McDonald and Auer 2006; Owen and Stokes 2007). Sections can also be cut at -90°C, thawed, negatively stained and examined in the TEM. Alternatively the sections can be plunge refrozen and visualized under cryo-conditions using a cryo-holder (Luther and Morris 2003).

Cryo-electron microscopy of vitreous sections (CEMOVIS)

CEMOVIS is a method for obtaining ultrathin sections of vitreous specimens and it is used mainly for the study of the macromolecular architecture of tissues and cells in a near-native state. Cryo-sectioning experiments on lysozyme crystals have shown a preservation of high resolution features up to 0.8 nm, resolution not previously observed in a sectioned specimen (Sader et al. 2009). Sections devoid of cutting artifacts show remarkable structure preservation. Nevertheless CEMOVIS is technically demanding and during the cutting process a series of artifacts can arise: the compression in the direction of cutting can be as high as 60%, the diamond knife can leave marks on the section, the section can vary in thickness (chatter) and crevasses appear easily due to the stress exerted on the specimen (Al-Amoudi et al. 2004; Al-Amoudi et al. 2005; Hsieh et al. 2006).

Focused ion beam milling (FIB-milling)

FIB-milling is a technique that bypasses artifacts that arise during cryo-sectioning. During FIB-milling a focused ion beam (usually gallium) is used to sputter atoms from the surface of the specimen, producing a thin vitreous lamella from HPF or plunge frozen samples. The thinning of the specimen is done in a scanning electron microscope to aid with the navigation during milling and to evaluate the thickness of the lamella. The method was used to successfully image lamellas through whole cells, cellular suspension and tissue using cryo-electron tomography. It was shown that during the milling process the water remains vitreous at the surface of the lamella (Marko et al. 2007; Hayles et al. 2010; Villa et al. 2013). Even though FIB-milling is showing promising results, the crucial experiment of testing how well resolution is preserved has not been conducted yet. This could be tested using a regular specimen that has been thoroughly investigated using EM, such as catalase or lysozyme protein crystals. For example catalase crystals could be deposited on EM grids and plunge frozen. The resolution could be monitored before and after the FIB-milling process by analysis of the diffraction patterns.

Plunge freezing of intact cells

The conditions of plunge freezing (see **1.2.4.1**) of intact cells are essentially the same as for isolated macromolecules. The thickness of whole cells constitutes a problem when it comes to imaging in the electron microscope as most of the times the cells are too thick for the electrons to go through, but this is not universally true. For example bacterial cells grown in minimal media can be deposited on a grid and plunge frozen in liquid ethane and visualized by cryo-EM or cryo-ET. Such studies have been employed to study magnetosomes (Komeili et al. 2006) or to characterize a potential new labeling method for cryo-EM (Wang et al. 2011). Plunge freezing has also been successfully employed to study small eukaryotic cells. Cryo-ET of *Ostreococcus* tauri, the smallest eukaryotic cell, which is less than a micron in diameter, was carried out. The strength of the method stems from enabling us to visualize cellular organelles their native cellular context (Henderson et al. 2007). Cells can also be grown on gold electron microscopy grids and plunge frozen. Even though most of the cell is too dense to image in the TEM, the edges of the cell are thin enough to allow analysis (Carlson et al. 2008) eg by tomography

1.2.5 Biological electron microscopy techniques

1.2.5.1 Electron crystallography

Electron crystallography is a method that is employed for the study of two-dimensional crystals. 2D crystals are very thin arrays of proteins that do not form 3D crystals suitable for X-ray crystallography. The method is particularly powerful because the electron micrographs collected contain the phase information that is lost during data collection for X-ray crystallography. Also the diffraction pattern, that forms in the back focal plane of the objective lens, can be recorded easily in a transmission electron microscope (Stahlberg and Walz 2008). The first protein structure solved by electron crystallography was that of a transmembrane protein, bacteriorhodopsin, and in the 0.7 nm reconstruction transmembrane helices were visualized for the first time (Henderson and Unwin 1975). The authors later published the first atomic structure determined by electron microscopy of the same protein, bacteriorhodopsin. The 3D structures can be determined by tilting the specimen and recording images at different tilt angles and recombining the information from 2D projections into a 3D structure (Henderson et al.

1990). In order to produce high resolution, three dimensional structures flat and highly ordered 2D crystals were required, these are not easily encountered or produced. A method was developed for the reconstruction of imperfect three dimensional crystals and it requires continuous tilt series of the specimen to be recorded (Saxton et al. 1984).

Electron crystallography is especially suitable for the structural study of membrane proteins mainly because obtaining 3D crystals of such proteins requires the presence of detergent. Since 2D crystals can be grown on lipid bi-layers the protein of interest can be studied in a near native environment and interaction between the protein and the lipids or other ligands can be observed (Ubarretxena-Belandia and Stokes 2012). As Z-discs have many of the features of 2D crystals, the methods developed for electron crystallography may be useful for them.

1.2.5.2 Single particle electron microscopy

Single particle electron microscopy aims to solve the three-dimensional structure of isolated particles or macromolecular assemblies. Single particle-EM is a powerful and still developing technique that can provide sub-nanometer structures of proteins and protein assemblies. Structures obtained of icosahedral viruses allow the tracing of the carbon backbone (Jiang et al. 2008). The new direct electron detectors are resulting in many more atomic and near-atomic resolution structures (Bai et al. 2013; Fernández et al. 2014; Voorhees et al. 2014). The thickness of the specimen is not the limiting factor for single particle-EM, but rather the size of the object of interest and the homogeneity of the sample. In the case of cryo-EM, complexes smaller than 300 kDa are difficult to image due to the the poor contrast in micrographs which limits particle picking, but also alignment for image averaging and 3D reconstruction (Orlova and Saibil 2011). Negative staining achieves ~ 2 nm resolution and therefore remains useful for particles <~300 kDa down to <10 kDa.

Whether using negative staining or plunge freezing the molecules can in suitable circumstances adopt random orientations on the electron microscope grid. Single particle-EM utilizes many single projection images of these molecules and establishes the geometrical parameters between different views of the molecules. Single particles are picked, aligned so that structural features are in register and then particles are classified. Averaging improves the SNR, which is low in single electron micrographs,

especially in cryo-EM. Classification provides information regarding the different views of the particle, molecules in the same orientation will be part of the same class average. The information gathered from thousands of particles is used to generate a three-dimensional model. Two methods have been developed for *ab initio* model generation: random conical tilt (RCT) and angular reconstruction. RCT is beneficial for the study of molecules that adopt preferred orientations on the grid and it consists of taking two images of the same area (one at 0° and the other at a high tilt angle).

The orientation parameters obtained by RCT are used for the generation of the model, usually by weighted back-projection. Weighted-back projection takes into account the point spread function of the microscope during reconstruction and ensures that the low frequencies (low resolution features) are not oversampled. The second method assigns orientation parameters to the obtained class averages, followed by the generation of the 3D model (van Heel et al. 2000; Cheng and Walz 2009). The model is refined iteratively by using the initial model to refine the orientation parameters of the particles. Care must be taken to ensure that model bias and over refinement will not affect the final result. The assessment of the final resolution is very important and currently it is still debated. Fourier Shell Correlation (FSC) is the most common method for resolution determination. The data set is split in two halves and two independent 3D reconstructions are generated followed by the calculation of the FSC curves. The resolution is defined as the value where the FSC curve falls below 0.5. A rule of thumb useful for assessing resolution , independent of the way the resolution was calculated, is that at 0.6 to 0.8 nm resolution α-helices are resolved and at 0.5 nm some side chains can be observed (van Heel and Schatz 2005; Cheng and Walz 2009). The resolution at which the correlation between the density computed from the entire data set and a perfect reference is equivalent to the crystallography figure-of-merit and can be assigned at the point where the FSC crosses the 0.143 threshold (Rosenthal and Henderson 2003).

Validation of the final model is an important test of single particle-EM projects. The best way to validate 3DEM structures is taking an additional picture of some of the particles (at a low tilt angle). By aligning the two images to the density map the differences should be consistent with the tilt angle used to image the tilted specimen (Henderson et al. 2012). Electron microscopy density maps can be interpreted using available crystallography data. If crystal structures can be accurately docked in the map the pseudo-atomic models generated can give insight into conformational changes,

protein orientation and interaction in macromolecular assemblies (Cheng and Walz 2009).

Another challenge that single particle-EM is facing is the heterogeneity of the samples. This refers to samples that could not be produced to the desired degree of purity or to structural heterogeneity that appears when molecules adopt different conformations or when subunits of a macromolecular complex dissociate during grid preparation. Methods have been developed to tackle this problem. For example the grid blotting technique allows the transfer of protein complexes from native polyacrylamide gels straight to the electron microscopy grid (Knispel et al. 2012). Another method, GraFix, combines the separation provided by gradient centrifugation with chemical fixation. Using GraFix protein complexes are centrifuged into a density gradient containing a chemical fixation reagent, this provides the separation of the fully formed complex from debris and dissociated subunits, while the fixative will stabilize the complex. Fractions are collected and can be used for single particle-EM (Kastner et al. 2008). An exciting perspective arises from the development of better microscopes and detectors. With better hardware and detection the differentiation between several conformations of the molecule can be achieved *in silico*, practically the proteins can be 'purified' using computational methods. This was demonstrated for the ribosome-sec61 complex, using excellent electron microscopy data and computational methods the authors could distinguish between actively translating ribosomes and quiescent ones (Voorhees et al. 2014). Besides the continual development of electron microscopy hardware, new methods are being developed for data processing. Currently one of the best image processing packages is RELION (REgularized LIkelihood Optimization), which can deal with conformational variability (Scheres 2012).

1.2.5.3 Electron tomography (ET)

Electron tomography is a technique that uses a series of projection images of the same object to provide a 3D reconstruction of the object. Electron tomography is particularly useful when studying pleomorphic structures which are not suitable for single particle methods. These include pleomorphic viruses (e.g. human respiratory syncytial virus), organelles (e.g. chloroplasts, mitochondria), cells and tissue. The resolution achievable through ET is lower than that of single particle-EM, but much

higher than that of light microscopy, thus the technique bridges the resolution gap between super-resolution light microscopy, allowing the identification of unique cellular structures or macromolecular assemblies and their visualisation to resolutions as high as 5 nm (Murphy and Jensen 2007; Leis et al. 2009).

In electron tomography the specimen is tilted in the microscope and micrographs are recorded at different angles to generate a tilt series. Tilt series are typically recorded to a maximum angle of ± 60° or ±70° because of the limitations imposed by the goniometer and the holder, but also due to the fact that at very high angles the thickness of the specimen is significantly higher, making the recording of useful data difficult. Most often the tilt series acquisition schemes use a linear angular step (1° to 3°), but other schemes are available (Koning and Koster 2009). The Saxton scheme is suitable for regular specimens (such as muscle), during acquisition the tilt step becomes increasingly smaller at higher tilt angles, this ensures a finer sampling at those angles and compensates for the relative thickening of the sample (Saxton et al. 1984). The dose to which the specimen is exposed during the tilt series is an important parameter that usually is monitored during acquisition. It is known that plastic sections shrink in the electron beam, thus it is recommended that these are irradiated prior to data collection to ensure that shrinkage does not occur during the recording of the micrographs (Luther 2005). In the case of cryo-electron tomography, where samples are extremely radiation sensitive, the total dose that can be tolerated by the specimen (around 100 $e^-/Å^2$) needs to be distributed across the entire tilt series. Typically at higher tilt angles a higher electron dose is used because of increased inelastic scattering due to the thickening of the sample (Murphy and Jensen 2007).

The individual images of tilt series are coarsely aligned using cross correlation to adjust for stage shifts. A finer alignment is generated using gold fiducial markers which can be added to the specimen to help tracking during data collection. Methods for marker-free alignment are also available (Winkler and Taylor 2006). Once the images are aligned the 3D structure (tomogram) is reconstructed by reprojection of all images. Due to the fact that the specimen cannot be sampled completely the tomogram has 'missing wedge' of information and is also characterized by anisotropic resolution (the resolution in x and y is better than in the z dimension). This causes structures to appear elongated in the z direction (Lucic et al. 2013). Slices through tomograms can be interpreted directly or be further processed using template matching and subtomogram averaging. In template matching, if there are multiple copies of a known structure (such

as the ribosome), the tomogram can be searched using known crystal or EM structures. Once these are found they can be averaged in order to increase SNR (Koning and Koster 2009). The strength of the subtomogram averaging technique stems from it enabling structural biology *in situ*, as described by John Briggs and colleagues (Schur et al. 2013). The low resolution of tomography (5-7 nm) is not sufficient to recognize molecular shapes, but by averaging subvolumes from a tomogram the resolution can be improved up to 2-3 nm, which opens new windows in the study of cellular processes. For example the use of this technique revealed the opened and closed conformation of glycoproteins present on the viral envelope of human immunodeficiency virus (HIV) (Tran et al. 2012; Briggs 2013). Cryo-electron tomography and subtomogram averaging also contributed to the understanding of chemoreceptor arrays in bacteria, which are huge macromolecular complexes that are characterized by a high degree of regularity, being assembled in a hexagonal lattice (Briegel et al. 2014). Currently the best resolution obtained by cryo-ET and subtomogram averaging is that of Gag protein from Mason-Pfizer money virus is 0.85 nm (Schur et al. 2013)

An exciting development is correlative light and electron microscopy (CLEM). Fluorescence microscopy delivers information regarding cellular processes mainly using fluorescently tagged proteins. On the other hand electron tomography offers the three dimensional cellular context by imaging the structures directly, but the field of view is limited to small areas. Currently fluorescence microscopy helps pinpoint the structures of interest, this is particularly important when studying transient cellular processes that are very well defined in time. By using labels that are visible by both fluorescence light microscopy and EM the structure can be identified reliably in the electron microscope and be studied using electron tomography. This technique was used successfully to study endocytosis and virus entry (Kukulski et al. 2011). CLEM is usually carried out using two different microscopes and problems may arise during grid transfer, such as bending of the grids or ice contamination. Effort are being made to develop integrated fluorescence and electron microscopy (Agronskaia et al. 2008), but also for integrated live fluorescence microscopy and vitrification, which will revolutionize the study of dynamic processes (Koning et al. 2014).

1.3 Mass spectrometry (MS)

Mass spectrometry is a proteomic technique which focuses on analysis of proteins isolated from tissues or cells. MS is well suited to deal with samples characterized by high complexity or with samples in which some proteins are found in relatively low concentration. Mass spectrometric measurements are carried out on ionized analytes in the gas phase. The mass spectrometer consists of an ion sourse, a mass analyser and a detector. The mass analyser measures the mass-to-charge ratio (m/z) and the detector records the numbers of ions at each m/z value (Aebersold and Mann 2003).
Two techniques are used to volatilize and ionize proteins for MS: ESI (electrospray ionization) and MALDI (matrix-assisted laser desorption/ionization). ESI ionizes proteins in solution, while MALDI sublimates samples from a crystalline matrix. ESI is mostly used for analysing complex protein mixtures, while MALDI is best suited for simpler samples (Aebersold and Mann 2003).

Mass spectrometry (MS) has been used routinely to study the peptide composition of purified proteins. However proteins need to be pure from biological contaminants and from certain buffers and detergents for this method (Kussmann et al. 1997). The protein composition of macromolecular complexes can be studied by combining 1D or 2D gel electrophoresis with tandem mass spectrometry analysis (MS/MS), by excising bands from polyacrylamide gels and processing them for mass spectrometry (Beranova-Giorgianni 2003). This approach is more convenient as it provides high mass range for detection of protein, high sensitivity and better tolerance to certain buffer conditions as compared with gel-free approaches. The peptide fragments obtained are checked against protein sequence databases (Henzel et al. 1993).

1.4 Thesis aims

The main goal of this project was to investigate the molecular organization of intact Z-disks by electron tomography. The work focused on the biochemical isolation of well preserved Z-disks from insect indirect flight muscles and vertebrate muscles.

In the past the structure of the Z-disk has been investigated by electron tomography of sectioned muscle (Cheng and Deatherage 1989; Luther 2009), however due to sectioning the resolutions is poor (5 nm at best). At 5 nm protein shapes cannot be distinguished in electron density maps, thus crystal structures cannot be docked accurately to inform about the molecular architecture of the Z-disk lattice. We would like to test the hypothesis that, by obviating the need for plastic sectioning, the resolution of tomography reconstructions can be improved to at least 2-3 nm, which would allow for recognition of protein shapes. Intact honeybee Z-disks that show a preserved hexagonal lattice have been isolated in the past (Saide and Ulrick 1974), thus we sought to improve existing preparation methods and to carry out ET. Even though isolated insect Z-disks have been reported in the literature for several decades the instrumentation and data processing methods were not sufficiently developed for a similar study to be carried out. Our aim was to study isolated Z-disks using modern electron microscopy techniques, such as cryo-electron tomography and subtomogram averaging. We considered that cryo-EM and ET was the best approach, since the specimen is visualized in a frozen-hydrated, near-native state. The resolution achievable is limited by radiation damage and sample preparation methods. Subtomogram averaging is a technique that enables the averaging of subvolumes from three-dimensional volumes in order to improve the signal to noise ratio and to improve resolution. Our aim was to combine cryo-ET with subsequent subtomographic averaging to study the structure of the Z-disk lattice and to achieve a resolution (2 nm) that will enable us to accurately dock crystal structures in the density map.

We also sought to develop a new method for isolation of Z-disks from vertebrate muscle, as there is no such method described in the literature. We consider that isolated vertebrate Z-disks, skeletal or cardiac, would constitute valuable specimens for the study of healthy and diseased muscle, thus a reproducible method for the isolation and purification of intact vertebrate Z-disks is needed.

2. General materials and methods

This chapter includes information on general materials and methods that are common to more than one chapter. Methods specific to a particular chapter are described in that chapter. Thus Chapter 3 contains information describing the preparation of cryo-electron microscopy grids of isolated Z-disks, subsequent image analysis using the ImageJ software and sample preparation for mass spectrometry. Chapter 4 contains information regarding tilt series acquisition schemes, tomogram reconstruction and sub-tomographic averaging. Methods describing protein purification and fluorescence microscopy are detailed in Chapter 5. All laboratory work has been carried out by the author at University of Leeds. Credits to contributors are given throughout the thesis.

2.1 Materials

Chemical reagents were supplied by Sigma-Aldrich Ltd. unless otherwise stated. Buffers were made up using water from Milli-Q or Milli-Elix purification systems (Millipore). After filtration, adsorption and deionization steps Milli-Q water had a resistivity of 18.2 MΩ.cm at 25°C and Milli-Elix a resistivity of > 5 MΩ.cm at 25°C.

2.2 Protein handling and analysis methods

2.2.1 Sodium dodecyl sulphate polyacrylamide gel electrophoresis (SDS-PAGE)

SDS-PAGE was used to analyze protein samples such as myofibril preparations or bacterial cell lysates and to monitor myofibril extraction conditions and protein purity (Weber and Osborn 1969). In the presence of small amounts of N, N'-methylene-bis-

acrylamide, acrylamide monomers form crosslinked polyacrylamide gels, which are used to separated proteins based of their molecular weight. The key to this is that SDS unfolds proteins and binds to them non-specifically, so that their charge is proportional to mass. Acrylamide polymerization is catalyzed by the addition of ammonium persulfate and the base N,N,N',N'-tetramethylenediamine (TEMED) (Walker 1996).

Polyacrylamide gels were made using glass plates, spacers (1 or 1.5 mm) and clamping holders from BioRad Laboratories. The acrylamide stock solution used for both the resolving and the stacking gel was 30% (w/v) acrylamide to bisacrylamide (37.5:1) stabilized Protogel solution (Gene Flow, National Diagnostics). The acrylamide concentration in the resolving gel varied from 7.5 to 12 %, depending on the sample to be analysed. The resolving gel contained 375 mM Tris-HCl (pH 8.8), 0.1 % SDS, 0.1 % ammonium persulphate (APS) and 0.05 % *N,N,N′,N′*-Tetramethylethylenediamine (TEMED), obtained from 99% stock solution (Sigma-Aldrich). The APS was either freshly made before preparing the gel mixtures or made up as a stock solution (10%) and stored in the freezer at -20°C.

After the resolving gel was poured it was covered with 70 % ethanol to ensure that the surface was flat and that air bubbles did not form on the top of the gel. The resolving gel was left to polymerize for 30-45 minutes before the layering of the stacking gel, which contained 3.9 % acrylamide, 125 mM Tris-HCl (pH 6.8), 0.1 % SDS, 0.1 % APS, 0.1% TEMED. A lane comb was inserted and the gel was left to polymerize. Polymerized gels were mounted in the BioRad gel tank and submerged in running buffer comprising 25 mM Tris-HCl pH 8.0, 192 mM glycine and 0.1 % SDS (National Diagnostics). The comb was carefully removed and 10-40 µl samples were added to the wells. For assessing protein size 5 µl of prestained molecular weight markers (PageRuler Protein Ladder – Invitrogen) were loaded in one of the wells.

Samples were prepared by diluting them with 2x denaturing buffer. The 2x sample buffer used was a modified Laemmli buffer (Laemmli 1970), which contains 63 mM Tris-HCl (pH 6.8), 2% SDS, 10% glycerol, 5% β-mercaptoethanol, 6 M urea and 0.004% bromophenol blue. Samples diluted with denaturing buffer were heated in a heating block to 100 °C for 5 minutes to induce heat denaturation of proteins.

Once the gels were loaded with protein samples and molecular weight standards they were run at a constant voltage of 160 V for 60-70 minutes or until the bromophenol blue front reached the bottom of the gel. After electrophoresis the gels were removed from the glass plates and rinsed briefly with MilliQ water, followed by staining for 3-4

hours or overnight using Coomassie Blue stain (3g/L Coomassie Brilliant Blue R250, 45 % methanol, 10 % glacial acetic acid, 45 % MilliElix water). After staining the gel was destained using 45 % methanol, 10 % glacial acetic acid, 45 % MilliElix water. Finally the gels were rinsed with MilliElix water and photographed using either a PC scanner (HP PSC 2210) or a BioRad GelDoc XR System.

Silver staining of polyacrylamide gels

Occasionally, samples under investigation were of a very low protein concentration, which made detection using Coomassie stain difficult. To overcome this silver stain was used as it is much more sensitive than Coomassie Brilliant Blue. Following electrophoresis gels were stained with the Pierce Silver Stain Kit (Thermo Scientific) according to the manufacturer instructions. Alternatively the gels were silver stained using in-house reagents.

The stock solutions needed for silver stain were: 50 % acetone, 50 % trichloroacetic acid (TCA), 20 % silver nitrate (stored in the dark), 20 % thiosulphate pentahydrate ($Na_2S_2O_3 \bullet 5\ H_2O$), 37 % formaldehyde (Sigma Aldrich). The gel was fixed for 5 minutes in fixing solution containing 60 ml acetone stock, 1.5 ml TCA stock and 25 µl formaldehyde. The gel was rinsed three times and washed in MilliQ water for 5 minutes, then treated with 60 ml acetone stock for 5 minutes. The acetone was replaced with 100 µl thiosulphate stock in MilliQ water and the gels was left incubating for 1 minute. The thiosulphate was rinsed away with MilliQ water and the gel impregnated with silver nitrate (0.8 ml $AgNO_3$, 0.6 ml formaldehyde, 60 ml MilliQ water) for 8 minutes. Prior to developing, the gel was rinsed twice with MilliQ water. The developer was prepared freshly before use and contained 1.2 sodium carbonate (Na_2CO_3), 25 µl formaldehyde, 25 µl thiosulphate in 60 ml MilliQ water. The developer was added and stirred gently until bands appeared. The developing process typically lasted no more than 1-2 minutes and was stopped by removing the developer and adding 1% acetic acid (Nesterenko et al. 1994).

2.2.2 Spectrophotometry

Protein concentration and bacterial cell culture density were measured using spectrophotometry. The readings were taken by a Cary 50 UV-Vis Spectrophotometer

(Agilent Technologies) connected to a PC. Software used for recordings was the Cary WinUV Bio package. The optical density of bacterial cell cultures was measured at 600 nm (OD_{600}) using disposable poly-methyl metacrylate (PMMA) sample cuvettes (Plastibrand).

Protein solutions were placed in clean quartz cuvettes (minimum 60 µl) and absorbance measured at 280 nm, 260 nm and 320 nm. Proteins absorb at 280 nm and the 260 nm measurement is required for nucleic acid quantitation. The 320 nm reading is use to detect background absorbance due to insoluble light-scattering aggregates, denatured proteins for example (Stoscheck 1990). A baseline value of the buffer without proteins was always recorded prior to absorbance measurements. The concentration was calculated using the Beer-Lambert law:

$$A = \varepsilon \times l \times c \tag{2.1}$$

Where A represents the absorbance, ε is the protein extinction coefficient (M^{-1} cm^{-1}), *c* is the molar concentration that is determined and *l* represents the path length (cm). The path length of the cuvettes used was 1 cm unless stated otherwise. The extinction coefficient of gelsolin was taken to be 115000 M^{-1} cm^{-1} (communicated by Prof. Carlier (LEBS, France)) with delivery of the gelsolin plasmid. For protein solutions for which the extinction coefficient was unknown, for example when working with myofibrillar suspensions, bacterial cell lysates or impure fractions collected during purification, absorbance was approximated by dividing the 280 nm value to the path length of the cuvette. To correct for nucleic acid contamination the following formula was used:

$$c = 1.55A_{280} - 0.76A_{260} \tag{2.2}$$

Where *c* represents the protein concentration in mg/ml, A_{280} and A_{260} are the absorbances at 280 nm and 260 nm, respectively (Stoscheck 1990). To convert the molarity of a protein solution to milligram per milliliter and vice versa the following formula was used:

$$c = \frac{M}{MW} \tag{2.3}$$

Where *c* is the concentration in mg/ml, M is the molarity and MW is the molecular weight of the protein (Stoscheck 1990).

2.2.3 Dialysis of protein solutions

Dialysis was routinely used for the removal of glycerol from myofibril suspensions stored in the freezer, for buffer exchange and the adjustment of salt concentration. Dialysis was typically carried out overnight in the cold room against a litre of buffer with gentle stirring. For small sample volumes (up to 1 ml) 6-8 and 12-14 kDa MWCO (Molecular Weight Cut-Off) Mini and Midi D-Tube Dialyzers (Novagen) were used. The dialysis membrane was hydrated before the start of the procedure as per manufacturer recommendations. The sample was carefully added to the D-tube Dialyzer, the cap was screwed on, and the tube was placed on a floating rack and immersed in cold buffer. For larger sample volumes (up to 50 ml) SnakeSkin dialysis tubing consisting of regenerated cellulose was preferred. The membrane does not need to be wetted before dialysis, the tubing was clamped at one end and the sample added, followed by clamping of the tubing with a plastic clip.

2.2.4 Concentrating protein samples

Protein solutions were concentrated using Amicon Ultra-15 filter units (Millipore). The centrifugal device consists of a sample holder which is separated from a polypropylene tube by a membrane (regenerated cellulose). The sample was pipetted in the chamber and centrifuged in a swing-out rotor at 4000 x g, 4°C for 15-30 minutes in a Jouan GR422 centrifuge. The concentrated protein solution was recovered from the sample chamber. Protein concentration was monitored using spectrophotometry (**2.2.2**).

Vivaspin 500 (Sartorius) centrifugal concentrators with high molecular weight cutoff (1000 kDa) were also used during myosin extraction from myofibrils. During centrifugation the myosin will go through the polyethersulfone membrane, leaving extracted myofibrils in the sample chamber. The recovery of extracted myofibrils was low and in order to improve the recovery rate the membrane was first blocked with several solutions as suggested by an application note of the manufacturer. The effect of the blocking solutions was compared by phase contrast light microscopy and SDS-

PAGE. The solutions used were: 1 % BSA in PBS, 5 % SDS, 5 % Tween-20 and 5 % Triton-X 100; however, recovery did not improve significantly.

2.3 Phase contrast light microscopy

Phase contrast light microscopy is an image contrast enhancing technique first described in 1934 by Frits Zernike (Zernike 1934). Phase contrast allows for transparent objects such as living cells or isolated organelles to be visualized with considerably improved contrast. The phase device has two parts: a condenser annulus and a phase plate. The condenser annulus is located in the front focal plane of the substage condenser. The phase plate is located near the objective back focal plane.

As light travels through the specimen, some of it is transmitted without scattering, while some is deviated. The amplitude and phase of the scattered waves are changed. The transmitted and the deviated rays are focused by the objective lens and combine through interference. Typically the resulting wave is phase shifted in relation with the unscattered beam. Contrast is determined by the difference in intensity (amplitude) of the resulting wave and the background, undeviated light, thus if the intensity is only slightly different the object appears as transparent in the light microscope. In phase contrast light microscopy contrast is enhanced by maximizing the differences between background light and the resulting wave. This is achieved by focusing the undeviated beam onto the ring of the phase plate, which alters its phase (Lodish et al. 1995; Burch and Stock 2002).

Prior to visualizing samples in phase contrast the microscope was aligned and Köhler illumination was established. Köhler illumination generates an even illumination of the sample, while the light source is not visible in the resulting image. With the 10x objective inserted the specimen was focused, the height of the condenser adjusted and the condenser centered. Next, one of the eyepieces was removed and a phase telescope was used to observe the phase plate. If necessary, the position of the phase plate was adjusted so that the condenser annulus and phase plate were overlapping and concentric. The phase contrast microscope was used to either visualize myofibrils directly or to monitor changes occurring during extraction in flow-cells. The flow-cells were assembled by sticking thin stripes of double-sided sticky tape onto a glass slide, followed by the addition of a droplet of myofibril suspension and a glass cover slip. The

volume of the flow cell was adjusted by changing the thickness of the sticky tape. After focusing on the desired area a drop of extraction buffer was placed on the right hand edge of the flow-cell and the left hand edge was touched with filter paper to ensure a continuous flow of buffer and the removal of extracted proteins. The flow cell was supplied with fresh buffer continuously to ensure that the samples did not dry.

2.4 Electron microscopy

2.4.1 Preparation of continuous carbon films

Grids covered in continuous carbon film were used for negative staining. Carbon coating of freshly cleaved mica sheets (Agar Scientific) was carried out in an E306A Vacuum Coating Unit (Edwards, Ltd.) The carbon film was deposited on the freshly cleaved surface of mica. The mica was placed on a filter paper in the center of the table in the vacuum chamber. Carbon thread (0.7 g/mm, 1 mm diameter, Agar Scientific) was suspended between electrodes directly above the mica at a distance of 15-17 cm. The coating unit was sealed and the air pumped out for 40 minutes to ~8×10^{-2} mbar, measured by a Pirani gauge. Once the initial rough vacuum was achieved a high vacuum was created by an oil diffusion pump. High vacuum ($1 \times 10^{-4} – 1 \times 10^{-6}$) was achieved after about one hour and a half and was assessed by a Penning gauge. Carbon was deposited on the mica by passing current through the carbon thread, effectively burning the carbon off. Once this is done the vacuum was broken and the mica sheets placed in a humid atmosphere next to a small beaker filled with MilliQ water under a glass bowl. This was done in order to facilitate carbon floating during grid coating. Copper grids (Agar Scientific) with 200 or 400 square mesh were cleaned in acetone, rinsed twice in MilliElix water and placed on a metal mesh submerged in MilliQ water. Prior to grid placement on the metal mesh the surface of the water was cleaned of impurities, such as dust particles, using lint free paper (Agar Scientific). The carbon films were floated off the mica by gently submerging the mica at a shallow angle (15°). The carbon film, being hydrophobic, detached and floated on the water surface. The grids were then raised gently to make contact with the carbon film. The grids were left drying overnight in a Petri dish.

2.4.2 Preparation of holey carbon films

Holey carbon films were used during the screening of freezing conditions suitable for isolated Z-disks and while learning how to carry out cryo-EM. The protocol for was obtained from University of California, San Diego. A solution consisting of 0.17 g of Formvar was dissolved in 50 ml choloroform. The solution can be stored for several months provided it is kept in a tightly sealed bottle, refrigerated and in the dark. A glass slide was cleaned thoroughly using detergent and warm water and rinsed with MilliQ water. A suspension of glycerol in the Formvar solution was produced by adding 50 droplets of 50 % glycerol/water and sonication in a Coplin jar. The tip of the sonicator probe was placed on the surface of the solution, which was sonicated until mixed. After sonication the solution appeared milky. The cleaned slide was coated with Formvar by dipping it in the solution and removing it gently with a continuous motion from the jar. Excess Formvar was drained by touching the edge of the slide on a filter paper. The slide was left to dry upright in a dust-free environment. A glass bowl was filled with MilliQ water and the surface of the water was cleaned using lint free paper. The edges of the Formvar film were scored with a clean razor blade and the film was floated by immersing the slide in water at a shallow angle (15°). The grids were placed shiny side down on the grey unwrinkled areas of the film. The grids were picked up by touching a piece of office paper onto the surface of the water. The paper with the Formvar coated grids was left drying in a Petri dish. After drying there is the possibility that thin films form over holes, creating “pseudo-holes”. In order to perforate these thin films the paper was placed on a filter paper soaked in methanol and left for 30 minutes. The grids were carbon coated as described in section **2.4.1** and inspected in the phase contrast to determine the quality of the film. The Formvar was dissolved by placing the paper on a filter paper soaked in ethylene dichloride. A half an hour treatment is sufficient to dissolve the Formvar without damaging the carbon film.

3. Isolation and characterization of insect Z-disks

3.1 Introduction

Early reports showed that the Z-disk of insect muscle is resistant to extraction with mild acids or high salt solutions, whereas the remainder of the sarcomere dissolved. The first mention of this was in 1888, when Kölliker described the Z-line as the most resistant part of the myofibril during treatment with dilute acids (Kölliker 1888). Later it was shown that, by exposing honeybee myofibrils to 0.5 – 1 ‰ lactic acid, round Z-disks that show a reticular structure are extracted (Garamvölgyi et al. 1962). A thorough report on the purification and properties of honeybee Z-disks was published by Saide and Ulrick (1974). The Z-disks were isolated using 0.43 % lactic acid and were purified on sucrose density. Electron micrographs showed that, remarkably, the hexagonal lattice of the Z-disk is preserved after acid extraction. Isolated Z-disks were pelleted and the ultra-thin sections of the pellet revealed fine projections (presumably the residue 'connecting filaments' that join Z-discs to thick filaments) extending to 130 nm from the thin Z-disk backbone, which may be a problem for electron tomography, causing excessive thickness of the specimen. Another interesting observation was that the diameter of the Z-disks varied between 2 μm and 9 μm depending on the pH of the suspending buffer, thus at very low or very high pH the Z-disks swell.

Intact honeybee Z-disks were also successfully isolated using high ionic strength Weber-Edsall solution containing 0.6 M KCl, 40 mM $NaHCO_3$, 10 mM Na_2CO_3 (Garamvölgyi et al. 1962; Harsányi and Garamvölgyi 1969). Prior to extracting the acto-myosin with Weber-Edsall solution the myofibrils were kept in distilled water. Giant water bug (*Lethocerus*) Z-disks were also isolated using high ionic strength solutions: 1.4 M KCl, 0.08 M $NaHCO_3$ pH 8.8 (Bullard and Sainsbury 1977) or 1 M KCl, 0.08 M $NaHCO_3$ pH 8.8 (Sainsbury and Bullard 1980). Similarly *Drosophila* Z-disks have been isolated using 0.7 M KCl, 0.04 M $NaHCO_3$ pH 8.5 (Saide et al. 1989).

Purified Z-disks were used to study protein composition by gel electrophoresis and Western-Blotting, and also were used to raise monoclonal antibodies to help identify proteins of high molecular weight in the Z-disk (Saide and Ullrick 1974; Sainsbury and Bullard 1980; Saide et al. 1989). Such studies are potentially valuable because they provide insight into the composition of the Z-disk interactome.

Purified Z-disks have not, however, been subjected to modern electron microscopy techniques such as cryo-EM and cryo-ET, nor to detailed composition studies exploring their full complexity, for instance by mass spectrometry sequencing. Our aim was to isolate intact Z-disks that show a well preserved hexagonal lattice and to carry out structural studies using cryo-EM, and study their protein composition using mass spectrometry sequencing. Although some proteins will be washed away during extraction, in proportion to the harshness of the method used, these studies could open the way to monitoring Z-disk structure and composition and how these change with circumstance. Components that had been washed away could, in principle, be added back, monitoring reattachment by fluorescence tagging and light microscopy, perhaps using super-resolution light microscopy. For example PALM (photoactivated localization microscopy) is a single molecule technique which enables the acquisition of images at ~ 20 nm lateral and ~ 50-100 nm axial resolution. The protein of interest (e.g. a component known to be washed away during extraction) could be labeled with a photoswitchable fluorescent probe. PALM probes consist of either genetically encoded fluorescent proteins or synthetic dyes that can be introduced in the sample using antibodies. During data acquisition only a subset of fluorophores are activated and images are recorded. The process is repeated several times until most of the molecules have been switched on. The raw data is analyzed to determine the center of the molecule with high precision. The resulting localizations are combined to generate a super-resolution image, which can provide information regarding the incorporation of the protein of interest within the lattice of the isolated Z-disk (Temprine et al. 2015). This information might then be correlated with appearance of new density in tomogram reconstructions.

We obtained well preserved Z-disks from honeybee by extracting washed myofibrils with high salt solution. We are grateful to Dr Belinda Bullard (York University) for advice and discuss about extraction conditions. We have successfully carried out cryo-EM on these preparations. Progress has been made in our attempts to

purify high salt extracted Z-disks and preliminary composition analysis of the preparation was carried out mass spectrometry sequencing of SDS gel bands**.**

3.2 Methods

3.2.1 Preparation of honeybee myofibrils

Honeybees (*Apis mellifera*) were kindly supplied by Mr. Lance Penketh, Dr. William Hughes and Dr. Katherine Roberts (School of Biology, University of Leeds). Prior to dissection the bees were exposed to carbon dioxide or kept on ice to ease their handling. Myofibrils were prepared from the indirect flight muscle according to methods described in the literature (Garamvölgyi et al. 1962; Bullard et al. 1973). Indirect flight muscles from the thorax were removed using tweezers and collected in ice cold sucrose containing buffer: 0.3 M sucrose, 0.1 M KCl, 0.01 M potassium phosphate (pH 7), 1 mM $MgCl_2$, 2 mM EGTA, 0.02 M NaN_3 and EDTA-free Protease Inhibitor Cocktail Tablets (1 tablet/50 ml buffer) (Roche Diagnostics).

Muscle was homogenized using either a Wheaton tissue grinder for small volumes (1-2 ml) or the Polytron homogenizer for larger volumes. Separated myofibrils were washed three time in sucrose buffer by spinning them down at 600 x g for 20 minutes at 4°C in a Sigma 2k15 bench top centrifuge, followed by resuspension; this step removed soluble proteins and most of the mitochondria and nuclei from the suspension. The sucrose was washed away by centrifuging at 600 x g for 10 minutes and resuspending myofibrils in 0.1 M KCl, 0.01 M potassium phosphate (pH 7) with protease inhibitors. Myofibrils were stored in the -80°C freezer in the same buffer containing 75 % glycerol. The quality of the myofibril suspension was checked throughout the preparation on a phase contrast microscope (Leitz Laborlux 12). Prior to extraction experiments, glycerol was removed from the preparation by overnight dialysis against 0.1 M KCl, 0.01 M potassium phosphate (pH 7) at 4°C and with protease inhibitors present.

3.2.2 Preparation of isolated Z-disks

Intact Z-disks were isolated from honeybee indirect flight muscle using mild acids and high ionic strength solutions, which are summarized in **Table 3.1** and described in detail in sections **3.2.2.1** and **3.2.2.2**. Extraction conditions were monitored by phase contrast light microscopy.

Table 3.1 – Extraction conditions used for the isolation of honeybee Z-disks

Mild acids	
Lactic acid	• 0.43 % lactic acid (Saide and Ulrick 1974)
High ionic strength buffers	
KCl	• 1.4 M KCl, 0.08 M $NaHCO_3$ pH 8.8 (Bullard and Sainsbury 1977) • 1 M KCl, 0.08 M $NaHCO_3$ pH 8.9 (Sainsbury and Bullard 1980) • 0.6 M KCl, 0.08 M $NaHCO_3$, 10 mM MgATP pH 8
KI	• 0.6 M up to 1 M KI
KCl+KI	• 0.7 M KCl, 0.6 M KI, 0.08 M $NaHCO_3$, pH 8

3.2.2.1 Preparation of isolated Z-disks using lactic acid

Flow cell experiments were carried out in the phase contrast microscope to determine the concentration of lactic acid that would cause Z-disk release. The tested concentrations were: 0.43 %, 0.1 %, 0.01 % and 0.001% lactic acid (Fluka DL-Lactic acid ~ 90 %). For gel electrophoresis and electron microscopy analysis samples were prepared by harvesting myofibrils by centrifugation at 1000 x g for 5 minutes. The suspending buffer was replaced with 0.43 % ice cold lactic acid and extraction was carried out on ice for 40 minutes.

Z-disks were purified further on discontinuous sucrose density gradients. The gradients were made up by dissolving sucrose in lactic acid and were layered in 5 ml polypropylene tubes (Beckman-Coulter) as follows: 2.2 ml 2.5 M sucrose, 2.2 ml 0.4 M sucrose. 0.5 ml Z-disk suspension was layered on top of the gradient and centrifuged in a swing-out rotor (SW 55 Ti, Beckman-Coulter) at 90000 x g for 16 hours at 4°C (Saide and Ullrick 1974; Bullard and Sainsbury 1977). 500 µl fractions were collected from the

top of the gradient manually by pipetting. Care was taken to ensure that the layers did not mix. Fractions were checked in the phase contrast microscope and some were further analysed in the electron microscope by negative staining (see **3.3.1**). Fractions found to contain Z-disks with little or no cellular debris were pooled and dialysed overnight against a buffer of physiological ionic strength: 25 mM HEPES (pH 7.2), 100 mM NaCl, 0.1 % NaN_3 and protease inhibitor cocktail tablets. Recovered samples were imaged using the electron microscope.

3.2.2.2 Preparation of isolated Z-disks using high salt solutions

Extraction using KCl based buffers

Potassium chloride extraction buffers have been used in the past to isolate intact Z-disks from *Lethocerus sp.* indirect flight muscles (Bullard and Sainsbury 1977, Sainsbury and Bullard 1980). Myofibrils were harvested by centrifugation at 1000 x g for 5 minutes and resuspended in ice cold extraction buffers (see **Table 3.1**). The extraction was carried out on ice for 60 minutes. The suspension was inspected in the phase contrast microscope.

Our attempts to isolate Z-disks using high salt potassium chloride based buffers (1 M and 1.4 M KCl) failed to yield a preparation composed mainly of Z-disks, instead the suspension contained mostly incompletely extracted myofibrils, as well as Z-disks. Adding ATP to the extraction buffers to promote thick filament depolymerization (e.g. 0.6 M KCl, 80 mM $NaHCO_3$, 10 mM MgATP) improved the yield of isolated Z-disks. Z-disks obtained using KCl extraction solutions were unsatisfactory for structural investigations by electron microscopy.

Extraction using KI

Iodide ions are chaotropic agents that destabilize folded proteins (Garamvölgyi et al. 1962; Zhang and Cremer 2006; Harsányi and Garamvölgyi 1969) and potassium iodide was used successfully used in the past to extract actin from muscle (Bullard and Sainsbury 1977; Corsi and Perry 1958; Remedios and Gilmour 1978; Maruyama et al. 1981); thus we incorporated KI in our extraction buffers to optimize extraction and to increase the concentration of isolated Z-disks.

Flow-cell experiments were carried out using increasing KI concentrations (0.6 M up to 1 M). At 1 M KI extraction occurs quickly and Z-disks fall flat on the glass slide surface. Z-disks were extracted in 1 M KI on ice for 30 minutes prior to gradient purification. Due to the difficulty of dissolving high concentrations of sucrose in 1 M KI, iodixanol gradients (Optiprep – Sigma Aldrich) were used for Z-disk purification. A discontinuous Optiprep gradient was prepared by layering 1.4 ml 40%, 30% and 20% iodixanol in 1 M KI solutions. The sample (0.8 ml) was placed on top of the gradient and centrifuged at 90000 x g for 2 hours at 4°C in a swing-out rotor (Beckman-Coulter, SW55Ti). Fractions were collected by taking aliquots from the top of the gradient and were checked in the phase contrast microscope, electron microscope and by SDS-PAGE.

Extraction using KCl and KI buffers

Better preserved Z-disks, as judged by their regular lattice, were obtained after extraction using 0.7 M KCl, 0.6 M KI, 80 mM $NaHCO_3$ pH 8. This preparation was taken further to cryo-EM and mass spectrometry for analysis. Z-disks were purified using both sucrose and iodixanol gradients. Collected fractions that were found to contain Z-disks were pulled and dialysed overnight against 25 mM HEPES pH 7.2, 100 mM NaCl, 0.01 % NaN_3 and protease inhibitors using D-Tube Mini Dialyzers MWCO 14-16 kDa (Novagen). SDS-PAGE of collected fractions before and after dialysis was carried out as described previously (**2.2.1**).

3.2.3 Negative staining of isolated Z-disks

Negative stain electron microscopy was employed for screening and assessing the quality of the sample throughout the preparation procedures. Several different stains were used: uranyl acetate, ammonium molybdate and phosphotungstic acid. For negative staining carbon coated grids were made hydrophilic by either UV treating grids for 30 minutes under a mercury lamp (UV Products Inc, Pasedena, Type R52), or by glow-discharging for 40 seconds at a high tension of 10 kV (Cressington 208 Carbon Coater). 7 µl of Z-disk suspension was pipetted onto the carbon and were left to settle for 10-15 seconds before washing with 2 droplets of low salt buffer (25 mM HEPES, 100 mM NaCl). The washing step was important as it removes the salts present in the

extraction buffer. Salt concentrations higher than 0.5 M impair negative staining (Sainsbury and Bullard 1980; Burgess et al. 2004b). Most often the stain of choice was 1 % ammonium molybdate pH 7 as it is not as dense as uranyl acetate and provides a moderate contrast (Saide et al. 1989; Bremer et al. 1992), making it easier to observe the lattice of the Z-disk. Lactic acid preparations were stained with 1 % phosphotungstic acid pH 2.5, as described by Saide and Ullrick (1974).

3.2.4 Cryo-electron microscopy of isolated Z-disks

Grids for cryo-EM were prepared by plunge freezing in liquid ethane. 200 mesh copper Quantifoil R 3.5/1 or lacey grids (Agar Scientific) were made hydrophilic by glow-discharge for 20 seconds at 10 kV HT (longer glow-discharge times made the carbon film brittle). 5 µl of Z-disk suspension were placed on the uncoated grid bar side of the grid. Due to the carbon film being hydrophilic the droplet migrates on both sides of the grids. This holds true for the washing droplets as well. The tweezers were placed on the work bench and the grids were washed once with the high salt solution to wash away extracted proteins and three times with a low salt solution (8 mM HEPES pH 7.2, 25 mM NaCl). Each wash consisted of a 7 µl buffer droplet that was carefully blotted from the carbon side of the grid using the cut edges of Whatman No. 1 filter paper. Manual blotting required finesse and special care was taken not to touch the carbon with the filter paper; thus the grids were blotted by touching the grid from its edge. Despite these precautions grids sometimes dried. An important aspect for the reproducibility of the experiment is that the size of the droplet which formed on either side of the grid did not differ greatly in size between different batches of grids. Best grids were obtained with 0.1 % Tween 20 was added to the washing solutions; this improved plunge freezing and more often thin ice formed over the grids. After washing grids were placed immediately in the Vitrobot chamber (4-5°C, 90 – 100 % humidity) and they were blotted for 4 – 6 seconds using blot forces 3-5. The best grids, showing a good distribution of Z-disks and 80 – 90 % ice coverage, were obtained after blotting them for 6 seconds at a blotting force of 4. **Figure 3.1** shows a comparative view of a grid blotted to dryness (**a**) and grid with Z-disks embedded in thin vitreous ice (**b**).

Data was collected under low dose conditions at a defocus of – 2 or – 3 µm. The total dose that the Z-disks can be exposed to before radiation damage occurred was determined by taking successive pictures with a dose of 2 $e^-/Å^2$/sec.

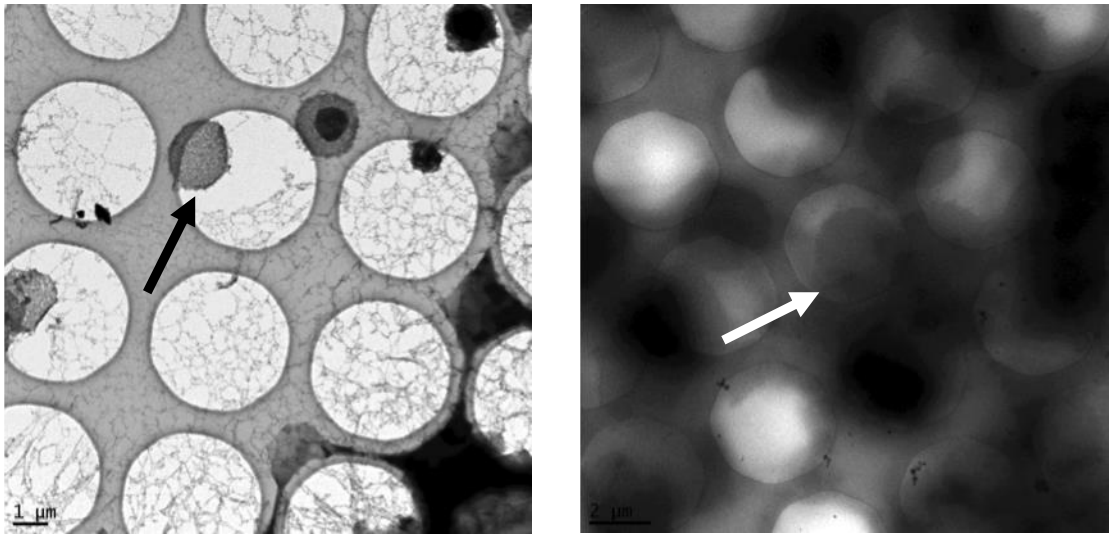

Figure 3.1 – Comparative view of a Quantifoil grid blotted to dryness and a grid with thin vitreous ice over holes. (a) Dried out Z-disks and (b) frozen hydrated Z-disks are indicated by black and white arrows, respectively.

3.2.5 Image analysis of electron micrographs

Electron microscopy data was recorded on film (Kodak SO-163) when using the JEOL 1200 and Phillips CM10 microscopes and were scanned using an Imacon scanner at 1270 ppi or 20 µm. Digital Micrograph was used to collect data on CCD (4k x 4k on the FEI F20 and 2k x 2k on the FEI T12 microscope). Micrographs were analysed using ImageJ (National Institutes of Health).

The Z-disks were subjected to two types of analysis. Firstly, the diameter of Z-disks was measured to allow a comparison between the two extraction methods. Secondly, the degree of lattice preservation was assessed by inspecting the Fast Fourier Transform (FT) of the image. ImageJ calculates the FT and displays the power spectrum, while the phases are also retained and can be accessed.

The relationship between the distance in reciprocal space (D) and the distance in real space (d) can be described by the equation: (3.1)

$$1/d = D/ PS \text{ x (box size)}$$

Where D is the distance in pixels to the furthest reflection in the power spectrum, PS is pixel size and box size is the boxed used for computing the FT. For scanned micrographs pixel size (PS) is calculated according to:

(3.2)

$$PS\ (Å/pixel) = 10000 \times SR \times DF/Mag,$$

Where SR is the scanning resolution of the scanner in microns, DF is the decimation factor and Mag is the magnification of the recorded image. For .DM3 files recorded using Digital Micrograph the pixel size is contained in the file header, which is recognized by a plugin in ImageJ (DM3Reader).

3.2.6 2D crystal unbending

Electron crystallography is a powerful technique that can deliver atomic structures of proteins (Henderson, 2004). Biological two dimensional crystals are rarely perfect, which constitutes the main impediment in reaching atomic resolution by most of the electron crystallography studies. Several lattice defects can appear in two-dimensional crystals including bending, stretching, dislocation of the lattice and cracks and degrade the Fourier Transform (FT) and reduce high resolution information. Filtering in the frequency domain essentially averages all the unit cells present in the FT, the averaged unit cell appearing blurred if the FT was degraded by lattice imperfections. Lattice unbending was developed as a method to correct distortions and to recover high resolution information (Henderson et al. 1986; Kunji et al. 2000; Gil et al. 2006). In practice lattice unbending translates into sharper diffraction spots and possibly the recovery of higher resolution spots that could not be resolved in the degraded FT.

Isolated Z-disks are essentially two dimensional crystals. Fourier Transforms of vitrified Z-disks have been shown to extend to 8 nm. With the goal of sharpening the diffraction spots in Fourier transforms, to correct for lattice distortions and to possibly resolve higher resolution spots, 2D lattice unbending was carried out at the University of Sheffield in the laboratory of Prof. per Bullough by Dr. Peiyi Wang using the MRC software 2dx (Gipson et al. 2006). Firstly the SNR of the 2D projection images was enhanced by optical filtering, which allows the selection of specific frequencies. This was done by setting all the frequencies unrelated to the periodicity to zero followed by

reprojection. A reference area consisting of a smaller region of the image is selected and lattice distortions calculated by cross-correlation, the distortions were represented graphically using lattice vectors.

3.2.7 Mass spectrometry of isolated Z-disks

Z-disks were extracted using high salt (0.7 M KCl, 0.6 M KI, 0.08 M $NaHCO_3$, pH 8) and purified by successive high speed (20000 x g, TLA 100 rotor, Beckman Coulter) centrifugation steps. The samples were spun four times; subsequently the supernatant was removed and replaced with fresh extraction solution. Prior to SDS-PAGE the electrophoresis apparatus was cleaned using 0.5 M NaOH to avoid any contamination. Precast gradient gels (4-12 % NuPAGE Invitrogen) were preferred as this limits the handling of the gels and lowers the chances of contamination from the environment (e.g. keratin from human skin). Gels were stained with 25 ml Instant Blue overnight and then rinsed with MilliQ water filtered through a Millipore filter with 0.22 μm pore diameter. Bands were excised using sterile razor blades and placed in LoBind Eppendorf tubes in 50 μl MilliQ water. Samples were sent to the Cambridge Centre for Proteomics (CCP), where mass spectrometry data was collected. The data obtained was cross-referenced against honeybee sequence data and analysed with the kind help of Dr. Charlotte Scarff.

3.3 Results

3.3.1 Preparation and EM observations of lactic acid isolated Z-disks

During the phase contrast light microscopy flow-cell experiments we observed that the three lowest concentrations of lactic acid (0.001%, 0.01% and 0.1%) caused gradual swelling in the myofibrils, but rarely Z-disk release. When using 0.43 % lactic acid the extraction was complete in a few seconds and round, pale Z-disks could be seen floating freely. If the myofibrils adhered firmly to the glass slide the Z-disks fell flat on the glass surface due to losing the support of the thin and thick filaments, as shown in **Figure 3.2.**

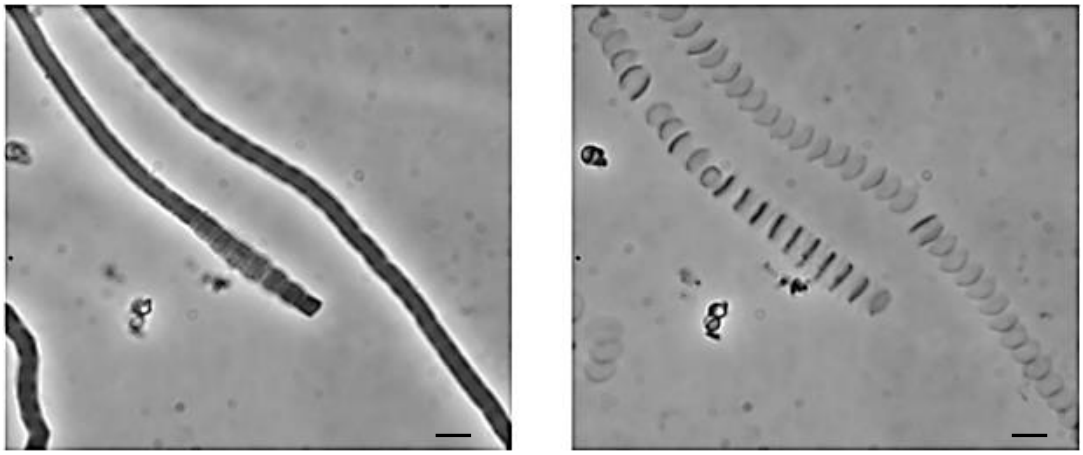

Figure 3.2 – Phase contrast micrographs of honeybee myofibrils before and after treatment with 0.43% lactic acid. The thin and thick filaments are removed by the lactic acid and the Z-disks are seen flat on the glass surface. Scale bars represent 5 μm.

Z-disks were further purified by centrifugation on discontinuous sucrose density gradients. Two distinct layers formed in the gradient (**Figure 3.3**). Upon inspection in the phase contrast microscope we found that the top layer (layer A) contained mainly Z-disks, while the bottom layer (layer B) contained Z-disks and a considerable of cellular debris.

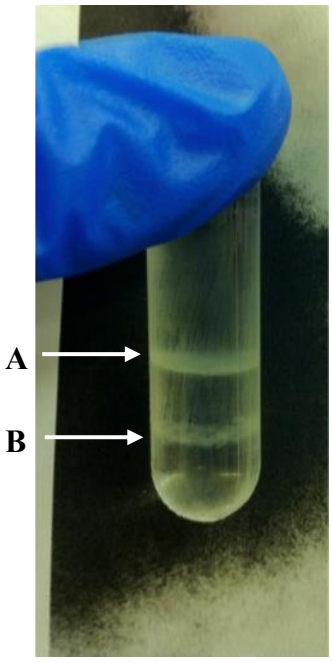

Figure 3.3 – Representative sucrose gradient showing two separate layers from lactic acid isolated Z-disks. Layer A contains mainly Z-disks, while in layer B cellular debris and contaminants are present.

The samples were stained using phosphotungstic acid pH 2.5, as described by Saide and Ulrick (1974). Our lactic acid extraction experiments were consistent with previously published data. It is remarkable that the Z-disk lattice survives the drop to acidic pH and that it maintains its structure. Well preserved Z-disks show a characteristic honeycomb appearance and their diffraction spots arranged in a hexagonal pattern can we recognized in their Fourier Transforms. Nonetheless our preparations also contained Z-disks that lost the lattice regularity did not diffract and were considerably swollen, having a diameter up to 6-7 μm (**Figure 3.4**). This indicates that the extraction can damage the structure of the Z-disk considerably. We estimate that the ratio between Z-disks that show a hexagonal lattice and the ones that are visibly damaged was 1:3.

Z-disks that diffracted and appeared round and were not folded or distorted in any way were selected for diameter measurements (**Figure 3.5 a**). Measurements were taken only from samples where Z-disks were still suspended in lactic acid prior to negative staining and EM. The average diameter of the Z-disk was 3.8 μm ± 0.5 μm (mean ± S.D., n = 25). The FT of the Z-disks shows a hexagonal pattern (**Figure 3.5 b)** extending to 34 pixels in reciprocal space, which corresponds to 60 nm in real space.

Density gradient purified Z-disks showed a similar regular structure in electron micrographs and FT (**Figure 3.5 c, d, e, f**). The recovery rate was very low, as judged by electron microscopy; presumably because the Z-disks adhere to the tube walls and are lost. Data was collected from 3 electron microscopy grids with only 8 Z-disks selected for diameter measurements. The diameter of purified Z-disks was measured to be 4.32 μm ± 0.76 μm (mean ± S.D., n = 8). Compared to the raw preparation the Z-disks swell significantly in the presence of sucrose (by ~0.5 μm). In **Figure 3.5 c** and **e** the Z-disks have a diameter of ~ 4.5 μm.

Purified Z-disks dialysed against physiological ionic strength buffer showed a dramatic change in size. **Figure 3.5 g** shows a Z-disk from a preparation dialysed against 25 mM HEPES pH 7.2, 100 mM NaCl. The FT power spectrum displays a second set of reflections (**Figure 3.5 h**). The furthest reflections extend to 97 pixels corresponding to 40.3 nm in real space. The change in the appearance of the FT suggests that the conformational changes that occur during extraction are partially reversible.

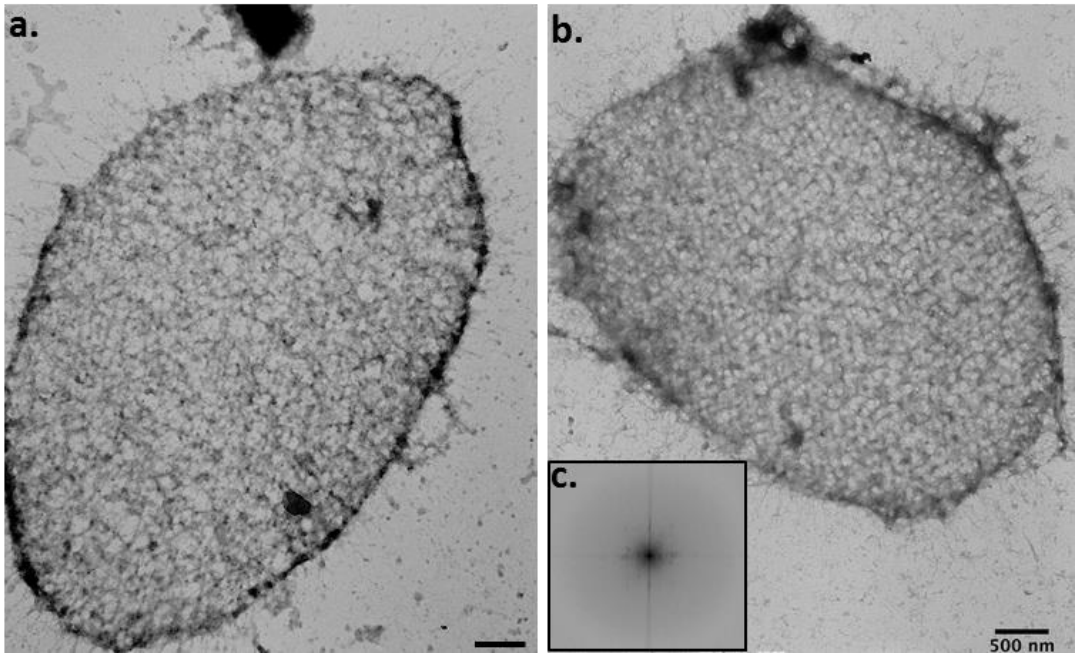

Figure 3.4 – Lactic acid isolated Z-disks damaged during extraction.
The Z-disks are swollen (a and b), the loss in the regularity of the lattice is observed in the FT (c). The specimen was stained with 1% phosphotungstic acid pH 2.5. Data was collected on film using the JEOL 1200 TEM.

Figure 3.5 – Electron micrographs and Fourier transforms of lactic acid isolated honeybee Z-disks. The Z-disks were stained with phosphotungstic acid pH 2.5.

a and b – isolated Z-disk suspended in lactic acid and its FT, showing the hexagonal lattice. The diffraction spots extend to 34 pixels, corresponding to 60 nm in real space. Scale bar represents 500 nm. Data was recorded on film on the JEOL 1200 TEM.

c and e – purified Z-disks suspended in the sucrose density medium and their FTs, showing the hexagonal lattice (**d and f**). Scale bars represent 1000 nm. Data was collected on CCD (4k x 4k) on the FEI F20 TEM.

g and h – purified Z-disk after dialysis against physiological buffer. Diffraction spots extend further, to 97 pixels which represent 40 nm in real space. Data was recorded on film on a Phillips CM10 TEM.

Figure on next page.

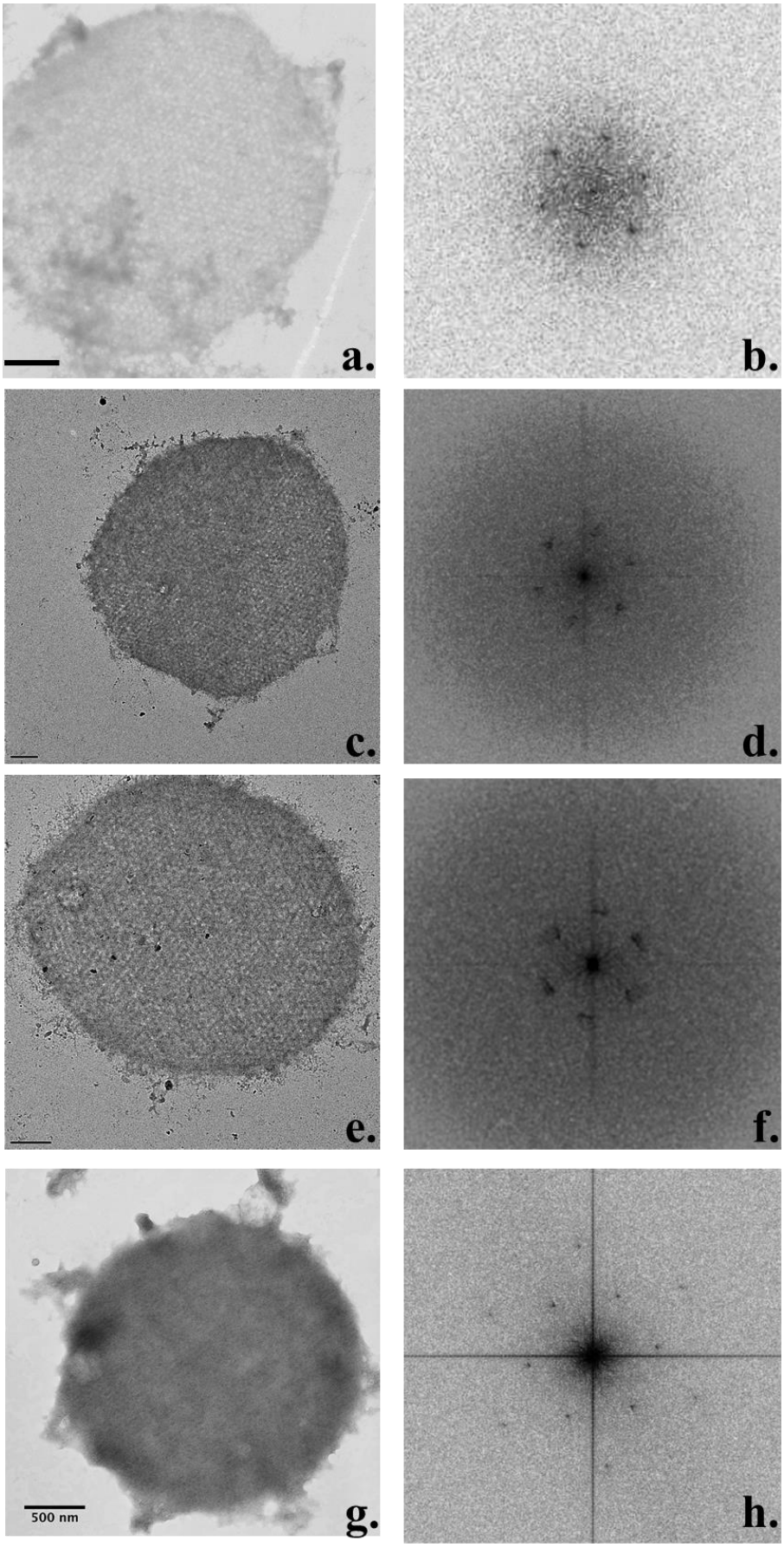
a.
b.
c.
d.
e.
f.
500 nm
g.
h.

3.3.2 Preparation and EM of high salt isolated Z-disks

KCl extraction

High ionic strength extraction solutions based on potassium chloride (1.4 M KCl, 0.08 M $NaHCO_3$ pH 8.8 (Bullard and Sainsbury 1977); 1 M KCl, 0.08 M $NaHCO_3$ pH 8.9 (Sainsbury and Bullard 1980) yielded suspensions composed primarily of incompletely extracted myofibrils, as well as Z-disks. To promote thick filament depolymerization, MgATP was included in the buffers (0.6 M KCl, 80 mM $NaHCO_3$, 10 mM MgATP pH 8. The addition of MgATP improved the yield of Z-disks, but their lattice was poorly preserved, as observed by electron microscopy (**Figure 3.6**).

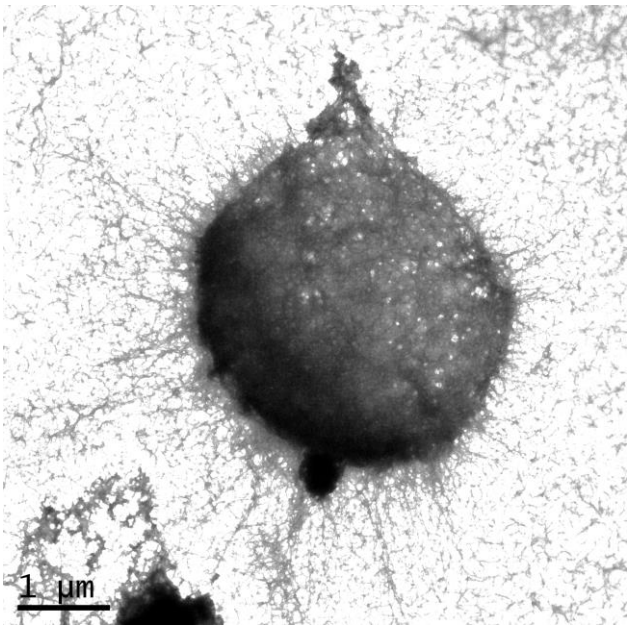

Figure 3.6 – Electron micrograph of a Z-disk showing poor lattice preservation. Specimen was stained with 1% ammonium molybdate pH 7. Data was collected on CCD (2k x 2k) on the FEI T12 TEM.

KI extraction

Flow-cell experiments where honeybee myofibrils were irrigated with 1M KI showed that extraction occurs quickly, actomyosin is dissolved and Z-disks fall flat on the glass surface. In such preparations the Z-disks appeared to be linked by some sort of connecting filaments that are visible in the phase contrast microscope (**Figure 3.7**). These connections were not observed in the electron microscope, indicating that protein extraction might have been incomplete in the flow-cell experiment, possibly due to the glass surface stabilizing the myofibrils.

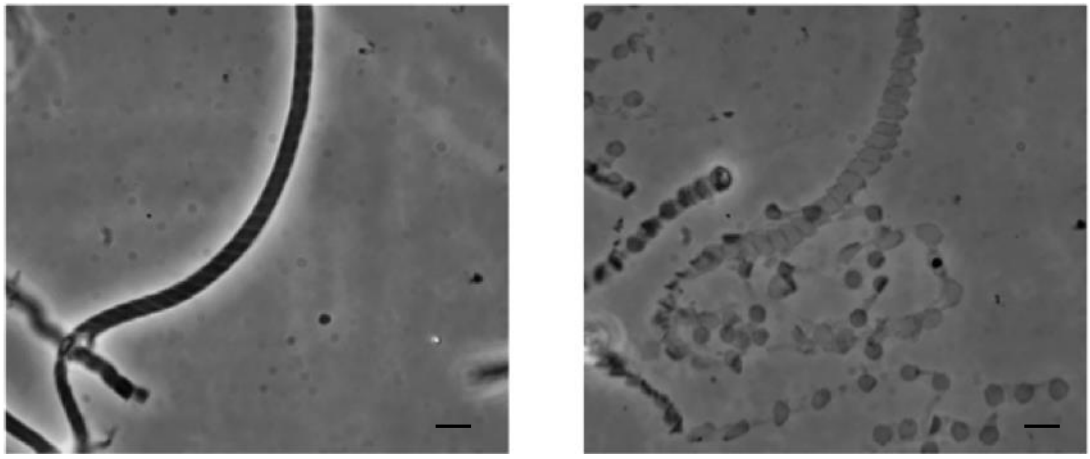

Figure 3.7 – Phase contrast micrographs of honeybee myofibrils before and after treatment with 1 M KI. Proteins in the I- and A-bands are removed, leaving Z-disks that fall flat on the glass surface. The Z-disks seem to be interconnected by filaments that resist KI solubilization (perhaps connecting filaments to thick filaments). Scale bars represent 5 μm.

Electron micrographs of negatively stained Z-disks revealed that only some of the Z-disks maintained the hexagonal lattice, whereas others appear to be degraded and do not show a regular lattice, possibly due to over-extraction (**Figure 3.8**). The ratio of well-preserved Z-disks to over-extracted ones was 1:10, indicating that the 1M KI treatment may be too harsh. Such preparations were not considered suitable for structural studies.

KCl+KI extraction

Z-disks isolated using the KCl-KI extraction buffer (0.7 M KCl, 0.6 M KI, 80 mM $NaHCO_3$ pH 8) were purified on discontinuous sucrose and iodixanol gradients. The removal of the density media used for purification, as well as decreasing salt concentration, were thought important for successful preparation of grids for cryo-electron microscopy, as high salt and the presence of sucrose or iodixanol might interfere with formation of thin vitreous ice layers and/or decrease contrast.

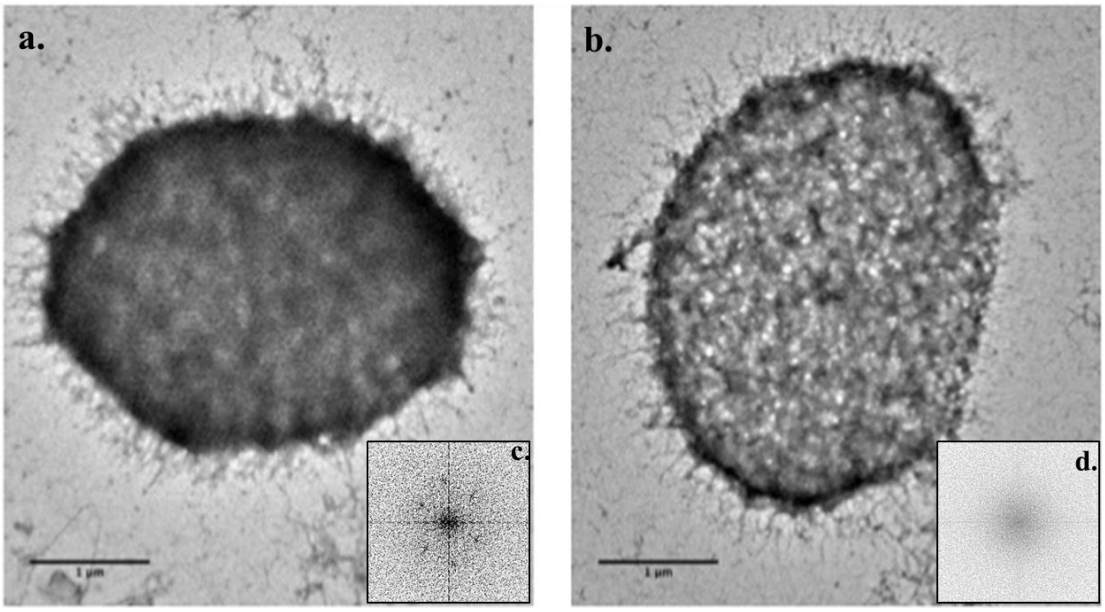

Figure 3.8 – Electron micrographs of KI extracted Z-disks and their Fourier Transforms. **a.** The Z-disk shows the honeycomb appearance that indicates a well preserved lattice, diffraction sport can be observed in the FT (b) **b.** Over-extracted and degraded Z-disk that has lost lattice regularities. The FT shows no diffraction spots (d). Specimen was stained with 1% ammonium molybdate pH 7. Data was collected on CCD (2k x 2k) on the FEI T12 TEM.

Fractions were collected and inspected in the phase contrast microscope; the ones that contained isolated Z-disks were dialysed overnight against a physiological buffer. Samples collected after dialysis did not contain any protein, as revealed by SDS-PAGE. The dialyzer membrane was cut and boiled in sample buffer for 10 minutes. Gel electrophoresis revealed that proteins were associated with the dialyzer membrane, indicating that the Z-disks adhere to it (**Figure 3.9**). Several dialysis membranes were tested including: Spectra/Por (Spectrum Labs), SnakeSkin (Pierce), SlideALyzer (Pierce) and Micro DispoDialyzers (Harvard Apparatus), but the Z-disks continued to adhere to the tubing.

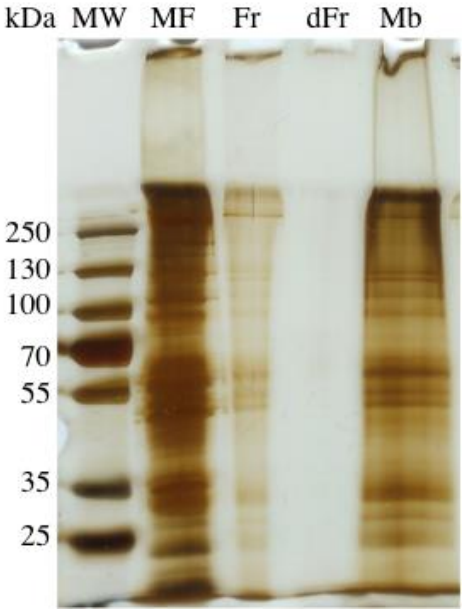

Figure 3.9 – During the post-purification dialysis isolated Z-disks adhere to the dialyzer membrane. A silver stained SDS gel is shown. MF represents myofibrils, Fr the fraction containing Z-disks collected from the sucrose gradient, dFr the sample after overnight dialysis and Mb the dialyzer membrane.

In electron micrographs negatively stained Z-disks showed remarkable preservation of the lattice, as compared to the lactic acid extracted ones. The best pictures were obtained when the stain (1 % ammonium molybdate) droplet was blotted slowly from the grid, allowing the heavy metal solution to penetrate the lattice. The specimens appear very dark in the field of view of the microscope and lattice features are not readily visible when observing the Z-disk on the fluorescent screen. Lattice regularities become evident when the data is visualised on the CCD, with the specimen covering the camera entirely (**Figure 3.10 a**). The FTs are also considerably richer than what was previously shown for lactic acid and KI extracted Z-disks. The power spectrum of our preparations reveals 3 orders of diffraction with the furthest reflections extending to 16.6 nm in real space (**Figure 3.10 b**).

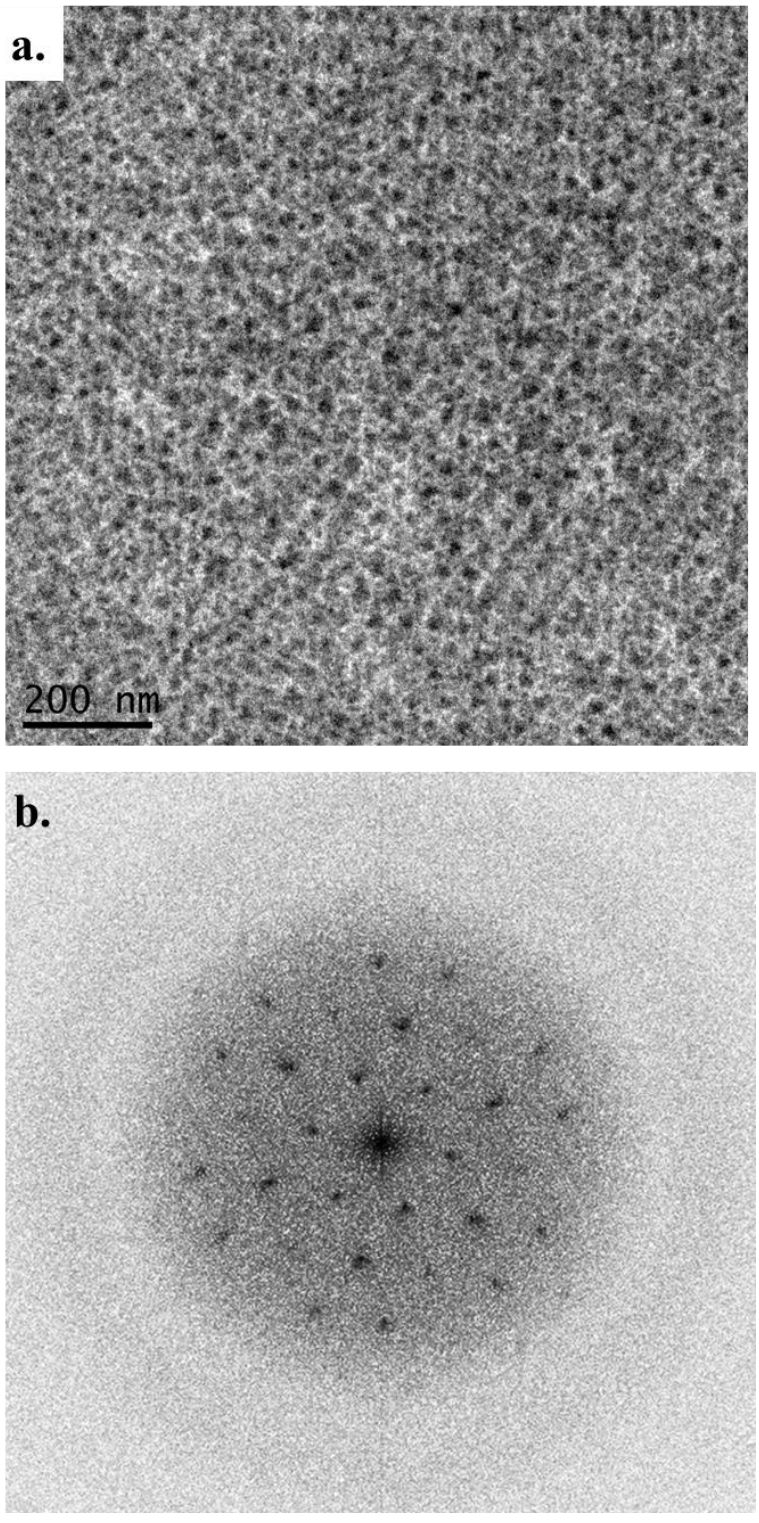

Figure 3.10 – Electron micrograph showing the central region of an isolated stained Z-disk and its FT. The FT (b) of the Z-disk (a) shows 3 orders of diffraction. The furthest reflection extends 16.6 nm in real space. Specimen was stained with 1 % ammonium molybdate pH 7. Data was recorded on CCD (2k x 2k) on the FEI T12 TEM.

Negative staining of macromolecular complexes is a powerful tool in determining three-dimensional structures of such specimens. Stain distribution and depth are important factors that contribute greatly to the final result. For example if the stain is extremely shallow it will not reveal the full structure of a thick, complex specimen such as the Z-disc (Saide and Ullrick 1974; Burgess et al. 2004b; Sainsbury and Bullard 1980; Saide et al. 1989).

In our preparations the stain distribution was not uniform within the same Z-disk (**Figure 3.11 a and b**). Uneven stain distribution affected all of the observed Z-disks. Occasionally (2-3 Z-disks/grid) extreme cases of stain accumulation were observed, such as the Z-disks having a patchy appearance as shown in **Figure 3.11 c**. The depth of the stain can also vary greatly within the specimen (**Figure 3.11 d**). These staining artifacts would also likely cause problems during tilt series tomogram reconstruction and sub-tomogram averaging.

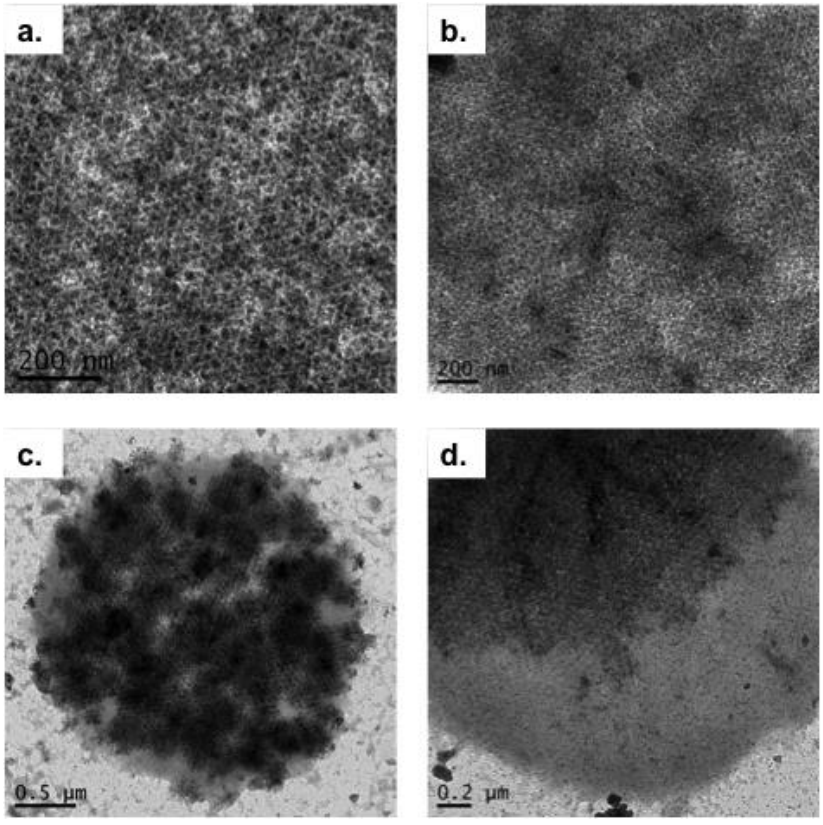

Figure 3.11 – Staining of high salt extracted Z-disks can give rise to artifacts. Stain is not evenly distributed within the specimen (a and b), accumulation of stain in pockets leads to a patchy appearance (c), the stain depth varies greatly within the same Z-disk. Specimens were stained using 1 % ammonium molybdate pH 7. Data was recorded on CCD (2k x 2k) on the FEI T12 TEM.

3.3.3 Cryo-electron microscopy of isolated Z-disks

Micrographs described in this thesis are the first cryo-electron microscopy images of unstained isolated Z-disks. Investigation and optimization of blotting conditions which yielded grids with suitable ice thickness took approximately 6 months. The dose tolerance of ice-embedded Z-disks was determined by repeatedly imaging a Z-disk until bubbles started appearing. After alignment of the microscope the beam intensity and electron dose were calibrated so that images were taken iteratively with the Record parameter set on 1 $e^-/Å^2s^{-1}$. **Figure 3.12 a** shows the Z-disk after 6 images were recorded, no radiation damage can be observed by naked eye. The samples usually start bubbling over areas where carbon is present; this is shown in **Figure 3.12 b**, where the arrow indicates bubbles appearing after 55 $e^-/Å^2$. At 70 $e^-/Å^2$, bubbling caused by radiation damage is clearly visible throughout the specimen, as indicated by arrows in **Figure 3.12 c**. The dose tolerance test is an important experiment that needs to be carried out and the information it provides is crucially important to be taken into consideration when micrographs are recorded. An important note to make is that we found the dose tolerance is sample dependent and variable, with some samples of frozen-hydrated Z-disks not showing bubbling even at 90-100 $e^-/Å^2$ total dose.

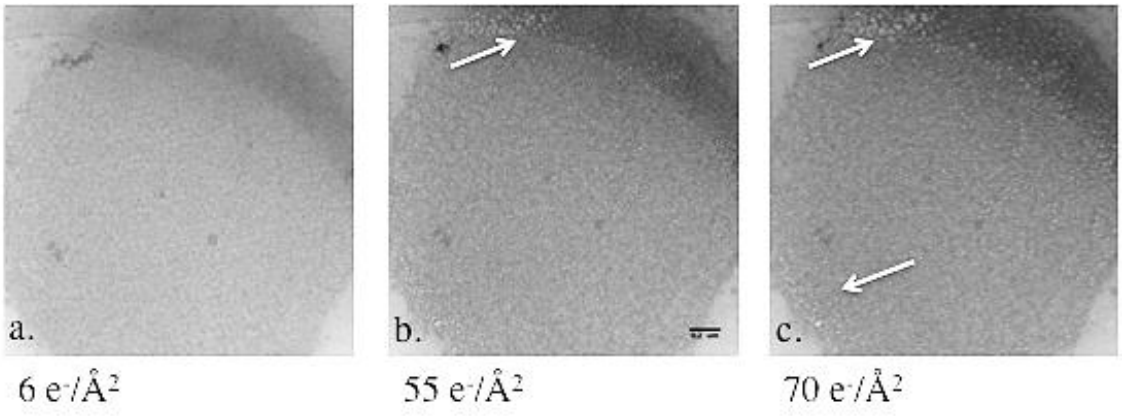

Figure 3.12 – Dose tolerance test of unstained frozen-hydrated isolated Z-disks. Bubbling caused by radiation damage appears first over area with carbon and is indicated by arrows. Data was recorded on CCD (2k x 2K) on the FEI T12 TEM operating at 120 kV. Scale bar represents 0.2 μm.

Micrographs of frozen-hydrated Z-disks showed a beautiful hexagonal lattice (**Figure 3.13 a**). The average diameter of high salt isolated Z-disks was measured to be 2.5 μm ± 0.2 μm (mean ± S.D., n = 292) with the minimum measured diameter being 1.96 μm and maximum 3.12 μm. The FT of ice embedded Z-disks reveals a rich diffraction pattern with 6 orders of reflections that extend to 252 pixels, which indicates a resolution of ~8 nm (**Figure 3.13 b**).

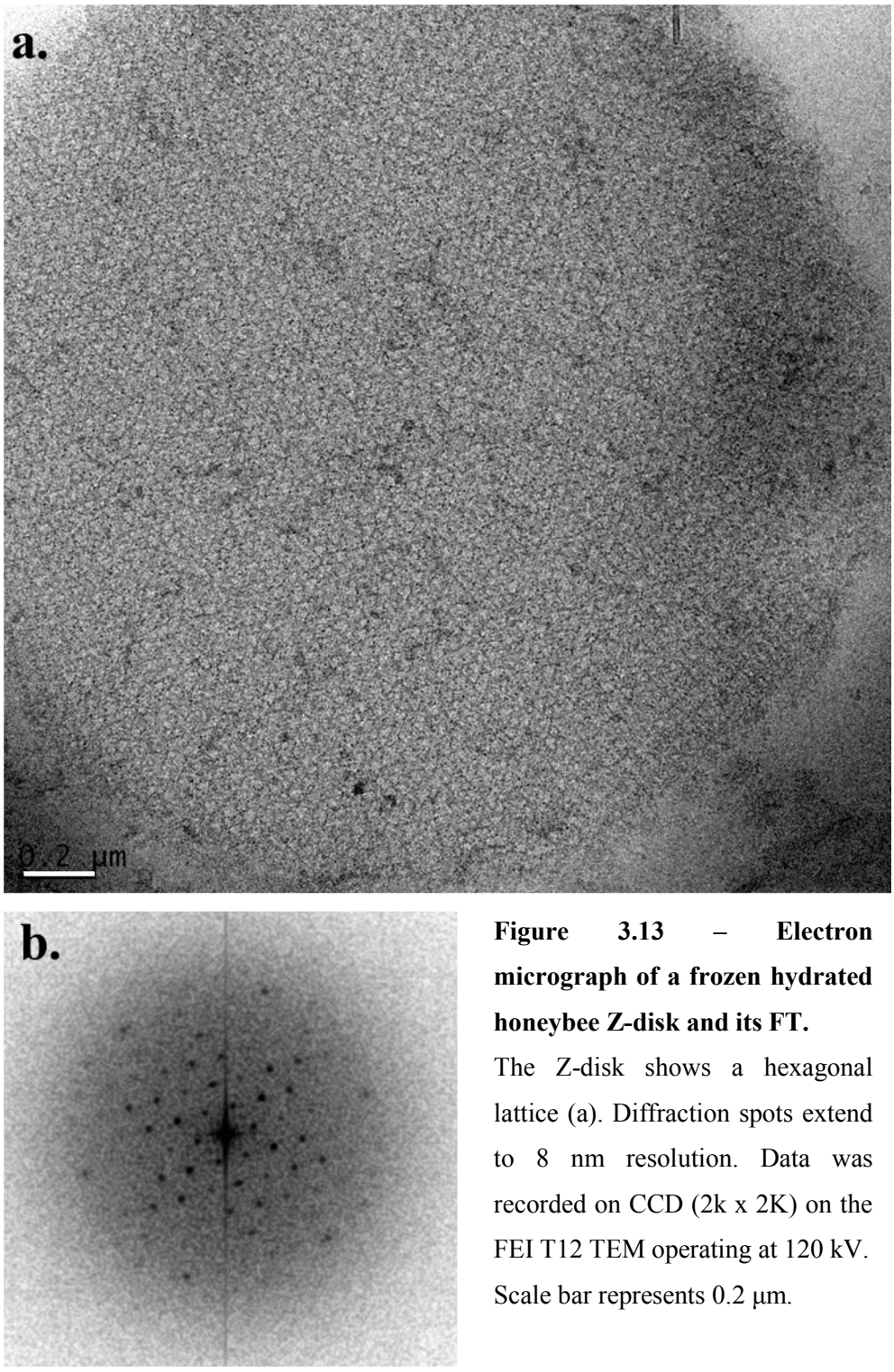

Figure 3.13 – Electron micrograph of a frozen hydrated honeybee Z-disk and its FT.
The Z-disk shows a hexagonal lattice (a). Diffraction spots extend to 8 nm resolution. Data was recorded on CCD (2k x 2K) on the FEI T12 TEM operating at 120 kV. Scale bar represents 0.2 μm.

3.3.4 2D lattice unbending

Isolated Z-disks are essentially two dimensional crystals, with diffraction spots in Fourier Transforms of vitrified Z-disks have been shown to extend to 8 nm. Ideally several images should be subjected to lattice unbending and data acquired from multiple images should be averaged to obtain projection maps that more accurately describe the Z-disk lattice. We have analysed one image of an isolated, frozen hydrated Z-disk and we present the data to demonstrate how powerful 2D lattice unbending is for structural studies of the Z-disk

Firstly the images were optically filtered to improve the quality of the image (**Figure 3.14).** By reprojecting only the information associated with the lattice periodicity the contrast was greatly enhanced and the new image was used to calculate lattice distorsions by computational correlation methods.

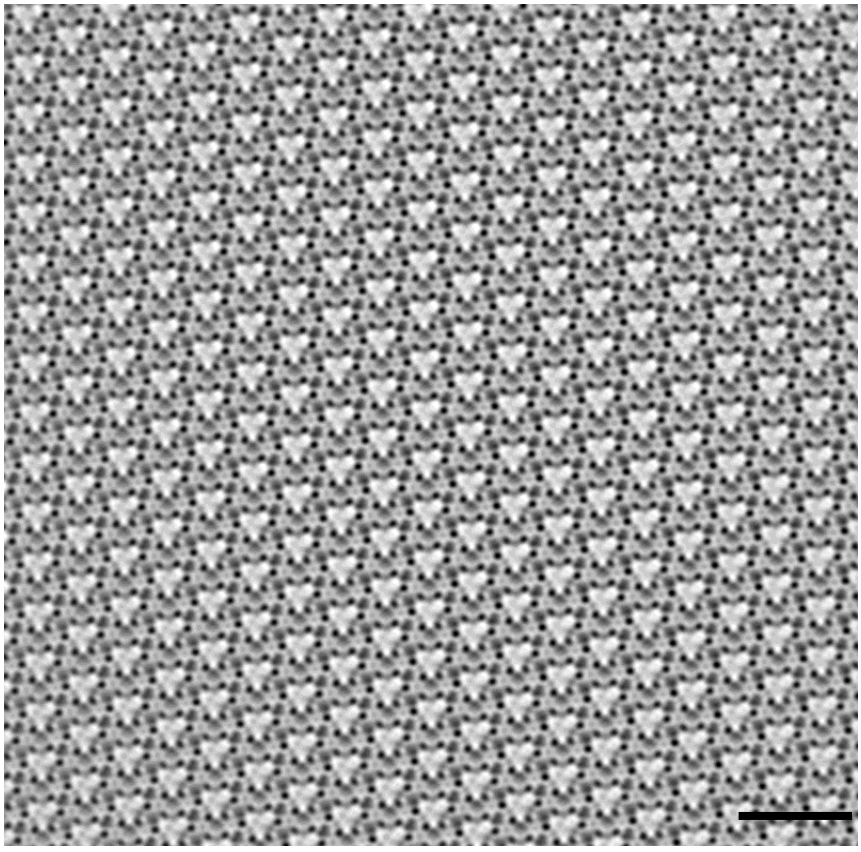

Figure 3.14 – Reprojection of the Z-disk after optical filtering. Frequencies unrelated with lattice regularities were set to zero, and the information was reprojected. Scale bar represents 0.2 μm.

The lattice vectors, showing lattice imperfections are shown in Figure **3.15 a**, while their corrected position is depicted in Figure **3.15 b**. Based on the corrected positions a new Fourier Transform was calculated (**Figure 3.16 b**). Compared with the Fourier Transform of the unbent Z-disk (**Figure 3.16 a**) the diffraction spots appear sharper, but no new, higher resolution spots were resolved.

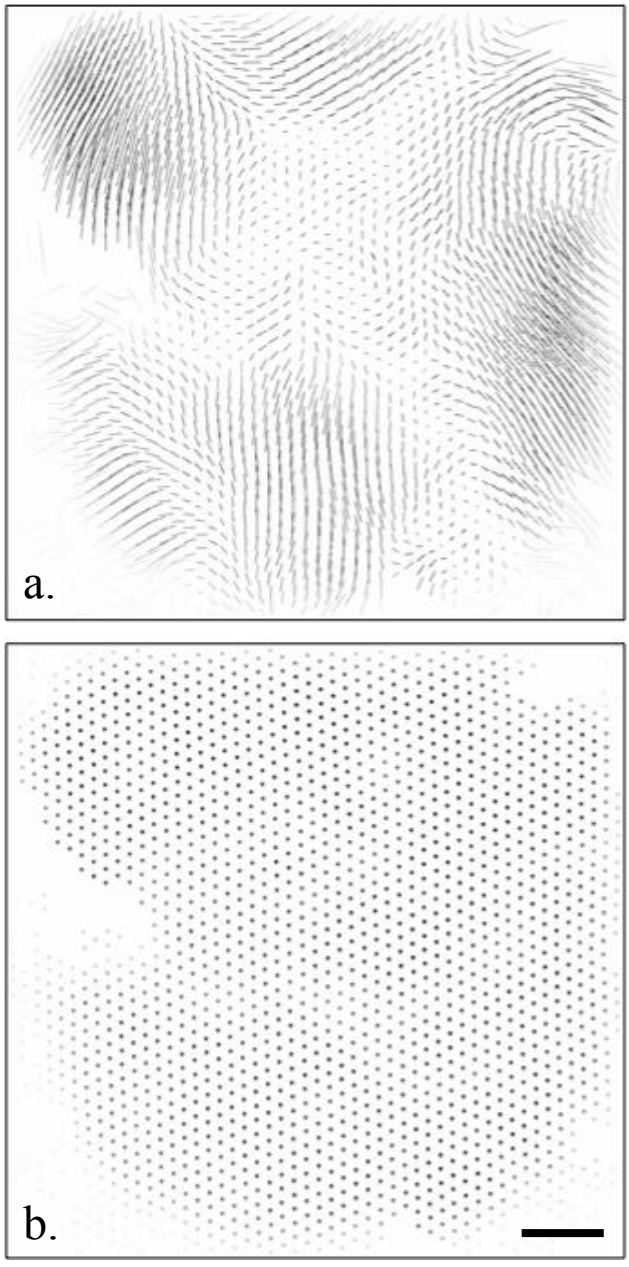

Figure 3.15 – Z-disk lattice vectors before (a) and after 2D crystal unbending (b) showing the lattice distortions (a) and their corrected position (b). Scale bar represents 0.2 μm

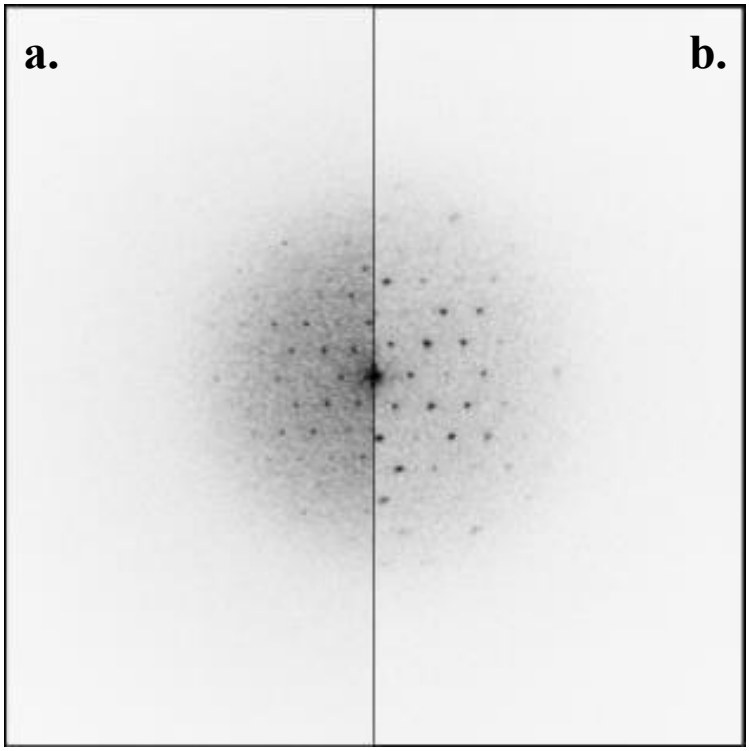

Figure 3.16 – Comparison view between the FT of an unbent Z-disk (a) and the FT after 2D crystal unbending (b).

Specific symmetry elements which are characteristic of the 17 two dimensional crystal spacegroups were tested. The results obtained from the analysis are shown in **Figure 3.17.** The conformity with applicable phase constraints is known as the phase error or phase residual. Phase errors are smallest for positions that relate the molecule by permissible symmetry operations. Analysis of our data set gave the lowest phase residuals for p3, p312 and p321 symmetry groups. The target residual is based on statistical calculations made by the software and is expressed as a percentage. A lower percentage indicates the likelihood that the symmetry elements correspond to a specific spacegroup. The lowest targets we have obtained were 25.2 % for p3, 25.7 % for p312 and 26 % for p321.

Based on the target residual a density map was projected with p3 symmetry imposed (**Figure 3.18**). In the projection map protein is represented by continuous lines. The projection map does not directly reveal three-dimensional information, thus we cannot draw conclusions regarding the arrangement of thin filaments or the positioning of cross-linking proteins. To retrieve this information we would need a three-

dimensional data set (a tilt series). **Figures 1.3** and **3.18** are not directly comparable. **Figure 1.3** represents a slice through the final three-dimensional model obtained by Deatherage et al. (1989) from tilt series; and it shows the central plane of the Z-disk. Electron micrographs are projection images and contain the information from the entire Z-disk lattice, thus the reprojected density map obtained after 2D crystal unbending does not offer accurate three-dimensional structural information. Also, ideally, the phases from more images should be aligned and averaged to obtain the density map. In **Figure 3.18** we tried to identify the potential position of the thin filaments, filaments A represent the ones that might be originating from the top sarcomere and filaments B from the bottom sarcomere. It is important to note that these observations are based on the analysis of one image and might not reflect the final result.

	SPACEGROUP	Phs.Res. (#) v.other spots (90 random)		Phs.Res. (#) v.theoretical (45 random)		OX	OY	Target
1	p1	25.2	176	18.4	176			
2	p2	54.8	88	27.4	176	-133.6	111.5	36.8
3b	p12_b	67.9	35	50.2	10	-107.4	-162.0	26.9
3a	p12_a	65.5	35	47.3	10	174.0	144.1	26.9
4b	p121_b	74.2	35	7.7	10	-138.4	-180.0	26.9
4a	p121_a	69.9	35	54.7	10	-180.0	88.8	26.9
5b	c12_b	67.9	35	50.2	10	-107.4	-162.0	26.9
5a	c12_a	65.5	35	47.3	10	174.0	144.1	26.9
6	p222	72.7	158	28.0	176	43.1	-72.1	31.7
7b	p2221b	69.5	158	27.4	176	-133.6	-68.5	31.7
7a	p2221a	66.1	158	27.9	176	43.6	-72.1	31.7
8	p22121	71.9	158	27.5	176	46.7	-68.9	31.7
9	c222	72.7	158	28.0	176	43.1	-72.1	31.7
10	p4	68.3	164	37.2	176	-102.0	137.2	31.5
11	p422	64.0	344	40.3	176	-109.9	133.9	28.2
12	p4212	69.7	344	28.0	176	44.7	-71.5	28.2
13	p3	38.2	108	--	--	45.2	-71.1	25.2
14	p312	46.1	262	7.0	20	45.7	-70.9	25.7
15	p321	36.5	269	9.6	34	44.9	-71.3	26.0
16	p6	48.1	304	27.8	176	44.8	-71.2	28.6
17	p622	45.7	619	28.0	176	45.2	-71.0	26.9

Figure 3.17 – 2dx results detailing the calculated phase errors for the 17 known symmetry groups. Lowest phase residuals and target residuals were calculated for spacegroups p3, p312 and p321.

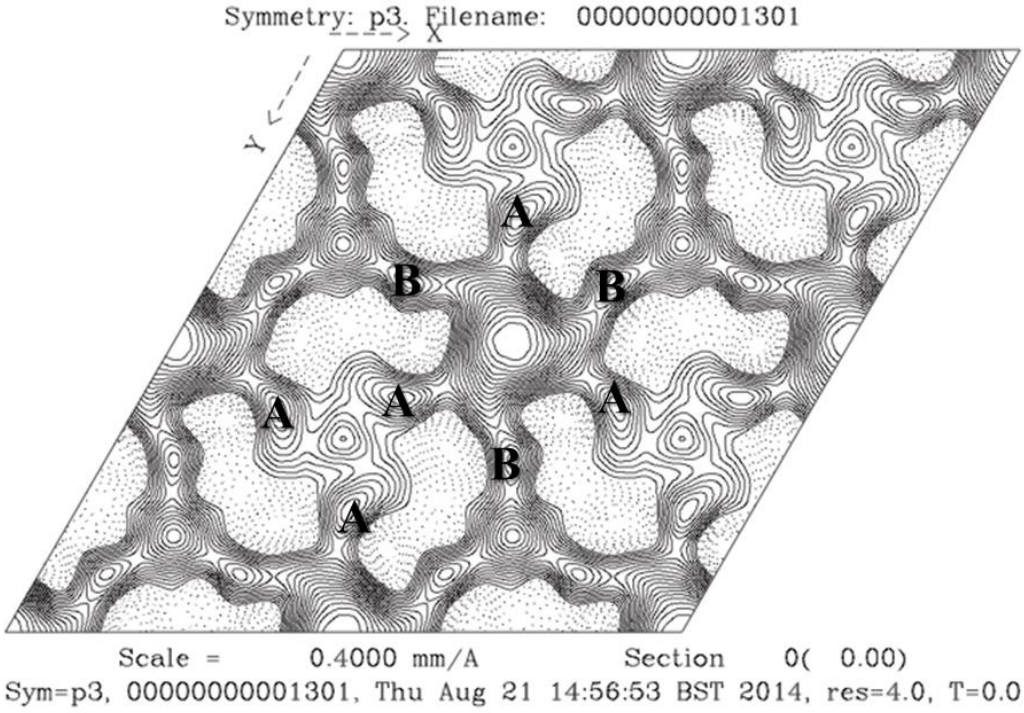

Figure 3.18 – Reprojected density map obtained after 2D lattice unbending of one isolated Z-disks. Potential thin filaments originating from the top (A) and bottom sarcomeres (B) are identified.

3.3.5 Mass spectrometry of isolated Z-disks

Z-disks were isolated using KCl+KI and purified by high-speed centrifugation (**3.2.7**) and gel electrophoresis was carried out. Excised bands from SDS-PAGE gels were sent the Cambridge Center for Proteomics (CCP) for analysis (**Figure 3.19**). Each band was digested using trypsin and analysed separately using an ESI-TRAP instrument. Peptide sequences were checked against the honeybee genome UNIPROT protein database. The results provided contained peptide sequences as well as accession codes from UNIPROT.

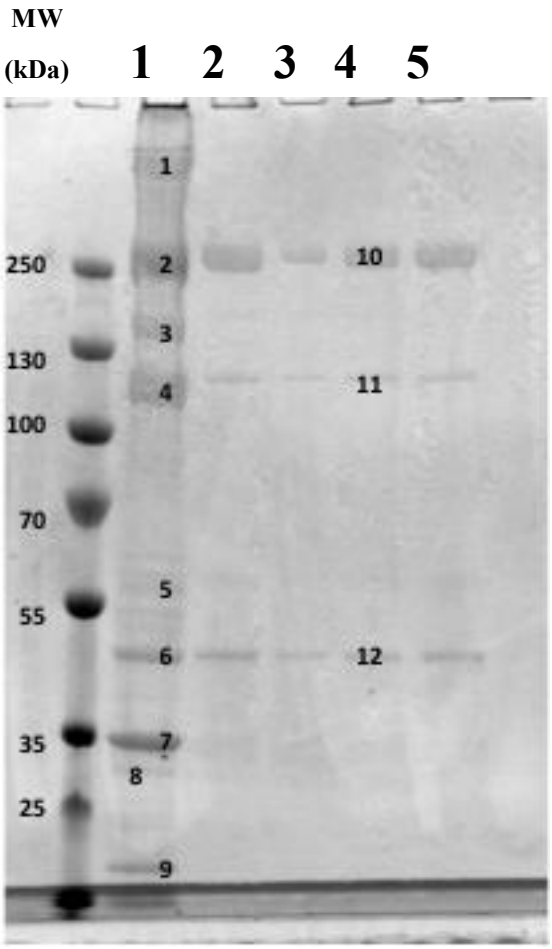

Figure 3.19 – Annotated SDS-PAGE gel sent for mass spectrometry analysis.
MW – molecular weight markers
1 – Isolated Z-disks, numbers on the gel indicate the bands excised for analysis.
2 – 5 – supernatants corresponding to the 4 washes carried out during purification by high speed centrifugation.

The results obtained from CCP, including the mass of the protein and the UNIPROT (Universal Protein Resource) accession code, as well as identified proteins are summarized in **Table 3.2**. The sequence data can be found in **Annex 1**. Sequences were also submitted for BLAST analysis (Basic Local Alignments Search Tool) on the NIH website (http://blast.ncbi.nlm.nih.gov).

Table 3.2 – Results of mass spectrometry analysis of isolated Z-disks.

Band No.	Protein mass (Da)	UNIPROT accession code	Identified protein or BLAST prediction, characteristics
1	1041645	H9K214	Uncharacterized protein from the Ig superfamily of proteins.
	1962476	H9KC31	
	849830	H9KD10	
2	264356	H9KU31	Myosin heavy chain.
	253106	H9KU35	Myosin heavy chain.
	175656	H9K4A8	Myosin heavy chain.
3	165578	H9KA35	Tripeptydyl peptidase II.
4	102051	H9KTR7	Paramyosin.
	102532	H9K1K1	α-actinin
5	55096	H9K918	ATP synthase subunit beta.
	59760	H9KC11	ATP synthase subunit alpha.
	49107	Q3B712	Troponin T.
6	42157	H9KNB7	Actin.
	42201	H9K667	Actin.
	42121	H9KKW7	Arp1 (actin related protein 1).
	38975	H9KTD0	Zasp 66 (PDZ and LIM domain protein 3).
	49647	H9K2W8	NADH dehydrogenase (ubiquinone) alpha subcomplex subunit 10.
7	32263	H9K538	Uncharacterized protein encoded by gene Mf (Myofilin).
	30634	H944R2	Porin.
	33193	Q6VQ13	ATP/ADP translocase.
	32977	H9KDY8	ATP synthase gamma chain.
8	21297	H9KF77	Heat shock protein β1.
	30753	H9KE53	Ubiquinone protein 3.
9	19822	H9KPG4	Ubiquinone subunit 10.
	21799	H9K1P1	Ubiquinone protein 4.

Band 1 comprised successful hits for 3 giant proteins; all of them uncharacterized in the honeybee genome, but containing Ig domains. Presumably these could be either kettin or projectin. To obtain better separation of high molecular weight components of isolated Z-disks gels containing lower acrylamide concentration should be used. Peptides obtained from band 2 were identified as part of the myosin heavy chain. Band 3 contained tripeptydyl peptidase II, but also fragments from myosin heavy chain, which were likely a product of proteolysis. Band 4 contained paramyosin and α-actinin Band 5 contained peptides associated with subunits α and β of ATP synthase, but also peptides found in troponin T isoform 4. Besides actin, band 6 is likely to contain actin related protein Arp1, NADH dehydrogenase (ubiquinone) and Zasp. Band 7 contains an uncharacterized protein in the honeybee genome encoded by the gene Mf (myofilin), as well as ADP/ATP translocase and porin. Band 8 and 9 contained NADH dehydrogenase subunits.

3.4 Discussion

The objectives of the work presented in this chapter were to establish protocols for the isolation of well-preserved intact insect Z-disks with the aim of carrying out cryo-electron microscopy. We have successfully isolated Z-disks from honeybee flight muscle using a variety of conditions ranging from dilute acids (lactic acid) to high salt solutions. As first shown by Saide and Ullrick (1974) the hexagonal lattice of lactic acid isolated Z-disks is retained, which is remarkable taking into consideration the very low pH (~ 3) of the extraction. Diffraction spots corresponding to 40 nm resolution were observed in lactic acid extracted Z-disks, this resolution being too low for high resolution studies. Z-disks tend to swell in these conditions and we report the average diameter of 3.79 ± 0.52 μm (mean ± S.D., n = 25). We have also shown that some Z-disks are severely damaged by the lactic acid and swell up to 6-7 μm, while losing the regularity of the lattice, which makes them unsuitable for structural studies. We have shown that lattice changes that occur during extraction are at least partially reversible by dialysing the Z-disks against a physiological buffer. Because of low recovery rates after dialysis and the presence of damaged Z-disks in a ratio of 3:1 to well preserved Z-

disks we sought to move away from these very harsh conditions by extracting Z-disks using high ionic strength buffers.

We found that the extraction buffer containing 0.7 M KCl, 0.6 M KI and 80 mM $NaHCO_3$ pH 8 causes the release of better preserved Z-disks, as compared to the lactic acid extracted Z-disks. Compared with previous work the resolution in negative stain has improved 2.5 times, the diffraction spots in Fourier Transforms extending to a resolution of 16 nm.

Isolated Z-disks were subjected for the first time to cryo-electron microscopy investigations. The frozen-hydrated Z-disks show a remarkably well preserved hexagonal lattice. The Fourier Transforms are richer, showing 6 orders of diffraction, with spots extending to 8 nm resolution. Such a high degree of structure preservation has not been demonstrated in a chemically isolated Z-disk, under room temperature or cryo conditions. The KCl/KI extraction buffer that we have used does not seem to have a significant impact on the diameter of the Z-disk. The average diameter was measured to be 2.5 ± 0.2 μm (mean ± S.D., n = 292), which is comparable with the diameter reported in muscle fibers (Cheng and Deatherage 1989).

Isolated Z-disks can be considered imperfect two-dimensional crystals, which can be affected by lattice distortions. Two-dimensional lattice unbending of vitrified Z-disks was carried out. This allowed the correction of lattice irregularities and the sharpening of diffractions spots in the Fourier Transform. The presence of specific symmetry elements was tested and, based on the analysis of a single Z-disk, we have determined that the symmetry is likely to be either p3, p312 or p321, in accordance with the data published by Cheng and Deatherage et.al (1989). In the available model the symmetry of the Z-disk was shown to be p312. Nevertheless the conclusions regarding the symmetry are preliminary, as a bigger data set is needed for averaging. We believe that 2D lattice unbending is very informative and, once a sufficient number of Z-disks are analysed, the symmetry data could be used for tomography and sub-tomogram averaging. It is interesting to note that Holmes et al. (1980) reported that the symmetry of myofilaments of the giant water bug (*Lethocerus cordofanus*) was p6, based on X-ray fiber diffraction. However, this is not comparable with the bee data quoted here, as it was from the whole muscle and a different insect species.

We sought to study the protein composition of our preparation, to monitor proteins lost during extraction. This was done by mass spectrometry of excised protein bands from SDS-PAGE gels. Attempts have been made to purify the Z-disks using a

combination of several continuous and discontinuous density gradients of different density media, followed by the removal of the density media by dialysis. Progress has been made towards obtaining a fraction containing isolated Z-disks, but this has proved somewhat difficult due to the tendency of the Z-disks to adhere onto tube walls and dialysis tubing. Mass spectrometry analysis of excised bands from 1D SDS-PAGE gels revealed that not only Z-disk components such as actin, α-actinin, Zasp are present in our preparations, but also a considerable number of contaminants associated with ribosomes and cellular organelles, such as mitochondria (indicated by the presence of ATPase and cytochrome c). Contaminants from other sarcomeric regions have been observed, troponin, tropomyosin and myosin are present in our preparation. It is disappointing that the myosin concentration is very high in the isolated Z-disk preparation, even though it is not a component of the Z-line. Similar studies regarding the composition of isolated Z-disks also show myosin as a contaminant of the preparation (Saide and Ullrick 1974; Bullard et. al 1989). The presence of myosin might prove somewhat detrimental for electron tomography, as it might increase the noise in the micrographs. However, post-processing in the form of subtomogram averaging will enable noise reduction, at least to some extent. Even though purity is not essential for successful data collection in the electron microscope for the study of protein component further optimization of Z-disk purification protocols is necessary. Proteins that might be present in lower concentrations have not been identified due to the low sensitivity of Coomassie Blue Staining. We consider that mass spectrometry is the best and obvious step for analyzing the proteome of isolated Z-disks, but further experiments need to be pursued to successfully purify isolated Z-disks.

The resolution of 1D SDS-PAGE gels is unsatisfactory, as bands contained several different proteins that had a similar molecular mass. Whole suspensions of Z-disk could be sequenced by mass spectrometry, but this might prove challenging in identifying components that are present in the lattice in low concentrations as the signal might be masked by the peptides found in higher concentration. In my opinion a better approach would be 2D gel electrophoresis coupled with sequence analysis using mass spectrometry. This would allow for the proteins to be firstly separated by Isoelectric Focusing (IEF) based on their isolectric point, followed by separation according to their molecular weight.

4. Electron tomography of isolated honeybee Z-disks

4.1 Introduction

As a technique, cryo-electron tomography delivers relatively low resolution (~ 5 nm) three-dimensional structures of pleomorphic samples. Resolution is primarily limited by radiation damage, because the same region is imaged ~ 100 times. The technique is particularly powerful when studying specimens in which many copies of the same structure are present, which enables subtomogram averaging, which improves SNR and resolution. Approximately 2 nm resolution is an important goal to allow accurate docking of known protein crystal structures in EM density maps, thus allowing for *in situ* structural biology to provide information regarding the 3D architecture of macromolecules in their cellular context. Theoretically, subtomogram averaging can be used to observe protein secondary structure. To date the best resolution achieved by cryo-ET combined with subtomogram averaging is 0.85 nm of Mason-Pfizer monkey virus Gag protein (Schur et al. 2013).

Muscle has been studied in the past by room temperature electron tomography of plastic sections. Even though the resolution is limited by embedding and sectioning, ET and subtomogram averaging have generated valuable information regarding muscle structure. For example it has lead to a characterization of myosin cross-bridges in the A-band of actively contracting insect flight muscle. In the study tomograms were generated from dual-axis tilt series of longitudinally sectioned muscles which were prepared by rapid freezing and freeze substitution. Subvolumes, consisting of repeats spaced axially at 38.7 nm and centered on the thin filament, were used to generate a global average of the structure. The global average was used further as a reference for multivariate data analysis (MDA), which was used to sort the highly heterogeneous cross-bridges into class averages. MDA employs Boolean masks to define a set of voxels in the tomogram in which patterns of density can be identified. In this particular

study subtomogram averaging and subsequent MDA improved resolution to ~ 5.5 nm from the 13 nm, the resolution of previous work. This allowed the authors to dock crystal structures of myosin in the EM density map and to identify novel interactions between actin and myosin. Based on the fitting of the crystallography data the study identified force producing and weak binding cross-bridges (Wu et al. 2012).

Another example of how electron tomography and subtomogram averaging can improve the understanding of muscle structure comes from a study focusing on myosin binding protein C (C-protein). Tomograms were generated from sections of skeletal muscle that was rapidly frozen. The unit used for subvolume averaging was the thick filament from half a sarcomere. In the final reconstruction of the thick filament density corresponding to C-protein was resolved. The results of this study showed that C protein bridges myosin filaments and thin filaments, thus answering a fundamental question concerning the *in situ* distribution of myosin binding protein C (Luther et al. 2011).

Sections through the Z-disk have also been investigated using electron tomography, albeit the data was not processed by modern subtomographic averaging techniques. Nonetheless such studies provide valuable insight into the geometry of the Z-disk. The reconstruction of a simple Z-line which resulted from dual-axis tomography revealed 2 sets of connections between interdigitating actin filaments, which are likely to contain α-actinin, but also protein density connecting filaments of the same polarity was observed (Luther 1991). Electron tomography of sectioned muscle allowed the study of Z-links, which contain α-actinin, and their relationship to the architecture and thickness of the structure. Fast muscle Z-disks, which are narrow, have 2-3 sets of Z-links, whereas skeletal muscle such as sartorius has 4 Z-links and slow muscle has 6 layers of Z-links. In nemaline myopathy the Z-disk is thickened and it consists of 7 layers of Z-connections. These reconstructions also provide insight into the flexibility of α-actinin, which was shown in nemaline rods to run axially parallel to the thin filaments before connecting the interdigitating actin filaments (Morris et al. 1990; Luther and Barry 2002).

Our aim was to investigate isolated Z-disks using cryo-electron tomography and to employ modern subtomographic averaging techniques to extract information, ideally to 2 nm resolution, allowing us to accurately dock crystal structures of Z-disk proteins into the EM density map. This in turn would provide a more accurate description of the Z-disk interactome. Even though the geometries of vertebrate and invertebrate Z-disks

and their differences and the transition of vertebrate muscle Z-disks from one lattice aspect to another are beginning to be understood, currently a detailed 3D model is not available from either type of muscle.

4.2 Methods

Negatively stained and cryo-electron microscopy grids were prepared as described previously, see **3.5.1** and **3.5.2**. At Leeds University data was collected by the author using the FEI Tecnai G2 Spirit (referred to as the T12) and the FEI Tecnai G2 F20 transmission electron microscopes. The microscopes are equipped with 2k x 2k and 4k x 4k Gatan CCD cameras, respectively. Electron tomography of stained Z-disks was carried out using a single tilt holder in the T12 electron microscope. Automated tilt series collection was carried out using SerialEM (Mastronarde 2005). For cryo-electron tomography a Gatan 626 cryoholder was used in the F20 electron microscope. For data collection the FEI proprietary software, Xplore 3D, was utilized. We also had the opportunity to visit the Medical Research Council's Laboratory for Molecular Biology (LMB) in Cambridge. With the kind help of Dr. Sonja Welsch (FEI), Dr. Sacha de Carlo, Dr. Shaoxia Chen and Dr. Greg McMullan (MRC LMB) tilt series of frozen hydrated isolated Z-disks were collected on an FEI Titan Krios microscope equipped with an FEI Falcon II Direct Electron Detector.

Tilt series alignment and tomogram reconstruction of negatively stained specimens with 1 % phosphotungstic acid pH 2.5 were carried out by the author using IMOD (Kremer et al. 1996; Mastronarde 1997). The LMB datasets acquired in cryo-conditions were reconstructed by Dr. Kenneth Taylor (Florida State University) using Protomo software (**4.2.2**) (Winkler and Taylor 1999; Winkler and Taylor 2006).

4.2.1 Microscope alignment and tilt series acquisition

The proper alignment of the electron microscope greatly influences the quality of the final image. Making sure the TEM is well aligned becomes a priority during data collection especially under low dose conditions, when one might get only one chance to record the micrograph. The specimen height was made eucentric, meaning that lateral movement of the image was minimal during tilting. The beam tilt pivot points were also

aligned to obtain pure tilts; this ensures the beam does not tilt when it is shifted and that it does not shift when it is tilted. The rotation center was adjusted to make sure the beam passes through the center of the objective lens (Sun and Li 2010). The alignments carried out ensure that movements during tilting are minimized. This is very important as it prevents the loss of information, as only the area of the specimen that is present in each micrograph can be subsequently utilized for reconstruction. Tilt series acquisition was carried out using automated software: SerialEM and Xplore 3D.

Tilt series of stained Z-disks were acquired using SerialEM employing a linear acquisition scheme, at 2° and 1° increments, most often over a tilt range of ± 55°. The software uses a prediction method to accurately assess the position of the specimen for each tilt. Once two images were acquired they can be used to predict the position of the specimen in the third image. The accuracy is assessed in the fourth image and if the reliability of the prediction is good enough tracking of the position and focus is not carried out for each tilt. If the reliability is not good enough it will collect tracking images and check focus for each position. The original setup, calibrations and optimization of SerialEM on the T12 electron microscope were carried out by Dr. Kyle Dent. Prior to tilt series acquisition several calibration steps were performed. Firstly the image shift was reset, which allows for the stage to be repositioned so that the feature of interest is centered in the image. Resetting the image shift is important as during tilt-series collection the side shifts of the specimen are compensated by image shifts. Secondly the tilt backlash, the changes in CompuStage position when the tilt direction is switched, was determined and is important for maintaining the position of the specimen. The coarse eucentricity was determined manually, but for low-dose tilt series acquisition the automated coarse eucentricity feature provided by SerialEM was preferred. During the procedure the stage was tilted to 13° starting with low tilting angles (0.6°) up to 5°. The Z-height was changed accordingly with the accuracy being 0.5-1 μm. The fine eucentricity was refined by taking 8 images between -24° and 24°. During refining SerialEM calculated the offset between the tilt axis and the optical axis and established eucentricity with an accuracy of 0.1 – 0.25 μm (Mastronarde 2005).

During cryo-electron microscopy data collection several positions on the grid and their corresponding recording parameters were defined. The grids were initially inspected at low magnification; the primary goal was to find ice of suitable thickness, while crystalline ice should be a rarity. Low magnification visualisation allowed the survey of large areas and minimized dose. Once the recording area containing a Z-disk

has been defined, the focusing area was displaced on the tilt axis by a few microns, this is needed in order to prevent radiation damage in the area of interest. Focusing can be carried out at the imaging magnification or slightly higher. Once focus has been established the image of the Record area was acquired. Typically the SerialEM setup for low-dose experiments was as follows: View (1900x, Spot size 5, dose 0.001 $e^-/Å^2$), Focus (11000x, Spot size 5, dose 3 – 3.5 $e^-/Å^2$) and Record (11000x, Spot size 5, dose 1 $e^-/Å^2$).

Tilt series of vitrified specimens were recorded under low-dose conditions using Xplore 3D. The acquisition scheme used was linear when recording on the F20 electron microscope. The Saxton scheme was preferred for data collection on the FEI Titan Krios, as suggested by Dr. Taylor. The Xplore 3D software relies on the reproducibility of CompuStage imperfections that arise during tilt series collection. This makes it possible to measure stage inaccuracies before tilting the samples and to use the data to predict image and focus shifts and to correct them automatically during tilt series collection. Robust calibrations are run once automatically by the software during the setup of Xplore 3D, while the specimen holder calibration needs to be repeated once a month (de Haas et al. 2012).

4.2.2 Tilt series alignment and tomogram reconstruction

During image acquisition the specimen will shift with each successive tilt, thus the need to align each 2D projection in a tilt series. During alignment the projections are brought to a common center of reference. Alignment can be aided by gold fiducial markers added to the specimen, as they can be tracked easily. Our specimens did not contain fiducial markers; we used alignment in Protomo (tomoalign) which based on cross-correlation to align the tilt series.

Alignment and reconstruction of cryo-EM data sets was carried out by Dr. Kenneth Taylor and Zhonjung Hu (FSU) without fiducials in Protomo. A reference image was taken in Protomo (the projection at tilt 0°) and the cross-correlation between that image and the next image of the tilt series was calculated. Translation and rotation factors were adjusted until the maximum correlation coefficient between the two images was found. The correlation coefficient represents the degree of similarity between the two projections. The newly aligned image was used as the reference for the next image in

the tilt series, and so on until all images had a common centre of reference (Winkler and Taylor 2006).

Following tilt series alignment the 3D volume, a tomogram, was generated by weighted back-projection. It is important to note that the Fourier transform of a projection represents a central section through the Fourier transform of the 3D object. Once the alignment is done the Euler angles, which describe the orientation of an object, can be calculated. Known Euler angles are used to place the Fourier transforms of the individual images in the 3D Fourier transform of the object. The inverse transform is calculated to generate a tomogram, this is known as back-projection. The weighted back projection takes into account the point spread function and allows enhancement of the high spatial frequencies (Frank 2005; Wolf et al. 2014).

4.3 Results

4.3.1 Electron tomography of phosphotungstic acid stained Z-disks

During electron tomography, at higher tilt angles the projected thickness of the specimen increases greatly, making the need of a thin specimen a crucial requirement for successful data acquisition so that post-processing might provide a high resolution structure. To determine whether or not isolated Z-disks were suitable for electron tomography preliminary analysis was carried out on negatively stained specimens. The concern was that after the isolation of the Z-disk filaments will protrude from either side of the Z-disk, as observed in earlier studies (Saide and Ullrick 1974). The protrusions might add thickness to the specimen or, alternatively, fold down during sample preparation. If this were to happen noise would be increased in the micrographs, but this can be averaged out during post-processing. Tilt series of Z-disks isolated using lactic and stained with 1 % phosphotungstic acid pH 2.5 acid were acquired using a linear acquisition scheme with a 2° tilt increment up to ± 50° tilt. Fiducial markers were not added to the preparation as we considered that the contrast provided by the stain was sufficient for the alignment in IMOD. The aligned stacks and tomogram show that the Z-disk is indeed a thin structure suitable for electro tomography. Filaments protruding from the Z-disk were not observed, indicating that either the removal of the material in the A- and I- bands was complete or that any residual filaments, at least in stained specimens, are flexible and are likely to be folded back onto the structure during

staining. Another possibility is that the thin projections were not visible due to the magnification used for the recording of the tilt series (9000x) (**Figure 4.1** and **Movie 1**).

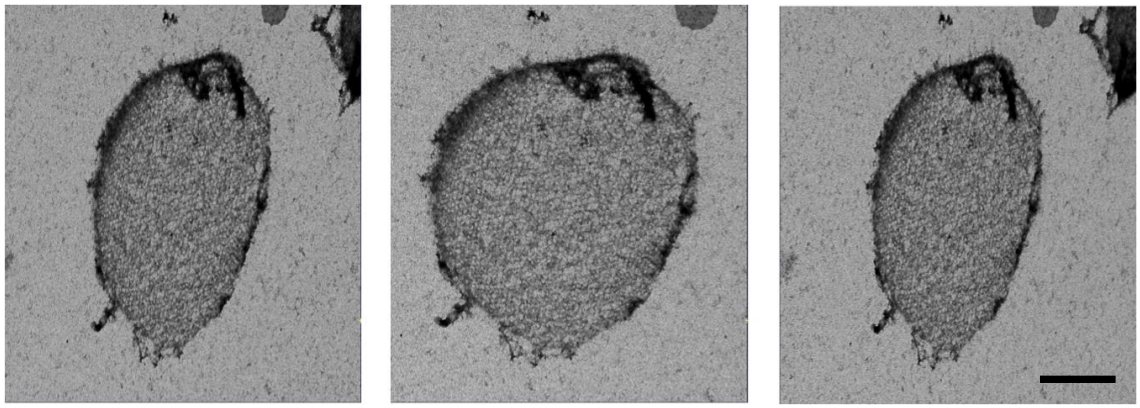

Figure 4.1 – Snapshots of lactic acid isolated Z-disks taken from the aligned tilt series at -50°, 0° and +50°. Z-disks were stained using 1 % phosphotungstic acid. Data was recorded on CCD (2k x 2k) on the FEI T12 TEM at an operating voltage of 120 kV. Scale bar represents 1 μm.

In the 3D reconstructions (**Movie 2** and **Figure 4.2**) it became apparent that the alignment accuracy of the fiduacialless protocol was limited. This was observed by inspecting transverse slices through the tomogram, where small reconstructed features present characteristic 'banana' shaped streaks. Slices through the center, the top and the bottom of the volume were chosen for inspection. In the center slice well aligned and symmetric missing wedge artifact were observed (**Figure 4.2 e**). In the bottom (**Figure 4.2 d)** and the top slices (**Figure 4.2 f**) the offset of the tilt axis was observed, translating in the appearance of the 'banana' shape artifact. We conclude that the marker-free alignment in IMOD was not satisfactory for high quality tomogram reconstruction.

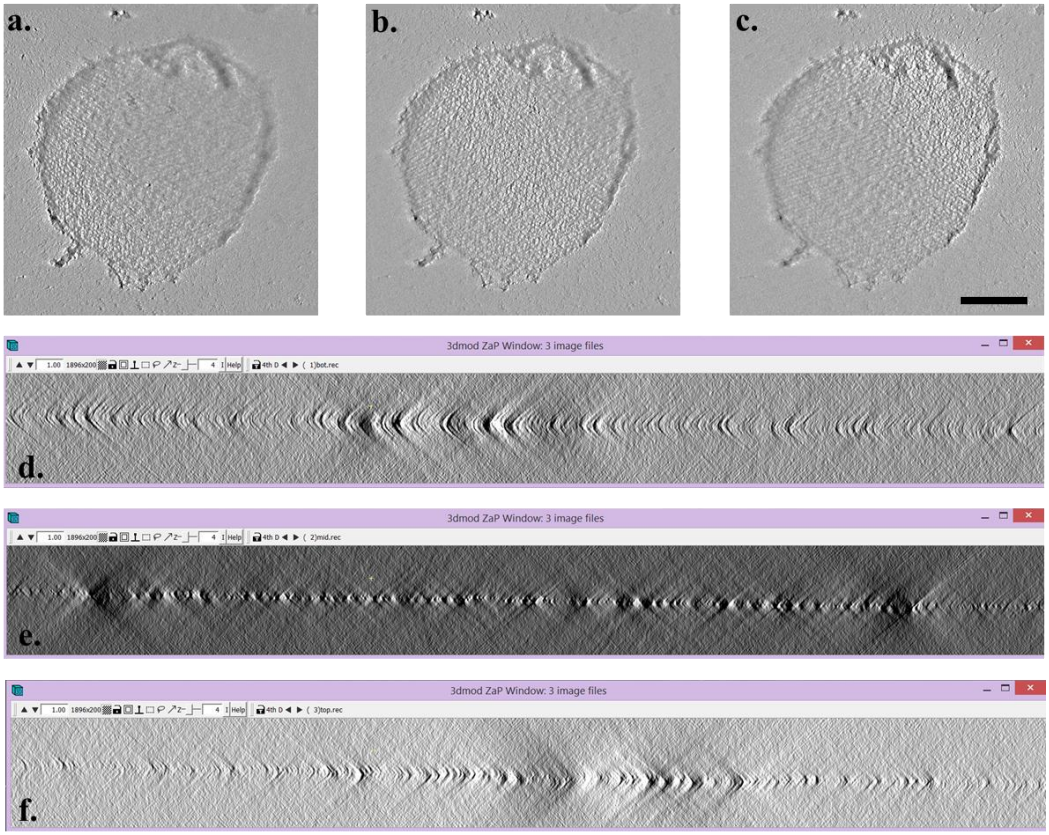

Figure 4.2 – Slices through the tomogram of a lactic acid isolated Z-disk. Transverse slices through the volume emphasize the existence of alignment artifacts, which appear as 'banana' shaped streaks.

4.3.2 Cryo-electron tomography of isolated Z-disks

Frozen specimens are essentially perfectly preserved until imaged and the main factor limiting resolution is radiation damage, which results when inelastically scattered electrons deposit energy into the sample. Radiation damage occurs immediately, even after a few electrons/Å^2, but at high doses the sample begins to bubble. The dose rate is dependent on the nature of the sample, with some specimens bubbling much faster than others, for example glycoproteins are much more sensitive to electron damage (Berriman et al. 2009). Typically biological specimens can withstand doses up to 120-150 e^-/Å^2. In the case of low-dose electron tomography this dose needs to be spread over the entire tilt series, making the SNR in individual micrographs very low (Murphy and Jensen 2007).

The total dose to which isolated Z-disks can be exposed before showing radiation damaged was determined (**Figure 3.12**). According to our data the Z-disks are prone to radiation damage at doses as low as 50 electrons/Å^2. The total dose should be distributed across the entire tilt series (140 images), leading to micrographs with very low SNR. This would not constitute a problem, since the alignment in Protomo uses information from reciprocal space to align the images. Nonetheless tilt series collection at Leeds University has proven challenging due to the microscopes being equipped with CCDs. Micrographs had to be recorded at a dose higher than ideal, which meant that radiation damage was visible half-way through data collection. The sensitivity of the CCD is considerable lower than that of a direct electron detector (Grigorieff 2013), thus we recorded data at MRC LMB Cambridge, using the FEI Titan Krios microscope operated at 300 kV and equipped with the FEI Falcon II Direct Electron Detector

Cryo-electron tilt series of ice embedded isolated Z-disks recorded at LMB Cambridge using the FEI Titan Krios electron microscope followed a Saxton acquisition scheme to ± 70° tilt. The dose was distributed throughout the tilt series with the specimen being exposed more at higher tilt angles to compensate for the increased thickness. The average electron dose per micrograph was 0.7 e^-/Å^2, making the total dose around 100 electrons. An aligned tilt series obtained from LMB data is shown in **Movie 3**. Due to low dose in each micrograph the Z-disk, little detail can be seen in the raw images, but the Fourier Transforms of the micrographs reveal diffraction spots and also the loss of regularity of the lattice (**Movie 4**).

Tomograms were generated by weighted back-projection using Promoto. An important thing to note is that during the alignment of the tilt series the last 15 images had to be discarded, as the loss of regularity within the lattice resulted in inability to align the tilt series properly. Also taking into consideration the performance of the direct electron detector we are considering lowering the dose further, to 30-40 total electron dose. As long as the FFT of individual frames shows diffraction spots, the algorithms of Protomo can align the tilt series.

During tomogram reconstruction it became clear that the honeybee Z-disk has p321 symmetry, this is in disagreement with the previous model (Deatherage et al. 1989; Cheng and Deatherage 1989). In the previous model of the honeybee Z-disk the three-fold symmetry axes were identified parallel to the axis of the myofibril, while the two-fold axes lie in the central plane of the Z-disk, perpendicular to the myofibril axis, along the diagonal of the unit cell (Deatherage et al. 1989). P321 symmetry elements are identified in **Figure 4.3a.** To decrease the effect of the missing wedge and to obtain higher resolution, p321 symmetry was imposed. P321 has three rotation centers of order three which are parallel to the myofibrils axis. The 2-fold axis lies in the plane of the Z-disks, along the unit cell edge. We report a resolution of about 8 nm of the reconstruction (**Movie 5**). The map was visualized using Chimaera. In the density map the position of the actin filament can be identified (**Figure 4.3**). Actin filaments maps were built from the PDB entry 2ZWH and fitted into the EM density. There are two groups of three actin filaments, in yellow the filaments converge in the front and extend in the back, while in the cyan group the actin filaments converge in the back and extend towards the front. **Figure 4.3 b** shows how two filaments converging (the third one is not shown).

Neighbouring yellow and cyan filaments are antiparallel and α-actinin (in red) can be identified crosslinking the two (**Figure 4.3 c**). α-actinin was modeled after the PDB entry 4D1E and fitted in the density map. However, we cannot see the convergence point and the protein connecting the actin filament trimers, the protein might have been extracted during preparation of the Z-disk. To note is that the data presented is still preliminary and might not reflect the final result. We are grateful to Dr. Kenneth Taylor and Zhonjun Hu for data processing, interpretation and **Figure 4.3**.

Subtomogram averaging

15 cryo-electron tilt series were collected at LMB. We present the first iteration of subtomogram averaging. 2200 volumes were averaged and generated 10 classes. The classes shown (**Figure 4.4**) were generated after one cycle of alignment and classification. The number of subvolumes averaged and their membership is shown in **Figure 4.5**. We observed that the averages segregate strongly by tomogram. The first 4 classes contained mostly information from tomograms 1, 2, 3 and 5; while the last 6 class averages almost exclusively from tomogram 4. To speed up the computational process the tomograms were binned by 4, making the resolution quite low, around 12

nm. The data therefore indicate that the individual Z-discs differ substantially, perhaps having responded differently to the extraction conditions used in their preparation.

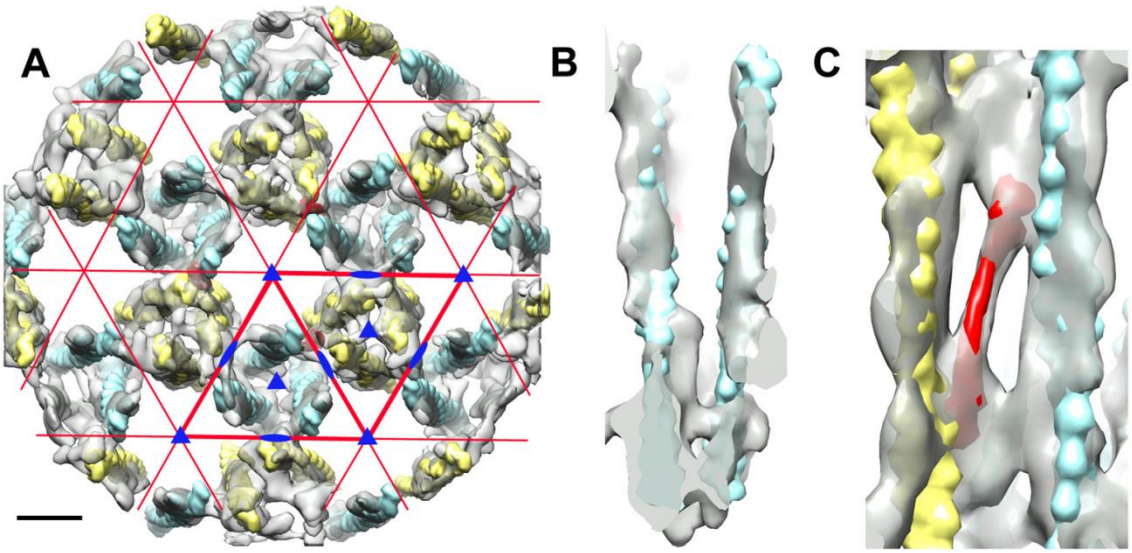

Figure 4.3 – Preliminary 3D structure of the honeybee Z-disk at a resolution of 8 nm. A. The Z-disk map with identifying p321 symmetry elements.
B. Two actin filaments converge at the bottom and extend towards the top. **C.** Crosslinking α-actinin is identified between antiparallel actin filaments. Z-disk density is gray, actin filaments are depicted in yellow and cyan, respectively. α-actinin is red. Scale bar represents 200 nm.

From the FT analysis of different Z-disks and the class averages we concluded that variation between Z-disks exists. Some of them were visibly damaged, most likely radiation damage occurring during data collection, which makes the interpretation impossible. Some Z-disks appeared to be too full, indicating that the extraction process was not complete or that extracted proteins have collapsed onto the structure, adding to its thickness and lowering the SNR to the point where interpreting the data reliably became challenging.

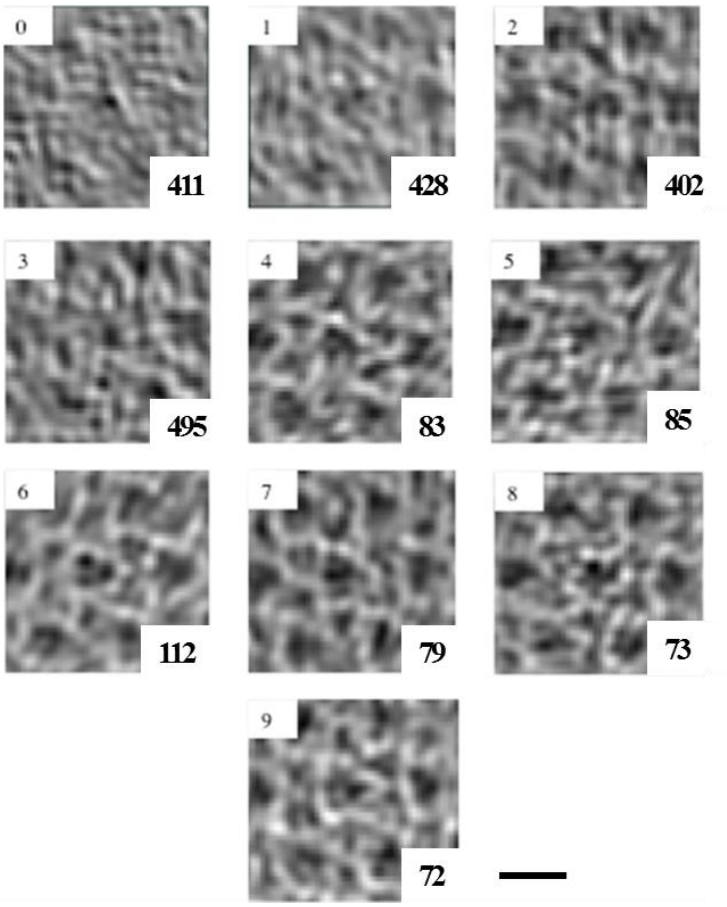

Figure 4.4 – Class averages generated by subtomogram averaging of 2200 subvolumes from cryo-electron tomogram of isolated Z-disks. Scale bar represents 500 nm.

Class		tomo1	tomo2	tomo3	tomo4	tomo5
0	010-000.mrc	3	13	5	1	389
1	010-001.mrc	103	207	93	20	5
2	010-002.mrc	26	172	178	25	1
3	010-003.mrc	39	162	273	12	9
4	010-004.mrc	0	0	0	83	0
5	010-005.mrc	0	1	5	85	0
6	010-006.mrc	0	2	0	110	0
7	010-007.mrc	5	0	0	74	0
8	010-008.mrc	0	5	0	68	0
9	010-009.mrc	2	6	7	57	0

Figure 4.5 –Class averages subvolume membership.

4.4 Discussion

The molecular organization of the Z-disk is not well known. This largely stems from the fact that plastic sectioning, which is typically required to obtain a thin specimen suitable for EM, has been shown to damage the specimen (Sader et al. 2007).

Our approach was to avoid sectioning entirely by isolating intact Z-disks from honeybee flight muscle and to perform cryo-electron tomography on the sample. We have shown that our preparation consists of separate Z-disks that are thin enough for cryo-EM. Cryo-electron tomography was carried out for the first time on isolated Z-disks. Dose tolerance tests which were carried out indicate that the Z-disk is prone to radiation damage at considerably lower doses than most biological specimens. Radiation damage in the form of bubbling of the sample appears as early as at 50 electrons/Å^2. Considering that during electron tomography the dose needs to be spread over the course of an entire tilt series we were not able to collect data on the equipment available at Leeds University, thus data was collected at LMB Cambridge on an FEI Titan Krios microscope equipped with Falcon II Direct Electron Detector. The LMB Krios facility is world-class and state of the art; however, time on it is available to external users on one day a week, which meant that only two Z-disk tomography sessions were possible before the 4 year deadline for submission of this thesis.

Based on this experience, we now know that high quality Z-disk tomograms can be recorded, but that at a total dose of ~70 e/Å^2 approximately the last quarter of the images in the tilt series show substantial radiation damage, indicated by the loss of regularity within the lattice, which can be observed in the FTs of individual micrographs. However, the data also demonstrates that images are relatively straightforward to align; suggesting that substantial reduction in dose is likely to be feasible. Future data will be recorded using a half or quarter of the previous dose (ie ~0.2-0.4 e/Å^2/image). To date, 15 tilt series of frozen-hydrated Z-disks have been acquired and tomograms generated. At the date of submission of this thesis 2200 subvolumes from one tomogram were selected and averaged to give an improved model of the honeybee Z-disk lattice.

Our data should still be considered preliminary, but based on it we concluded that the symmetry of the honeybee Z-disk is p321, in disagreement with previously published data (Deatherage et al. 1989; Cheng and Deatherage 1989). We have identified the two-fold symmetry axis along the edges of the unit cell, whereas

Deatherage et al. have identified the two-fold axis along the unit cell diagonal, which is characteristic cu p312 symmetry. In comparison with the Deatherage model, where thin filaments had no substructure and appeared as amorphous cylinders, the filaments in our model show greater detail. We have fitted F-actin models into our density and we have found groups of 3 actin parallel filaments which converge. These were also reported by Deatherage as well as a trimeric protein that crosslinks the parallel filaments. The positioning of the protein (identified as C4 in the model) is consistent with the position on the thick filaments in the A-band, thus it is hypothesized that C4 might be kettin or projectin. In out reconstruction we have not identified the protein connecting the parallel actin filaments; this might be an indication that the protein was extracted during sample preparation. For future work milder extraction conditions or lower extraction times might prove beneficial.

Antiparallel thin filaments have also been identified in our EM density map and the presence of crosslinking density was confirmed. We have modeled α-actinin based on the newly published crystal structure of the α-actinin 2 homodimer in its closed conformation (de Almeida Ribeiro et al. 2014) and fitted the model within the EM density map. The resolution is around 8 nm, but this should improve once more data is acquired and more subvolumes generated. The resolution is still relatively low, this could be due to radiation damage or to noise added by myosin and other contaminants in the sample. For tomogram reconstruction we had to discard a quarter of the images due to radiation damage, which lead to loss on lattice regularity. We have shown that sub-tomogram averaging is powerful, as protein shapes are somewhat recognizable in the tomogram. We consider that the acquisition of new data sets (with images sampling the entire tilt range) and subsequent sub-tomogram averaging might considerably improve resolution.

5. Strategies for vertebrate Z-disk isolation

5.1 Introduction

Vertebrate Z-disks have mainly been studied by electron microscopy of plastic sections, nonetheless a method for Z-disk extraction from rabbit psoas muscle was first described in 1962 by Garamvölgy and collaborators. Myofibrils were suspended in distilled water followed by Weber-Edsall solution extraction for 10-30 minutes (Garamvölgyi et al. 1962). Weber-Edsall solution is of high ionic strength containing 0.6 M KCl, 40 mM $NaHCO_3$, 10 mM Na_2CO_3 (Harsányi and Garamvölgyi 1969). Negative stain electron micrographs of the preparation reveal highly disorganized and distorted, with no longer circular Z-disks.

Much like the honeybee Z-disk, the vertebrate one is resistant to extraction using high salt buffers containing potassium iodide that remove most of the thick and thin filaments. Exposure of rabbit skeletal myofibrils to a potassium iodide solution (0.6 M KI, 0.1 M Tris-HCl, 3 mM EGTA, 3 mM $MgCl_2$, 3 mM $Na_2P_2O_7$, 0.1 mM DTT, pH 7.5) removed most of the sarcomeric proteins leaving behind a filamentous network comprising Z-disks, and thin strands, presumably titin and/or nebulin. Electron micrographs showed that remaining Z-disks were fragmented, having stellate shapes (Wang and Ramirez-Mitchell 1983).

Phase contrast microscopy of Z-disks sheets and myofibrils from chicken skeletal muscle extracted by 0.6 M KI showed that most of the A-band is extracted, but insoluble material appears to collapse onto the Z-disk. Immunofluorescence and SDS-PAGE reveals that residual myosin, tropomyosin, titin and nebulin remain associated with the Z-disk (Granger and Lazarides 1978). Such specimens are not suitable for cryo-electron tomography mainly because the collapsed insoluble proteins will make specimens thicker and can be expected to decrease the SNR in cryo-electron micrographs.

The relative ease with which skeletal myofibrils can be prepared and handled makes them an ideal specimen for Z-disk isolation. Nonetheless protein extraction experiments done so far have resulted in highly disordered and poorly preserved Z-disks that are thickened by sarcomeric proteins that collapse during extraction (e.g titin and nebulin). A key component of vertebrate sarcomeres is the giant protein nebulin (500 - 900 kDA) that is closely associated with thin filaments. Its C-terminus is an integral part of the Z-disk (Labeit et al. 2011). Our concern is that after extraction of actin, nebulin might collapse onto an isolated Z-disk, which would increase specimen thickness and add noise to images. However cardiac myofibrils express nebulin in very small amounts (Kazmierski et al. 2003). This suggests that cardiac myofibrils could be an attractive specimen for our studies. Instead of nebulin cardiac expresses a shorter protein, nebulette (107 kDa), which associates with the Z-disk (Pappas et al. 2011).

Gelsolin (84 kDa) is a member of a superfamily of proteins that are involved in actin cytoskeleton organization. Gelsolin can bind, sever and cap actin filaments. Alternative splicing of the gelsolin gene results in cytoplasmic and plasma isoforms of the protein. Gelsolin function is regulated by Ca^{2+}, intracellular pH, phosphoinositides and tyrosine phosphorylation. At a pH of 7.4 gelsolin requires 10 μM Ca^{2+} to function, but this decreases with pH to 3 μM Ca^{2+} at a pH of 6.5. At even lower pH activation can occur in the absence of calcium altogether (Silacci et al. 2004). N-terminal gelsolin fragments (FX-45) exhibit actin binding and severing properties in the absence of calcium. FX-45 was successfully used to remove actin filaments from muscle fibers while avoiding Ca-induced proteolysis (Trombitás and Granzier 1997; Granzier and Wang 1993). Upon Ca^{2+} activation gelsolin quickly binds to the actin filament and slowly severs it. After severing the protein caps the barbed end of one of the resulting shorter filaments and prevents the addition of actin monomers. The gelsolin cap is removed from the actin filament upon interaction with either phosphatidylinositol 3,4 or 4,5 bisphosphate (PiP2) (Sun et al. 1999).

In 1990 Takashi Funatsu and collaborators showed that thin filaments can be selectively removed from skeletal myofibrils by plasma gelsolin. Treatment of myofibrils with plasma gelsolin will remove thin filaments from the A- and I-band. But, critically, not from the Z-disk, as shown by fluorescence light microscopy (Funatsu et al. 1990). Similar results were observed in cardiac muscle (Funatsu et al. 1993).

Titin is the third most abundant protein in muscle, after myosin and actin. Titin is the largest protein found in nature and spans half the sarcomere, being over 1 μm long

(Tskhovrebova and Trinick 2003). This aspect is important to take into consideration when trying to isolate intact Z-disks from vertebrate muscle. The concern is that, if all other components of the sarcomere are extracted, titin will collapse onto the Z-disk adding thickness and decreasing the SNR in cryo-electron micrographs. However, if titin can be cleaved in the I-band, homogenization of relaxed myofibrils should result in separated A- and I- segements (the latter also known as I-Z-I brushes). Depolymerization of actin using gelsolin should then result in Z-disks.

Titin has been successfully cleaved in the I-band of skeletal and cardiac muscle using trypsin. A mild trypsin digestion step was used to specifically cleave titin in cardiac cells to study the contribution of titin to passive tension (Granzier and Irving 1995). Electron microscopy data of skinned frog muscle fibers suggests that trypsin selectively cleaves titin at longer sarcomere lengths (3 μm) after 4 minutes of incubation with 0.25 μg/ml trypsin in relaxing buffer. After 8 minutes the overlap between thin and thick filaments is lost completely and dislocated A-segments and I-Z-I brushes is observed (Higuchi 1992).

With the aim of isolating well preserved vertebrate Z-disks suitable for structural studies using cryo-electron tomography we employed a combination of biochemical methods to gradually disassemble the sarcomere under ionic conditions as close as possible to physiological. We have tried several approaches, initially we considered the removal of the A-band by high salt extraction, but this might not be necessary as long as thin filaments are depolymerised in the I-band and titin cleaved. Removal of actin filaments protruding from either side of the Z-disk, but without disrupting the actin network in the Z-disk can be achieved using gelsolin, an actin severing protein (Funatsu et al. 1990). At long sarcomere lengths titin is selectively cleaved close to the Z-disk by trypsin. Cleavage of titin close to the Z-disk followed by gentle homogensation may enable separation A-segments from I-Z-I brushes. Washing away the bulk part of titin would prevent it collapsing onto the Z-disk (Higuchi 1992). Even though this approach did not result in a preparation of isolated vertebrate Z-disks, overall the results look promising, with successful depolymerization of actin from the I-band and cleavage of titin being achieved.

5.2 Methods

5.2.1 Preparation of skeletal myofibrils

Myofibrils from psoas muscle were prepared according to the methods described by Knight and Trinick (1982) with a few modifications. Psoas muscles were removed from a male rabbit (2.5 kg) and teased into thin strips that were tied to wooden rods using string. The muscle was incubated overnight on ice in Ca-free Ringer solution (100 mM NaCl, 2 mM KCl, 2 mM $MgCl_2$, 6 mM potassium phosphate, 1 mM EGTA, 0.1 % glucose, pH 7.0, protease inhibitor cocktail tablets). For long term storage in a freezer at -20°C, muscle strips were incubated overnight at 0°C in a mixture containing 50% glycerol and 50% 13.3 mM potassium phosphate pH 7.0 to allow glycerol to infiltrate the muscle. Before storage, the solution was changed and muscle strips were transferred to the freezer. If the strips are stretched prior to tying them onto wooden sticks the muscle will go into rigor at longer sarcomere length; thus isolated myofibrils will also have longer sarcomeres, which favors proteolysis of I-band titin.

Separated myofibrils were prepared from the muscle strips by homogenization in rigor buffer (0.1 M KCl, 2 mM $MgCl_2$, 1 mM EGTA, 10 mM potassium phosphate pH 7.2, 0.1 % NaN_3, protease inhibitors) using either a Sorvall Omnimixer (for volumes < 1 ml) or a Polytron Homogenizer (for volumes > 2 ml). The resulting suspension contained myofibrils, mitochondria, nuclei, cellular debris and soluble proteins. The myofibrils were washed at least three times in rigor buffer by sedimentation at 2000 x g, 4°C and gentle resuspension. This step is crucial for the removal of soluble proteins and other cellular components. The quality of the preparation was monitored in the phase contrast light microscope (Knight and Trinick 1982).

If necessary the protein concentration can be estimated by spectrophotometry. An aliquot of the myofibril suspension is dissolved in warm SDS (1%). The protein concentration is calculated from the OD_{280} taking using an the extinction coefficient of 0.7 ml/mg.

5.2.2 Preparation of cardiac myofibril bundles

Cardiac myofibril bundles were prepared from rabbit and pig hearts. Fresh pig hearts were acquired from the slaughterhouse (Rowland-Agar Ltd., Ilkley). Hearts were immediately perfused through the aorta with ice cold cardioplegic solution containing

277.5 mM glucose, 30 mM KCl, 25 mM $NaHCO_3$, 34.3 mM mannitol, 2 units of heparin / ml and protease inhibitors (0.3 g/l leupeptin, 0.1 g/l pepstatin A – Sigma Aldrich). Cardioplegic solutions were used to arrest metabolic activity in the heart and to prevent cell death (Donnelly and Djuric 1991). Until dissection, which was carried out in the cold room, the heart was kept on ice in cardioplegic solution. Ventricular papillary muscles were excised and tied to wooden rods. Papillary muscle was preferred over wall muscle because the myofibrils are more likely to be parallel (Fawcett and McNutt 1969). This aspect was useful when stretching the muscle strips while immobilizing them onto the wooden rods, since for titin cleavage and actin depolymerization a longer sarcomere length is desirable (Higuchi 1992).

The muscle strips were immersed in calcium depleting solutions and incubated overnight in the cold room. Several conditions for overnight calcium depletion were explored and are summarized in **Table 5.1**. Each preparation was checked in the phase contrast microscope and electron microscope. The glycerination procedure was essentially the same as for skeletal muscle. A recent study suggested that the mechanical response is altered and the filament order begins to degrade if myofibrils are stored at -20°C, while myofibrils stored at -80°C are essentially immortal with unchanging mechanics (Perz-Edwards and Reedy 2011). Thus, cardiac muscle strips were stored at -80°C in rigor buffer (100 mM KCl, 2 mM $MgCl_2$, 1 mM EGTA, 10 mM potassium phosphate, pH 7) with 75% glycerol.

Table 5.1 – Buffers used for calcium depletion of cardiac papillary muscle strips

Buffer	Buffer composition
Ca-free Ringer buffers (adapted from Knight and Trinick 1982)	100 mM NaCl, 2 mM $MgCl_2$, 6 mM potassium phosphate pH 7, 1 mM EGTA, 0.1 % glucose, protease inhibitor cocktail tablets (Roche Diagnostics).
	100 mM NaCl, 2 mM $MgCl_2$, 6 mM potassium phosphate pH 7, 1 mM EGTA, 0.1 % glucose, 0.5 % Brij 58, protease inhibitor cocktail tablets (Roche Diagnostics).
	100 mM KCl, 2 mM $MgCl_2$, 6 mM potassium phosphate pH

	7, 1 mM EGTA, 0.1 % glucose, protease inhibitor cocktail tablets (Roche Diagnostics).
	100 mM KCl, 2 mM $MgCl_2$, 6 mM potassium phosphate pH 7, 1 mM EGTA, 0.1 % glucose, 0.5 % Brij 58, protease inhibitor cocktail tablets
	100 mM NaCl, 2 mM $MgCl_2$, 6 mM potassium phosphate pH 7, 1 mM EGTA, 0.1 % glucose, 1 % Triton X-100, protease inhibitor cocktail tablets (Roche Diagnostics).
MOPS	100 mM potassium methane sulphonate, 20 mM MOPS, 5 mM EGTA, 5 mM ATP, 6 mM $MgCl_2$, 1 mM DTT, 3% dextran T-500, protease inhibitor cocktail tablets (Roche Diagnostics) (Perz-Edwards and Reedy 2011).
TES	132 mM NaCl, 5 mM KCl, 1 mM $MgCl_2$, 7 mM glucose, 10 mM TES pH 7.1, 5 mM EGTA and 1 mg/ml leupeptin (Linke et al. 1993).

5.2.3 Myosin depolymerization using high-salt buffers

The A-band of skeletal and cardiac myofibrils can be extracted by high ionic strength buffers, in the presence of ATP or sodium pyrophosphate (Hanson and Huxley 1953). The A-band of skeletal myofibrils and cardiac bundles was extracted using the Guba-Straub solution (0.3 M KCl, 50 mM K_2HPO_4, 100 mM KH_2PO_4, 1 mM $MgCl_2$, 10 mM ATP, pH 7). The process was monitored in a phase contrast microscope in a flow cell experiment.

The most efficient way to extract myosin is in a flow-cell where the depolymerised myosin is continually washed away and the constant flow of fresh buffer will promote further myosin depolymerization. The flow-cell extraction is not a preparative method, thus myosin extraction is carried out in Eppendorf tubes. The myofibrils are spun gently (1000-2000 x g, 3-4 minutes) and the supernatant is replaced with Guba-Straub solution. The mixture is left incubating on ice for 30 minutes. To better extract myosin

the myofibrils can be centrifuged again and the Guba-Straub solution containing myosin is discarded and replaced with fresh solution. Extracted myofibrils need to be spun harder to be harvested, but pelleting and resuspending extracted myofibrils can damage their structure and protein is lost after each consecutive centrifugation step.

A new method for A-band extraction, which resembles more the environment of a flow cell, was developed. The myofibril suspension is filtered through a nitrocellulose filter with 0.45 μm pore size. For small volumes (500-1000 μl) a syringe filter (Millipore, UK) is sufficient. When working with larger volumes or very concentrated samples a Millipore filtering unit connected to a vacuum pump was used. This was to prevent the clogging of the syringe filter and to avoid overpressure. The myofibrils were immobilized on the surface of the filter where they could be washed effectively with Guba-Straub solution. The pore size of the filter is too small to allow myofibrils to go through, but it is big enough to let extracted proteins be filtered in the flow-through. Myofibrils can be bathed with various buffers or different extracting solutions and proteins that are washed away can be monitored easily by spectrophotometry and SDS-PAGE of the filtrate. For A-band extraction myofibrils were first washed on the filter with rigor buffer followed by Guba-Straub solution. Much like in a flow cell the constant supply of fresh buffer will promote myosin depolymerization. Extracted myofibrils can be recovered from the filter by washing it with rigor buffer from the opposite side.

SDS-PAGE was employed to monitor each step of the preparation. This allowed us to have a protein profile corresponding to the filter membrane and filtrate. The extraction was carried out on a Millipore syringe filter, 2 cm diameter. The starting volume of the myofibril suspension was 1 ml. 20 μl of the starting suspension were kept for SDS-PAGE. The myofibrils were washed with an additional 1 ml rigor buffer after the initial filtration. Care was taken to ensure that the filter was kept wet at all times, to avoid drying of the myofibrils. Myofibrils were washed slowly with 1 ml Guba-Straub solution without ATP, followed by 1 ml Guba-Straub with 10 mM ATP. Extracted myofibrils were recovered by washing the filter with 1 ml rigor buffer. SDS-PAGE samples of the starting suspension, the rigor filtrate, both Guba-Straub flow-through and recovered myofibrils were run on a 12% SDS-PAGE gel.

5.2.4 Expression and purification of human gelsolin (hGSN)

With the goal of using human gelsolin to remove thin filaments from both skeletal and cardiac myofibrils we expressed and purified the protein. Protein expression and purification optimization were carried out with the help of Dr. Marcin Wolny.

5.2.4.1 Expression in bacterial cells

The plasmid containing hGSN was a kind gift from Marie-France Carlier (Le Laboratoire d'Enzymologie et Biochimie Structurales – LEBS, Paris, France). Besides hGSN the plasmid contains the ampicillin resistance gene to ensure that bacteria expressing the protein of interest can be grown. 25 µl of *E.coli* competent cells (BL21 DE3, Novagen) were transformed with 1 µl hGSN plasmid. The mixture was incubated on ice for 30 minutes followed by 45 seconds at 42°C in a water bath. 250 µl Luria Broth (LB) medium (Invitrogen) were added and the cells were incubate at 37°C for 1 hour. After incubation 100 µl of bacteria were plated on LB Agar-ampicillin plates (0.1 mg/ml ampicillin) and incubated overnight at 37°C.

The following day single colonies were picked and used to inoculate 10 ml of LB-Amp precultures. The small cultures were incubated overnight in a shaking incubator at 37°C and 220 rpm. Large scale cultures for protein expression were set up by diluting 1 ml preculture/100 ml LB-Amp media. Cultures were induced with 0.7 mM IPTG (isopropyl β-D-1-thiogalactopyranoside) when the absorbance at 600 nm reached ~ 0.8 and were left shaking at 37°C, 220 rpm for 4 hours. Cells were harvested by centrifugation at 4°C and 3000 x g for 30 minutes in a Jouan GR422 centrifuge. Pellets were stored in the -80°C freezer until use.

5.2.4.2 Bacterial lysate preparation

Pellets were thawed on ice and resuspended in 3 ml lysis buffer (50 mM Tris-HCl pH 7.8, 1 mM EDTA, 100 mM NaCl, 1mM PMSF, protease inhibitor cocktail tablets (1 tablet/ 50 ml buffer – Roche Diagnostics) and 3 ml BugBuster Protein Extraction Reagent (Novagen). 25 units of benzonase per ml of BugBuster were added to the mixture. Benzonase is a nuclease that hydrolyzes nucleic acids, reducing the viscosity of the bacterial lysate. The cell suspension was incubated at room temperature on a rocking table for 20 minutes, and then centrifuged for 20 minutes at 16000 x g and 4°C

using a Beckman-Coulter ultracentrifuge (JA 25.50 rotor). The supernatant containing hGSN was collected and dialysed against 20 mM Tris-HCl pH 7.8, 1 mM EGTA, 0.01% NaN_3.

5.2.4.3 Human gelsolin purification

Throughout the purification procedure buffers were kept at ~ 4°C and fractions were stored immediately on ice to help the purified protein to maintain activity. Purification of hGSN comprised three column chromatography steps: anion exchange using DEAE Sephadex or DEAE Cellulose resins, cation exchange using SP Sepharose resin and a final polishing gel filtration step.

DEAE anion exchange purification of hGSN

- DEAE Sephadex A-50 (GE Healthcare) was suspended in binding buffer (20 mM Tris-HCl pH 7.8, 1 mM EGTA, 0.01% NaN_3) and left to swell completely for 2 hours, at 100°C, over boiling water. After swelling the ion exchanger was washed extensively on a Buchner funnel. The slurry was prepared by mixing the rinsed resin with binding buffer in a ratio of 3:1. The slurry was poured carefully in a polypropylene column (Qiagen) to prevent the introduction of air bubbles. The column was attached to a peristaltic pump and the resin was left to settle under a continuous flow of degassed binding buffer (5ml/min) until a desired 10 cm bed.
- DEAE Cellulose (Sigma-Aldrich) was regenerated from dry resin by suspending it in distilled water and was left to settle for 30 minutes. The resin was poured into a Buchner funnel, filtered and washed with 0.5 M NaCl containing 0.1 M NaOH for 10 minutes. NaOH was washed away using 0.5 M NaCl, followed by an acidic wash containing 0.1 M HCl in 0.5 M NaCl. Finally the resin was washed with MilliQ water. The column was packed in a polypropylene column (Qiagen) under gravity flow of binding buffer. The resin bed was 10 cm. The reconstituted DEAE Cellulose resin was stored in 1 M NaCl at 4°C.

The dialysed sample was applied on top of the column and the flow-through was collected. The column was washed with 2 column volumes (20 ml) of binding buffer to ensure that proteins that do not bind to the beads were washed away. Gravity flow

purification was preferred to an automated purification system (AKTA) because, due the properties of the DEAE Sephadex resin, during automated runs the column pressure was fluctuating and this leads to resin decompression and the appearance of cracks in the column. Also pumping may cause channeling in DEAE Cellulose columns, which is not desirable.

A step-wise gradient consisting of 6 washes (10 ml each) with 20 mM Tris-HCl pH 7.8, 1 mM EGTA and increasing salt concentration (50 mM NaCl → 300 mM NaCl) was used to elute the protein. The column was regenerated by washing it with a high ionic strength buffer (1 M NaCl, 20 mM Tris-HCl pH 7.8, 1 mM EGTA) followed by equilibration in binding buffer. The binding buffer was replaced with 20% degassed ethanol for long-term column storage at 4°C. The flow-through and fractions were assessed by SDS-PAGE. Fractions containing hGSN were pooled and dialysed overnight against 10 mM MES (2-(*N*-morpholino)ethanesulfonic acid) ph 6.5, 1 mM EGTA, 0.01% NaN_3.

Preceding the cation exchange column the pH of the protein was checked and if needed it was adjusted to 6.5. The 5 ml SP Sepharose column (GE Healthcare) was attached to the AKTAPrime Plus and equilibrated with the binding buffer (10 mM MES ph 6.5, 1 mM EGTA, 0.01% NaN_3). The protein was bound to the column and eluted using a continuous salt gradient (0 mM NaCl → 500 mM NaCl in binding buffer).

A final polishing size exclusion chromatography step yielded a considerably purer protein. Before applying the protein on the gel-filtration column (Superdex 200, GE Healthcare) samples were dialysed overnight against 10 mM MES ph 6.5, 1 mM EGTA, 0.01% NaN_3 and concentrated using 10 kDa MWCO Vivaspin concentrators (Sartorius) by centrifugation for 10 minutes at 4°C and 3000 x g. The proteins were eluted from the column isocratically using the SP buffer system (10 mM MES ph 6.5, 1 mM EGTA, 0.01% NaN_3), at a constant flow-rate of 1 ml/min.

5.2.5 Thin filament removal using gelsolin

The effect of hGSN on vertebrate myofibrils was studied by fluorescence microscopy. The solutions used were: EGTA-Rigor buffer (0.17 M KCl, 1 mM $MgCl_2$, 10 mM MOPS pH 7, 1 mM EGTA) and Ca-Rigor buffer (0.17 M KCl, 1 mM $MgCl_2$, 10 mM MOPS pH 7, 0.1 mM $CaCl_2$) (Funatsu et al. 1990), both containing protease inhibitor cocktail tablets (1 tablet/50 ml buffer – Roche Diagnostics). The control

consisted of myofibrils suspended in EGTA-Rigor buffer. Myofibrils were spun and were resupended in Ca-Rigor buffer and hGSN was added to a final concentration of 0.1 mg/ml. After 20 minutes incubation on ice 20 µl of each sample was placed on an isopropanol cleaned microscope coverslip (13 mm diameter). The myofibrils were left to settle for 10 minutes and then rinsed twice with PBS. Samples were fixed for 15 minutes with 1 % paraformaldehyde in PBS, followed by two PBS washes. Thin filaments were stained with a 1% FITC (Fluorescein isothyocyanate) phalloidin conjugate in PBS (Sigma-Aldrich) for 40 minutes at room temperature, in the dark. The unbound phalloidin was removed by extensive washes with PBS. The coverslips were left in the dark to dry for 5-10 minutes before mounting them on glass slides using ProLong Gold Antifade Reagent (Life Technologies). This mounting agent helped suppress photobleaching and help retain the fluorescent signal for long term storage. For data collection a Zeiss Axiovert 135 TV Fluorescence Microscope with an attached AxioCam HRC camera was used.

After incubation with gelsolin for 30 minutes rabbit psoas myofibrils were spun and the protein composition of the supernatant and pellet was analysed by SDS-PAGE.

5.2.6 Titin cleavage using trypsin

Titin cleavage experiments were carried out on suspensions of skeletal myofibrils and cardiac bundles rather than on skinned fibers. This was preferred because the thickness of skinned fibers impairs the penetration of trypsin. Also, the trypsin treatment can be halted easily by adding trypsin soybean inhibitor and gentle homogenization should promote the separation of A-segments and I-Z-I brushes.

Skeletal myofibrils stored in the freezer were dialysed overnight against rigor buffer to remove traces of glycerol. Protease inhibitors were washed away by 3 cycles of centrifugation (1000 x g, 5 minutes) followed by resuspension in rigor buffer which did not contain protease inhibitors. Trypsin digestion was carried out in relaxing buffer which contained 0.01 % trypsin (Sigma Aldrich – Type III) (w/v).

Trypsin preferentially cleaves titin in skeletal muscle at longer sarcomere lengths, leaving other sarcomeric proteins largely unaffected (Higuchi 1992). We presume that a similar situation holds true in cardiac muscle as well. The slack length of cardiac sarcomeres is 1.8-1.9 µm. In most of our preparations from stretched cardiac muscle the

myofibrils do not exhibit sarcomeres longer than slack length, which could have prevented the selective cleavage of titin by trypsin. Further digestion experiments at long sarcomere length would be desirable.

The effect of endogenous proteases on titin was also explored by incubating muscle strips in Na-Ringer with 0.5 % Brij-58, but without added protease inhibitors. Muscle was homogenized in rigor buffer without any inhibitors. To verify that titin was cleaved myofibrils were resuspended in relaxing buffer followed by homogenization. On the negatively stained electron microscopy grids of samples prepared from autodigested fibers an array of intact myofibrils with disorganized Z-bands, incomplete A-segments, myofibrils with no Z-disks were observed. Even though there are indications that endogenous proteases will cleave titin, due to the likelihood of other sarcomere components being digested, experiments where with myofibrils prepared from fibers incubated in buffers containing protease inhibitors were preferred.

Prior to trypsin treatment, cardiac myofibrillar bundles were washed four times in rigor buffer without protease inhibitors, to help ensure that trypsin activity was not hindered by residual protease inhibitors. Rigor buffer was replaced with relaxing buffer (53 mM KCl, 5.4 mM $MgCl_2$, 4.3 mM ATP, 10 mM EGTA, 20 mM PIPES pH 7.0 - (Higuchi 1992)). To the relaxed myofibrils trypsin (Sigma Aldrich – Type III) in relaxing buffer was added to a final concentration of 0.25 % (w/v). This was followed by either vigorous or gentle homogenization using a pipette with an attached gel-loading tip. Samples were incubated at room temperature. To determine the suitable incubation time, negatively stained grids were prepared from samples at several time points during the course of the trypsinisation (0, 2, 4, 8 and 15 minutes). In addition to trypsin digestion, experiments were also carried out using a trypsin substitute (TrypLE-Express – Invitrogen) used for cell culture that does not have animal origin.

A concern was that the diffusion rate of the EGTA Ringer buffers containing protease inhibitors within cardiac muscle strips is too low, thus muscle does not enter the rigor state fast enough and endogeneous proteases digest several sarcomere components. To speed up rigor development we blocked ATP production by bathing muscle strips in 100 mM NaCl, 2 mM $MgCl_2$, 6 mM potassium phosphate, 1 mM EGTA, 5 mM 2-deoxyglucose, 1 mM iodoacetic acid, 2 mM NaCN, 0.5 % Brij-58. Iodoacetate and 2-deoxyglucose inhibit glycolysis reactions, while sodium cyanide blocks the mitochondrial electron transport chain (Lancaster and Harrison 1998). After 30 minutes incubation muscle strips were rinsed with EGTA Ringer to remove the

cyanide and were homogenized using the Polytron homogenizer. Myofibrils were suspended in either rigor buffer or relaxing buffer without any protease inhibitors and 1x TrypLE-Express was added to the suspension, followed by gentle homogenization.

5.3 Results

5.3.1 Preparation of skeletal myofibrils and cardiac myofibrillar bundles

Homogenization of glycerinated psoas muscle strips yields a suspension containing mainly single myofibrils, which show clear Z-disks and H-zones, indicating that the myofibrils are not contracted. Fresh preparations of myofibrils are mostly straight (**Figure 5.1**), whereas older ones are curvy, suggesting breakdown (Knight and Trinick 1982).

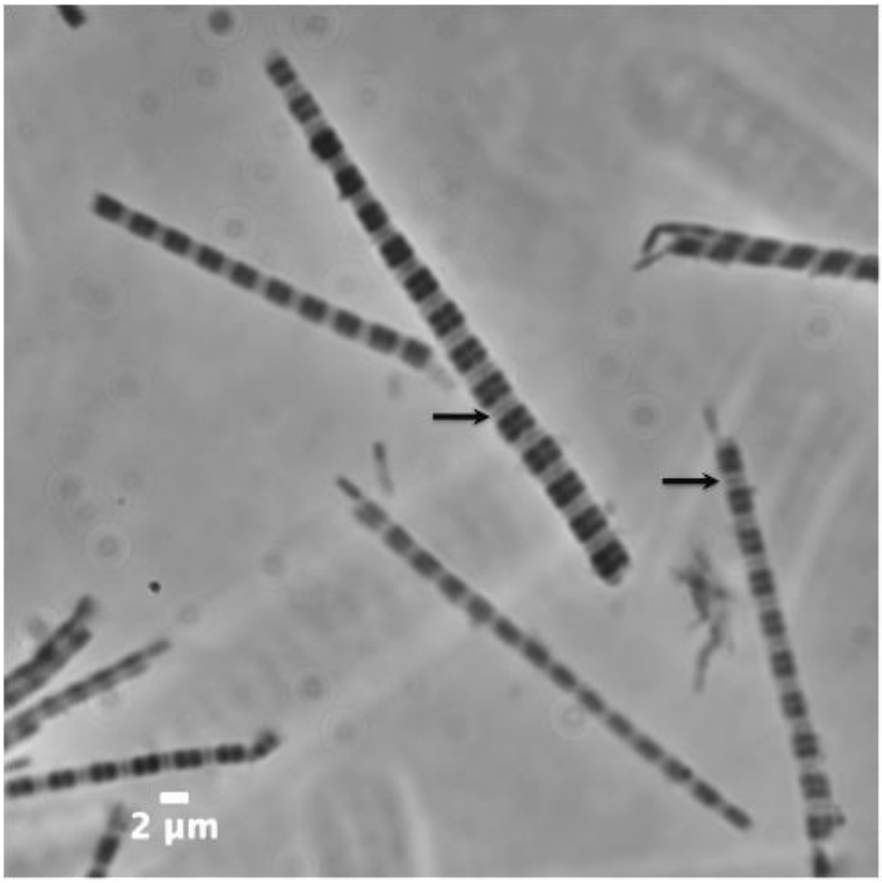

Figure 5.1 – Phase contrast light microscopy of rabbit psoas myofibrils. Myofibrils show clear Z-lines (arrows) and H-zones. The image was taken using an oil immersion objective (100x, Leitz Wetzlar) on a Leitz Diaplan Phase Contrast Microscope.

Homogenization of cardiac papillary muscle strips yields a suspension composed mainly of cardiac myofibrillar bundles, while single cardiac myofibrils are found only sporadically in preparations. Presumably this is because cardiac muscle is rich in connective tissue and has a desmin content as high as 2%, ie 2.8 fold higher than skeletal muscle (Paulin and Li 2004). Also, myocytes are mechanically coupled *via* intercalated disks (Small and Fürst 1992), which might hinder the separation of the bundles in single myofibrils. Smaller cardiac bundles were obtained when muscle fibers were skinned using detergents such as Triton X-100 and Brij-58 (**Figure 5.2**). Due to the thickness of the bundles, specimens stain heavily and appear dark in the electron microscope. The average length of the sarcomeres in our pig cardiac cardiac bundles prepared from muscle kept in Ca-free sodium Ringer buffer with 1 % Triton X-100 was measured to be 1.8 μm, comparable with the 1.85 μm slack length measured in rat cardiomyocytes (Granzier et al. 1997).

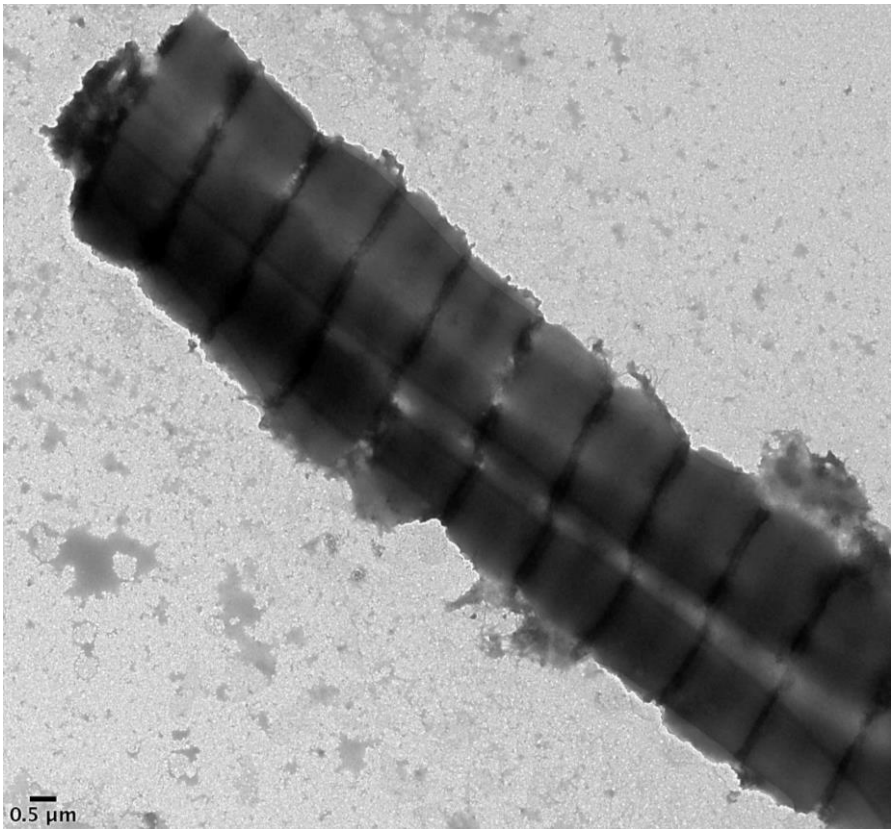

Figure 5.2 – Electron micrograph of a rabbit cardiac myofibril bundle. Papillary muscle was incubated overnight in Ca-free sodium Ringer containing 1 % Triton X-100. Myofibrils were stained with 1 % ammonium molybdate pH 7. Data was collected on CCD (2k x 2k) on the FEI T12 TEM.

5.3.2 Guba-Straub extraction of the A-band

A-band extraction was monitored in the phase contrast light microscope using flow-cells. After irrigation with Guba-Straub solution most of the A-band of rabbit psoas myofibrils disappeared, but darker bands in the H-zone were still noticeable, indicating that myosin extraction was not complete (**Figure 5.3**).

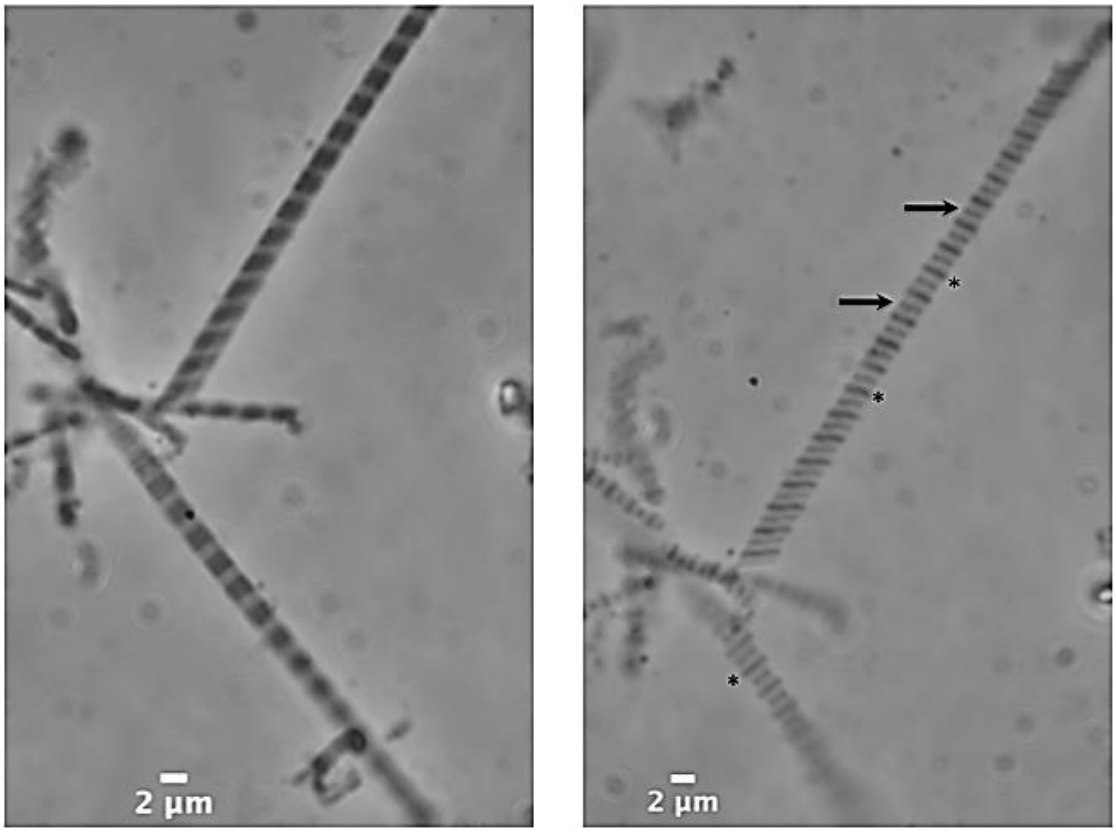

Figure 5.3 – Phase contrast microscopy of rabbit psoas myofibrils before and after A-band extraction. The Guba-Straub solution removes most of the A-band, residual protein is found in the H-zone (stars). Arrows indicate Z-disks.

Similarly, myofibrils extracted by successive centrifugation and resuspension steps showed a similar structure, with myosin still being present in the center of the sarcomere. The newly developed method for myosin extraction, the filter method, ensures the continual removal of myosin during filtration. The downside of the filter extraction method is that in order to recover myofibrils large volumes of buffer are needed, diluting the sample. Also the recovery rate of extracted myofibrils from the

filter is low, around 5-10 %. Dilute samples can be concentrated by centrifugation, but this is not ideal for structural work as extracted myofibrils are easily distorted by centrifugation.

Even though the filter method is more efficient at removing myosin, gel analysis reveals that residual myosin is found in extracted myofibrils, this being confirmed by electron microscopy (**Figure 5.4**). Estimating from the density of the actin band the recovery rate from the filter is less than 50%. Further experiments are needed to fully optimize this method.

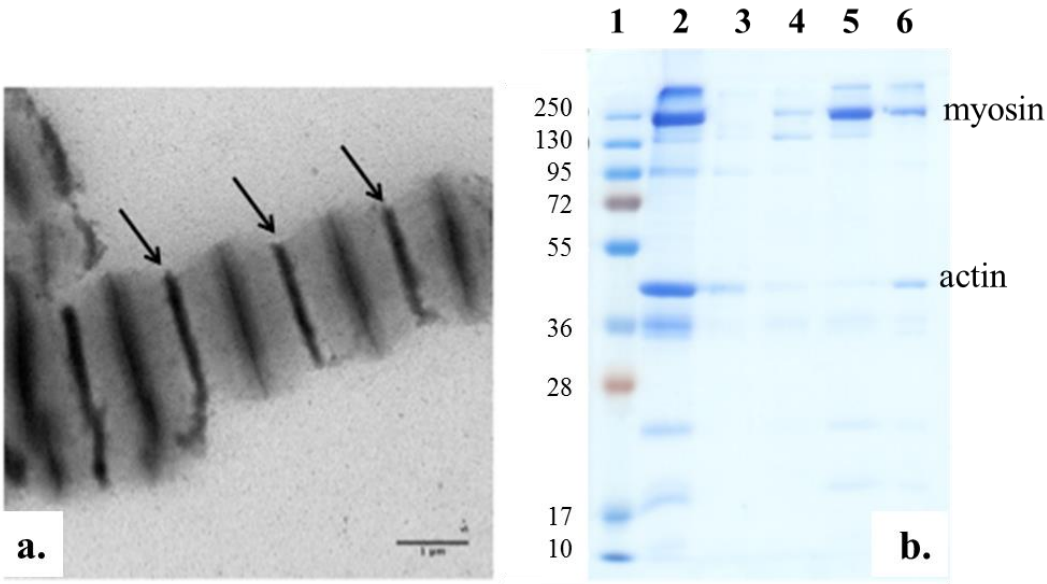

Figure 5.4 – Electron micrograph and SDS-PAGE analysis of extracted pig cardiac myofibril bundles using the filter method.

(a) Extracted cardiac bundles show residual myosin in the center of the sarcomere. Arrows indicate Z-disks. Specimens were stained with 1 % ammonium molybdate. Data was recorded on CCD (2k x 2k) on the FEI T12 TEM. Scale bar represents 1 μm.

(b) SDS-PAGE was used to monitor every step of the filter extraction. 1 – Molecular Weight markers (kDa); 2 – myofibrils in rigor buffer, 3 – flowthrough (rigor buffer); 4 – flowthrough after the filtration of Guba-Straub buffer without ATP; 5 - flowthrough after the filtration of Guba-Straub buffer with ATP; 6 – extracted myofibrils recovered from the filter.

5.3.3 Purification of human gelsolin

During gravity flow purification using DEAE Sephadex A-50 gelsolin eluted in the fractions containing 100 - 250 mM NaCl, 20 mM Tris-HCl pH 7.8, 1 mM EGTA, as revealed by SDS-PAGE of collected fractions (**Figure 5.5**). The detected protein size does not accurately correspond with the molecular weight of the provided hGSN construct (80.6 kDa), since hGSN migrates just above the 100 kDa molecular weight marker.

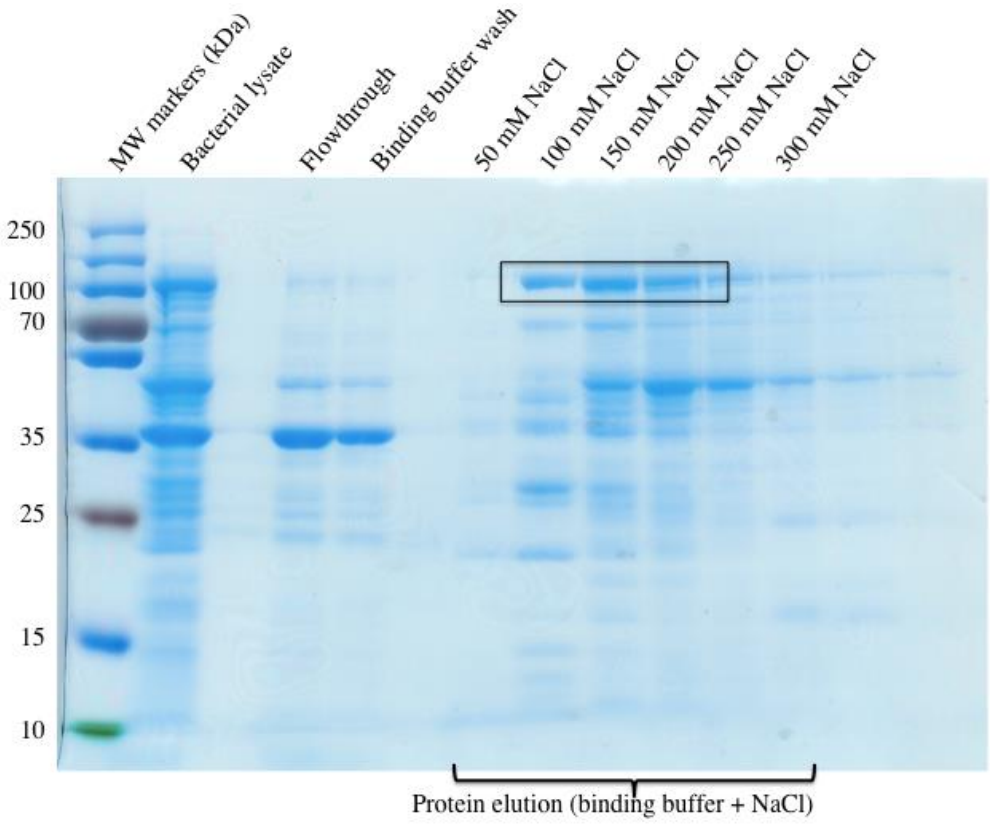

Figure 5.5 – SDS-PAGE analysis of anion exchange purification of hGSN on a DEAE Cellulose column. Samples were collected at all stages during purification (flow-through, wash and elution). hGSN eluted between 100 - 250 mM NaCl, 20 mM Tris-HCl pH 7.8, 1 mM EGTA. Black selection area indicates the fractions that were pooled together and dialysed for further purification.

The elution profile of the cation exchange purification (SP Sepharose) showed hGSN eluted in a single peak at around 150 mM NaCl. Nonetheless contaminants were still present in the preparation.

The chromatogram obtained from size exclusion chromatography (Superdex 200) revealed a good separation between gelsolin and contaminants, as two peaks well separated peaks can be resolved. hGSN eluted first, as expected, due to having a higher molecular weight than the contaminating protein. SDS gel analysis confirmed that the fractions collected contain pure hGSN (**Figure 5.6**).

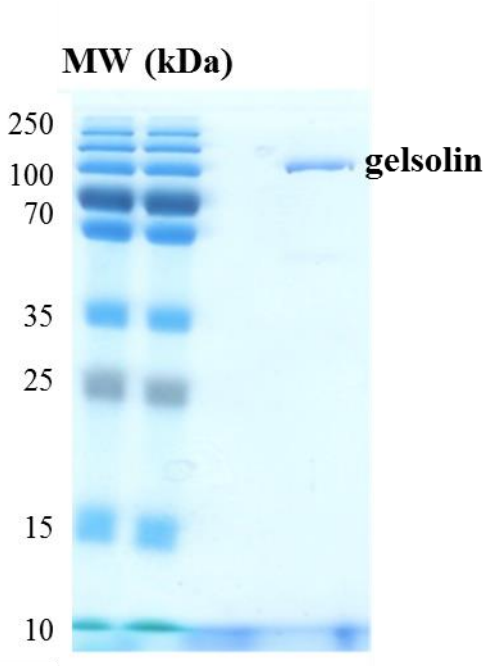

Figure 5.6 - SDS-PAGE analysis of the main peak obtained after size exclusion chromatography. hGSN eluted in a single absorbance peak and is pure.

5.3.4 Thin filament removal using gelsolin

Fluorescence light microscopy of gelsolin treated myofibrils revealed that the distribution of actin within the sarcomere was drastically changed by gelsolin. While in untreated myofibrils most of the sarcomere is labeled with FITC phalloidin, with the exception of the H-zone, in myofibrils treated with hGSN in Ca-Rigor most of the thin filaments in the I-band are removed. The highest fluorescence signal corresponds to the actin filaments in the Z-disk (**Figure 5.7**).

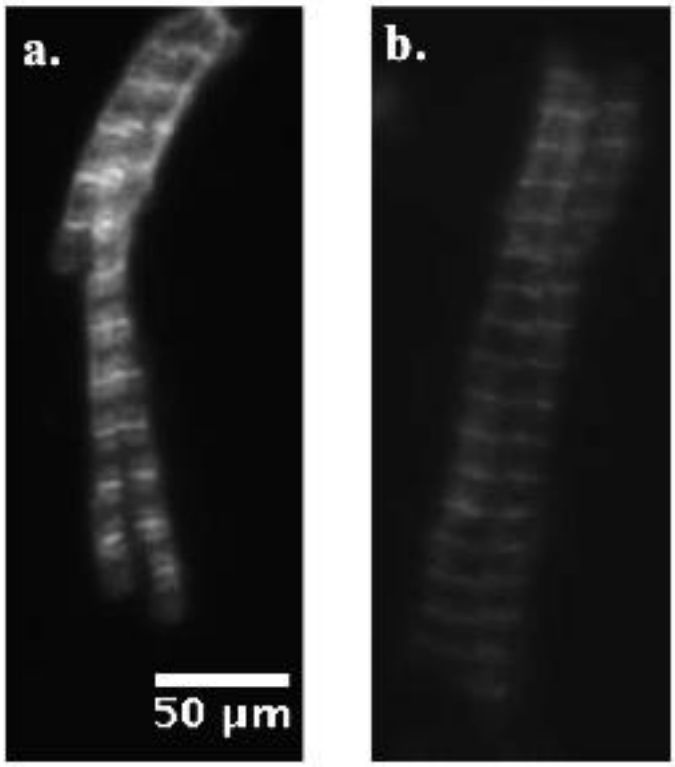

Figure 5.9 – Fluorescence micrographs of gelsolin treated cardiac myofibrils. a - In untreated myofibrils suspended in EGTA-Rigor buffer FITC phalloidin labels the entire sarcomere, with the exception of the H-zone. **b** – In myofibrils exposed to gelsolin the actin in the I-band is depolymerized, while the actin in the Z-disk is not removed. Magnification 400x.

SDS-PAGE analysis of intact and extracted myofibrils, as well as the post-extraction supernatant was carried out. The supernatant contained mainly gelsolin and actin, while other proteins associated with the thin filament, such as tropomyosin and troponin were not detected. The pellet, consisting of extracted myofibrils, contains residual gelsolin as well as a considerable amount of actin. Data confirms that the purified protein maintained its activity in the presence of calcium. The results are therefore consistent with the published data that most of the thin filament actin is susceptible to depolymerization by gelsolin, but the actin in the Z-disk is most resistant, presumably due to protection by its binding partners there.

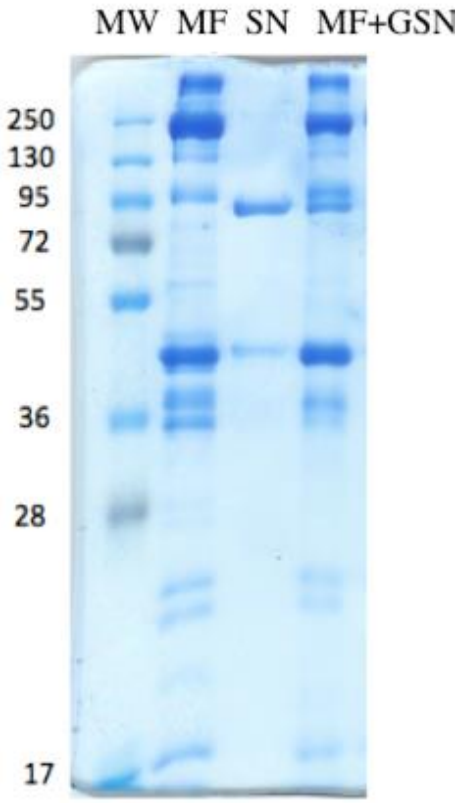

Figure 5.10 – SDS gel analysis of rabbit psoas myofibrils treated with hGSN. (MW) – Molecular weight markers, (MF) – untreated myofibrils, (SN) – supernatant collected after incubation with hGSN and centrifugation, (MF+GSN) – pellet containing myofibrils treated with hGSN. The supernatant contains gelsolin and actin, while in the pellet residual gelsolin, but also actin can be found.

5.3.5 Titin cleavage

Vertebrate muscle

Titin cleavage experiments were carried out on both skeletal and cardiac muscle. In the case of skeletal muscle sample freshness and storage proved to be very important. Psoas muscle that was stored in the -20°C freezer for more than 1.5 years was degraded to the point where gentle homogenization in relaxing buffer (0.15 M KCl, 5 mM $MgCl_2$, 10 mM MOPS pH 7, 1 mM EGTA, 4 mM ATP) would result in a suspension of thin and thick filaments, as revealed by negative stain electron microscopy (**Figure 5.11**). The loss of Z-disk width and structure suggests that proteins within the lattice were degraded during long-time storage in the freezer.

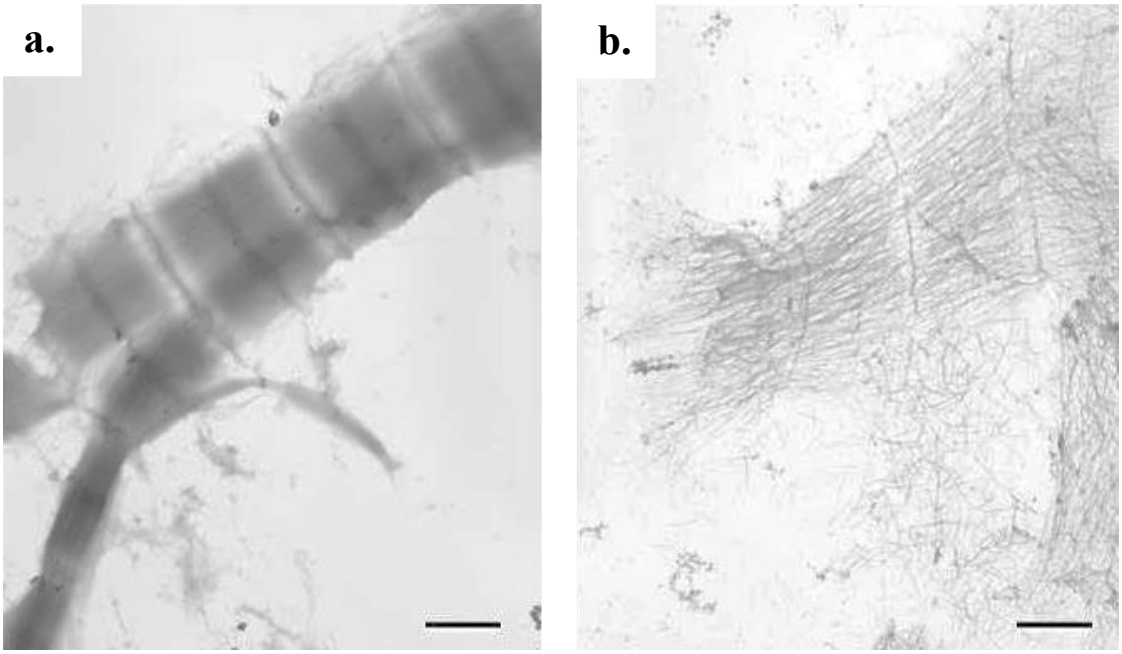

Figure 5.11 – Electron micrograph of negatively stained rabbit psoas myofibrils before (a) and after gentle homogenisation in relaxing buffer (b). The homogenized myofibrils fall apart into thin and thick filaments. Micrographs were recorded on film on a JEOL1200 TEM and scanned using an Imacon Flextight 848 digital scanner. Scale bars represent 1 μm.

Cardiac muscle

In the case of cardiac muscle we observed complete myofibril digestion after 4 minutes, as judged by phase contrast light microscopy and EM. This is to be expected because, unlike Higuchi, our experiments were carried out on myofibrillar bundles in suspension where buffer exchange is more efficient than in skinned muscle fibers. The Ringer buffer used for overnight calcium depletion of freshly dissected muscle strips seemed to influence the outcome of the trypsin digestion experiments. The highest concentration of A-segments and I-Z-I brushes was obtained from myofibrils made from cardiac strips incubated in Na-Ringer with 0.5% Brij-58 (**Figure 5.12**). After 2 minutes incubation with trypsin 5 μl of suspension were negatively stained with ammonium molybdate and checked in the electron microscope. Observed A-segments are approximately 1.5 μm in length with the M-line clearly visible (**Figure 5.12 a**). I-Z-I brushes are characterized by thin filaments protruding from either side of the Z-disk (**Figure 5.12 b**). In both micrographs the protein concentration in the background is very high. Even though A-segments and I-Z-I brushes were present in this preparation

their concentration was still very low and most of the grid was covered in thick and thin filaments.

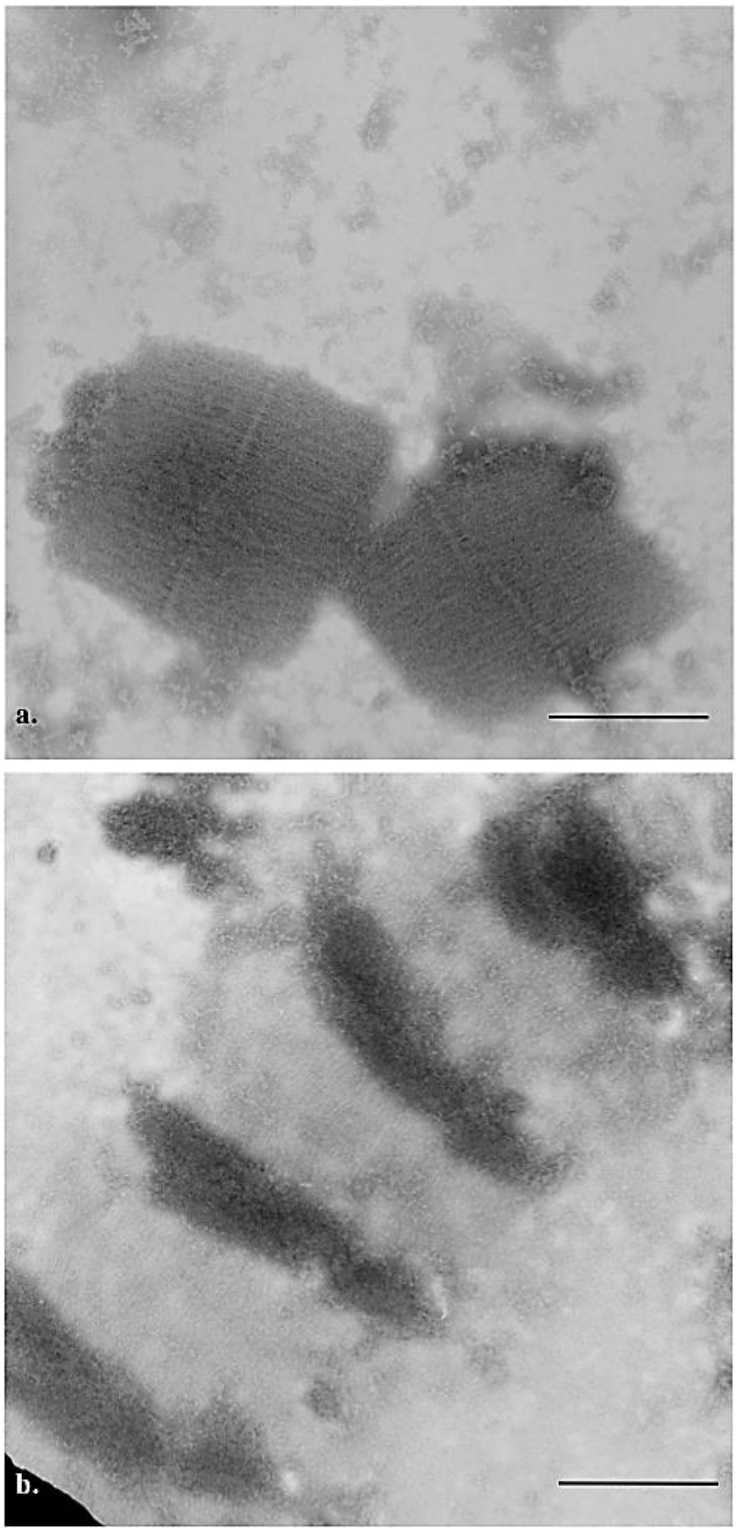

Figure 5.12 – Electron micrographs of negatively stained (ammonium molybdate) pig cardiac A-segments (a) and I-Z-I brushes (b). Micrographs were recorded on film on the JEOL1200 TEM. Scale bars represent 1 μm.

Incubation of the suspension containing I-Z-I brushes with hGSN should allow for thin filaments depolymerization and Z-disk release. Titin cleavage experiments were characterized by low reproducibility; most of the screened preparations did not contain any A-segments or I-Z-I brushes. We hypothesize that this might related to the relative shorter sarcomere length (aprox. 1.8 – 2 μm) where trypsin does not selectively cleave titin, but might digest other sarcomere components.

We also took into consideration that the trypsin used was purified from bovine liver and might contain traces of chymotrypsin, thus we substituted trypsin with TrypLE-Express. We have also sped up the transition of myofibrils into rigor by incubating them in 100 mM NaCl, 2 mM $MgCl_2$, 6 mM potassium phosphate, 1 mM EGTA, 5 mM 2-deoxyglucose, 1 mM iodoacetic acid, 2 mM NaCN, 0.5 % Brij-58. Muscle strips can be homogenized after only 30 minutes incubation. Myofibrils showed well defined M-lines and H-zones, narrow I-bands and had a sarcomere length of approximately 1.8 - 2 μm (**Figure 5.13 a**). Under relaxing conditions the arrangement of sarcomeres was preserved even though most the myofibril was digested by TrypLE-Express. There was no clear distinction between A-segments and I-Z-I brushes (**Figure 5.13 b**). On the other hand, TrypLE-Express treatment in rigor buffer produced well preserved A-segments with well-defined M-lines, while the I-band was missing and the Z-disks appeared either thickened (**Figure 5.13 c**) or disorganized, potentially partly digested (**Figure 5.13 d**).

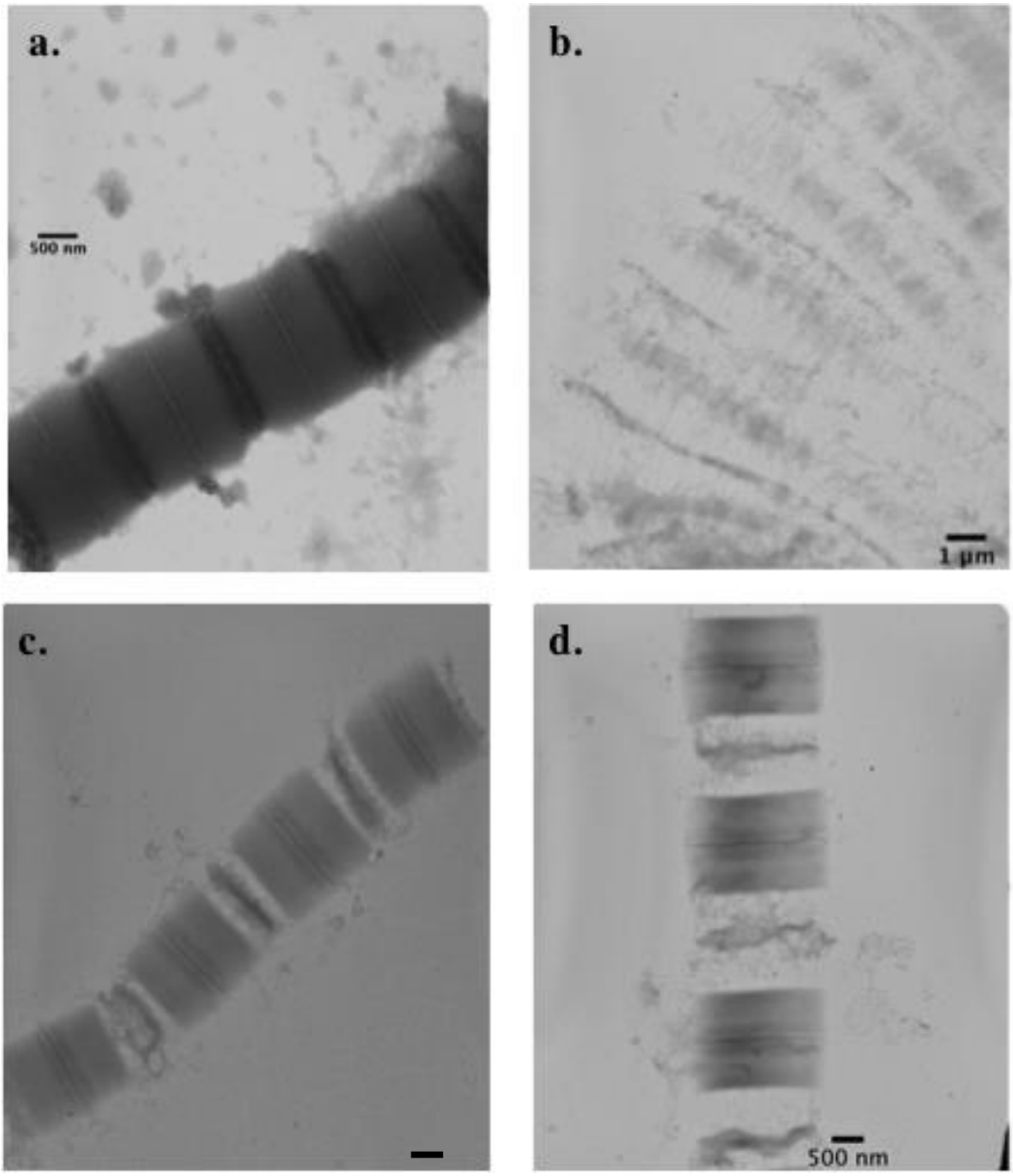

Figure 5.13 – Electron micrographs of pig cardiac myofibrils treated with TrypLE-Express. (a) Untreated myofibril obtained after incubation in Ca-free sodium Ringer containing sodium cyanide and iodoacetic acid; (b) Myofibril after digestion under relaxing conditions; (c and d) Myofibrils in rigor treated with TrypLE-Express. Samples were negatively stained with ammonium molybdate and micrographs were recorded on film using a JEOL1200X TEM.

5.4 Discussion

The aim of the work presented in this chapter was to establish reproducible methods, using physiological ionic conditions, unlike the more extreme conditions used on the insect indirect flight muscle, for the isolation of vertebrate Z-disks showing a well preserved tetragonal lattice. Methods for obtaining isolated Z-disks from vertebrate striated muscle are not described in the literature. If successful, the Z-disks were to be analysed by negative stain and cryo-transmission electron microscopy.

The work was carried out on both skeletal and cardiac muscle. We opted for a gradual disassembly of the sarcomere under conditions as mild as possible. The A-band was extracted in the presence of ATP using the high salt Guba Straub solution. Residual myosin was present in the middle of the sarcomere as corroborated by SDS-PAGE and EM analysis. The filter extraction method was developed to better wash away the myosin during extraction and to allow the constant flow of fresh buffer to promote myosin depolymerization even further. The advantage of the method is that it allows for better monitoring of proteins extracted by Guba Straub buffer. Extracted myofibrils can be recovered in the buffer of choice with little to no contaminants from the filtrate. The disadvantage of the method is that myofibril recovery from the filter is low, less than 40-50%, which was not enough for further experiments. Myosin extraction was considered necessary to allow easier access of gelsolin to thin filaments, especially when working with cardiac myofibril bundles which have shorter sarcomere length and are slightly over-contracted. Calcium dependent human gelsolin expression and purification from bacterial cultures was successful. Fluorescence light microscopy confirmed that in rigor conditions gelsolin depolymerises thin filaments. This worked as expected on both myofibrils that were previously extracted with Guba Straub solution and untreated myofibrils.

Past studies had shown that during various protein extractions titin and nebulin are likely to have collapsed onto the Z-disk (Ohashi et al. 1982; Wang and Ramirez-Mitchell 1983). From a structural point of view this is not desirable because such collapsed proteins would thicken the specimen and can potentially be a source of noise in the micrographs that might hinder 3D reconstruction. We decided to work with cardiac muscle because it expresses nebulette, which is a sixth the size of nebulin and localizes in the Z-disk (Pappas et al. 2011). Titin can be preferentially cleaved by trypsin at long sarcomere lengths (Higuchi 1992). Under relaxing conditions the A-band

and I-band appear dislocated indicating that titin was cleaved in the I-band region of the protein. Experiments were carried out on pig cardiac myofibril bundles using trypsin and trypsin substitutes of non-animal origin. Conditions that would yield I-Z-I brushes and A-segments in high concentration were screened thoroughly. Promising conditions were repeated several times, but were not easily reproducible. This might be due to the fact that sarcomeres are not stretched beyond slack length, thus titin is not cleaved preferentially. The lack of reproducibility lead us the idea that during overnight rigor development protease inhibitors and EGTA do not penetrate the muscle strips fast enough, thus permitting contraction of myofibrils and possibly autodigestion. Faster rigor development could be achieved by adding cyanide, iodoacetate and 2-deoxyglucose to the Ringer buffer. The work proved far more challenging than expected and well preserved Z-disks were not found.

The demonstration of the use of trypsin and gelsolin to produce I-Z-I brushes and to sever thin filaments protruding from either side of the Z-disks with the final goal of isolating the Z-disk provides a basis for future work. In my opinion future work should focus on obtaining stretched myofibrils from cardiac muscle. This can be achieved for example by gluing one end of the muscle strip and tying the other end to a hook and slowly stretching it while muscle is immersed in the buffer of choice. Also adding BDM (butadiene monoxime) to the buffer should inhibit myosin function and prevent over-contracture. Once myofibrils are sufficiently stretched, adding trypsin followed by gentle homogenization should yield I-Z-I brushes that once treated with gelsolin will release intact Z-disks.

6. Discussion

6.1 General considerations

Much of the molecular organization of sarcomeres remains to be determined, which is a major impediment to understanding muscle function and homeostasis. Electron microscopy is a powerful technique that can deliver high resolution information on protein-protein interactions in muscle within the cellular context (Batters et al. 2014). Since myofibrils are relatively thick, several hundred nanometers in diameter, sectioning methods have been needed for successful imaging in the electron microscope (Reedy et al. 1983a; Taylor et al. 1984; Deatherage et al. 1989; Luther 2000; Luther and Barry 2002).

The lack of understanding of the molecular architecture of the A-band, M-line, I-band and the Z-disk arises from the shortcomings associated with sample preparation methods for electron microscopy. Traditionally intact muscle and sarcomeres have been studied by cutting ultrathin sections of tissue embedded in resin. It has been shown that muscle fibers within resin blocks can be very well preserved, up to 1.3 nm resolution (Sader et al. 2007), but after ultramicrotomy the resolution is ~ 5 nm at best, indicating that sectioning is where damage occurs. This resolution is not satisfactory to study the 3D structure of muscle. Only at a resolution of 2-3 nm the shapes of proteins can be recognized, allowing known crystal structures to be accurately docked in the EM density map. This in turn will allow for protein-protein interactions to be studied in healthy or diseased muscle, which is critical to a comprehensive understanding of underlying mechanisms.

For many years the Z-disk has been regarded as a passive structural component of muscle that can withstand contraction forces, having a purely mechanical role. However we now know the Z-line has over 40 protein components, many of which have the ability to shuttle between the Z-disk and other cellular compartments, such as the

nucleus, and are involved in important signaling pathways (Atkinson et al. 2000; Faulkner et al. 2001; Bang et al. 2001; Bassel-Duby 2006; Bertz et al. 2009; de Almeida Ribeiro 2014). The Z-disk is also thought to act as a stretch sensor in muscle as it is coupled mechanically to the sarcolemma through the costameric region and several protein components have been linked with signaling pathways triggered by mechanic stimuli (Epstein and Davis 2003). Mutations within Z-disk proteins have been associated with a number of diseases like cardiomyopathies and muscular dystrophies (Frank et al. 2006). The image of the Z-disk has shifted from a passive one to an active one, with the Z-band being considered a 'control centre' that governs muscle homeostasis (Gautel 2011). However, for the reasons above the molecular organisation of this crucially important part of the sarcomere is not known in detail.

Many studies have been carried out and we are beginning to understand the geometry of muscle, but due to the poor resolution in plastic sections the detailed molecular architecture of the Z-disk remains unknown. Tomography of honeybee Z-disks gave insight into the symmetry of the lattice, the localization of thin filaments and revealed connecting densities which bridge anti-parallel and parallel actin filaments. This information is important, but crystal structures of know lattice components could not be fitted in the density map (Deatherage et al. 1989; Cheng and Deatherage 1989). Tomography of vertebrate Z-disks revealed the overall organization of α-actinin Z-bridges in healthy and diseased muscle (Morris et al. 1990; Luther 1991; Luther 2000; Luther and Barry 2002; Luther and Squire 2002). X-ray fiber diffraction revealed that the transition between the two observed lattice appearances in vertebrate muscle, small-square and basketweave, relates to the movements of tropomyosin on the thin filament (Perz-Edwards and Reedy 2011). Progress towards the understanding of the 3D structure of the Z-disk has been made; nevertheless the detailed molecular landscape remains largely unexplored.

My project focused on obtaining a 3D EM density map of intact Z-disks. For this project we employed electron tomography, a relatively low resolution technique. However, by exploiting the paracrystalline nature of the Z-disk we hope to improve the final resolution by sub-tomogram averaging. This approach is different from what was done in the past and it obviates the need for sectioning and its damaging effects. We pursued the isolation of intact Z-disks from fresh and glycerinated myofibrils from vertebrate and insect flight muscle using new biochemical approaches in order to

obviate the need of sectioning. The Z-disk is a naturally thin structure and is clearly well suited for 3D reconstruction and cryo-EM.

6.2 Findings

6.2.1 Preparation and electron tomography of insect Z-disks

If insect flight muscle myofibrils are irrigated with mild acids, such as lactic or formic acid, the myofibrils fall apart, with the exception of the Z-disks, which are very resistant structures. This property of the Z-disk has made it possible to isolate the intact structure which shows the characteristic hexagonal lattice regularity. Studies on the properties of lactic acid extracted Z-disks have been carried out 40 years ago and revealed that the Z-disk can change diameter depending on buffer conditions. Initially, in our studies, we isolated Z-disks from honeybee indirect flight muscles as described in the literature. We confirmed that the hexagonal lattice is preserved and that they show an expanded conformation in acidic environments, which can be reversed by changing to conditions closer to the physiological ones. The resolution of the best specimens was around 40 nm. Electron tomography of lactic acid isolated Z-disks has been carried out for the first time and has shown that the isolated Z-disks are thin enough to successfully acquire tilt series. We have shown that exposing the Z-disks to very acidic conditions will damage their structure. This has been observed as loss of regularity within the lattice and the absence of diffraction spots in the Fourier Transforms. The ratio of preserved Z-disks to damaged ones was 1:3 in the lactic acid preparations, which was considered an obstacle for high resolution imaging and 3D reconstruction.

We sought out to isolate Z-disks in milder conditions, using high salt buffers rather than mild acids to extract proteins from the A-band and the I-band. Previous work from the Bullard laboratory suggested that this can be achieved using high potassium chloride buffers. In ort hands the specimens we prepared were not suitable for electron microscopy, with the ratio between single Z-disks and incompletely extracted myofibrils being skewed in the favor of the latter.

A new method for Z-disk extraction has been developed and used a combination of high potassium chloride and iodide to remove the A- and I-bands. The Z-disks obtained show the best preservation seen in preparations of isolated Z-disks, with diffraction spots extending to 16.6 nm resolution, much improved when compared with the lactic

acid specimens. Separated Z-disks have distinct advantages; they can be purified and used to study protein composition. Progress has been made towards the purification of isolated Z-disks, nonetheless our effort failed to yield a suspension containing only Z-disks. The approach was to purify the Z-disk in discontinuous gradients, as it was previously described in the literature (Saide and Ulrick 1974; Bullard and Sainsbury 1977; Sainsbury and Bullard 1980). We have found that the Z-disks adhere to the tubes used for purification, as well as to the dialysis tubing used for the removal of the density media. Further efforts are necessary to optimize the purification of isolated Z-disks.

The protein composition of the specimens can be easily monitored by gel electrophoresis. We have investigated the protein make-up of isolated Z-disks by mass spectrometry of excised bands from SDS-PAGE gels. Analysis of obtained sequences has confirmed that the samples are not pure with contaminants being present in the preparation. The nature of the contaminants has been identified as extracted proteins from the A- and I-band in the form of myosin, paramyosin, and troponin. Beside sarcomeric proteins the samples were also contaminated by cellular organelles, such as mitochondria, as suggested by the identification of ATP synthase and ubiquinone.

Suspensions of Z-disks can be easily handled and rapidly prepared for electron microscopy. We presented here the first report of cryo-electron microscopy and tomography of unstained frozen-hydrated isolated Z-disks. Fourier Transforms of cryo-EM micrographs are much richer than what was previously shown in negative stain, with 6 order diffraction spots extending to 8 nm resolution being resolved. Since isolated Z-disks can be regarded as two dimensional crystals we have decided to employ 2D lattice unbending to correct for lattice imperfections and to sharpen the diffraction peaks. 2D lattice unbending was carried out by Dr. Peiyi Wang in the laboratory of Prof. Per Bullough at the University of Sheffield. Data was generated only from one image and it should be considered preliminary and taken as a proof of principle which demonstrates that 2D lattice unbending is a powerful technique suitable for the analysis of isolated Z-disks.

Cryo-electron tomography of frozen hydrated Z-disks has generated an EM density map which shows improvements in resolution compared with the available Deatherage model. Cryo-electron microscopy and tomography were carried out for the first time on isolated Z-disks. Tilt series were collected using state-of-the-art equipment at the Laboratory for Molecular Biology in Cambridge. The data is currently being processed and analysed in collaboration with Dr. Kenneth Taylor and Zhongjun Hu (Florida State

University). Presented data should still be considered preliminary and conclusion that were drawn might not reflect the final result.

In the current working model we have we were able to identify the symmetry elements of the Z-disk lattice. We have found that the honeybee Z-disk is based on a p321 lattice, in disagreement with results published in the literature (Deatherage et al. 1989; Cheng and Deatherage 1989). Deatherage has found the symmetry of the Z-disk to be p312, whereas we consider that the symmetry is p321. Compared to the available model in which the thin filaments had no substructure and appeared like cylinders, we are beginning to distinguish details pertaining to the actin filament in our structure. Actin models have been generated and fitted into the EM density map. The model revealed crosslinking densities between actin filaments of opposite polarity. α-actinin was modeled and fitted into the Z-bridges density with perfect agreement. Deatherage reported a connecting density between three actin filaments of the same polarity. This protein presented 3-fold symmetry and its location was in accordance with the position of thick filaments in the A-band (Cheng and Deatherage 1989). Our model reveals the three converging parallel actin filaments, but no crosslinking density was observed, suggesting that the protein was washed away during extraction.

In conclusion we have developed a Z-disk extraction method based on high ionic strength buffers which we have shown to yield well preserved Z-disks in a reproducible manner. We have carried out for the first time cryo-EM and cryo-ET and preliminary data suggests that the resolution is improved when compared with previous reports.

6.2.2 Preparation of vertebrate intact Z-disks

The vertebrate Z-disk is different from the insect one not only in its protein composition, but in its geometry, with the thin filaments overlapping in a tetragonal lattice. The tetragonal lattice has two different appearances depending on the state of the muscle: small square in relaxed muscle and a basketweave lattice in muscles under tension (Goldstein et al. 1987; Perz-Edwards and Reedy 2011).

A method describing how intact Z-disks can be isolated from vertebrate myofibrils is not currently available in the literature. We pursued the isolation of skeletal and cardiac Z-disks in conditions as mild as possible taking into consideration the need to

successfully remove the actin from the I-band, but not from the Z-line; also the need to avoid the collapse of the giant proteins titin and nebulin onto the structure.

Gelsolin was expressed, purified and actin was removed successfully from the I-band, while the actin in the Z-disk was not removed. Cardiac muscle was preferred due to its low contents of nebulin, which might collapse onto the isolated Z-disks adding noise and thickness to the specimen. Titin was successfully cleaved in the I-band of the cardiac sarcomere which caused the release of A-segments and I-Z-I brushes. Even though titin cleavage was successful to some extent the method was characterized by low reproducibility and low concentrations of I-Z-I brushes. On an electron microscopy grid only 2-3 I-Z-I brushes were identified. Hundreds of grids were checked in the EM and several conditions explored, but optimal conditions for vertebrate Z-disk have not yet been identified.

6.3 Future work

With this work as a starting point we hope that the stepping stones for future research of isolated Z-disks were set and the methods developed and knowledge generated will help answer unresolved questions regarding the organization and function of the Z-disk from both vertebrates and invertebrates. The availability of isolated Z-disks opens many new possibilities and has great potential. Electron tomography has been shown to be capable of sub-nanometer resolution after sub-tomogram averaging (Briggs 2013) and there seem no reason why a regular structure such as the Z-disk should not be solved to reveal the component protein shapes. What is limiting the resolution of our models presented here could be radiation damage or the presence of substantial amounts of contaminating myosin; however both these factors should be capable of substantial improvement. The fact that the composition of the Z-disks can easily be monitored also has great potential, including the following the gain and loss of individual components monitored by gels, mass spec or microscopy, for instance with antibodies and light or electron microscopy. The fact that Z-disks usually lie flat even in the light microscope should be an advantage for such work, and the fact that super-resolution light microscopy reveals detail smaller than the Z-disk lattice spacing offers exciting possibilities.

Regarding the work presented here we identify few directions for improvement. The methods for purification of honeybee Z-disks should be optimized to minimize the concentration of contaminants in the preparation. Also milder isolation methods should be explored, to minimize the protein loss occurring during extraction. Our data showed that Z-disks are unusually susceptible to radiation damage. Considering that we had to discard a quarter of our cryo-tilt images we consider that for future data collection lower doses should be used (as low as 0.3 -0.4 electron/$Å^2$).

Even though the vertebrate Z-disk isolation attempts did not yield the desired outcomes we believe we have identified a potential strategy for the preparation of isolated vertebrate Z-disks. The method was not reproducible, but further investigations into titin digestion using either trypsin or trypsin substituents are needed. Also the use of the gelsolin fragment FX45, which does not require calcium to depolymerize actin in the thin filaments may be valuable.

Bibliography

Aebersold, R., & Mann, M., 2003. Mass spectrometry-based proteomics. *Nature*, *422*(6928), 198-207.

Afzelius, B.A. and Maunsbach, A.B., 2004. Biological ultrastructure research; the first 50 years. *Tissue and cell*, 36(2), pp.83–94.

Agarkova, I. and Perriard, J.-C., 2005. The M-band: an elastic web that crosslinks thick filaments in the center of the sarcomere. *Trends in cell biology*, 15(9), pp.477–485.

Agronskaia, A.V.; Valentijn, J.A.; van Driel, L.; Schneijdenberg, C.; Humbel, B.M.; van Bergen en Henegouwen, P.M.; Verkleij, A.J. Koster and Gerritsen, H.C., 2008. Integrated fluorescence and transmission electron microscopy. *Journal of structural biology*, 164(2), pp.183–189.

Ahuja, P., Perriard, E., Perriard, J. C., Ehler, E., 2004. Sequential myofibrillar breakdown accompanies mitotic division of mammalian cardiomyocytes. *Journal of cell science*, *117*(15), 3295-3306.

Al-Amoudi, A.; Chang, J.J.; Leforestier, A.; McDowall, A.; Salamin, L.M.; Norlen, L.P.O.; Richter, K.; Sartori Blanc, N.; Studer, D. and Dubochet, J., 2004. Cryo-electron microscopy of vitreous sections. *The EMBO journal*, 23(18), pp.3583–3588.

Al-Amoudi, A., Studer, D. and Dubochet, J., 2005. Cutting artefacts and cutting process in vitreous sections for cryo-electron microscopy. *Journal of structural biology*, 150(1), pp.109–121.

Al-Khayat, Hudson, L., Reedy, M.K.; Irving, T.; Squire, J., 2003.Myosin head configuration in relaxed insect flight muscle: x-ray modeled resting cross-bridges in a pre-powerstroke state are poised for actin binding. *Biophysical journal* 85.2 (2003): 1063-1079.

Al-Khayat, H.A.; Wensler, R.W.; Squire, J.M.; Marston, S.B. and Morris, E.P., 2013. Atomic model of the human cardiac muscle myosin filament. *Proceedings of the National Academy of Sciences*, 110(1), pp.318–323.

Alamo, L.; Wriggers, W.; Pinto, A.; Bartoli, F.; Salazar, L.; Zhao, F.-Q.; Craig, R. and Padrón, R., 2008. Three-Dimensional Reconstruction of Tarantula Myosin Filaments Suggests How Phosphorylation May Regulate Myosin Activity. *Journal of molecular biology*, 384(4), pp.780–797.

Alberts, B.; Johnson, A.; Lewis, J.; Raff, M.; Roberts, K. and Walter, P., 2008. *Molecular Biology of the Cell* Fifth. M. Anderson and S. Granum, eds., Garland Science.

Arber S, Halder G, Caroni P., 1994. Muscle LIM protein, a novel essential regulator of myogenesis, promotes myogenic differentiation. *Cell,* 79:221–231.

Atkinson, R.; Joseph, C.; Dal Piaz, F. and Birolo, L., 2000. Binding of [alpha]-Actinin to Titin: Implications for Z-Disk Assembly. *Biochemistry,* (39), pp.5255-5264.

Au, Y., 2004. The muscle ultrastructure: a structural perspective of the sarcomere. *Cellular and molecular life sciences : CMLS*, 61(24), pp.3016–3033.

Bai, X.-C.; Fernandez, I.S., McMullan, G., Scheres, S.H.W. and Kühlbrandt, W., 2013. Ribosome structures to near-atomic resolution from thirty thousand cryo-EM particles. *eLife*, 2, p.e00461.

Bang, M.L.; Mudry, R.E.; McElhinny, A.S.; Trombitás, K.; Geach, A.J.; Yamasaki, R.; Sorimachi, H.; Granzier, H.; Gregorio, C.C. and Labeit, S., 2001. Myopalladin, a novel 145-kilodalton sarcomeric protein with multiple roles in Z-disc and I-band protein assemblies. *The Journal of cell biology*, 153(2), pp.413–427.

Barua, B., Winkelmann, D. A., White, H. D., & Hitchcock-DeGregori, S. E., 2012. Regulation of actin-myosin interaction by conserved periodic sites of tropomyosin. *Proceedings of the National Academy of Sciences*, *109*(45), 18425-18430.

Bassel-Duby, R; Olson, E.N., 2006. Signaling pathways in skeletal muscle remodeling. *Annual Review of Biochemistry,*75, pp. 19-37.

Batters, C.; Veigel, C.; Homsher, E. and Sellers, J.R., 2014. To understand muscle you must take it apart. *Frontiers in physiology*, 5, p.90.

Beranova-Giorgianni, S., 2003. Proteome analysis by two-dimensional gel electrophoresis and mass spectrometry: strengths and limitations. *Trends in Analytical Chemistry*, 22(5), pp 273-281.

Berman, Y. and North, K.N., 2010. A gene for speed: the emerging role of alpha-actinin-3 in muscle metabolism. *Physiology (Bethesda, Md)*, 25(4), pp.250–259.

Berriman, J.A.; Li, S.; Hewlett, L.J.; Wasilewski, S.; Kiskin, F.N.; Carter, T.;Hannah, M.J. and Rosenthal, P.B., 2009. Structural organization of Weibel-Palade bodies revealed by cryo-EM of vitrified endothelial cells. *Proceedings of the National Academy of Sciences of the United States of America*, 106(41), pp.17407–17412.

Bertz, M., Wilmanns, M. and Rief, M., 2009. The titin-telethonin complex is a directed, superstable molecular bond in the muscle Z-disk. *Proceedings of the National Academy of Sciences*, 106(32), pp.13307-13310.

Bismuth, K. and Relaix, F., 2010. Genetic regulation of skeletal muscle development. *Experimental cell research*, 316(18), pp.3081–3086.

Bos, J. M., Poley, R. N., Ny, M., Tester, D. J., Xu, X., Vatta, M., Towbin, J., Gersh, B., Ommen, S., Ackerman, M. J., 2006. Genotype–phenotype relationships involving hypertrophic cardiomyopathy-associated mutations in titin, muscle LIM protein, and telethonin. *Molecular genetics and metabolism*, *88*(1), 78-85.

Bremer, A.; Henn, C.; Engel, A.; Baumeister, W. and Aebi, U., 1992. Has negative staining still a place in biomacromolecular electron microscopy? *Ultramicroscopy*, 46(1-4), pp.85–111.

Briegel, A.; Wong, M.L; Hodges, H.L.; Oikonomou, C.M.; Piasta, K.; Harris, M.J.; Fowler, D.J.; Thompson, L.; Falke, J.J.; Kiessling, L.L. and Jensen, G.J., 2014. New Insights into Bacterial Chemoreceptor Array Structure and Assembly from Electron Cryotomography. *Biochemistry*, 53(10), pp.1575–1585.

Briggs, J.A., 2013. Structural biology in situ-the potential of subtomogram averaging. *Current opinion in structural biology*, 23(2), 261-267.

Bullard, B. and Sainsbury, G.M., 1977. The proteins in the Z line of insect flight muscle. *The Biochemical journal*, 161(2), pp.399–403.

Bullard, B.; Burkart, C.; Labeit, S. and Leonar, K., 2006. The function of elastic proteins in the oscillatory contraction of insect flight muscle. *Journal of muscle research and cell motility*, 26(6-8), pp.479–485.

Bullard, B., Dabrowska, R. and Winkelman, L., 1973. The contractile and regulatory proteins of insect flight muscle. *The Biochemical journal*, 135(2), pp.277–286.

Burch, C.R. and Stock, J.P.P., 2002. Phase-Contrast Microscopy. *Journal of Scientific Instruments*, 19(5), pp.71–75.

Burgess, S., Walker, M., Knight, P.J., Sparrow, J.; Schmitz, S.; Offer G.; Bullard, B.; Leonard, K.; Holt, J. and Trinick, J., 2004a. Structural studies of arthrin: monoubiquitinated actin. *Journal of molecular biology*, 341(5), pp.1161–1173.

Burgess, S.A., Walker, M.L., Thirumurugan, K., Trinick, J. and Knight, P., 2004b. Use of negative stain and single-particle image processing to explore dynamic properties of flexible macromolecules. *Journal of structural biology*, 147(3), pp.247–258.

Campbell, N.A. and Reece, J.B., 2005. *Biology* 7th Edition, San Francisco: Pearson-Benjamin Cummings.

Carlson, L.-A.; Briggs, J.A.G; Glass, B.; Riches, J.D.; Simon, M.N.; Johnson, M.C.; Müller, B.; Grünewald, K. and Kräusslich, H.G., 2008. Three-dimensional analysis of budding sites and released virus suggests a revised model for HIV-1 morphogenesis. *Cell host and microbe*, 4(6), pp.592–599.

Cheng, N.Q. and Deatherage, J.F., 1989. Three-dimensional reconstruction of the Z disk of sectioned bee flight muscle. *The Journal of cell biology*, 108(5), pp.1761–1774.

Cheng, Y. and Walz, T., 2009. The advent of near-atomic resolution in single-particle electron microscopy. *Annual review of biochemistry*, 78, pp.723–742.

Clark, K.A.; McElhinny, A.S.; Beckerle, M.C. and Gregorio, C.C.; 2002. Striated muscle cytoarchitecture: an intricate web of form and function. *Annual review of cell and developmental biology*, 18, pp.637–706.

Corsi, A. and Perry, S.V., 1958. Some observations on the localization of myosin, actin and tropomyosin in the rabbit myofibril. *The Biochemical journal*, 68(1), pp.12–17.

Crabtree, G.R., 2001. Calcium, calcineurin, and the control of transcription. *The Journal of biological chemistry*, 276(4), pp.2313–2316.

Craig, R., 2006. Structure and function of myosin filaments. *Current opinion in structural biology*, *16*(2), 204-212.

Craig, R. and Padrón, R., 2004. Molecular structure of the sarcomere. *Myology 3rd ed Myology 3rd* Ed., Chapter 7, pp.129-166.

de Almeida Ribeiro Jr, E., Pinotsis, N., Ghisleni, A., Salmazo, A., Konarev, P.V., Kostan, J., Sjoeblom, B., Schreiner, C., Polyansky, A.A., Gkougkoulia, E., Holt, M.R., Aachmann, F.L., Zagrovic, B., Bordignon, E., Pirker, K.F., Svergun, D.I., Gautel, M., Djinovic-Carugo, K., 2014, The Structure and Regulation of Human Muscle α-Actinin., *Cell*, 159, pp. 1447 -1460.

de Carlo, S. and Harris, J.R., 2011. Negative staining and cryo-negative staining of macromolecules and viruses for TEM. *Micron (Oxford, England : 1993)*, 42(2), pp.117–131.

de Haas, F., Schoenmakers, R.; Voigt, A.; Voorhout, W. and van Duinen, G., 2012. *Xplore 3D. Application instructions*, FEI Nanoport Life Sciences.

Contompasis, J. L., Nyland, L. R., Maughan, D. W., Vigoreaux, J. O., 2010. Flightin is necessary for length determination, structural integrity, and large bending stiffness of insect flight muscle thick filaments. *Journal of molecular biology*, *395*(2), 340-348.

Deatherage, J.F., Cheng, N.Q. and Bullard, B., 1989. Arrangement of filaments and cross-links in the bee flight muscle Z disk by image analysis of oblique sections. *The Journal of cell biology*, 108(5), pp.1775–1782.

Donnelly, A.J. and Djuric, M., 1991. Cardioplegia solutions. *American Journal of Health-System Pharmacy*, *48*(11), 2444-2460.

Dubochet, J. and Lepault, J., 1984. Cryo-electron microscopy of vitrified water. *Le Journal de Physique Colloques*, 45(C7), pp.C7–85–C7–94.

Dubochet, J., Adrian, M. and Lepault, J., 1985. Emerging techniques: Cryo-electron microscopy of vitrified biological specimens. *Trends in Biochemical Sciences*, *10*(4), 143-146.

Epstein, N.D. and Davis, J.S., 2003. Sensing stretch is fundamental. *Cell*, 112(2), pp.147–150.

Eppenberger, H. M., Perriard, J. C., Rosenberg, U. B., & Strehler, E. E., 1981. The Mr 165,000 M-protein myomesin: a specific protein of cross-striated muscle cells. *The Journal of cell biology*, *89*(2), 185-193.

Erickson, H. and Klug, A., 1971. Measurement and Compensation of Defocusing and Aberrations by Fourier Processing of Electron Micrographs. *Philosophical Transactions of the Royal Society of London. Series BBiological Sciences*, 261(837), pp.105–118.

Ervasti, J.M., 2003. Costameres: the Achilles' heel of Herculean muscle. *Journal of Biological Chemistry*, 278(16), pp.13591–13594.

Faruqi, A.R. and Subramaniam, S., 2000. CCD detectors in high-resolution biological electron microscopy. *Quarterly reviews of biophysics*, 33(01), pp.1–27.

Faul, C., Dhume, A., Schecter, A. D., & Mundel, P., 2007. Protein kinase A, Ca2+/calmodulin-dependent kinase II, and calcineurin regulate the intracellular trafficking of myopodin between the Z-disc and the nucleus of cardiac myocytes. *Molecular and cellular biology*, *27*(23), 8215-8227.

Faulkner, G., Lanfranchi, G. and Valle, G., 2001. Telethonin and other new proteins of the Z-disc of skeletal muscle. *IUBMB life*, 51(5), pp.275–282.

Faulkner, G., Pallavicini, A., Comelli, A., Salamon, M., Bortoletto, G., Ievolella, C., Trevison, S., Kojić, S., Vecchia, F., Laveder, P., Valle, G, Lanfranchi, G., 2000. FATZ, a filamin-, actinin-, and telethonin-binding protein of the Z-disc of skeletal muscle. *Journal of Biological Chemistry*, *275*(52), 41234-41242.

Fawcett, D.W. and McNutt, N.S., 1969. The ultrastructure of the cat myocardium. I. Ventricular papillary muscle. *The Journal of cell biology*, 42(1), pp.1–45.

Ferguson, C., Lakey, A., Hutchings, A., Butcher, G. W., Leonard, K. R., Bullard, B., 1994. Cytoskeletal proteins of insect muscle: location of zeelins in Lethocerus flight and leg muscle. *Journal of cell science*, *107*(5), 1115-1129.

Fernández, I.S.; Bai, X.C.; Murshudov, G.; Scheres, S.H.W. and Ramakrishnan, V.; 2014. Initiation of Translation by Cricket Paralysis Virus IRES Requires Its Translocation in the Ribosome. *Cell*, 157(4), pp.823–831.

Filatov, V.L.; Katrukha, A.G.; Bulargina, T.V. and Gusev, N.B., 1999. Troponin: structure, properties, and mechanism of functioning. *Biochemistry. Biokhimiiâ*, 64(9), pp.969–985.

Frank, D. and Frey, N., 2011. Cardiac Z-disc signaling network. *The Journal of biological chemistry*, 286(12), pp.9897–9904.

Frank, D.; Kuhn, C.; Katus, H. and Frey, N.; 2006. The sarcomeric Z-disc: a nodal point in signalling and disease. *Journal of Molecular Medicine*, *84*(6), 446-468.

Frank, J., 2006. Three-dimensional electron microscopy of macromolecular assemblies. Visualization of biological molecules in their native state. Chapter 5 - Three-dimensional reconstruction, *Oxford University Press*, 173-277.

Franzini-Armstrong, C., 1973. The structure of a simple Z line. *The Journal of cell biology*, 58(3), pp.630–642.

Franzot, G., Sjöblom, B., Gautel, M., & Carugo, K. D., 2005. The crystal structure of the actin binding domain from α-actinin in its closed conformation: structural insight into phospholipid regulation of α-actinin. *Journal of molecular biology*, *348*(1), 151-165.

Frey N, Olson EN, 2002. Calsarcin-3, a novel skeletal muscle- specific member of the calsarcin family, interacts with multiple Z-disc proteins. *J Biol Chem*, 277:13998–14004.

Frey, N., Barrientos, T., Shelton, J. M., Frank, D., Rütten, H., Gehring, D., Kuhn, C., Lutz, M., Rothermel, B., Bassel-Duby, R., Richardson, J., Katus, H., Olson, E. N., 2004. Mice lacking calsarcin-1 are sensitized to calcineurin signaling and show accelerated cardiomyopathy in response to pathological biomechanical stress. *Nature medicine*, 10(12), 1336-1343.

Funatsu, T.; Kono, E.; Higuchi, H.; Kimura, S.; Ishiwata, S.; Yoshioka, T.; Maruyama, K. and Tsukita, S., 1993. Elastic filaments in situ in cardiac muscle: deep-etch replica analysis in combination with selective removal of actin and myosin filaments. *The Journal of cell biology*, 120(3), pp.711–724.

Funatsu, T., Higuchi, H. andand Ishiwata, S., 1990. Elastic filaments in skeletal muscle revealed by selective removal of thin filaments with plasma gelsolin. *The Journal of cell biology*, 110(1), pp.53–62.

Garamvölgyi, N., Metzger-Torok, G. and Tigyi-Sebes, A., 1962. The Z- and M-formations of straited muscle. *Acta physiologica Academiae Scientiarum Hungaricae*, 22, pp.223–233.

Gautel, M., 2011. The sarcomeric cytoskeleton: who picks up the strain? *Current Opinion in Cell Biology*, 23(1), pp.39–46.

Gautel,M., Goulding, D., Bullard, B.,Weber, K., Furst, D., 1996. The central Z-disk region of titin is assembled from a novel repeat in variable copy numbers. *J. Cell Sci*. 109, 2747–2754.

Geeves, M.A. and Holmes, K.C., 1999. Structural mechanism of muscle contraction. *Annual review of biochemistry*, 68, pp.687–728.

Geier, C., Gehmlich, K., Ehler, E., Hassfeld, S., Perrot, A., Hayess, K., Cardim, N., Venzel, K., Erdmann, B., Krackhardt, F., Posch, M., Bublak, A., Nagele, H., Scheffoldt, T., Dietz, R., Chien, K., Spuler, S., Fürst, D., Nürnberg, P., Özcelik, C., 2008. Beyond the sarcomere: CSRP3 mutations cause hypertrophic cardiomyopathy. *Human molecular genetics*, *17*(18), 2753-2765.

Gest, H., 2004. The discovery of microorganisms by Robert Hooke and Antoni Van Leeuwenhoek, fellows of the Royal Society. *Notes and records of the Royal Society of London*, 58(2), pp.187–201.

Gil, D., Carazo, J.M. and Marabini, R., 2006. On the nature of 2D crystal unbending. *Journal of structural biology*, 156(3), pp.546–555.

Gipson, B., Zeng, X., Zhang, Z. Y., & Stahlberg, H., 2007. 2dx—User-friendly image processing for 2D crystals. *Journal of structural biology*, *157*(1), 64-72.

Goldstein, M.A.; Michael, L.H.; Schroeter, J.P. and Sass, R.L., 1987. Z band dynamics as a function of sarcomere length and the contractile state of muscle. *FASEB journal : official publication of the Federation of American Societies for Experimental Biology*, 1(2), pp.133–142.

Golji, J., R. Collins, M. R. Mofrad., 2009. Molecular mechanics of the alpha-actinin rod domain: bending, torsional, and extensional behavior. *PLOS Comput.* Biol. 5:e1000389.

Gontier, Y.; Taivainen, A.; Fontao, L.; Sonnenberg, A.; van der Flier, A.; Carpén, O.; Faulkner, G. and Borradori, L., 2005. The Z-disc proteins myotilin and FATZ-1 interact with each other and are connected to the sarcolemma via muscle-specific filamins. *Journal of cell science*, 118(Pt 16), pp.3739–3749.

Gordon, D.A. and Lowey, S., 1992. Distribution of developmental myosin isoforms in isolated A-segments. *Journal of muscle research and cell motility*, 13(6), pp.654–667.

Granger, B. and Lazarides, E., 1978. The existence of an insoluble Z disc scaffold in chicken skeletal muscle. *Cell*, *15*(4), 1253-1268.

Granzier, H.L. and Irving, T.C., 1995. Passive tension in cardiac muscle: contribution of collagen, titin, microtubules, and intermediate filaments. *Biophysical journal*, 68(3), pp.1027–1044.

Granzier, H.L. and Wang, K., 1993. Passive tension and stiffness of vertebrate skeletal and insect flight muscles: the contribution of weak cross-bridges and elastic filaments. *Biophysical journal*, 65(5), pp.2141–2159.

Gregorio, C.C.; K Trombitás, K.; Centner, T.; Kolmerer, B.; Stier, G.; Kunke, K.; Suzuki, K.; Obermayr, F.; Herrmann, B.; Granzier, H.; Sorimachi, H. and Labeit, S., 1998. The NH2 terminus of titin spans the Z-disc: its interaction with a novel 19-kD ligand (T-cap) is required for sarcomeric integrity. *The Journal of cell biology*, 143(4), pp.1013–1027.

Gregorio CC, Poller W, Schaper J, Schultheiss HP, Chien KR, 2002. The cardiac mechanical stretch sensor machinery involves a Z-disc complex that is defective in a subset of human dilated cardiomyopathy. *Cell*, 111:943–955.

Grigorieff, N., 2013. Direct detection pays off for electron cryo-microscopy. *eLife*, 2, p.e00573.

Hall, C.E., 1956. Method for the observation of macromolecules with the electron microscope illustrated with micrographs of DNA. *The Journal of biophysical and biochemical cytology*, 2(5), pp.625–628.

Hampton, C., Taylor, D. and Taylor, K., 2007. Novel Structures for [alpha]-Actinin: F-Actin Interactions and their Implications for Actin-Membrane Attachment and Tension Sensing in the Cytoskeleton. *Journal of molecular biology*, *368*(1), 92-104.

Hanson, J. and Huxley, H.E., 1953. Structural basis of the cross-striations in muscle. *Nature*, 172(4377), pp.530–532.

Harsányi, V. and Garamvölgyi, N., 1969. On the Z-substance of striated muscle. *Acta biochimica et biophysica; Academiae Scientiarum Hungaricae*, 4(3), pp.259–264.

Hayat, M.A., 2000. *Principles and techniques of electron microscopy - Biological application* 4 ed, Cambridge University Press.

Hayles, M.F.; Matthijs de Winter, D.A.; Schneijdenberg, C.; Meeldijk, J.; Luecken, U.; Persoon, H.; de Water, J.; de Jong, F.; Humbel, B.M. and Verkleij, A.J., 2010. The making of frozen-hydrated, vitreous lamellas from cells for cryo-electron microscopy. *Journal of structural biology*, 172(2), pp.180–190.

Henderson, G.P., Gan, L. and Jensen, G.J., 2007. 3-D ultrastructure of O. tauri: electron cryotomography of an entire eukaryotic cell. *PloS one*, 2(1), p.e749.

Henderson, R., 2004. Realizing the potential of electron cryo-microscopy. *Quarterly reviews of biophysics*, *37*(01), 3-13.

Henderson, R. and Unwin, P.N., 1975. Three-dimensional model of purple membrane obtained by electron microscopy. *Nature*, 258(5533), pp.351–352.

Henderson, R.; Baldwin, J.M.; Ceska, T.A.; Zemlin, F.; Beckmann, E. and Downing, K.H., 1990. Model for the structure of bacteriorhodopsin based on high-resolution electron cryo-microscopy. *Journal of molecular biology*, 213(4), pp.899–929.

Henderson, R.; Sali, A.; Baker, M.; Carragher, B.; Devkota, B.; Downing, K.H.; Egelman, E.H.; Feng, Z.; Frank, J.; Grigorieff, N.; Jiang, W.; Ludtke, S.J.; Medalia, O.; Penczek, P.; Rosenthal, P.B.; Rossmann, M.G.; Schmid, M.F.; Schröder, G.F.; Steven, A.C.; Stokes, D.L.; Westbrook, J.D.; Wriggers, W.; Yang, H.; Young, J; Berman, H.M.; Chiu, W.; Kleywegt, G.J. and Lawson, C.L., 2012. Outcome of the first electron microscopy validation task force meeting. *Structure*, 20(2), pp. 205–214.

Henderson, R.; Baldwin, J.M.; Downing, K.H.; Lepault, L. and Zemlin, F., 1986. Structure of purple membrane from halobacterium halobium: recording, measurement and evaluation of electron micrographs at 3.5 Å resolution. *Ultramicroscopy*, 19(2), pp.147–178.

Henzel, W.J.; Billeci, T.M.; Stults, J.T.; Wong, S.C.; Grimley, C. and Watanabe, C., 1993. Identifying proteins from two-dimensional gels by molecular mass searching of peptide fragments in protein sequence databases. *Proceedings of the National Academy of Sciences,* (90), pp.5011-5015.

Higuchi, H., 1992. Changes in contractile properties with selective digestion of connectin (titin) in skinned fibers of frog skeletal muscle. *Journal of biochemistry*, 111(3), pp.291–295.

Holmes, K. C., R. T. Tregear, J. Barrington Leigh. 1980. Interpretation of the low angle X-ray diffraction from insect flight muscle in rigor. *Proceedings of the Royal Society of London. Series B. Biological Sciences* 207.1166, 13-33.

Holmes, K., 2011. Steric blocking mechanism explains stretch activation in insect flight muscle. *Proceedings of the National Academy of Sciences*, 108, pp.7–8.

Hooper, S.L. and Thuma, J.B., 2005. Invertebrate Muscles: Muscle Specific Genes and Proteins. *Physiological reviews*, *85*(3), 1001-1060.

Hsieh, C.-E.; Leith, A.; Mannella, C.; Frank, J. and Marko, M., 2006. Towards high-resolution three-dimensional imaging of native mammalian tissue: electron tomography of frozen-hydrated rat liver sections. *Journal of structural biology*, 153(1), pp.1–13.

Hunter, E.E., 1993. *Practical Electron Microscopy: A Beginner's Illustrated Guide*, Cambridge University Press.

Huxley, H.E. and Hanson, J, 1954. Changes in the cross-striations of muscle during contraction and stretch and their structural interpretation. *Nature* 173:973–976.

Huxley, A.F. and Niedergerke, R, 1954. Structural changes in muscle during contraction. *Nature* 173:971–973.

Iancu, C.V.; Tivol, W.F.; Schooler, J.B.; Dias, D.P.; Henderson, G.P.; Murphy, G.E.; Wright, E.R.; Li, Z.; Yu, Z.; Briegel, A.; Gan, L.; He, Y. and Jensen, G.J., 2006. Electron cryotomography sample preparation using the Vitrobot. *Nature protocols*, 1(6), pp.2813–2819.

Iwamoto, H., Nishikawa, Y., Wakayama, J. I., Fujisawa, T., 2002. Direct X-ray observation of a single hexagonal myofilament lattice in native myofibrils of striated muscle. *Biophysical journal*, *83*(2), 1074-1081.

Iwamoto, H. and Yagi, N., 2013. The molecular trigger for high-speed wing beats in a bee. *Science (New York, NY)*, 341(6151), pp.1243–1246.

Iwamoto, H., Inoue, K. and Yagi, N., 2006. Evolution of long-range myofibrillar crystallinity in insect flight muscle as examined by X-ray cryomicrodiffraction. *Proceedings. Biological sciences / The Royal Society*, 273(1587), pp.677–685.

Jésior, J., 1986. How to avoid compression II. The influence of sectioning conditions. *Journal of Ultrastructure and Molecular Structure Research, 95*(1), 210-217.

Jésior, J.C., 1985. How to avoid compression: a model study of latex sphere grid sections. *Journal of ultrastructure research*, 90(2), pp.135–144.

Jésior, J.C., 1989. Use of low-angle diamond knives leads to improved ultrastructural preservation of ultrathin sections. *Scanning microscopy Supplement*, 3, pp.147–52; discussion 152–3.

Jiang, W.; Baker, M.L.; Jakana, J.; Weigele, P.R.; King, J. and Chiu, W., 2008. Backbone structure of the infectious ε15 virus capsid revealed by electron cryomicroscopy. *Nature*, 451(7182), pp.1130–1134.

Jin, J. P., Wang, K., 1991. Nebulin as a giant actin-binding template protein in skeletal muscle sarcomere Interaction of actin and cloned human nebulin fragments. *FEBS*

letters, *281*(1), 93-96.

Josephson, R.K., Malamud, J.G. and Stokes, D.R., 2000. Asynchronous muscle: a primer. *The Journal of experimental biology*, 203(Pt 18), pp.2713–2722.

Kastner, B.; Fischer, N.; Golas, M.; Sander, B.; Dube, P.; Boehringer, D; Hartmuth, K.; Deckert, J.; Hauer, F.; Wolf, E.; Uchtenhagen, H.; Urlaub, H.; Herzog, F.; Peters, J.M.; Poerschke, D.; Lührmann, R. and Stark, H, 2008. GraFix: sample preparation for single-particle electron cryomicroscopy. *Nature methods*, 5(1), pp.53–55.

Katzemich, A.; Liao, K.A.; Czerniecki, S. and Schöck, F., 2013. Alp/Enigma Family Proteins Cooperate in Z-Disc Formation and Myofibril Assembly. *PLOS Genetics*, 9(3), p.e1003342.

Kazmierski, S.T.; Antin, P.B.; Witt, C.C.; Huebner, N.; McElhinny, A.; Labeit, S. and Gregorio., C.C., 2003. The complete mouse nebulin gene sequence and the identification of cardiac nebulin. *Journal of molecular biology*, 328(4), pp.835–846.

Klaavuniemi, T.; Kelloniemu, A.; Ylänne, J., 2004. The ZASP-like motif in actinin-associated LIM protein is required for interaction with the alpha-actinin rod and for targeting to the muscle Z-line. *J Biol Chem.,*279(25):26402-10

Knight, P. and Trinick, J., 1982. [2] Preparation of myofibrils. *Methods in enzymology*, 85, pp.9–12.

Knispel, R.W.; Kofler, C.; Boicu, M.; Baumeister, W. and Nickell, S., 2012. Blotting protein complexes from native gels to electron microscopy grids. *Nature methods*, 9(2), pp.182–184.

Knöll R, Hoshijima M, Hoffman HM, Person V, Lorenzen-Schmidt I, Bang ML, Hayashi T, Shiga N, Yasukawa H, Schaper, W, McKenn, aW, Yokoyama M, Schork NJ, Omens JH, McCulloch AD, Kimura, Gregorio, C., Schaper, J., Schultheiss, H., Chien, K., 2002. The cardiac mechanical stretch sensor machinery involves a Z disc complex that is defective in a subset of human dilated cardiomyopathy. *Cell*, *111*(7), 943-955.

Knöll, R. and Buyandelger, B., 2012. Z-disc Transcriptional Coupling, Sarcomeroptosis and Mechanopoptosis. *Cell Biochemistry and Biophysics*, 66(1), pp.65–71.

Kölliker, A., 1888, Zur Kenntnis dei quergestreiften Muskelfasern, I., *Zeitschf f. wiss Zool*. 47: 689-710.

Komeili, A.; Li, Z.; Newman, D. and Jensen, G.J., 2006. Magnetosomes Are Cell Membrane Invaginations Organized by the Actin-Like Protein MamK. *Science*, 311(5758), pp.242–245.

Koning, R.I. and Koster, A.J., 2009. Cryo-electron tomography in biology and medicine. *Annals of Anatomy - Anatomischer Anzeiger*, 191(5), pp.427–445.

Koning, R.I.; Faas, F.G.; Boonekamp, M.; de Visser, B.; Janse, J.; Wiegant, J.C.; de Breij, A.; Willemse, J.; Nibbering, P.H.; Tanke, H.J. and Koster, A.J. 2014. MAVIS: an integrated system for live microscopy and vitrification.

Ultramicroscopy, 143, pp.67–76.

Kremer, J.R., Mastronarde, D.N. and McIntosh, J.R., 1996. Computer visualization of three-dimensional image data using IMOD. *Journal of structural biology*, 116(1), pp.71–76.

Kukulski, W.; Schorb, M.; Welsch, S.; Picco, A.; Kaksonen, M. and Briggs, J.A.G., 2011. Correlated fluorescence and 3D electron microscopy with high sensitivity and spatial precision. *The Journal of cell biology*, 192(1), pp.111–119.

Kulke, M.; Neagoe, C.; Kolmerer, B.; Minajeva, A.; Hinssen, H.; Bullard, B and Linke, W.A, 2001. Kettin, a major source of myofibrillar stiffness in Drosophila indirect flight muscle. *The Journal of cell biology*, 154(5), pp.1045–1057.

Kunji, E.R.S.; von Gronau, S.; Oesterhelt, D. and Henderson, R., 2000. The three-dimensional structure of halorhodopsin to 5 Å by electron crystallography: A new unbending procedure for two-dimensional crystals by using a global reference structure. *Proceedings of the National Academy of Sciences,* (97), pp.4637-4642.

Kussmann, M.; Nordhoff, E.; Rahbek-Nielsen, H.; Haebel, S.; Rossel-Larsen, M.; Jakobsen, L.; Gobom, J.; Mirgorodskaya, E.; Kroll-Kristensen, A.; Palm, L. and Roepstorff, P., 1997. Matrix-assisted Laser Desorption/Ionization Mass Spectrometry Sample Preparation Techniques Designed for Various Peptide and Protein Analytes. *Journal of Mass Spectrometry*, 32(6), pp.593–601.

Kühlbrandt, W., 2014. The Resolution Revolution. *Science (New York, NY)*, 343(6178), pp.1443–1444.

Labeit, S.; Gibson, T,; Lakey, A.; Leonard, K., Zeviani, M.; Knight, P., Wardale, J. and Trinick, J., 1991. Evidence that nebulin is a protein-ruler in muscle thin filaments. *FEBS letters*, 282(2), pp.313–316.

Labeit, S., Ottenheijm, C.A.C. and Granzier, H., 2011. Nebulin, a major player in muscle health and disease. *The FASEB journal*, *25*(3), 822-829.

Laemmli, U.K., 1970. Cleavage of structural proteins during the assembly of the head of bacteriophage T4. *Nature*, 227(5259), pp.680–685.

Lancaster, M.K. and Harrison, S.M., 1998. Changes in contraction, cytosolic Ca2+ and pH during metabolic inhibition and upon restoration of mitochondrial respiration in rat ventricular myocytes. *Experimental physiology*, 83(3), pp.349–360.

Landon, F., Gache, Y., Touitou, H., & Olomucki, A., 1985. Properties of two isoforms of human blood platelet α-actinin. *European Journal of Biochemistry*, *153*(2), 231-237.

Lange, S., Himmel, M., Auerbach, D., Agarkova, I., Hayess, K., Fürst, D. O., Ehler, E., 2005. Dimerisation of myomesin: implications for the structure of the sarcomeric M-band. *Journal of molecular biology*, *345*(2), 289-298.

Leis, A.; Andrees, L. and Baumeister, W., 2009. Visualizing cells at the nanoscale. *Trends in Biochemica*l *Sciences,* 34(2), pp.60-70.

Lek, M. and North, K.N., 2010. Are biological sensors modulated by their structural scaffolds? The role of the structural muscle proteins alpha-actinin-2 and alpha-actinin-3 as modulators of biological sensors. *FEBS letters*, 584(14), pp.2974–2980.

Linnemann, A., van der Ven, P. F., Vakeel, P., Albinus, B., Simonis, D., Bendas, G., Fürst, D. O., 2010. The sarcomeric Z-disc component myopodin is a multiadapter protein that interacts with filamin and α-actinin. *European journal of cell biology*, *89*(9), 681-692.

Linke, W.A., 2008. Sense and stretchability: the role of titin and titin-associated proteins in myocardial stress-sensing and mechanical dysfunction. *Cardiovascular research*, 77(4), pp.637–648.

Linke, W.A., Bartoo, M.L. and Pollack, G.H., 1993. Spontaneous sarcomeric oscillations at intermediate activation levels in single isolated cardiac myofibrils. *Circulation research*, 73(4), pp.724–734.

Littlefield, R.S. and Fowler, V.M., 2008. Thin filament length regulation in striated muscle sarcomeres: pointed-end dynamics go beyond a nebulin ruler. *Seminars in cell and developmental biology*, 19(6), pp.511–519.

Lodish, H.; Baltimore, D.; Berk, A.; Zipursky, S.L.; Matsudaira, P. and Darnell, J., 1995. *Molecular Cell Biology* 3rd ed, Scientific American Books.

Lucic, V., Rigort, A. and Baumeister, W., 2013. Cryo-electron tomography: The challenge of doing structural biology in situ. *The Journal of cell biology*, 202(3), pp.407–419.

Luther, P., 2000. Three-Dimensional Structure of a Vertebrate Muscle Z-band: Implications for Titin and α-Actinin Binding. *Journal of structural biology*, 129(1), pp.1–16.

Luther, P., Barry, J., Squire, J., 2002. The three-dimensional structure of a vertebrate wide (slow muscle) Z-band: lessons on Z-band assembly1. *Journal of Molecular Biology*, *315*(1), 9-20.

Luther, P. and Squire, J., 2002. Muscle Z-band ultrastructure: titin Z-repeats and Z-band periodicities do not match. *Journal of Molecular Biology,* (319), 1157-1164.

Luther, P., 2005. Sample shrinkage and radiation damage of plastic sections. Chapter 1 - Electron tomography. Methods for three-dimensional visualization of structures in the cell. Second Edition. J. Frank, ed., Springer., 17-49.

Luther, P.K., 2009. The vertebrate muscle Z-disc: sarcomere anchor for structure and signalling. *Journal of muscle research and cell motility*, 30(5-6), pp.171–185.

Luther, P.K., 1991. Three-dimensional reconstruction of a simple Z-band in fish muscle. *The Journal of cell biology*, 113(5), pp.1043–1055.

Luther, P.K. and Morris, E.P., 2003. Cryoelectron microscopy of refrozen cryosections. *Journal of structural biology*, 142(2), pp.233–240.

Luther, P.K., Winkler, H.; Taylor, K.; Zoghbi, M.; Craig, R.; Padrón, R.; Squire, J.M.; and Liu, J., 2011. Direct visualization of myosin-binding protein C bridging myosin and actin filaments in intact muscle. *Proceedings of the National Academy of Sciences*, 108(28), pp.11423–11428.

Lymn, R.W. and Taylor, E.W., 1971. Mechanism of adenosine triphosphate hydrolysis by actomyosin. *Biochemistry*, 10(25), pp.4617–4624.

MacArthur, D. G., Seto, J. T., Chan, S., Quinlan, K. G., Raftery, J. M., Turner, N., Nicholson, M., Kee, A., Hardeman, E., Gunning, P., Cooney, G., Head, S., Yang, N.n North, K. N. 2008. An Actn3 knockout mouse provides mechanistic insights into the association between α-actinin-3 deficiency and human athletic performance. *Human molecular genetics*, *17*(8), 1076-1086.

Maiellaro-Rafferty, K.; Wansapura, J.P.;Mendsaikhan, U.; Osinska, H.; James, J.F.; Taylor, M.D.; Robbins, J; Kranias, E.G.; Towbin, J.A. and Purevjav, E., 2013. Altered regional cardiac wall mechanics are associated with differential cardiomyocyte calcium handling due to nebulette mutations in preclinical inherited dilated cardiomyopathy. *Journal of molecular and cellular cardiology*, 60, pp.151–160.

Marko, M.; Hsieh, C.; Schalek, R.; Frank, J. and Mannella, C.; 2007. Focused-ion-beam thinning of frozen-hydrated biological specimens for cryo-electron microscopy. *Nature methods*, 4(3), pp.215–217.

Maruyama, K.; Kimura, S.; Ohashi, K. and Kuwano, Y., 1981. Connectin, an Elastic Protein of Muscle. Identification of "Titin" with Connectin. *Journal of biochemistry*, *89*(3), 701-709.

Masaki, T.; Takaiti, O., 1974. M-protein. *Journal of biochemistry*, *75*(2), 367-380.

Mastronarde, D.N., 2005. Automated electron microscope tomography using robust prediction of specimen movements. *Journal of structural biology*, 152(1), pp.36–51.

Mastronarde, D.N., 1997. Dual-axis tomography: an approach with alignment methods that preserve resolution. *Journal of structural biology*, 120(3), pp.343–352.

McDonald, K.L. and Auer, M., 2006. High-pressure freezing, cellular tomography, and structural cell biology. *BioTechniques*, 41(2), pp.137-141.

McElhinny, AS, Kolmerer, B, Fowler, VM, Labeit S, Gregorio CC., 2001. The N-terminal end of nebulin interacts with tropomodulin at the pointed ends of the thin filaments. *J Biol Chem*, 276:583–592.

McLendon, P. M., & Robbins, J., 2011. Desmin-related cardiomyopathy: an unfolding story. *American Journal of Physiology-Heart and Circulatory Physiology*, *301*(4), 1220-1228.

McMullan, G., Clark, A.T.; Turchetta, R. and Faruqi, A.R.; 2009. Enhanced imaging in low dose electron microscopy using electron counting. *Ultramicroscopy*, 109(12), pp.1411–1416.

Michel, R. and Dunn, S., 2004. Calcineurin and skeletal muscle growth. *Proceedings of the Nutrition Society* (2004), 63, 341–349.

Mohapatra, B., Jimenez, S., Lin, J. H., Bowles, K. R., Coveler, K. J., Marx, J. G., Chrisco, M., Murphy, R., Lurie, P., Schwartz, R., Elliot, P., Vatta, M., McKenna, W., Towbin, J., Bowles, N. E., 2003. Mutations in the muscle LIM protein and α-actinin-2 genes in dilated cardiomyopathy and endocardial fibroelastosis. *Molecular genetics and metabolism*, *80*(1), 207-215.

Molkentin JD, Lu JR, Antos CL, Markham B, Richardson J, Robbins J, Grant SR, Olson EN, 1998. A calcineurin- dependent transcriptional pathway for cardiac hypertrophy. *Cell* 93:215–228.

Moncman, C.L. and Wang, K., 1995. Nebulette: a 107 kD nebulin- like protein in cardiac muscle. *Cell Motil. Cytoskeleton,* 32, 205– 225.

Moncman, C.L. and Wang, K., 2002. Targeted disruption of nebulette protein expression alters cardiac myofibril assembly and function. *Exp. Cell Res*. 273, 204–218.

Moreira, E. S., Wiltshire, T. J., Faulkner, G., Nilforoushan, A., Vainzhof, M., Suzuki, O. T., Valle, G., Reeves, R., Zatz, M., Passoss-Bueno, M. R., Jenne, D. E., 2000. Limb-girdle muscular dystrophy type 2G is caused bymutations in the gene encoding the sarcomeric protein telethonin. *Nature Genet*. 24, 163-166.

Morris, E., Nneji, G. and Squire, J.M., 1990. The three-dimensional structure of the nemaline rod Z-band. *The Journal of cell biology*, 111(6), pp.2961–2978.

Mould, A.P.; Holmes, D.F.; Kadler, K.E. and Chapman, J.A. 1985. Mica sandwich technique for preparing macromolecules for rotary shadowing. *Journal of ultrastructure research*, 91(1), pp.66–76.

Mues, A., van der Ven, P. F. M., Young, P., Furst, D. O., Gautel, M., 1998. Two immunoglobulin-like domains of the Z-disc portion of titin interact in a conformation-dependen t way with telethonin. *FEBS Lett*. 428, 111–114.

Murakami, K.; Yasunaga, T.; Noguchi, T.Q.P.; Gomibuchi, Y.; Ngo, K.; Uyeda, T.Q.P. and Wakabayashi, T.; 2010. Structural basis for actin assembly, activation of ATP hydrolysis, and delayed phosphate release. *Cell*, 143(2), pp.275–287.

Murphy, G.E. and Jensen, G.J., 2007. Electron cryotomography. *BioTechniques*, 43(4), pp.413-417.

Narita, A.; Takeda, S.; Yamashita, A.; Maeda,Y; 2006. Structural basis of actin filament capping at the barbed-end: a cryo-electron microscopy study. *The EMBO journal*, 25(23), pp.5626–5633.

Nesterenko, M.V., Tilley, M. and Upton, S.J., 1994. A simple modification of Blum's silver stain method allows for 30 minute detection of proteins in polyacrylamide gels. *Journal of biochemical and biophysical methods*, 28(3), pp.239–242.

Ohashi, K., Mikawa, T. and Maruyama, K., 1982. Localization of Z-protein in isolated

Z-disk sheets of chicken leg muscle. *The Journal of cell biology*, *95*(1), 85-90.

Ohi, M.; Li, Y.; Cheng, Y.; Walz, T., 2004. Negative Staining and Image Classification - Powerful Tools in Modern Electron Microscopy. *Biological procedures online*, 6, pp.23–34.

Olivé, M.; Goldfarb, L.; Shatunov, A.; Fisher, D.; Ferrer, I., 2005. Myotilinopathy: refining the clinical and myopathological phenotype. *Brain : a journal of neurology*, 128(Pt 10), pp.2315–2326.

Ono, S., 2010. Dynamic regulation of sarcomeric actin filaments in striated muscle. *Cytoskeleton*, 67(11), pp.677–692.

Orlova, E.V. and Saibil, H.R., 2011. Structural Analysis of Macromolecular Assemblies by Electron Microscopy. *Chemical Reviews*, pp.7710–7748.

Otterbein, L. R., Graceffa, P., & Dominguez, R., 2001. The crystal structure of uncomplexed actin in the ADP state. *Science*, *293*(5530), 708-711.

Owen, G. and Stokes, D.L., 2007. An introduction to low dose electron tomography-from specimen preparation to data collection. *Modern Research and Educational Topics in Microscopy*, *2*, 939-950.

Papa I, Astier C, Kwiatek O, Raynaud F, Bonnal C, Lebart MC, Roustan C, Benyamin Y, 1999. Alpha actinin-CapZ, an anchoring complex for thin filaments in Z-line. *J Muscle Res Cell Motil* 20:187–197.

Papageorgopoulos, C., Caldwell, K., Schweingrubber, H., Neese, R. A., Shackleton, C. H. L., & Hellerstein, M., 2002. Measuring synthesis rates of muscle creatine kinase and myosin with stable isotopes and mass spectrometry. *Analytical biochemistry*, *309*(1), 1-10.

Pappas, C.T.; Bhattacharya, N.; Cooper, J.A.; Gregorio, C.C., 2008. Nebulin interacts with CapZ and regulates thin filament architecture within the Z-disc. *Molecular biology of the cell*, 19(5), pp.1837–1847.

Pappas, C.T.; Bliss K.T.; Zieseniss, A.; Gregorio, C.C., 2011. The Nebulin family: an actin support group. *Trends in cell biology*, 21(1), pp.29–37.

Paulin, D. and Li, Z., 2004. Desmin: a major intermediate filament protein essential for the structural integrity and function of muscle. *Experimental cell research*, 301(1), pp.1–7.

Peckham, M.; Cripps, R.; White, D., 1992. Mechanics and Protein Content of Insect Flight Muscles. *The Journal of experimental biology*, (168), pp.57–76.

Perz-Edwards, R.J. and Reedy, M.K., 2011. Electron microscopy and x-ray diffraction evidence for two z-band structural States. *Biophysical journal*, 101(3), pp.709–717.

Perz-Edwards, R. J., Irving, T. C., Baumann, B. A., Gore, D., Hutchinson, D. C., Kržič, U., Porter, R., Ward, A., Reedy, M. K., 2011. X-ray diffraction evidence for myosin-troponin connections and tropomyosin movement during stretch activation

of insect flight muscle. *Proceedings of the National Academy of Sciences*, *108*(1), 120-125.

Purevjav, E., Varela, J., Morgado, M., Kearney, D. L., Li, H., Taylor, M. D., Arimura, T., Moncman, C., McKenna, W., Murphy, R., Labeit, S., Vatta, M., Bowls, N., Kimura, A., Boriek, A., Towbin, J. A., 2010. Nebulette mutations are associated with dilated cardiomyopathy and endocardial fibroelastosis. *Journal of the American College of Cardiology*, *56*(18), 1493-1502.

Pyle, W. G., & Solaro, R. J., 2004. At the Crossroads of Myocardial Signaling The Role of Z-Discs in Intracellular Signaling and Cardiac Function. *Circulation Research*, *94*(3), 296-305.

Pyle, W.G., Hart, M.C, Cooper, JA, Sumandea, M.P; de Tombe, P.P; Solaro, R.J., 2002. Actin capping protein: an essential element in protein kinase signaling to the myofilaments. *Circulation research*, 90(12), pp.1299–1306.

Reedy, M.C., Reedy, M.K. and Goody, R.S., 1983a. Co-ordinated electron microscopy and X-ray studies of glycerinated insect flight muscle. II. Electron microscopy and image reconstruction of muscle fibres fixed in rigor, in ATP and in AMPPNP. *Journal of muscle research and cell motility*, 4(1), pp.55–81.

Reedy, M.K.; Goody, R.S.; Hoffman, W.; Rosenbaum, G., 1983b. Co-ordinated electron microscopy and X-ray studies of glycerinated insect flight muscle. I. X-ray diffraction monitoring during preparation for electron microscopy of muscle fibres fixed in rigor, in ATP and in AMPPNP. *Journal of muscle research and cell motility*, 4(1), pp.25–53.

Remedios, dos, C.G. and Gilmour, D., 1978. Is there a third type of filament in striated muscles? *Journal of biochemistry*, 84(1), pp.235–238.

Rosenthal, P.B. and Henderson, R., 2003. Optimal determination of particle orientation, absolute hand, and contrast loss in single-particle electron cryomicroscopy. *Journal of molecular biology*, 333(4), pp.721–745.

Royuela, M., Fraile, B., Arenas, M. I., Paniagua, R., 2000. Characterization of several invertebrate muscle cell types: a comparison with vertebrate muscles. *Microscopy research and technique*, *48*(2), 107-115.

Ruskin, R.S., Yu, Z. and Grigorieff, N., 2013. Quantitative characterization of electron detectors for transmission electron microscopy. *Journal of structural biology*, 184(3), pp.385–393.

Qiu, F., Brendel, S., Cunha, P. M., Astola, N., Song, B., Furlong, E. E., Bullard, B., 2005. Myofilin, a protein in the thick filaments of insect muscle. *Journal of cell science*, *118*(7), 1527-1536.

Sader, K.; Reedy, M.; Popp, D.; Lucaveche, C; Trinick, J., 2007. Measuring the resolution of uncompressed plastic sections cut using an oscillating knife ultramicrotome. *Journal of structural biology*, 159(1), pp.29–35.

Sader, K.; Studer, D.; Zuber, B.; Gnaegi, H.; Trinick, J., 2009. Preservation of high

resolution protein structure by cryo-electron microscopy of vitreous sections. *Ultramicroscopy*, 110(1), pp.43–47.

Saide, J.D. and Ullrick, W.C., 1974. Purification and properties of the isolated honeybee Z-disc. *Journal of molecular biology*, 87(4), pp.671–683.

Saide, J.D., Chin-Bow, C.; Hogan-Sheldon, J., Busquets-Turner; Vigoreaux, J.O.; Valgeirsdottir, K.; Pardue, M.L., 1989. Characterization of components of Z-bands in the fibrillar flight muscle of Drosophila melanogaster. *The Journal of cell biology*, 109(5), pp.2157–2167.

Sainsbury, G.M. and Bullard, B., 1980. New proline-rich proteins in isolated insect Z-discs. *The Biochemical journal*, 191(2), pp.333–339.

Sanger, J.W.; Wang. J.; Fan, Y.; White, J.; Sanger, J., 2010. Assembly and Dynamics of Myofibrils. *Journal of biomedicine and biotechnology*, 7, pp.1–8.

Sanger, J.W., Kang, S., Siebrands, C.C; Freeman, N.; Du, A.; Wang, J.; Stout, A.L.; Sanger, J.M., 2006. How to build a myofibril. *Journal of muscle research and cell motility*, 45(3), pp.317–337.

Saxton, W.O., Baumeister, W. and Hahn, M., 1984. Three-dimensional reconstruction of imperfect two-dimensional crystals. *Ultramicroscopy*, 13(1-2), pp.57–70.

Scheres, S. H., 2012. RELION: implementation of a Bayesian approach to cryo-EM structure determination. *Journal of structural biology*, *180*(3), 519-530.

Schiaffino, S., 2010. Fibre types in skeletal muscle: a personal account. *Acta physiologica (Oxford, England)*, 199(4), pp.451–463.

Schoenauer, R., Bertoncini, P., Machaidze, G., Aebi, U., Perriard, J. C., Hegner, M., & Agarkova, I., 2005. Myomesin is a molecular spring with adaptable elasticity. *Journal of molecular biology*, *349*(2), 367-379.

Schur, F., Hagen, W.; de Marco, A.; Briggs, J., 2013. Determination of protein structure at 8.5Å resolution using cryo-electron tomography and sub-tomogram averaging. *Journal of Structural Biology,* 184 (3), pp. 394-400.

Selcen, D., 2011. Myofibrillar myopathies. *Neuromuscular disorders : NMD*, 21(3), pp.161–171.

Sethi, R., Seppälä, J., Tossavainen, H., Ylilauri, M., Ruskamo, S., Pentikäinen, O. T., Permi, P., Ylänne, J., 2014. A Novel Structural Unit in the N-terminal Region of Filamins. *Journal of Biological Chemistry*, *289*(12), 8588-8598.

Shalaby, S., Mitsuhashi, H., Matsuda, C., Minami, N., Noguchi, S., Nonaka, I., Nishino, I., Hayashi, Y. K., 2009. Defective myotilin homodimerization caused by a novel mutation in MYOT exon 9 in the first Japanese limb girdle muscular dystrophy 1A patient. *Journal of Neuropathology & Experimental Neurology*, *68*(6), 701-707.

Silacci, P.; Mazzolai, L.; Gauci, C.; Stergiopulos, N.; Yin, H.L.; Hayoz, D., 2004. Gelsolin superfamily proteins: key regulators of cellular functions. *Cellular and*

molecular life sciences : CMLS, 61(19-20), pp.2614–2623.

Sjöblom, B., Salmazo, A. and Djinović-Carugo, K., 2008. Alpha-actinin structure and regulation. *Cellular and molecular life sciences : CMLS*, 65(17), pp.2688–2701.

Small, J.V. and Fürst, D.O., 1992. The cytoskeletal lattice of muscle cells. *European journal of biochemistry / FEBS*, 208, pp.559–572.

Somlyo, A.P. and Somlyo, A.V., 1994. Signal transduction and regulation in smooth muscle. *Nature*, 372(6503), pp.231–236.

Sousa, D.R., Stagg, S.M. and Stroupe, M.E., 2013. Cryo-EM structures of the actin:tropomyosin filament reveal the mechanism for the transition from C- to M-state. *Journal of molecular biology*, 425(22), pp.4544–4555.

Stahlberg, H. and Walz, T., 2008. Molecular electron microscopy: state of the art and current challenges. *ACS chemical biology*, 3(5), pp.268–281.

Stoscheck, C.M., 1990. [6] Quantitation of protein. *Methods in enzymology*, *182*, 50-68.

Sun, H.Q.; Yamamoto, Y.; Mejillano, M.; Yin, H.L., 1999. Gelsolin, a multifunctional actin regulatory protein. *Journal of Biological Chemistry*, 274(47), pp.33179–33182.

Sun, J. and Li, H., 2010. How to Operate a Cryo-Electron Microscope. In *Methods in enzymology*. Methods in Enzymology. Elsevier, pp. 231–249.

Taylor, K.A. and Glaeser, R.M., 1974. Electron Diffraction of Frozen, Hydrated Protein Crystals. *Science, New Series*, 186(4168), pp.1036–1037.

Taylor, K.A.; Reedy, M.C.; Cordova, L.; Reedy, M.K., 1984. Three-dimensional reconstruction of rigor insect flight muscle from tilted thin sections. *Nature*, 310(5975), pp.285–291.

Temprine, K., York, A. G., Shroff, H.,2015. Three-Dimensional Photoactivated Localization Microscopy with Genetically Expressed Probes. In *Advanced Fluorescence Microscopy* (pp. 231-261). Springer New York.

Tran, E. E., Borgnia, M. J., Kuybeda, O., Schauder, D. M., Bartesaghi, A., Frank, G. A., Sapiro, G., Milne, J., Subramaniam, S., 2012. Structural mechanism of trimeric HIV-1 envelope glycoprotein activation. *PLoS pathogens*, *8*(7), e1002797.

Trinick, J., Knight, P. and Whiting, A., 1984. Purification and properties of native titin. *Journal of molecular biology*, 180(2), pp.331–356.

Trombitás, K. and Granzier, H., 1997. Actin removal from cardiac myocytes shows that near Z line titin attaches to actin while under tension. *The American journal of physiology*, 273(2 Pt 1), pp.C662–70.

Tskhovrebova, L. and Trinick, J., 2003. Titin: properties and family relationships. *Nature reviews Molecular cell biology*, 4(9), pp.679–689.

Tskhovrebova, L., & Trinick, J., 2012. Molecular rulers?. *Current Biology*, *22*(9), R317-R318.

Tskhovrebova, L. and Trinick, J., 2012. Making muscle elastic: the structural basis of myomesin stretching. *PLoS biology*, 10(2), p.e1001264.

Tyler, J.M. and Branton, D., 1980. Rotary shadowing of extended molecules dried from glycerol. *Journal of ultrastructure research*, 71(2), pp.95–102.

Ubarretxena-Belandia, I. and Stokes, D.L., 2012. Membrane protein structure determination by electron crystallography. *Current opinion in structural biology*.

Vainzof, M.; Moreira, E.; Suzuki, O.; Faulkner, G.; Valle, G.; Beggs. A.; Carpen, O.; Ribeiro, A.; Zanoteli, E.; Gurgel-Gianneti, J.; Tsanaclis, A,; Silva, H.; Passos-Bueno, M. Zatz, M., 2002. Telethonin protein expression in neuromuscular disorders. *Biochimica et Biophysica Acta*, 1588(1), pp.33–40.

van Heel, M. and Schatz, M., 2005. Fourier shell correlation threshold criteria. *Journal of structural biology*, 151(3), pp.250–262.

van Heel, Gowen, M.B.; Matadeen, R.; Orlova, E.V.; Finn, R.; Pape, T.; Cohen, D.; Stark, H.; Schmidt, R.; Schatz, M. and Patwardhan, A.; 2000. Single-particle electron cryo-microscopy: towards atomic resolution. *Quarterly reviews of biophysics*, 33(4), pp.307–369.

van Straaten, M.; Goulding, D.; Kolmerer, B.; Labeit, S.; Clayton, J.; Leonard, K. and Bullard, B., 1999. Association of kettin with actin in the Z-disc of insect flight muscle. *Journal of molecular biology*, 285(4), pp.1549–1562.

Villa, E.; Schaffer, M.; Plitzko, J.M. and Baumeister, W. 2013. Opening windows into the cell: focused-ion-beam milling for cryo-electron tomography. *Current opinion in structural biology*, 23(5), pp.771–777.

Voorhees, R.M.; Fernández, I.S.; Scheres, S.H.W. and Hegde, R.S. 2014. Structure of the Mammalian ribosome-sec61 complex to 3.4 å resolution. *Cell*, 157(7), pp.1632–1643.

Von der Ecken, J., Müller, M., Lehman, W., Manstein, D. J., Penczek, P. A., & Raunser, S., 2014. Structure of the F-actin--tropomyosin complex. *Nature*. 1-3.

Vorgerd, M., van der Ven, P. F., Bruchertseifer, V., Löwe, T., Kley, R. A., Schröder, R., Lochmüller, H., Himmel, M., Koehler, K., Fürst, D.m Huebner, A., 2005. A mutation in the dimerization domain of filamin c causes a novel type of autosomal dominant myofibrillar myopathy. *The American Journal of Human Genetics*, *77*(2), pp.297-304.

Vreeker, A.; van Stuijvenberg, L.; Hund, T.J.; Mohler, P.J; Nikkels, P.G.J and van Veen, T.A.B 2014. Assembly of the Cardiac Intercalated Disk during Pre- and Postnatal Development of the Human Heart. *PloS one*, 9(4), p.e94722.

Walker, J., 1996, The Protein Protocols Handbook, Chapter 11 - SDS Polyacrylamide Gel Electrophoresis of Proteins, *Humana Press*, pp. 55-67.

Wallgren-Pettersson, C.; Sewry, C.A.; Nowak, K.R. and Laing, N.L. 2011. Nemaline Myopathies. *Seminars in Pediatric Neurology*, 18(4), pp.230–238.

Wang, K., and Williamson, C. L., 1980. Identification of an N2-line protein of striated muscle. *Proc. Natl. Acad. Sci. USA*, 77, pp.3254–3258.

Wang, K. and Ramirez-Mitchell, R., 1983. A network of transverse and longitudinal intermediate filaments is associated with sarcomeres of adult vertebrate skeletal muscle. *The Journal of cell biology*, 96(2), pp.562–570.

Wang, Q., Mercogliano, C.P. and Löwe, J., 2011. A ferritin-based label for cellular electron cryotomography. *Structure (London, England : 1993)*, 19(2), pp.147–154.

Weber, K. and Osborn, M., 1969. The reliability of molecular weight determinations by dodecyl sulfate-polyacrylamide gel electrophoresis. *Journal of Biological Chemistry*, 244(16), pp.4406–4412.

Weins, A.; Schwarz, K.; Faul, C.; Barisoni, L.; Linke, W.A. and Mundel, P. 2001. Differentiation and stress-dependent nuclear cytoplasmic redistribution of myopodin, a novel actin-bundling protein. *The Journal of cell biology*, 155(3), pp.393–404.

Westerblad, H., Bruton, J.D. and Katz, A., 2010. Skeletal muscle: energy metabolism, fiber types, fatigue and adaptability. *Experimental cell research*, 316(18), pp.3093–3099.

Williams, D.B. and Carter, C.B., 2009. Transmission Electron Microscopy. In *Transmission Electron Microscopy*. Boston, MA: Springer US, pp. 3–22.

Winkler, H. and Taylor, K.A., 2006. Accurate marker-free alignment with simultaneous geometry determination and reconstruction of tilt series in electron tomography. *Ultramicroscopy*, 106(3), pp.240–254.

Winkler, H. and Taylor, K.A., 1999. Multivariate statistical analysis of three-dimensional cross-bridge motifs in insect flight muscle. *Ultramicroscopy*, *77*(3), 141-152.

Witt, C. C., Burkart, C., Labeit, D., McNabb, M., Wu, Y., Granzier, H., & Labeit, S., 2006. Nebulin regulates thin filament length, contractility, and Z-disk structure in vivo. *The EMBO journal*, *25*(16), 3843-3855.

Wolf, D., Lubk, A. and Lichte, H., 2014. Weighted simultaneous iterative reconstruction technique for single-axis tomography. *Ultramicroscopy*, 136, pp.15–25.

Wolny, M., Colegrave, M., Colman, L., White, E., Knight, P. J., Peckham, M., 2013. Cardiomyopathy Mutations in the Tail of β-Cardiac Myosin Modify the Coiled-coil Structure and Affect Integration into Thick Filaments in Muscle Sarcomeres in Adult Cardiomyocytes. *Journal of Biological Chemistry*, *288*(44), 31952-31962.

Woodhead, J.L., Zhao, F.Q.; Craig, R.; Egelman, E.H; Alamo, L.; R Padrón, 2005. Atomic model of a myosin filament in the relaxed state. *Nature*. 436(7054):1195-9.

Wright, J., Huang, Q. Q., & Wang, K., 1993. Nebulin is a full-length template of actin filaments in the skeletal muscle sarcomere: an immunoelectron microscopic study of its orientation and span with site-specific monoclonal antibodies. *Journal of Muscle Research & Cell Motility*, *14*(5), 476-483.

Wu, S.; Liu, J; Reedy, M.C.; Perz-Edwards, R.J.; Tregear, R.T.; Winkler, H.; Franzini-Armstrong, C.; Sasaki, H.; Lucaveche, C.; Goldman, Y.E.; Reedy, M.K. and Taylor, K.A, 2012. Structural changes in isometrically contracting insect flight muscle trapped following a mechanical perturbation. *PloS one*, 7(6), p.e39422.

Yamashita, A., Maeda, K. and Maéda, Y., 2003. Crystal structure of CapZ: structural basis for actin filament barbed end capping. *The EMBO journal*, 22(7), pp.1529–1538.

Yang, S.; Barbu-Tudoran, L.; Orzechowski, M.; Craig, R.; Trinick, J.; White, H. and William Lehman, 2014. Three-Dimensional Organization of Troponin on Cardiac Muscle Thin Filaments in the Relaxed State. *Biophysical journal*, 106(4), pp.855–864.

Young, P. and Gautel, M., 2000. The interaction of titin and alpha-actinin is controlled by a phospholipid-regulated intramolecular pseudoligand mechanism. *The EMBO journal*, 19(23), pp.6331–6340.

Zeng, W., Conibear, P. B., Dickens, J. L., Cowie, R. A., Wakelin, S., Málnási-Csizmadia, A., & Bagshaw, C. R., 2004. Dynamics of actomyosin interactions in relation to the cross-bridge cycle. *Philosophical Transactions of the Royal Society-Ser B-Biological Sciences*, *359*(1452), 1843-1856.

Zernike, F., 1934. Diffraction theory of the knife-edge test and its improved form, the phase-contrast method. *Monthly Notices of the Royal Astronomical Society*., 94, pp.377-384.

Zhang, Y. and Cremer, P.S., 2006. Interactions between macromolecules and ions: The Hofmeister series. *Current opinion in chemical biology*, 10(6), pp.658–663.

Zhao, F. Q., Craig, R.,2003. Ca^{2+} Causes Release of Myosin Heads from the Thick Filament Surface on the Milliseconds Time Scale. *Journal of molecular biology*, *327*(1), 145-158.

Zhou Q, Chu PH, Huang C, Cheng CF, Martone ME, Knoll G, Shelton GD, Evans S, Chen J., 2001. Ablation of Cypher, a PDZ–LIM domain Z-line protein, causes a severe form of congenital myopathy. *J Cell Biol* 155:605–612.

Zoghbi, M.E.; Woodhead, J.L.; Moss, R.L. and Craig, R., 2008. Three-dimensional structure of vertebrate cardiac muscle myosin filaments. *Proceedings of the National Academy of Sciences*, 105(7), pp.2386–2390.

Zou, P., Pinotsis, N., Lange, S., Song, Y.H., Popov, A., Mavridis, I., Mayans, O.M., Gautel, M., Wilmanns, M., 2006. Palindromic assembly of the giant muscle protein titin in the sarcomeric Z-disk. *Nature*, 439, 229-23.

Annexes

Annex 1 – Protein sequences obtained from mass spectrometry analysis of SDS-page of isolated Z-disks

Band 1 – H9K214
MGVADDFAPSFTQKPQLRQEDDGNRLIFECQLISSPKPEISWYRGEVELGPDTRTNFRMQSVGTN
KFLVVLELDDVIETDAGLYKVKAKNKMGEVAASINLNFSPVDEPREKQIDGIAPTFAKKPAIRQE
DDGKRLLFECRITADPTPKVTWFHDGNMVKDSPRHKLTVDKDGHSYFATLEIKNVTVEDAGKY
KVTAKNELGESNATISLNFDSDEAPVPDDGIKPTFTERPVIRQSDDGNTITFECRLVGDPKPTVKW
YHGSEELKEDGRYRMSLELDQKLYHLARLRIDNVAKGDAGEYRAVAKNKHGQGVATINLNFE
GGDKLKIPDGKPPRFPKKPTIRQEGDVLIMECILEAHPVPDITWYQGQKTITDSKRVKMSRKATG
KDTYLLTLEISNPTKADGGNYRCNAFNNFGESNANISLNFQDTEEGPGFAPTFVEKPRIIPNETGT
LITMKCKCKANPKPEVTWFRGANVVKESSKISIKTKTVEEDVYELIMEIKDPSAPDGGTYRCHVK
NEYGESNANLNLNIEAEPEPEGDGPTFVEKPRIQSQNQGKLVIMDCKVKANPKPEIVWTHAGKIV
KESSKISISIVQEKQDIYYIKLTLNDPGAEDSGLYKCNIKNALGELNANLTLNVEIIPVIKEKPKVV
KIVKKRTVIVECHVLSKFTPECTWFKETNAVKADNRHKVHVEQVKEGEFAVKLEIEQVSASDKG
VYKLVARNEKGEATSQVVEVTEIMEEGEKPKIISGLKSATIEEGKSIELVASLSKQDRKVTITWYR
DSTVVKASKDIMISFNGVDMKLSITSASTSYSGTYKVVVSNEYGQDESSARLVVKDIPDHTPNGI
DKSTPKKKLEVIQEALLKAEKTVSRKQSISKVEELRTESRRSSLIATDEKIEEVKTESRRASIIEKKV
ITEKVDREIPKFRSTIIPTHHTKILPTDRDIEHYEPEPDDDDEIEDIWASVPREPEIRSIIKREPKLQPD
NANELLLDNYEDTSTPRASRPSKNIENESKIIPKQIEELDNDIEDIWADRPQEPEIKSILREDTWKSN
LINNESETLKEKSKLPLIDDKVEEKVEPKLKKTRKKVGTGKDEEPTSDSKERDNVSNGTKKDEV
VAKAKTVGKEEKKEELKSTLKIEESKESIAKSKTPVDKPVEEVKKKEPVPKLKTTLAKPEEAKKE
EPAPKPKPTLTKPEELKKEEPALKPKTTLAKPEEAKKEEPALKSKITLAKPEEAKKEEPALKPKTT
LPKPEETKKEEPALKSKTTLTKPEEAKKEEPALKPKTTLAKPEEAKKEEPALKRKTTLAKPEEAK
KEELALKSKTTVAKPEEAKKEEPALKPKTTLPKPEQTKKEEPALKSKTTIAKPEEAKKEEPVLKP
KTTLAKPEEAKKEESALKPKSTLIKPEEAKTEEPALKPKTTLAKSEEAKKEEPALKPKTTLAKPEE
TKKEKSALKPKTTLTKPEEAKKEEPALKPKPTLAKPEEAKKEESALKSKTTLAKPEETKKEESAL
KPKTTLAKPEEAKKEEPALKPKTTLAKPEEAKKEEPALKPKTTLAKTEEAKKEELAPKPKTTLTK
PVEAKKEEPAPKPKVTLTKPEEAKKEEPAQKPKTTLGKPEEAKKEEPAPKPKVTLGKPERKEEEQ
TRKLSLKPGAKIEEEAKTLNKVELKPVAAEMNEKKSGLRKPPKYEIKADSFQSIQLKPVSRDPKT
PQKAENGGIELKKTEKTEKVEAKKMKIGKAGKEKSYELPEIPDYERPVLEKPQEFEFGEHVARD
KTKLERPATQPKVPEIKAPEAPKIEVIKDVTPAGSRKSSLIPGSGTTSRRGSLIPPEELGRRPSLIISD
ELGKLRPGEVLDTKRRRPSTDVRRPSVADLENKINQPSTPLRDVGPPGPPQIIDVQESYSAVEDST
AYLTVGVEGTPAPTFKFYKGITEIIEGGRFKFLTDTETNTITLCMRKTKPNDEGTYKIVVSNIHGE
DSAEMQLYVSDASGMDFRAMLKKRRYQKWAREEQEQEKVDLKEVEKPIPALKKVEKKPESFL
KPLVDQYAKEGKDKKVVFEANFSKPNCKPKWFFRKDELFPSSKYKFKNEEDCYQLIIMNPKVED
TGKYTIEISGVSSTAFLNVEEPDPTYTFTKPLSKKTSGYTKHEVYMECTVSSNLAQVTWYKGKTK

LEDGDTYSISKDMNGVCRLTIKSATLEDSGEYICKINKQTDKTETVLTVVEYPYKFVKVLKSQQL
VEKETLTLVCELDDAGGEVKWFKGDQEIVPDKRVQIKEDGRKRKLIIKDTKVTDAGQYSCVSNA
DKTEAEIVINYANRFNKKLKDTVAVEREKLVLDVELQDQTAPAIFFFNGNRIEPNERVEIKNLGG
GKHQLIFNRVEMTDDGEISCESGQLKSSCKLTVKKGESKPIVEIPDKVEGPCNTPLVFVVPYKIEG
TKQSQVEAKLLKDGKALPLKDVEIVVGEDKITFKIKKPSRDQSGVYQVKISNNQGEEVNDVNIN
MQDVPSPPRDVDVNEIFQDSCVVSFKPSKDDGGTPITKYVIERLDLSLKAQWDNVGEVMPGEKC
SYKVQDLVAKKEYKFRIRAVNKLGSSEPAMFGKPVLAKDPWDEPSKPKNVEVTDWDKDHADL
KWTKPESDGGAPITGYIIEYKEKFGKEWVKGKEIEGDITEATIDGLKEGTQYEFRIRAVNKAGPG
EPSDATKPIIAKCRFVKPYIVGDGLTNLIVKKGQIIKYDIKYAGEPEPEVHWFLGEKELVQDTAERI
TIDKYERNTVLTVRKTTRPDSGKYKLVLSNSSGTCESVGDVVVLDKPSKPTGPLKVEEVRADHV
KVKWEKPEDNGGTDITGYVLEKMDMDTGRWIPAGEVGPDETSFNFTGLTPKKKYKFRVKAVN
KEGESEPLEVEEAILARNPYDEPDKPGKPVIFDYDNVSVSLKWEKPQNDGGRPITHYTVEMKDK
FAVDWVEVTKTTDATPEAKVEGLKEKMIYQFRVRAHNKAGPSQPSEPTDNHLCKHKNLKPRID
RTNFKSIVIKAGRTHKWSVDIIGEPPPEVKWIWRDNIPLTTTERIKIENVDYHTDFTIVNAMRKDT
GKYTLIAENVNGKDEETVELTVLGKPDAPKGPLEVTDITATSAKVKWEKPEDDGGVPIKEYEIEK
LDTKTGKWVRVGKVPGNAPLTEFEVTGLNPGSEYKFRVTAVNDEGDSEPLESERGIIARNPYDEP
HKPGTPEITDYDNESISLKWTAPDFDGGAPIEKYIIEKKDRYKPDWEKAMEVPGNQLEAKVGDL
KERGEYQFRIIAVNKAGPSPPSDASKMQICKHKALKPRIDRTNLKPITVRAGKPIKYDVDVRGEPP
PEITWYHANQAVQSGGNIEIVNVDYNTKLNITDCVRKNTGVWKIKAVNPHGEDEAEVEVTILSA
PGKPKGPLKVYDVTKSGLKLKWEKPEDDGGLPITSYQIEKLDKATGRWVPVGRTSDTEMDVKG
LQEGHEYEFRVKAINEEGESEPLVTDSSTIAKNPYDVASKPGVPEFEDWDVDRVDLKWEPPKST
GGAPITGYIIEMKEKPSPNWQEATVTDSPQPKGRVTGLKKGSVYQFRVRAVNKAGPSEPSDPTKP
HVAKARHLKPHINRDKLKTIKVRAGQMVKLEVDIEGEPPPTVTWNFGGAVLQTSANVKIDNED
YLTKIHLTQTSRKLSGKYTIKAVNDSGQDEADVEIIIQDKPGKPEGPLEVTDIHKEGCKLKWNKP
RDDGGLPLSGYLVEKMDVTTGRWVPVGIVDPDKTEQTITGLEPGKRYEFRVKAVNEEGESEPLQ
TDVPIIAKNPYDPPSAPGLPEIIDWAENMVKLKWEPPIRDGGAPITGYIIEMKDRFGTTFVKAADV
EGRVCTGTVTRLEEGNQYQFRVRAVNKAGPGEPSEATNPHTAKARWLKPFIDRTNLQPITVKVG
LTVTLDVNIIGEPPPNVTWFFQDKEIVSDDTIRVDNIDYNSKFFILKTKRAHTGKYVIKAKNEVGE
DTADVEIIVIGKPSKPKGPLEISDVNKHGCKLKWEKPDDDGGVPVEYYEIEKLDPLTGQWIPCAK
SVEPEVTVTGLQEGKPYKFRVKAVNREGESDDLEADKSIIAKNPFDEPGKPGRPEIKNWDKDFV
DLEWTPPKDDGGAPIEKYIVQMRDKEGRQWIDVAKVLGDRTTAKVTDGIEEGHEYEFRIVAVN
RAGPGEPSDTSRSVVAKPRFLAPRIDRKNLHKKVMRVGQLLRIEADVQGEPPPLVTWKLKDAVL
KSMDRLKIENEDYHTTFIISKLQRSDTGTYTVVAKNDSGTDQVDVEILVVSKPSKPKGPLEVSDV
TAEGCKLKWDKPDDDGGEPVDHYVIERMDVDTGRWVPCATSKTPEAEVTGLNEGKDYMFRVK
AVNSEGESEPLETAIPTTAKNPYTEPDAPGKPDLKDWSKQHVDLKWKAPKKDGGAPIEKYIIEKK
DQYGKWQKAAEVPGDKTEGRVEGLIEGQKYQFRVKAVNKGGQSKPSEPSDSLVAKDRYAAPRI
DRTNLKDVTIKAGTNIRLDVKVTGEPPPTKTWYLNKAKQESGGVLTIELEDYRTKFLVSSASRAH
CGTLTLKAENSSGKDEASIEVLVLDKPGKPEGPLKVSDVHKEGCTLKWNPPLDDGGVPLDHYV
VEKMDTETGRWIPVGRTKEPGMVVENLVPGQEYKFRVSAVNAEGESEPLETDHGIVAKNPFDEP
GPPGRPEAADWDKDHIDLRWTPPLNDGGSPITGYIIEKREKDGPRWIKACETGPECKGRVDNLDE

GVEYEFRVKAVNIAGPGEPSDTSKPITAKSRRLAPKIDRKNLRDITVRENEGFHFDVKIIGEPPPDV
TWVINNKSIQQTTFRRIQNVPYNSKFFNDKPERKDSGIYKITAVNQYGSDTAEVEVTVVSKPAKP
EGPLEVSDIHAEGCTLKWKKPKDDGGEPIEGYLVEKFDPDTGVWLPVGKTTGPEMKVEGLTPG
HEYKFRVKALNKEGESEPLETYSSIVAKDPFTVPSPPGAPEPVDWTANQVELSWKEPVSDGGSPI
TGYIIEKKDKYSTMWEKALEIETPTTKGLVHGLIEGNEYLFRVIAVNKAGQSEPGDTSKTFTAKP
RYLAPKIDRRNLRDVTLSAGSLLRFDVNVIGEPPPHIEWRYGAIPLHSDRKVQIDNSEYNTKFSIRP
VSRDDSGDYTITATNSSGRDSVTVQVTVTDKPMPPEGPLQVSDVHKEGCKLKWKRPKDDGGTPI
EYYQVEKMDPETGCWVPCGRSTEPNLEVSGLTPGKEYLFRVTAVNAEGESKPLEAEQAILAKNP
YDEPGKPGDLRATDWDKDHVDLAWSPPTSDGGSPITGYIIEKKDKYGEWEKAVEVPAYETSAT
VPDLIEGQPYEFRVRAVNKAGPGEPSDPTPTIIAKPRNQPPKIDRTNLIEVRIKAGQNFSFDVKVSG
EPPPTTKWLLGKREVRPTERVKVKHVDYSTSLSVRMATRAESGRYTITAENINGEDEAFVKVTV
LDVPSPPQGPLRASDVHAEGCTLTWKPPEDDGGQPIDKYVVEKMDEATGRWVPAGETDGPQTS
LQVEGLTPGHKYKFRVRAVNKQGKSEPLAAMQSIEAKNPFDEPGKPGTPVVSDYDSDFVELQW
DRPQEDGGSPITGYIIEKRDKYNPNWEKCAEVEGDVNRGKVNDLVEGIHYEFRVRAVNKAGPGE
PSDASKSHLARPKNLPPKIDRKYMLDVKVKAGGFYDFDVPVIGEPPPSKEWSLKGTVLLSNDRIK
IVNEDYNTKVRVMEARRSDSGVYTLEARNINGKDSATLTVNVLDVPSPPEGPLKIDGVTKNGCN
LKWRPPKDDGGSEILYYQVEKMDTENMRWVPVAEATSTYAHVDHLIEGHDYQFRVRAVNKQG
ESLPLTGMDTITAKDPYDKPDKPGTPVATDWDKDRVDLEWTPPKKDGGSPITGYIVEKKPRFGQ
WEKALEIDGAKTSARVPDLVEGQEYEFRVIAVNKAGPGEPSEASSPIVAKPRFLAPSFDPHALSDL
VVRAGQKINYIIPIQASPKPTATWSVDGAVIMADSRHEMYTTSTETTFEIPFSVRSDTGRYTLTLE
NEHGKFSASARVTVLDRPSPPQKPLEISKITKEGCHLAWGHPLDDGGSPILHYVIEKMDLSRGTW
SDAGMSMILSHEVARLIHRKEYLFRVKAVNTIGESDPLEAPKSIVAKNEFDEPDAPGKPQITDWD
KDHVDLQWPVPSSDGGSPITEYIVQKKEKGSPYWVNAIHVPPTQTNATVPDLTEGQEYEFRVIAV
NAAGQSEPSEPSDLVTAKPRYLAPKIKTPLQDIRVKAGLIFHVDIDFIGEPTPEVIWTVGSRELESD
KRTTVTSIGYHTIVHTVNAQRSDSGLYHLLLKNSSGIDEGSFQVIVLDRPGPPEGPLQYEEITSQSV
TLSWKPPKDNGGSEITTPTPRVPRLLEGTTYEFRISAENLQGRSDPLTTDHSIVAKNQFVAPGQPG
KPECVDADKDHIKIRWTAPISNGGSKIIGYDVERRDRATGRWLKLTKEPARYAEYYDDHVTEGH
QYEYRVTAINAAGAGKPSDTSAVFIAKPMKEKPKLNLDALIGRKIKVRAGEPINVNIPLSGAPTPT
IVWTKDGKPLFETLRISTETKSDRTNLLVEKSVREDGGIYTITATNEHGKDSADIEVIVVDRPGPP
QGPLQYTGTTQESVSLSWNRPVDDGGSDITNYIVEVSDYGTDNWRQTPGYCPRTSYTAKGLTEG
KKYVFRVRAENMYGVSEPLEGKPVIAKSPYDPPDAPSQPEILGYTPNSCSLFWNPPLNTGGKPIT
GYYVERRERGGEWLKVNNYPTPNTTFTVQDLHEGSKYEFRVIAVNEAGPGKPSKPTEPITAGHQ
RLRPDAPEPPKPDRITKDSVTLSWRPPRSDGGAKIRGYIIQMKQRGQDEWDDVNGALIPTNVYTV
PKLTEGEEYLFRVIAVNDVGNSDPSRPSNPIVIEEQPNKPVMDLGGVRDITVRAGEDFSIHVPYIGF
PKPTATWYANDVIKDETEPRVHQQLGDDYASLVVKNAKRSDGGQYRLQLRNSSGFDTATINVK
VLDRPNPPENLHADEFGGDALTLFWNPPKDNGGADITNYVVEKREPKGSWSKVSSYVTTPFFRV
RNLTVGSMYEFRVMAENQYGTSDPVTTMDPIKARHPFDPPGAPGTPKGVETTEDSITITWTKPRH
DGGSPILGYVIEKRLLSEDKWVKATPSLVHETNYRVTGLIENHDYEFRVAAENAAGRGPWSSNS
DVIRASAPPFPPRITSDLSIRDMTVIAGEPFTITVPFTANPKPRPSWSINGEEVLTSDRIKFDTTDIAS
QFINKKAKRSDTGTYTIYLTNTVGTDSASCRVLVVDKPSPPQGPLDISDITPETCTLSWKAPFDDG

GSPVTNYIVEKLDPAGYWVKLSSFVRNTHYDVIGLEPNRQYNFRVRAENQYGISEPLQADEPITA
KFPFTVPDPPGQPRVIDWDTSNATLVWTRPISDGGSRVQGYKIEFRDPADDAQWRVANDYLVK
DTTYICYNLLSGHEYEFRIRAKNAAGFSKPSPSSPPFKLKSKFNVPSPPGTPQVVKVGKNYVDLK
WEAPISDGGSRITGYVIEKREVGSAIWAKCNEYNVTDTEYTVLHLIERGDYEFRIFAVNAAGRSE
PSSCTTPVKICEVEGGEKPEFVRTLPISTNVPLGKTCVLECEATGKPLPTARWLKNGREITIGGRFR
AEAFDGIYRLVISDVSDSDTGDYSCQISNPLGLATTTCRLKIGSPPRIERMPDILYLAENDNTKIKIY
YSGDQPMDVTLKKDGRKVVETSHIKYTVFDEYLIIFIKDIEKDDAGVYDVSITNDSGSVSGSFNV
CITGLPGPPSEPLEVTDVNKHTCTVSWRPPKFDGGVRVTHYVVERRDVSHAHWIIASSFCKDCSF
VVQGLTEGQEYLFRVMAVNDNGMGPPLEGTNPVKAKAPFDPPGPPGTPKVTEVGGDFVNLSWE
KPETDGGSKIQGYWIDKREVGSQAWVRVNVIICLPTQINVTNLIEGRQYEFRVFAQNAAGLGPES
KASTSVKIADPQAAKPPEVIQPLHKVSCVQNHNAHFQCKIVGVPRPTITWFKGAREIVTGSRYNI
YSEGDVHNLIIHDVFGEDADEYFCRAVNKCGVKSTKGELLIKTPPKLNVPPRFRDTAFFDKGVNV
VIKIPFTGYPKPKITWVREGELIESGGHYTVEVKERHAVLTIIDGNRIDSGPYRITAENDLGQDSAII
KIQISDRPDPPRFPQVDNVGHDSLALTWKPPVWDGGSNITNYLVEKREHPMTSWIRVGNTRFCS
MAVTGLSPGHQYDFRVCAENIYGRSDPSEVTPLITTKGTVKREFKQKEYKVDETGKKIRGRSDE
KPRDYDQFVFDVYSKYVPQPVEIKHISVYDRYDILEEIGTGAFGVVHRCRERSTGNIFAAKFIPVS
HAMEKELIRKEIDIMNQLHHPKLINLHDAFEDDDEMVLIFEFLSGGELFERITAEGYTMSEAEVIN
YMRQICEGVKHMHEKNIIHLDIKPENIMCQTRNSTNVKLIDFGLATKLDPNEVVKISTGTAEFAA
PEIVEREPVGFYTDMWACGVLAYVLLSGLSPFAGDNDIETLKNVKACDWDFDEEAFRDVSEEG
KDFIRRLLIKNKEKRMTAHECLLHPWLTGDHSNRTTPIASSRYLNFRDRLRAKYENWDKYVLPI
GRLAEYSSLRKLLIDKYKIYDSCFDRRQAAPRFVIKPTSAFAYEGQSVKFTCRVIAIASPTLTWFH
NNQELRQSVKFMKRYHGDDYTFIINRVKLEDRGEYVIRAENHYGYREEVVFLNVQPLPKEIPKY
RPELHPVRRREPLGYNVWLETIESAPSFTFLLRPRVIQVRQTCKLLCCLSGNPSPTVKWYKDREEL
SKYHYPMTHADGVVTMEIIDCKPEDSGKYRCVATNVHGKDETSCVVIVEGTGETEEQVKLAHD
LLHSGDRKFIEQPLKPAPPPIVTVHKAGGYSGYSSTTTQGYNYSSSSAKNTSSSSFSYKATDSSTE
KRSVKKYGLDSTGSPSRSRSTTKELIYPPDESMRAPKFTKKLSDLTINDGEQLELSVNVDGDPEPQ
VTWSKNGKTLSSSGIMSLKYKGGVATLVINEVFPEDEGEYSCQASNSIGTVTTSCKLTVKPMTSG
SSKKKTDDKPPKIVDHVSSMFVKDGEPVTLSCRIIGAKKFDVVWLHNNKEIKPSKDFQYSSEANI
YKLNIAEIFPEDSGTYTCEAFNDAGESFSSCTLNVLVPNEEPKSPVFATFPQSATVSEGESVTFVCK
TETAPLKVTWLKDGKALPESSSRYLFSSDGDKSFELRIKSCTASDVGQYVARAIGKKGETNAAFA
LNVTSANE

Band 1 – H9KC31

MFGFDGFQGEIVMQTTPTVPTFTGRPGDPSPPVFEQIFKNARFAQGGNAIFEGRVRGNPKPIVCW
THKGAPLLESWKIHMSYDEKTGAVTLQINQIGPGDEGEYTCSAKNQYGEAICSVYIQPEGFGPPP
QQQMGGYRKEFAQTFQSTEQKTQTGTQSFQQRSYQQTIDKRSYVNGTSVSIEDFKVDTFEYRLL
RETEFRESITRRFVGESDVQISTVVDRNLGPVAPPQITQKPRNSKLVEGSDAVFTAKISGNPKPRLT
WFKNGQRIRESQRVEMSYSNQQASLRIRVALPEDSGHYTLLSENPQGCTVSSAYLAIESSDQVDQ
AYQAQRETIKTQQVETIGETDSGKVLPPNFVRTCTDRDATEGKMTRFDCRVTGRPYPEVTWYIN
GQQVANDLTHKILVNESGNNSLMITNVSRADAGVVTCVARNKAGETSFQCNLNVIEKEQVVAP

KFVERFTTTNVKEGEPVVFMARAVGTPVPRITWQKDGVPITPGPDVRISTDGSGASTLDIPYAKL
SDAAWYQCTAQNVAGSTATRARLFVETPKGAAPEPRRLNLPRPTKVIEPEPAPGPEVIYLRHVER
AKPYLPPPEEDRIYPPPRFIIPLKDVHQIEGGRIHFEARIEPVGDPTMRVEWYVNGRALDASSRATS
IFRFGFISLDLISIVLQDSGEYLCRVVSSTGVAESRATLSVTPRATIEQTSQHPDSLQYIQQLEDYSK
YQRQESVEDISPQRPVFIRPLQDLGELQEGRNAHFEAQLTPVSDPTMKVEWFKDGRPITASSRITT
IFNFGYVSLNILHLRAEDAGSYTVRAVNRLGEAVSSASLRVFARTSVTTDLGIPEQQRYIEAAEEL
EAYQQAMHQKYVQEQPEPTSPPEFKSPIKDQNSIREGGFAHFEARLEPVGDSDLRVEWLKDGRP
VEASSRITTFFNFGYVALTIKYVTIHDVGIYTCRAYNRVGEAHTTAQLSVISKNDVIYDSQHPTGL
QKIQTLEDSSRYSRQLQEETQVTQAPRFLGTLKGTNKIVEGQRAHFEARVEPQSDLTMAIEWYH
NGKPITAANRIQTYHDFGYVAIDILQVRSEDAGTYTVVARNSLGEARLSATMVVETRSSVDTSS
MHRTSYEKTQRLEESKFVEPQYHIEEISKSKPIFVQPLSDPKPVSEGKNIHLECRLEPMGDPTMRV
EWFQNGRPVTVGSRFRTYYDFGFVALDIVHSTVLDSGEYTVRATNHLGTAHTSACVRVIGKSDV
VTETQHEQSLEQIQMLEDSSRYRKTQQEEVTVMQAPQFTRPLHNIETVELTNVHLECRLQPVGDS
TMRVEWFVNGRPVKTGHRFRPSYEFDYVALDILGVYPEDSGVYTCQARNQLGEAVTSCSVRVH
AKKDLLLESQHPEGLERIQYLEDASRYKRQEMVDEVVTVKPRFITAPKSQENLREGEHAHFECK
LEPVTDSNLKVEWFKNGRPVTIGHRFRPIHDFGYVALDVIDLIAEDSGTYTCRAVNLVGSDEVSC
TLTCRSTAQVLTDSKNEIGLEQIHYLEDRSRYQRREDVEETTTQAPIFTTSLNNVEIKEGQRAHFE
CRLIPVSDATMKVEWFHNNKPVKAGSRFVETNSFGFVALDIMYAYPEDSGTYTCRAKNIIGEAIT
SASAVVHSKKSIYTESQNEETLQRLHYLEDTSRYQRKTTTEEIITQAPVFTMPIKDLKVAENQAA
HFEARVIPVGDSKLKVEWLRNGVPIAASNRVTTMHDFGYVALNMKYVNPEDSGTYTCRAVNDL
GEAVTSATLFVQSKAALQFESQHESALSKIQALEDTSKYQRREEEEIVVKERPSFTVQLNGPTAL
VEGQSAHYECRIEPYPDPTMKVEWFHNGKPLSTGHRYRTTCDFGFAALDVLTVYAEDSGTYTC
QATNRLGSAKSSINLDVKSRSSIIRETQHESALKKIQYLEDDSRYKRVEEEDLIVAERPKFGRPLK
NIEHLPEGKSAHLEATLTPVNDPTMVVEWFRDGRPIPQGHKFKTTYDFGYVALDILYAYPEDSGT
YMCKARNAVGEAVTTCVISVDSKQGLYLDTLDAQRLQKIRELETVEVKQEVEKEVVHQKPVFL
TPLNNLDHLKEGEHAHLECRVEPINDPNLKIEWFVNGVAVKTGHRFRKTHDFGYVALDILYTYP
EDAGTYMCKATNLAGEAVNTCTIKIGSKKERSFPPRFLPLKSPERACNVKRYESRKIYSPPYFRRG
DTSAVKPRFGPFSLTTFRCDKQFMDSGKVHKNRLYDKNQYEYANSSYKSCPARRSILLDTQHPD
GLEKIRELEAQGRPARLEVEEPPVTPPRFVTELRGTTEVYEGQTAHFECQVEPLHDANLRIEFFHN
GKPLPSASRFHVTFDFGYVALDIGHAVPEDAGEYSVRAINALGQCVSSIELRVIPRDNIILDSQRPE
GMDKIRELEAQQPWKRPEVPEPQTRQRPVFTQPLQNIDAIPEGHTAHFECRLIPVGDPTLKVEWF
RNEIPLETSSRITKVHDFGYVSLDITHVREEDEGVYMCRATNPLGEAVTTASMKIRSKASIQLDTQ
HPEAQRKIAQLEADKGPSRTEEPEKVFDKPIFTQLLTGPTELWEGQTARYECRVVPVGDASLRFE
WYINGVELKMGSRFHVSHDFGYVTLDILKVITEDSGVYTCKAINKAGEAVSSISLKVKARSAIDA
ESLQPDAWQKIQLKEAEMNKVPEMFVDTTPQQAPVFTKHLESYDKLVEGQHVYLEAQVEPRAD
PNLRVEWFKNGIALQTGTRLRSTFDFGLVTLSINGLRSDDSAIYTCKATNLLGEAVSTCSLKIVDR
HWLLGDTLHPDALPKIDALEQPHVTTVEQPEPIYEVPVFITHLNNVECVEGDNAHFECNVEPSKD
PTMKIEWFINGKPLPTGARFKSTYDFGYVALDLTHAYEEDSGVVIVKATNSKGSAQTSGTLKCTS
KQSIYLQTQHPQGEAGLEKVKEVEDAYLSKLKRPDAGPEQEYPKPVWTVPLQPEFKLGESEPLH
LEGQVEPKDDPNLKIEWYFNGKALEHGSRFKMTSDFGFVTLDLTDVYDRDSGIYTCKAYNKAG

EAFTSTTIYCSTKENIIEKSQHPKGKEGLEAIQDLEESLKRQEGAPPESEEGHPPVFTSQFENLTNLS
EGEIAHFEASLTPTGDQTMVVEWFYNGKSLEASHRTRTVYAFGMVVLEVLGTKIEDSGTYSCRA
TNKWGQAEISVQLECVDKSKGQKPKFTTHIQSLEGLKDGQSAHFECTLIPVGDPHMKVEWFHNG
QPLRHSSRFKMVSDFGFVVMDIAGVMAHDTGEYVCKASNKFGEDYTKATLKCFGKSGVYLDSL
QPDSLARIRELESYGGEQPTTPTTPVAEPPKFITQISDITKLVEGQSAHFEARLTPVNDPDLKVEWY
YNGKKLPHGHRYRTFHDFGIVILDILYCYEENSGVYECRAFNKYGEDTTKATLKCYSKSSLILES
QLPKGMEGGLEKIQTLEDSMIRTRDEKIVEERGKAPVFTVPLSNIDGLREGESAHFEARLTPTDDP
KLKVEWFWNGKPLRTGTRFRTFCDFGFVILEISPIYPEDSGEYSCRATNDYGEAVTTCTMKCTGK
RSIILESQLPKGMEGTIDKIAELEGLGNEPGEVIPDDDTGKPPEFITTPSDLTLTENSLAHFECRLTPI
NDSSMRVEWFHNGKPLLAGTRIKTIHDFGFVILEVANCYQRDSGLYTCKATNRHGEATVSCKLQ
VRGRQGIILEPQLPTNFKTGTESIQKLEEALYKKDEILTEEETPNPPKFTVELKDIEVEEGAPSHFD
CRVEPVGDSTMRIDWFHNGRSFATGSRVHQINDFGFISLDMSYTYARDSGEYICRATNKWGSAT
TKATITCKSKKTIDFDSQLPSGMSGEKLKELERGPVSEPPPAEEPPRQPPKFITHIQSATVDESEAV
RFECRVEPKDDPNLRIEWYRNGKLIPAGHRYRTMYDMGFVSMDILYVYPEDSGEYVCKAINDL
GEDTTRASVSCKKLPNIILQNQVPKGMKKSEALMQMEATIKKYTSEVHLTEDDLYDADKKQPPR
FVTQIQDQTELVEMNSTKFECQLAPVGDPNMKVEWFFNGKPLPHKNRFTPIYDFGYVAMNFGW
VYPEDSGEYLCRATNLYGMDETRAVIRTAGKPGIIYESQLPKGMKSIEKIREMEAAWQIVPEEEG
EEEKVRAPPTFVSKPEPVTVEEGDWSRFCCRVTGHPRPRVMWIINGHTVVNGSRYKLTYDGMY
HLDIPKTRQYDHGKVEVIARSSVGEARTETTLTVKPRSDDYRGVLKNSPRPWYDYGLTQYQTER
QNTELERVFDERHHNISQGIEIATEHLGQKVYKEPETEWQKSVKSKKNEDYYNKLMTLEEEQVL
KESRLRESSHQFAIPGEKVVAHSVAKGMAQQYEETLEDKKDEKIQETQQTTTKFVKKPHTTEVD
IDMERVKGRYPPEPSESTVHGREVHVAKQKQIQKEVKGDLEITRKITATETTEVEHKAKTQERIV
QGPTKPAKPPVFTKKIQPCRAFEQEQARFEVEFDGDPLPSIKWYREDFPIQNSPDLQIYTFSTKSVL
IIRQVFMEDSGVFSVIAENRGGKAKCSANLVVEERRRQPGRGGVVPPSFLSTIQSTSVTTGQLARF
DAKVTGTKPLDVYWLKNGKKVTADIRYKTLEEDNTYTLLILETIPEDSGKYECVAINSAGEARC
DADCMVRGPQSPAKTAKPTTPGVEKAPQVLEPLKDQTIREGTSVAFACRITGKPVPTVQWKKGD
KVIKPSKYFQMQKDGDLCTLRISEAFPEDEGVYKCIAKNPAGDVTTSANLRVLAPDAADVLPKL
SPLKDQIVFEGQPAQFKTQVTPAKPKPTIQWYREGALIPQSPDFQMIHEGNNAVLLIATTYEEDTG
TFTCRATTSAGTVETSAKLIVKKRKGAYYEVPTETGPGVKSSTNYGRDIILEPLTLDENGLPLESL
PLQSGDESLPWRKGRVHHRPRLGDVTPWRKSKSRDTSLDKLQAVEGQVKPWTEEAVVLKKTPQ
VPREMPREKLEEVELKPTKIEKKDIARASLEAVDLKPVLREMTKEIKTEEEKITQLDKTTEEIYVE
EEDSRFVKTSKRIDETVQRKKEEVKPWTEEKVTLKKSKLDRKEIPRETLETVELKPSKIVKKEVD
KATLEKVDLKSIPIVTEKITEETISKSEYLEQEDTSMLDVTKIEEKPKEEKPEEVKLKPIPKSVSEKV
EEKPEDEAEKILPWRRGKKTKKIVDFREEVTVVPIDQEKVITEIHDEEIKIVEQKVEAKKIVQAEIK
EFKEEKPELPWRTTKEVKEIIEEKVVVEEIKPETVLKEDEVIEDVTESSEVSWRKRRKPKKPEKEK
EVVELKPVEKHEEFVERIEEIVLKPVEKEKFEEKPKEEELKPLKLEKPKKLEEEEIEEEKVTEMLW
KKPEEIPVPVEKEVSTQEVQVIEATKVEKIVEDVVEVEKKKVQVEDRRRKHKQRTQVEISITDKD
KKIAPRFIQKLQPVIAQPETTAKFTCTVFGNPFPEITWYRNEQELHASEKYIMTIYETTASLEITKV
KEEDAGMYSCRASNPAGVATSTVNLVIFEKEEEGIAPHFATPIKPLMVEEHKPALLECIVTGTPMP
EVKWYRGEEELKPEKGREITFNPETGEAKLHILEPTEEDETIYRVRAVNKFGRAECRANLVISNV

VRVSKPEVLRSPKITRPLPALVAEFGKPLTLSADFESKPTPEVKWYRNGAEIVPSDKRVIKIYENT
TELYIPEVTKKDGGKYEVRVENPVGEARSSGSVTVKKREDKTDEVKAPRFIEPLQPQIVTEGEVV
IMETRVDSYPTASFQWFHDTRPLESTPQVRIVTQENKSILMIKEIKPEYSGTYTCRAENVGGSVTC
TATINLLDTPWEETVELVSPTFVKRLSPVRVMDGESANLTCIVQGKPTPRVEWYHDNKPIKEGKE
ITIVQDTEGVCSLAITEVFPEDAGEYTCRAVNPVGEAVCTSSLIVEAYEYVPDSEIASSIVATSLTT
GQSGSEEDLLSPKETPLFDTDEESAPEIVKKLPQLIPTKVGELTRLEVKVKGKPKPEGKWYKQGV
EIVSSQEFLIEEFEDGTSVLTIAETYPDDMGEIVFEVHNPLGVSTTTTYLSVEGIVGTKEYRKPSWV
TQMEEMQEALRGKSRQSEAIDCMLSEAECSFSTDSLDRAIREESSQRDSSTMISEFSSTRTLMNID
DEGKRCFEEEDPHQKGFFLSRRFSDSLEIEQEITTTEYSWEMSASNKETSSFECVENALFENTKRE
SKNGEQRGKMDKKTRTERVSKVVRKKKLESMEEKTVTKKCTETKSHPVKNRRDSASGTSSKYS
NVHKMRLSRPLTVEKSIKGTNVNVKARSLSPDQVKYSKMTESSEKHRNVKSSSPTRSRQVRSND
KLIATKCAKFKEEEASIINDEVACRRMESMNKMSIESENRSERRKKIVLDFNEFPPPKSERKNQAR
SDLSNIQEAGFYLSPIEENSEASTGSGQSKQVIEHYGKMMETSMEYDHVRKYHTYPKSRIPVARW
SKERRFGNLMMDPKMYPLEPREIDLEAFQQLHTADSQEELQEFLLLESQCSGNLGLAGNMSTSE
VSCNEHHSEDERGTMSATQSVPRFIQEITDVYAKEGETAVFECIYSGNPVPDVVWYKNDKMIINT
PNVKIRLLDEEKKTILTIKHATEEDDATYVCKATSEIGLTTTKAKLHVTEITGKKIFMDEEQFEEKI
VDIEETQTLETTEIIEEQPTEVTRAKKVMPIQEPLITEATASLKKIDDEKAREIILKTEERAKRVLEE
REGVVVSEMAIEDTARDFTIESVVDRAQITSETLQTVSVSEVHTEASVQEIRRVDTKRKAKKTVV
TEEEELPREIVVEEKPKKKKKEKLKVREEVTIEEIVERQKENIAREVEEIMETLHAKEFGPGEAPL
RELATIGFLVRQGVSVNEINESLYKTDNFPALKTPEAQNALVQLVEREGHGPLITQVLTEETTTDE
SVVAATVGFRAFMRMIELQHVTVEEVLTHFAPEDFRPRAWEVTEATEVETEERITERVDVIHKTE
VHFMEYEDTRQAHTTLRERKLTKPKEQIEEKKEDRGVGVQVVEIEEIEETETGRKKTKDAEEIEE
EIETIIIETDSKHKLAQKEKKRVDVEEEEIIEKERKELIPKRPHIRRNEVEMEEIEEFEIKEDRSMPSLI
LNVPSQRHQIIPLDRTIEQAPGKPELEKAKLTMDTITPLTEHFVPIQEKEIDDISQIKLIERKASLSISP
IEPYSIMETTVQASTGEFAGIFKPTFYEATRGIVPSESLVISETLANDAGLSSLIINKQEISKTADVSV
ALQEATTVYETMVSQKEAPTEDFVSPLTVRAEDIILPQIGLSVYEIQEGLTEDKLEPLKTLPTKPRV
NIAAVEPLVVEEVRAEDKPGKYYPELVVPTEVATETVIPQRQRVTEEMYAPEKEGMYVPGRLPP
SQKAQVGISYGNETATVQQNIVQESEGVFISERKTDTFEATPNVTVLEGISVSTVQAQDIESDLTIE
EMKKAVADLNIIEITSAVTSETVPSEKEKEYQLEDKPAIKTAETSISLLEIGSIASTIIQESEGIYHPD
QKPTKVLAETSIKPEEYVQISEIQTADYPSDFKEELKYVQESGTIAVQLIEAKMIQETMTHDREAK
MEELIKPEERVVKTSYDAIKSVEVFQTTSIEKEADLKIFEMPESHRGKTVPTHPVVSLEIEMTQPE
DNLGMIKKEVPSSSIAKIEPIALQETIIGETVIAEDVAXXXXXXXXXXXXXXXXXXEKKAISSVAQS
SHIPLESVTIAMQELAEKEDLYMTEIQPNKKIAIVELTEPRPGPIILEVISHDRENVYNPNVKPQDY
TAETLVSGHKVALKSETLVEQSTANMSIDKPQSKKAIPQRDILEELIVTETTIAETEKIREADILPTI
QSAEIEIQSKTEKLTVIEVTSIQEEEKLEIEKIPKERKVVLGITGGHEVAEMQETVLASNVNILKEE
KIKEDHANQQQSGLEVVEQTEISISEKESPLQKDIRPDIKIVEVTFQEGESIVVGITHPEDKEGIFTPE
EKPKNVEATVDIITQGVASKFEILSDTGLSDLPDETVQKMKPKTTILPIEAAIAQEVHTRETEAPFS
EIKPNDKKANLEFVTGEGLIISAITTEDKESLLPETEKPKTKSASFDIPTHFVAQTIETTTTDNVGEF
KREEIHVATAITDHITFRSVITSETATGDLEKPMEDFIQPEKKMIDVSFQEEEGITVIETIASDKEKE
YFKKLEMQGEQATASFDAHKVAQLTEINPASISGDLTMLAPITVAAKEERLPFESIVQTETIVSET

EKEFKDKPIITNKAEVSINEIISATTTTEIPADKEDILQIFEKPSEKQASIEVTVDSSAGKLKKIKPVS
ALAVPSSIPLEAVISSEIQPTEIEGPFIKDKRPLKAIADLSVVEEQSVQVSAVIMEDKEEEYKSKNLP
EIKTAGKSLVSGHIVAETTMQIVDFSTGEFIQEKPSGAIAISEHVPFISLIESQPIIQESEDKFIPGQLP
ENKTAIVDLEESKKIVIVSQVTPADKESLYISEELPSKHAASFGLDTIHGIAETTTISVEDSISEVKL
KKPDTKKASTTQELYQSLLVTQDIVQDQENTFEEKFKPTVQKIEVSIEEGKRVTNVIEVSAADKE
EILKTVQEEIRSVVPIIVSGHEVAERSEIIPHLSTGEMDIIKPTTATAQVGQKPFETIEMIEQVLAEKE
IDKVEEISPQKTNARITVDENRFIAITEATTAQDVEAEMSIIKKPREEMAKSSMEGKEVAEQMEVS
LREELGNLPVAQRPTTFEAYPTQITLECVDISETIPQEHSTVFEEKMKVDERSAKVSFVEGKSINIS
HVISQDKEDTMIIQKREESTAEMTLTKVGMDVAQKAQVFIEQSTGLVQPFEKREVQAHHKQDAL
EPIIVEEIPSAESEGVFDKYPKTVFSTAIQTFEQDHGISITEVTSAEVESVLKEKKMDISQTANSTLI
MERNIVETSMIESQISIPDKIEQISMKPQVAVPEQDTFESIIVNENIVEESERTFEDVFQPQTQKADI
DIQKVTSLQVSETITEDKESVFDVVPKREEVKATQDISLHETVIGSLVESVQSIQEIHEEKRISSQAT
MAQTVIETAVKIETTVGEREDTFEGKNFKLEQQKGKPQMEGLSTVIVTEIVSNEIEDVLPATVTPK
EQQAQPILTGREVPEVTQVIAASTTEEFEKVTQLKKQQGKIEMEEMSSVTISEVISNETEDIFVLKT
IPKDQKANFNILGNEIAETSQVTTIIETEDLALKRPEEQKGKPTLDELTSLTVSHVVSEEAEETLSL
AKVPKEKTAHPSLTGRDVAEIIQILAIASVEKFVASKAPEEQKGKIQVEELAPLTVSQVISQEAEET
LPTPEIPVEREAQPSLISRDVAQTMEILTMANIDTLAEDKKPGEQKSVPGLEEFVPLSVLQTISTET
EDVLVSPKVPTKKIAQSSLTGHDVAETMQILTMMATKELIADRAPEKQKGKPNIEELTSVMVSQ
TVFHETEETLEEQVAPSTVIAKPALTGREVAEISQVLTVANVEELEKGKLPEQQKGKPNVEELTSI
TVSQAVFHETEETLEKQAAPSTVIAKPALTGREVAEVSQILTVANVEELEKDKLPEQQKGKPNVE
ELTSITVSQTVSHETEEILKQITPSTMIAKPALTGREVAEVSQVLTEVSIKELEKDKPPEQHKGKLN
VEELTSITVSQTMFHEIEETLEKQVAPSTVIAKPALTGREVAEVSQILTVANVEELEKDKLPEQQK
GKPNVEELTSITVSQTVFHETEETLEKQVAPSTVIAKPALTGREIAEVSQILTVANVEELEKDKLPE
QQKGKPNVEELTSITVSQTVFHETEETLEKQAAPSTVIAKPALTGREVAEVSQILTVTSAEELEKD
KLPEQQKGKPNVEELTSITVSQTVFHETEETLEKQIVPSTVIAKPALTGREVAEVSQILTVTSAEEL
EKDKLPEQQKGKPNVEELTSITVSQTVSHETEETLEKQIVPSTVIAKPALTGREVAEVSQILTVTTT
PALLGREVAEISQVLTVTSIEELEKRTLPEEQKGKPRLDELTSITISQIVSIELEDKLPSPEKPSEKIA
QPQIAGREVAQKTEILTVTNVEELEKSEKPESQKGRPDVEELSFLTVSEVVSTEAEKELPTPKAPK
EHKALPQLDSIEVAETSEILTITNTEELPKSKIPEEQKGKPQLEELLSLSVSEIAFGEMEKNLATPDE
PTIQTAKPSLIGIQVAQKSQVIPSVTAGELQKEMKPAAKQIIPEQIPFESIEQLQAVAQESEDIFVVE
KIGKSVKAEMSFRVSESVEVTQVMATEQESKEVIKGVAKEVSAQPDVIKHEVALKTEVQLADVA
DEFKVIKPEGKMAKGVDEIQQSVIVTEPLNAGEIESEMSESVLPSAKLANIIVEAEHLEHVMETTE
VPAQQHHITITQHTTKHDTPQLIESDTEVIEEYTTKFRRGSKEDETAAVKTKKTIIRKKKPKNEED
NVVVIEEELEDIKPKIPSIPKKQFMPIEEVTTTIDVEEIIPTRIEEAEEVEQKEIKALPAQEKVKPTEIE
EVKEQITVTEDTTKLGKPKKTTKKKIIKRHGKEQKVTEVVTVEEEEKAPETTVTEGPVEEIVEETI
KSLPGLEMVVPTEVEEVKEQVTVTEEITKLGKPKKTTKKKIIKRRGKEQQVTEVVTVEEEGKAPE
TTVTEGPVEEIVEETIKPLPGLEKVVPTEVEEVKEQVTVTEETTKLGKPKKTTKKKIIKRRGKQQQ
VTEVVTVEEEGKAPETTVTEGPVEEIVEETIKPLPGLEKVVPTEVEEIKEQVTVTEETTKLGKPKK
TTKKTIIKRRGKEQQVTEVVTVEEEGKAPKTTVTEGPVEEIVEETIKPLPDLEKVVPTEVEEVKEQ
VTVTEEITKLGKPKKTTKKKIIKRRGKEQQVTEVVTVEEEGKTPKTTVTEGPVEEIVEETIKPLPG

LEKVVPTEVEEVKEQVTVTEEITKLGKPKKTTKKKIIKRRGKEQQVTEVVTVEEEGKAPKTTVTE
GPVEEIVEETIKPLPGLEKVVPTEIDQVKEQVTVTEEITKLGKPKKTTKKKIVKRRGKQQQVTEVV
TVEEEGKAPETTVTEGPVEEIVEETIKPLPGLEKVVPTEVEEVKEQVTVTEEITKLGKSKKTTKKK
IIKRRGKEQQVTEVVTVEEEGKAPKTTVTEGPVEEIVAETIKPLPGLEKVVPTEVEEVKEQVTVTE
EITKLGKPKKTTKKKIIKRRGKEQQVTEVVTVEEEGKAPETTVTEGPVEEIVEETVKPLPGLEKVV
PTEIEEVKEQVTVREEITKLGKSKKTTKKKIIKRRGKEQQVTEVVTVEEEGKAPKTTVTEGPVEEI
VEETIKPLPGLEKVVPTEVEEVKEQVTVTEEITKLGKPKKTTKKKIIKRRGKEQQVTEVVTFEEEG
KAPETTVTEGPVEEIVEETVKPLPGLEKVVPTEVEEVKEQVTVTEEITKLGKPKKTTKKKIIKRRG
KEQQVTEVVTVEEEGKAPKTTVIEGPVEEIVEETIKPLPGLEKVVPTEVEELKEQVTVTEEITKLG
KPKKTTKKKIIKRRGKEQQVTEVVTVEEEGKAPKTTVIEGPVEEIVEETIKPLPGLEKVVPTEVEE
LKEQVTVTEEITKLGKPKKTTKKKIIKRRGKEQQVTEVVTVEEEGKAPKTTVIEGPVEEIVEETIK
PLPGLEKVVPTEVEEVKEQVTVTEEITKLGKPKKTTKKKIIKRRGKEQQVTEVVTVEEEGKAPET
TVTEGPIEEIVEETIKPLPGLEKVVPTEVEEVKEQVTVTEEITKLGKPKKTTKKKIVKRRGKQQQV
TEVVTVEEEGKAPETTVTEGPIEAIVEETIKPLPGLEKVPTEVEEVKEQVTVTEEVSQEGKPKKVT
KKKVIRRKGKQQQVTEFVTIEEQGKAPVTSVTETPLEEIIDEIVVSLPVLEDIKPTEVEEMQRHIIV
TEDVIKKSKEKEIIESADKEQQVTEIVSIEQKENLPITISGGPMGEILEVLSKIEYIKPIECVHEEITVV
EEITKEGKPKKVIKKRITIREGKEQRVIEETTVEEHGKSPVTTIIEGPVEEVLQEFLKSIPTSDYVGK
SNEVEEIREQVTVTEGTKEDKPIKTTKKRIIKRQGKKQQITELVTVEERGKTPISILTEGPMEELIEE
IIKPLPAPEQIKPSEVEKVCEQITMTEEVTKEGKPKKIVKKKIIKRKGREQQVSEVVTIEERDKPPV
TIITDGPIEEIVEETIKALPMKSGEVEEIREQVTVTQEITKEDKPRKTTKKKIIKHKGKEQQVTEVIT
VEEQGKEPVTTVTEGPVEKVIEEMIKSLPISERMKPTEIEEVHEQVTVAEEIKEGKPKKKITKKKQI
RQKGREQHVSETITVEEEGKLPVITITEGPTEEIIEETLKVLSAPEYAKPDELEEIRKQVTITQEMTE
EGKSKQITKQKAIKRKGKKQQVTEIVLVEEEGKSPVTIITEGPIEEIVKETVRALPTVERVDPIKVE
EVVEEVTVTEIVTEEVKLERLKVTKVEATKLEVQKIPMDKPQFAQIKLRKTPTMKRPVEKKEKIP
RVLLRSRIIPIKWPPAIKYLKIEEFEPNEVQNGILSRNVEEAAILSKSKKKKVKRLEKEIAKLEKLD
QEFEELKKELPLEKLVEPLIEKPEKKVKKKKPVEKLKGEKPQLMKISIKEQKPIKPKFEESVTPLFA
QIKLKKAPVKPKKKEDKDEIKFPKVLLRSRITEHEWPPSIKYCIITELEPNYVQNGELSRTMEEAL
KLKKMKHKKVKFPEKEITELEKVDQEFEKLKKIPLEKGEEIAPYERKPKSKESEEEKPKKLKIGK
GKPRSAEEEEPEIIKLKKIPEKVPSVPEKLAPIAKKKDEVDKPEKEKEEKEYPKLKPFEPYEIETTEI
ELEELEELEYPKKPEKVPKKMLTKKPKKEHKTPVQETEAVPIVPGVPKPREPQEEEEIKRRIPESE
ASKEKPEKIKLKPWKKPEEEKEQEKKPEYYLKFVPKDDDIVETVEIVTTVNMEETPEKKQRKIKK
KKTTTKRGDEKPKVIEEITIEEEGVEPMVTVEEIVEDKLEAVSIELKPVPIEEIKEEIVTSEIMSEDG
AKKTVRKKRVTKKREGKEQITEEVIVEEEGKKPLTATTELHEDTTQEIHEKPKHKRPTKPKADEK
VTEDITEEIVEQKAVEEIKKPKIIKKKPLKAKNEVTEEVVEGIIIEQPDEQEAQPIMEELETVTITEH
DVRNIPKKKKEVVIKEEEEIFETIETPTQKIIRKKIRPMKKGGEEIVVEEIIQKPREETIEMEKQRIIE
VIETPIKKVVKKIKAVVKDDGVPEEIVEEIVIEKPQKEKAKSIIEEEKEKVKVMKIDLKQAPKKPEE
IVEEEEEIIEIIETPMQKIIKKKSKDKKKKIVEEVIQKTIEDAKAMEERKIVEIIETPTKKIIKKKKAIF
TEGKTPEEEVEEIVIEKPVNEKVQKDVVPQEGIEITEIIAETSIEQLPEKKLKPEESKVSEVEEEKTEI
TQIEMEKIPKKKKPIATIEPEDKEEIIEEIKPEMKKEKAKPTEKESVEITEVISEVITEKLPEEIMKKK
ATKIKETEEKIIKKEIKIKEAPKEAVPQTEEQLEEEVQELITEKLKKTKAKKEVMSQDSIIITEVISTT

AEEALEVKKPEEDKAVIIKEKEEKGKVEEKKVIVKKAKKKLIPTEAEEEQIEEIIEEITPEELKMKK
AKKTILPKEEIQITEMIPEIKTEEIKEKQPKEEKAVPKEEEKVEEEAKITEVSVKKVPKEEEKKEIIT
NGEIGEKPKVKEIPEERPELKEAPKTEKFKKEKPKEIKPEEKEEKLKKKKIPEKKPIITEEEQFDEKI
EEIVEEKPRKVEPKKEIISKETISEIVAEELSTRKPEEHKVISVEEKSDEKFTVEEVLVEKDLEKKEK
EILEEKSIEEIHEKPKEIKKKKKKKIVKKENIEEWVEPEYERPVLEPMPEKIQWEPKKKKVKKPLP
ESLQKLVPQKIERKEIKPMKLKYSEPTETVQFAAIKLKKVVIPKKKEIEESKFPKIMLRSRITFVGD
YPPEIQYPKISELEVNPVQTGILSRNTEEALEILKRKVKKIKLPKKEVTELEKLDQEFEELKKVPLE
KIEDKLIYERPPKKPAEKPEEPQKLVVGKGKVPEEKKAEPEMMKLKKIPEKKPEKIEEPLKKPVK
PESEEKIKAEKKEKPKMKLEHEELRPLEFDKSELEKYVPEEHEESEKPPPEPMPKPYEREKKKKPD
QEIEQIPLIKGEPKLPEPDKEPEVKFRIPQKEKPEEEPEKITLKGWKKDKPEDEDIKEFPAKEEEEEA
PTAPKKEAEEIILKRKVKLKKPKEKATKEEEVTFKKPEEKKPKEVIEEITLKKEPEKSMEQVPEIFI
KKPVVEEKEIEEKETITEVTLKKPEEKISEEIIEEIKKPEAKKPVKKETSDEITVKKSIVEEKKEEEIP
EQIILKKKKPKEKPIPEEIKEEITLKKLKEKVSEEEQIEIKKPKEKKSVEKEATSEITIKKPVENEEEEI
LEEVTLKKKKPVLEEVKEEITLKKPIPKEKVPEEISEQIEIKKPKKKKPVEEEAADEITIKKPETVEK
EEEEITEEVTLKKKKPKEKPVLEEVKEEVTLKKPIPKEKVPEEVTEQVEIKKPKKKKPVEEEAADE
ITIKKPVSIEKEEEEITEEVTLKKKKPKEKPVLEEVKEEVTLKKPIPKEKVPEEITEQVEIKKPKKKK
PVEEEAADEITIKKPEPIEKEEEEIIEEVTLKKKKPKEKSVLEEVKEEVTLKKPVPKEKVPEEITEQV
EIKKPKKKKPVEEEAADEITIKKPEPIEKEEEEIIEEVTLKKKKPKEKSVLEEVKEEVTLKKPVPKE
KVPEEITEQVEIKKPKKKKPVEEEAADEITIKKPEPIEKEEEEIIEEVTLKKKKPKEKSVLEEVKEEV
TLKKPIPKEKVPEEVTEQVEIKKPKKKKPVEEEAADEITIKKPEPVEKEEEEITEEVTLKKKKPKEK
PVLEEVKEEVTLKKPIPKEKVPEEVTEQVEIKKPKKKKPVEEEAADEITIKKPELVEKEEEEITEDI
TLKKKKPKEKPVLEEVTEEITLKKPKEKEKVLEEVTEKIEVKKSKKKKPIVEEAADEVTIKKIVEE
ETKEEEAPEEVVLRPKSKRKSIVEEEEEVTEVTITKPKPVEEEKKSKEVEVFLKKKKPVVEEEVAD
VTVKKLISTEAEEVPEEFTIKKKKKPEKKPTVPEEVEETAITIKKVRGPEERKEEGEVSTEIQIKKK
KPERKVKEEATEELTIKKFEELKEPEEKEEVQEFTVKRKPPKQPPKPIEEIYEDVTLRKLRPKRKPR
PDINEVTEVENVTFRPRSTKTKEDVEQEFKISLNTYEEEDISMSGKVRLKPKKRPMTYSEEAGEET
IKIIQEIEDDSGPIIEEIIESDEEAKDQYSIEELETDEMRLPFRKRKKKEPKPYKVEDVEEGDVKLKL
KHERKYSIEEIDETLALKLKAKRRVSTYEEEEASLSITREEDISEGEEIEYVVRDGDTMFSICSYVA
ETDEAINLVEGERVYIIDHTNQDWWFVKKHLTEEKGWVPAQYLLNEVHYTHYLQRKLHEKIDK
LPVFEKPGPGEKTSAPRFIEKLQPIHTPDGYTVQFECQVEGLPRPQITWFRQTAIIKPSPDFQMYYD
DDNVATLIIREVFPEDAGTFTCVAKNAAGFASSTTELIVEAPLSDHGSDLTGPSRKSLSRESSLADI
LEGIPPTFSRKPKAKYVNEGEDVILECRLVAVPEPEITWYYKDMQITTKENIVVATESDMHMYCS
VIKITKVQKKQEGKYTIIAKNREGEATIEIPMKVKTGKHEPPEILEPLQSYVIREGETVVLSTQIVG
NPAPKVTWYKNGKPLKDLIPKQDGHVNTLTLIQPQVSDSGDYSVTAINDLGKVETKATLTVEKIP
SGAPEPPLFTERFQELTVPQKGTFKLVAKVTGNPVPEVTWLRNNKPLEKSPNIIETYDGENIVLEI
RNADSEVDAGDYKCIASNPVGKASHGAKVTVDVEKVTFTKTLEKEMIVDEYKTLELICETSHTV
STKWWHNDKEISGMDHREIVQEGRVHKLVIKRTSPTDEGTYKCTVKNQSTSSKVTVKATKPEFV
KKLQDCEVKERDVTILEVEITSQTADVKWFKDGESLGPSKEKLEFVKDGTIRKLLIRNTSVHDEG
EYTCTLMDEKCTAEVTVIELPPEIITKMQDVTIARGERATFEIELTKGDALVRWFKDGQELQFSEH
VQLSIDGKRQRLKIYDTEPEDAGVYSCEVGQQKSSAKLIVEEPGVDFITRLPDVTLVPLNADAVF

LIEISRDVPVTWMRKSEVIKESSKYSIVDEGTIKKLIVKKCTTKDISEYTAAVTNVKTSSKLRVEVI
EVAPKINPDTPKKYKVRKGEDVEIVVKFSSTPKPNDEWTVNGHVVTKSKRVVPSIDEESAILTIRK
IQEEDVGDYTLKLVNNVGEASIEINVVIVQVPSAPGAPEPLEITENSVTLHWKKPDSNGNSPIVEYI
LEHQEKTETTWTKIAETIKETTHKVTKLTTNKEYTFRVTAANEAGPGETSPTSPYIKITKPSAAEPP
IILEPLKSVVVGLGETVSLTCVIGGTPAPEITWLRNGEIFEDINITYENRVSKYTITRTTETSSASFTV
KAKNDIGTAETTCELKVQEPPKIIYDETLASQNLPVNGQWKIEIQMSGFPKPEITWLKNNKKIVD
KRVSIETVENTSTIFISSLSREDSATYTVKAVNEAGSSSVELHLRVIDKPSKPQGPVVFKKIRQDRV
TIEWRPPEDDGGIELEKYTIEKYEPGKTWTKVVDIDKEVESFCVHKLQQNAEYKFRIIARNAVGA
SEPLESETVKMRTSFEPPGPPRGPLEVSGMTKTSFTIKWQAPENDGGTPITEYIIEIKEESKKAWQK
IGSTKHETTQFGVSNLKTDVPYNFRITAKNSVGTGPPYVAEEPIAPGRRIKITKMTESTMYALLGIF
PPTKIIISKTPPSSPQHVQVINVTSKSVTLSWSPPASNGGTELTGYIIEKRPLIGKGARWTKVVTLD
ATTLQYCIENLKESEFIFRIFAENNMGLSLPTNSEPVTLMTHANVPSPPTAPLEIRQIAANTVVISW
GRPESDGGAPLESYKIAIRDAKKTMWMEVGRVNADTQKLNIRDLQENHMYLIRIFAKNEVGLSD
PLESDEPVKIIPASELAVVEPIAEMTEKGETASVSFSTENTSSWLREHNMDADIHSYARARLLRQD
EYFFRIWHYAKKLFE

Band 1 – H9KD10

MSETPPKSASPGGSRASPGSPSTPRGGRLRDRVNFFVELFEDKEGRRNAGQYRSPTNPRPGSGPSS
RPSSRASDSSFEESFERLVEEGELNGSKVVKFEKITVRKSVREVGAGGGASTRASLAESSRTPSEE
HALEDSAYQSHSHGAPNYGSKSSSVTSFTRFPSEESLSHRRGSSPHQHLGLDDRTPSEWYAEYRT
QSFHNVATRIEYVRSKSEYDAHIAEIKDEQERVQKKTFVNWINSYLSKRSPPLRVDDLIEDLKDG
TRLLALLEVLSGEKLPVERGRNLKRPHFLSNANTALQFLQSKKIKLVNINSSDLVDGRPPVVLGLI
WTIILYFQIEENTRALEYLGQTWGSQSSLESLSTQGSATSERKRISSEKWKQGARKTLLQWVTNA
LPKDIKVRDFGESWRDGNAFLAIIDAIKANLVNIAAMREATNRTRLATAFHVAESELGIAKLLDP
EDVDVPQPDEKSIMTYVAQFLHKYPEPGSAASDSFAAVQQEYDGLLAWLYERLKYLEQMGSSP
LGYDEYATVKGEVEQQRIVYNKLQRLVETPSMISITRDSWRHVQNLWKTLEMLMLRWLWVLD
SYLPGELSVVGRWLCHAEDLLLSDNNIPEEMTEETANIISNKLEEHKKFFLDLPSMTERFQAARSS
EAALKVHPQQLNEMAARLDSLPDRAAKRRIRLKFLEHKCCLIAFLFLVETKLKGWSVKYGTEES
VHQMLEQYRNFVSRNRIFQEFQKAYLDMQQIVEDYKREGNVDQEESANIDRFMRETSDKWKSV
SMDLRCVQSMLEEVVAYWRRWNVISDEFVTWLNRAEPALHLPEEDKMEFFQDISVWKDKHQQ
LSDTVTFLIATSDESVALQLKQRYSSLTSRWESLFQEAKQYMHAGDVIRNRKDYRAGVETLQK
WLRNVETALSATDLTTTEKIKAYGEKLQIFHNEVEGIEDLFKSISKKFQTLIQDLSRDEVDKMMN
TLKKEKEALVKVRALIPMQLHLYHQLLVQQESLEAGQKEIAAWLDEAERMLTNVDLSRGREHIL
TQLDRHKAFFSRTLYYKSMLESKNKVFTSIVKSVDSHADVATAEGGKTLRELNERFNRVSQAAQ
ALEQRLQEAVRCWTKFKECERQVCEWLSVAETMMNDKHTDNRRSIEYHKNFFSNVNEKWIQD
FVNAGQDLKSILPVEQQAPISEAVESLQKRWKEVLTFAPLHLMRLEFRLDEATFLQYLKEIEVEV
NSEQQALMKNDNVESILQRNKEFFVNRGTVLEVEKCLQTLKKISDAYSQLKPNDTSLAEAAQHA
ENLWEDSAQRVERLREQLKQVPEQWAAYKKKFDEMVRWMDHVDSNLRTILHEVNTLEEFETE
KTIFQKICREADSKREEMKWLVQTLDSLTSNRSDHEALSEQNRLEQLITRYKNLIPTIEITMTKTDI
YSKSYTYRKEVREVCTLLHKVKDQSKIDVVAESPETLKTAVTHQESRLSQLEQQRSNIVSMLQR

GKDLLKDQHAPPFVSLEVQQLESSWNDTYGQSVETLKSLKSSQKLWNTYLQQKEEILKLIEQAE
EELRKIESTTYYDASQVSSDLQSKQDFSSTLRKSAEELLKKLQETYSHLTEVAAPEKKEILKKEIIH
TEKRMETTLKTVQEKVVYLQEHSTRWNKFQTKLNELQLWTQQSAPQSIADTENLATTPEEMVY
RTESLQKEIIERTRTLKFLEEESQKLVKGGVDSLPAKQLRSDIITLERSIETLQKSIVAQRQTAEQNL
QTWKEYEKGIQELKPWIEEAESKAATIGSKPTTLAQAAHMLETARAFETRCQQHFPQIQDLSLIS
QRITGKTSASDEVDAVHTRWNAVHDIAVQTTTKLDKLVTSWNSFESEIKEFNEWLERSERTVLV
EPNAETPEISVLEKELVRLKDFNKTISDHQAQLISLTQVSDHISHGLSLEGATNLKARISDIKARVS
KLADTVRLQINRVSDSLLARQEFQMKITDFENWMSRLRSNIAEISDATVDTVDTNLQAVHAYIQE
HSEKQPSLEAICQEVKDICSKGSMQATVALVDTYTNLEKKYKALGDDLQQKKKGLEKWIELLS
WLNDANAQLSHCKYEAEARKPTIADLERFSSELRTIYDKIETWKQHVLPDSAIGIQIRDKQGKPLS
ASGLLIDLENKALSLQNEISAKRDRLENLGAKWNNFRTLQQTITEKILNTQTALQETVYNVDSCK
QLAPAVEKIDQLIEEHQKREQEKEILHFEGSSLMKEDQRSTTNIQVVLSSVDANWEKVNELLREQ
RKKYADMNTDWKDYEEARQKVEKSIKDAINLCQSVKGISYDITQANITLEKHKKALDTLKKGR
HFLDKMDSKAQQLTKEASLMPRFNSELIENDLTEVRQRYQDTYNDISEKLQAYETQVIIWKQIEE
SKSELIKWLTNTNEALTTAFERLMDAENCQIRLIRYREELPGYQQVYQNIVTKIEQLVKLNNNSDI
PTLNSLHQLLDDQFKVVKTSAEKLESLTSTLNERERTIRQEMKRCGDLISKIREDIIKCDDLTGEN
TKILGRINKCQELKTELEQCDYTLSKVEETLTKISTEYPSISRSSLPKELQALQLRRDGVANHANK
VIATLVAFLTKLYHEKFGALQRMVVTLKEKVAWCEPEQSSDRYNLEVKMASLMDVEVGIADCI
ARKEDTDNSLKLLASVESVETMAALKSDRDKVEVDLESLKSSYNKIKNDLERNIALWQRYELTS
ENVLSWLKENENKIRAEASALLNLDDIEQKIAEMTEMQKSVMEYQSELKDLTVLAEDITRVSSES
RVNQYISHLNTRYDYVLKFLAQHLDRLRELKENRDQYVANKKKLEIWIENAEKTLKAYDEITGP
KPITFYQSRLKELKAFAEEREVGQAILNKTAEAGEALFARITPDQREMIRTELRNFRNRVDAMAD
RSNVIYKKIESDMMHRSSFEDKFSQVKQWLADAQNKLGEKQDLLPTLQEKKLALHLYRTVAQD
VTVHKNILQQLQDRLSTAPDDDASEMLGNVIEAYEKLSNEVEGRINIAEKHVSNHEAYLQTFEKT
RDWINTVINEGTPIVEDFSVERETAQSKITTIENLLQQKAEGDRILADCNQQLNIVLEQTSMPGHS
ALLSNFEQQKKMWEDFLKRCVTARDKLKHMFNQWSEFEKIVEGLEAWIKQMETQLKDQSLKS
TEEAKRAHLQKLKSLEESIIAKGAEFNAAIEKSQSIEAEADLVTRVSRQTTKYQAIKNQIKEAVMR
YEQFVKEHNTFNMKYNQLLQWITDIKSELKKHSEIVGDLSVLQSRQKLIRDLGDTRTKENARFES
VIDLGEKLYVHTSPDGREIIRQQLRNLRTLWDGFTEDLQNTMQKLDQCLMQFAEFSLSHEQLTA
WLRDVERAMHQHTELKCTLEEKRAQLQNHKIMHQEIMSHQSLVESVCDKAQQLVDQTKDTSL
NVFLPSIKQLFHNIVAKSKDLLENLDDCVEKHHKFNLQVKSFSDWLNGEKDKLAECNDMTGER
TDICRRLATLAILKDDQMQGAEQLGKLKELSDTVIKRTAPKGWDAINKEIVILEGNLRQYLNEIES
VEDKQKTALQKWQDFEDKLETHTKWFSTMEAAFRDQQLQPTLQDKEARLQTLKEKRDAILKEE
LKIDEFIDKSHSLLHASGVERIKPLISQISNRYQLLHVLSKEVVTRCQSVVDDHRTYEEKLKVVDA
WLTQLEQSLASLKKDETGGNLEEKVSRLQILLAEKEQGEHRLASLISFGERILADTSAQGREIIRH
ELRQARERWDKLVEGIAEQQKKQDAQSLQWTNYQETLQQILAWLDTMERSVKQDSTITWSSLQ
EIKSKLLKSKKNISNLETLLDTFQQFYDLQKSYQDYQKQQWEQLANYSDYTGNKAALQIQLTKI
MELQDGQREGELKLDILSEHVSQSAHNLSPRSLESMERDLATLRFEHKKFATAVNDIIRCIEERIQ
QWSEYENSLERLLAWLADAESSLKNYSLKNTLDEKQEQLEKYQMLIVNLRQNEAEFDKMSDES
SELMQISGETRFSASVQQITSRFQSIQATAKELVKKCEQAVADHAAYLERYKQCSEWLANTRTT

YQSIKDDFSGTRQELTSNVTTLKDLLARQSSATLLINNTVEAGERLYSTTGMEGREIVRQQLLDL
QRAFEELYDSIASTERELQSKISRWSGFDESNESFDKWLRTVETQLKPEIELKTTLDEKRAQLQIY
RSFLHDIQSHQQDLLDLRDKADNLPDSTDKVHLTLKKLSERHATVLKRAVAFVERYEGIVSDHQ
QYSKAVLDTHEWIDATHNAVILWGDTELERVSLHTNLDRLKNLLHGLPEDKPRVQQIRILGEKVI
PGTLESGQINIRSQIDSSQQEWESLVTAVKSTIETLENKLQQWNEFEMSKERCLAWMRETDTKLH
AVDLKATLQEKKDQLELLRTLQGQVRAKELEIDAVTEKAQQLHKNITSRTTHMSELSIKYQQISN
KVKDLNSRWHQYVTTHQEFDNQVAECTRWLDDIRKKLAYCSDLGASSQKDLENKMEIVQDLL
LYKEDGFAKVQGIVELAQAVLANTAPIGHKAINDAVGKLQEQWSALASKMLETKTNLDDSINK
WAGLLEQIQSMNKTALEEKVRCENIEVDSLKIKVAEMIASGPQGLAASQAQSILNRFDTLFEKIKS
LLTEREEQYKDHRLYKEAHDDIINWLSRAREKIPSMKQRPLSDKLAIENAVAPLESLLNKKAQGE
LLVEHLQHTGKVVCASTSPQGQEIIKNEVKALTQSFEELFREIKQQKDQLEQTVSQWRDYKDEY
ERLSDWLQQFDILIKAQKNSLLPNVAEKEKQVQEVKEILENLLKGQEQIDKFNKTASSLLSSHLD
TYINNQLRHLNSRYQVQVNLAKDVLNKVETNLAQHKEYEANLEKTRAWIENAKQIIRKGTEAA
STSSREELQNRLDNIQELLRKREEGQNLVHLTVNCGEKVMRNTRSDGREEINAQLKEIQNDWER
LVKKISTTKVRLETSLLQWADYSSSYLQLQQWINDREAKLQQVCEQKVSKARKGLAGLSSLAIG
ERKANLRQTNSIVQDIVAFEPMIQSVTTKAEDLRQATPATEISIKYETLSKQAQELYAKQKETVEQ
HQAFIDSGNEFIQWIRAAKERLGKCSEPTGDKESLANKITQLKVLQSELPEGQKKLQHALEQGNA
ACQIADEEDKEIIEEEVALLQEEYDSYVDSLNNTKSLLEVGIVKWTEYEDQFSEATEWLTQTEQL
VQSFNKLQDSLEEKKNVLEQFQIHLQTLFDWQKELDRLNMKAQMLLETCADTRISNAITQLTTK
YNALLSLAKEIMRRLELHYQDQLRSNMAGLLSSWEQLSIDLNTVQAQLKSLLHRWDDHSEAHE
KLKQWLEETENGMQDLPDTKGEFGDMKTMLERYKHIQEEVRDKKTELDHLMDEASELSKLAK
KNTPLERTKELLKRWENLSENVDERKRLIENEMQEYNAYHAALQETEKWLLQISFQLMAHNSL
YITNKEQTVSQIQQHENLLAEIENYTSVLNDLKLKGNGQITRYVAVNPEIKTIIETQLQNVQESYN
SLLNTALQIKKRLAESLVKFQEYENTLESIMKNLDAYEPEIAQEMEAPMDTLDAAKQRFENART
LHNKLQGEKTRLALAVEACEAAVACVSRPGSPLDAPPVQIPAREVEVRNKLEELIDQAQGHLMN
VTKALNELEEQTRQKNVLRAWINQQRALCAEWKSRPAKLRSEAALAELQAMNDLLGNVGERR
THALTELSLHDDDQDIEEGLNKLETELTDAIAGKQAAQDLIQKYRTQVQNMQSWLDTLSKKVD
VIEKGNGQTIGQKIASVKEITTEFESQGPGKLNEVKTLSDQVMDSVSNLDSQQIEEQIKSVERRYA
DIGKKLQRKAQVLDMTAQGIEATRQEIEENRDWIQQKKKQAQMSEPVGFDSKQAEERLLALKA
MLKEAEGKQMVIDTLEKRVGNMQNELESNEQQQLENETKALRGEQSQLCTILTEGISSATAAAD
ARRKFEADLERARSWIKSKSNNLKKLSGYLPLKASKVEQDIVQHGELETDIDSFSEKDLNDILKQ
GNNLLKECSEEDRARLNKILDELNKDYEELKSEAQEKQAALADLLQGRKAFENEIDKCQRWINE
AEVATSSDLRTSSIDILREQLAKYDRLKKEAKEYADDIEKLMQQGKSILPTVTDADKLELNEQLQ
NMKEAHGRVAGIINERALVLQKNIDEAEESLARVAEAIQFMTDVQKELHELNKPIGSRVEDVEA
MLDAYERILNDLKANKAKLSDLQSINVADLHGVLTQQDDLMKAIESQIAKLRQLLLLRQQFIALI
TEITTFIAKYTEIVRDIENSGQTTEEKIKRYDDAILKIQECEATLASATDKGQQIAAEGSTVDRNNI
TEQLQSLKQQLQGLRRAVETQREQHELAAAEHKRLANELAEILDWLEDKEKEVKSRPLLERDPI
SVEAELQKHNELCDAVNEHLDRIRNLKNSVPHEEGMPGSLKEMLSEAVSLLTSLPREMEERGNY
LESNMKLRQEYAALTEKLRSWVREAEIRLESDKDGLDFENILSDLEEHKIYFSSEPSIRELVSQQIQ
QAGDKIWPSLNTSEQEELSAEQQQHTQLLKNTLNTAKSQRARLEQGAETWRDYTQTLERVRAVI

ARSRFTDEPVTTLAGLQFNIQKITHALNDIQNQQFELDLLIERSQEVLRLADASNKRTIEAQICEIS
AEWKELVSGLEGRRDALEALSKHWEDLEAQWSLIETKVNAIEEKGKLLDTVVRSKQHLHDTIKS
LHELVTEAEKLKPMAAEVKALSGPVLAYLAAFTEAPAHALEEKLNKLQNSVESLIDTLQTKSRK
ADEDLEAFESTEREIDQLRKRLNEARERASNLYIFGPDQDATEEELDELRWAVEQLLESGKKFSG
STKARYQASQQLVPSDLAQHLTALELCAEATAQAMEEKQREQKRARTVRSDYLTDLDEVQAWI
RQAELKVQDRSIEPVPLKDQLRQVQEELGTISDKLERLTRNGRTIAENTRDDTEKQLIDSTVHNV
TEQLNQVRNWLDERKQVVADTIDAWQRFLSLYEAVRTWTEEKRQFLVEPLKLSTLVQARQRLH
EYSTAVKSCKQINKNLSDMGKELESIGQVCSVGDLPEKLLEAEEAKVQVEGQLLERNALLQETS
EEWEQCERKMKEVKTWIEKAKQSLESPQNKKKPLRDQHSIREKMLSDIAIQKTKIGISMEKLQV
HFRSGIGGDSRIGETVDELLAELDNLHANVKEQTTALEGCLAQIDQYQQEIQQLRQQIMQVEQQL
RTVLSPTYLSTDKEKALQEQQICREKIKSLQSKIQARTERSKILAQRGRPDPELLDP

Band 2 – H9KU31

MPKPKPQEGEDPDPTPYLFVSLEQKRIDQTKPYDAKKACWVPDEKEGYVLGEIKATKGDVVSV
GLPGGETKDFKKDQLQQVNPPKYEKCEDMSNLTYLNDASVLHNLKQRYYAKLIYTYSGLFCVA
INPYKRFPVYTQRCAKLYRGKRRNEVPPHIFAISDGAYVNMLTNSENQSMLITGESGAGKTENTK
KVIAYFATVGASTKKADDPTQKKGSLEDQVVQTNPVLEAFGNAKTVRNDNSSRFGKFIRIHFGPS
GKLAGADIETYLLEKARVISQQALERSYHIFYQMMSGSVPGLKEMCCLTNDIHDYVFVSQGKTTI
PNVDDGEEYMCLLSNNIYDYVNVSQGKITIPNVDDGEECVLTDQAFDVLGFTQEEKNDIYKITA
AVMHMGGMKFKQRGREEQAEADGTEEGERVAKLLGCDCADLYKNLLKPRIKVGNEFVTQGRN
KDQVAYSVGAMSKAMFDRLFKWLVKKCNETLDTKQKRQHFIGVLDIAGFEIFDYNGFEQLCINF
TNEKLQQFFNHHMFVLEQEEYKKEGIVWQFIDFGMDLAACIELIEKFNSFEQLCINFTNEKLQQFF
NHHMFVLEQEEYTKEGIHWEFIDFGMDLLACIELIEKFNGFEQLCINFTNEKLQQFFNHHMFVLE
QEEYKKEGIVWQFIDFGMDLASCIELIEKLQQFFNHHMFILEQEEYKREGIEWTFIDFGMDLQQTI
DLIEKPMGILSILEEESMFPKATDKTFEEKLNNNHLGKSPNYLKPKPPKPGQQPAHFAIGHYAGN
VPYNITGWLEKNKDPLNDTVVDQFKKSGNKLLVEIFADHPGQSGDAGGGGGKGGRGKKGGGF
STVSSSYREQLNNLMTTLRATQPHFVRCIIPNEMKQPGVIDSHLVMHQLTCNGVLEGIRICRKGFP
NRMVYPDFKLRYMILAPAAMANEPDPKKAAQKCFDEVGLDPDMYKILAPAAVDKVASDPKKA
AEAILESTGLDPDQYKILCANAIKEPCDPQKATQLILDAINLEPELYRMGNTKVLDAFDKLASKP
VEGKNARYFGYLMRGGEKECLYKYDWGTDEEEGNFGKSNQSNGRRDRVFFRAGVLGQMEEFR
DERLSKIVSWMQAYIRGYLSRKDYKKLQEQRLALVVVQRNLRKYLQIRTWPWWKLWQKVKPL
LNATRIEDELAGAAGEKKSGNEGDAESQLQALEEKARKTQEALEKEEKLRKELEEQNSKLVTER
DALQRQLDGEKGSLSEYMEKSLKLAAQKADLESQLQDLNDRFKEEEDTRNNLFQNKKKLEQEV
AGLKKDIEDLELNLQKSEQDKATKDHQIRNLNDEIAHQDELINKLNKEKKNQGEVNQKTAEELQ
AAEDKVNHLNKVKIKLEHTLDELEDSLEREKKSRADVEKAKRKVEGDLKLTQEAVADLERNKK
ELEQTIQRKDKELSSLTAKLEDEQSLVGKLQKQIKELQARIEELEEEIEAERGSRVKAEKQRSDLA
RELEELGERLEEAGGATSAQIELNKKREAELSKLRRDLEEANIQHETTLANLRKKHNDAVAEMG
EQIDTLNKLKARVEKDKVQYFSELNDMRASVDQLSNEKAAQEKIVKQLQHQLNETQGKLEEVN
RTLNDFDAAKKKLSIENSDLLRQLEEAESQVNQLSKIKISLTTQLEDTKRLADEESRERATLLGKF
RNLEHDLDNIREQVEEEAEGKADLQRQLSKANAEAQLWRTKYESEGVARAEELEEAKRKLQAR

LAEAEETIESLNQKVLALEKTKQRLSTEVEDLQIEVDRATAIANAAEKKQKAFDKIIGEWKLKVD
DLAAELDASQKECRNYSTELFRLRGAYEEGQEQLEAVRRENKNLADEVKDLLDQIGEGGRNIHE
IEKARKRLEAEKDELQAALEEAEAALEQEENKVLRSQLELSQVRQEIDRRIQEKEEEFENTRKNH
QRALDSMQASLEAEAKGKAEALRMKKKLEADINELEIALDHANKANAEAQKNIKRYQQQLKD
VQTALEEEQRARDEARELLGISERRANALQNELEESRTLLEQADRGRRQAEQELADCHEQLNEL
GAQNASISAAKRKLEAELQTLHSDLDELLNEAKNSEEKAKKAMVDAARLADELRAEQDHAQTQ
EKLRKALETQIKELQVRLDEAEANALKGGKKAIQKLEQRVRELENELDGEQRRHADAQKNLRK
SERRIKELSFQADEDRKNHERMQDLVDKLQQKIKTYKRQIEEAEEIAALNLAKFRKAQQELEEAE
ERADLAEQAITKFRTKGRGGSAARGLSPAPHRPAFKPQLDGSAFPPRFDLQPDGEL

Band 2 – H9KU35

MPKPKPQEGEDPDPTPYLFVSLEQKRIDQTKPYDAKKACWVPDEKEGYVLGEIKATKGDVVSV
GLPGGETKDFKKDQLQQVNPPKYEKCEDMSNLTYLNDASVLHNLKQRYYAKLIYTYSGLFCVA
INPYKRFPVYTQRCAKLYRGKRRNEVPPHIFAISDGAYVNMLTNSENQSMLITGESGAGKTENTK
KVIAYFATVGASTKKADDPTQKKGSLEDQVVQTNPVLEAFGNAKTVRNDNSSRFGKFIRIHFGPS
GKLAGADIETYLLEKARVISQQALERSYHIFYQMMSGSVPGLKEMCCLTNDIHDYVFVSQGKTTI
PNVDDGEESFDVLGFTQEEKNDIYKITAAVMHMGGMKFKQRGREEQAEADGTEEGERVAKLLG
CDCADLYKNLLKPRIKVGNEFVTQGRNKDQVAYSVGAMSKAMFDRLFKWLVKKCNETLDTKQ
KRQHFIGVLDIAGFEIFDYNGFEQLCINFTNEKLQQFFNHHMFVLEQEEYKKEGIVWQFIDFGMD
LAACIELIEKFNSFEQLCINFTNEKLQQFFNHHMFVLEQEEYTKEGIHWEFIDFGMDLLACIELIEK
FNGFEQLCINFTNEKLQQFFNHHMFVLEQEEYKKEGIVWQFIDFGMDLASCIELIEKLQQFFNHH
MFILEQEEYKREGIEWTFIDFGMDLQQTIDLIEKPMGILSILEEESMFPKATDKTFEEKLNNNHLG
KSPNYLKPKPPKPGQQPAHFAIGHYAGNVPYNITGWLEKNKDPLNDTVVDQFKKSGNKLLVEIF
ADHPGQSGDAGGGGGKGGRGKKGGGFSTVSSSYREQLNNLMTTLRATQPHFVRCIIPNEMKQP
GVIDSHLVMHQLTCNGVLEGIRICRKGFPNRMVYPDFKLRYMILAPAAMANEPDPKKAAQKCF
DEVGLDPDMYKILAPAAVDKVASDPKKAAEAILESTGLDPDQYKILCANAIKEPCDPQKATQLIL
DAINLEPELYRMGNTKVLDAFVLGQMEEFRDERLSKIVSWMQAYIRGYLSRKDYKKLQEQRLA
LVVVQRNLRKYLQIRTWPWWKLWQKVKPLLNATRIEDELAGAAGEKKSGNEGDAESQLQALE
EKARKTQEALEKEEKLRKELEEQNSKLVTERDALQRQLDGEKGSLSEYMEKSLKLAAQKADLE
SQLQDLNDRFKEEEDTRNNLFQNKKKLEQEVAGLKKDIEDLELNLQKSEQDKATKDHQIRNLN
DEIAHQDELINKLNKEKKNQGEVNQKTAEELQAAEDKVNHLNKVKIKLEHTLDELEDSLEREKK
SRADVEKAKRKVEGDLKLTQEAVADLERNKKELEQTIQRKDKELSSLTAKLEDEQSLVGKLQK
QIKELQARIEELEEEIEAERGSRVKAEKQRSDLARELEELGERLEEAGGATSAQIELNKKREAELS
KLRRDLEEANIQHETTLANLRKKHNDAVAEMGEQIDTLNKLKARAEKGRHDIHAELNNSRAAT
DQVSREKAAQEKIVKQLQHQLNETQGKLEEVNRTLNDFDAAKKKLSIENSDLLRQLEEAESQVN
QLSKIKISLTTQLEDTKRLADEESRERATLLGKFRNLEHDLDNIREQVEEEAEGKADLQRQLSKA
NAEAQLWRTKYESEGVARAEELEEAKRKLQARLAEAEETIESLNQKVLALEKTKQRLSTEVEDL
QIEVDRATAIANAAEKKQKAFDKIIGEWKLKVDDLAAELDASQKECRNYSTELFRLRGAYEEGQ
EQLEAVRRENKNLADEVKDLLDQIGEGGRNIHEIEKARKRLEAEKDELQAALEEAEAALEQEEN
KVLRSQLELSQVRQEIDRRIQEKEEEFENTRKNHQRALDSMQASLEAEAKGKAEALRMKKKLEA

DINELEIALDHANKANAEAQKNIKRYQQQLKDVQTALEEEQRARDEARELLGISERRANALQNE
LEESRTLLEQADRGRRQAEQELADCHEQLNELGAQNASISAAKRKLEAELQTLHSDLDELLNEA
KNSEEKAKKAMVDAARLADELRAEQDHAQTQEKLRKALETQIKELQVRLDEAEANALKGGKK
AIQKLEQRVRELENELDGEQRRHADAQKNLRKSERRIKELSFQADEDRKNHERMQDLVDKLQQ
KIKTYKRQIEEAEEIAALNLAKFRKAQQELEEAEERADLAEQAITKFRTKGRGGSAARGLSPAPH
RPAFKPQLDGSAFPPRFDLQPDGEL

Band 2 – H9K4A8

MTAVFFFFFYLCSPFAFLPPPPPLLGLEQFNSFEQLCINFTNEKLQQFFNHHMFILEQEEYKREGIE
WTFIDFGMDLQQTIDLIEKPMGILSILEEESMFPKATDKTFEEKLNNNHLGKSPNYLKPKPPKPGQ
QPAHFAIGHYAGNVPYNITGWLEKNKDPLNDTVVDQFKKSGNKLLVEIFADHPGQSGDAGGGG
GKGGRGKKGGGFSTVSSSYREQLNNLMTTLRATQPHFVRCIIPNEMKQPGVIDSHLVMHQLTCN
GVLEGIRICRKGFPNRMVYPDFKLRYKILAPAAVDKVASDPKKAAEAILESTGLDPDQYRLGHT
KVFFRAGVLGQMEEFRDERLSKIVSWMQAYIRGYLSRKDYKKLQEQRLALVVVQRNLRKYLQI
RTWPWWKLWQKVKPLLNATRIEDELAALEEKARKTQEALEKEEKLRKELEEQNSKLVTERDAL
QRQLDGEKGSLSEYMEKSLKLAAQKADLESQLQDLNDRFKEEEDTRNNLFQNKKKLEQEVAGL
KKDIEDLELNLQKSEQDKATKDHQIRNLNDEIAHQDELINKLNKEKKNQGEVNQKTAEELQAAE
DKVNHLNKVKIKLEHTLDELEDSLEREKKSRADVEKAKRKVEGDLKLTQEAVADLERNKKELE
QTIQRKDKELSSLTAKLEDEQSLVGKLQKQIKELQARIEELEEEIEAERGSRVKAEKQRSDLAREL
EELGERLEEAGGATSAQIELNKKREAELSKLRRDLEEANIQHETTLANLRKKHNDAVAEMGEQI
DTLNKLKARAEKGRHDIHAELNNSRAATDQVSREKAAQEKIVKQLQHQLNETQGKLEEVNRTL
NDFDAAKKKLSIENSDLLRQLEEAESQVNQLSKIKISLTTQLEDTKRLADEESRERATLLGKFRNL
EHDLDNIREQVEEEAEGKADLQRQLSKANAEAQLWRTKYESEGVARAEELEEAKRKLQARLAE
AEETIESLNQKVLALEKTKQRLSTEVEDLQIEVDRATAIANAAEKKQKAFDKIIGEWKLKVDDLA
AELDASQKECRNYSTELFRLRGAYEEGQEQLEAVRRENKNLADEVKDLLDQIGEGGRNIHEIEK
ARKRLEAEKDELQAALEEAEAALEQEENKVLRSQLELSQVRQEIDRRIQEKEEEFENTRKNHQR
ALDSMQASLEAEAKGKAEALRMKKKLEADINELEIALDHANKANAEAQKNIKRYQQQLKDVQ
TALEEEQRARDEARELLGISERRANALQNELEESRTLLEQADRGRRQAEQELADCHEQLNELGA
QNASISAAKRKLEAELQTLHSDLDELLNEAKNSEEKAKKAMVDAARLADELRAEQDHAQTQEK
LRKALETQIKELQVRLDEAEANALKGGKKAIQKLEQRVRELENELDGEQRRHADAQKNLRKSE
RRIKELSFQADEDRKNHERMQDLVDKLQQKIKTYKRQIEEAEEIAALNLAKFRKAQQELEEAEE
RADLAEQAITKFRTKGRGGSAARGLSPAPHRPAFKPQLDGSAFPPRFDLQPDGEL

Band 3 - H9KA35

MAEVIDCNFPVWGLLPKKETGVTQFLTKYPEYDGRGVIIAIFDSGIDPGAPGMQETSDGKPKIIER
YDCSGAGDVDTSKIVQAPDGYIIGITGRKLKVPSNWVNPSGQYHIGIKNLYSLYPGKLRERVLVE
RKKRLWDNNHKSALAEASRQLQEFEAKNPQLTTLKERLEKEELEARVEILNNIEKKYSDVGPTY
DCVVFHDGEVWRACIDTSEEGNLETGVFLGEYTITRQYAPLIPEDQLNISINIHDDGNTLEIVSLCS
SHGTHVASIAAAYFPDNPELNGVAPGAQIISLSVGDGRIGTMETGTAVVRAMIHVMKHKEKIHVI
NMSYGEHAHWSNTGRIGELMNEVIDKYGVTWVASAGNLGPALCTIGTPPDISSNSVISVGAYVS

PDMMVAEYSLREKMPGMSYTWSSRGPMIDGGAGITVCAPGGAITSVPNFTLRKSQLMNGTSMA
APHVTGAIAILISGLVAKGCSYSPYSIKRALENTAHYIQNLDPFAQGSGLLQVERAFDNLITYCDV
PERDVRFTINCGPNNAKGIHMRSSIIDRPKDYAITVEPVFLNSENTDPTLKIAFNLKLTLVCDASW
VHFPTHLDLMNMVRAFAIKVDGFNLPEGVHTTSVRAYDVTDVAKGPVFQIPVTVVQPQTLPKT
AILPDLTYTNILFKPNTIYRHFILVPEDATWAVIRLKSTEKDKTGRFVIHSVQLKPRLSCKTLEVNK
LFTVTSQSEIVHPFAVQGGLILELVIAKYWANIGDMLVDYVIEFHGVRMISGNLTMQSGDGINRL
EVRSSLRNEEVVPSICLKSSVQILKPTDSRIAPLRERDIIPPSRQIYELQLTYTFHCAKATEITPNAAL
LSDLLYESEYESQMWMIYDSNKQLICCGDAYPSKYSNQKIEKGDYTLKIHIRHEKKDLLDRLTE
MPFLLSHKLSNPINLDVYASQSQAIIGGKKMIAASVPPGHILPLYIAPISNENKVSRGITLGSGSYL
QGTLTFCKDDNGKKVDCHTFKYILSEPNKKSSSSSSSSSSSSYSSSNKEKPTKWDEYNEALRDFK
CSWLTKLEPGEYANLLYGELKNLFSDHLPVHTAMLISLDSPEARRHVPHDDISEESVSLANQIISV
ADAVITNIDQDKLLAYYGLKSDQRDDATKIRATMEKQKFSLIKALVKKGCALSRLYVHSAKKGE
GDRQSYEHLLDSVTHHWQEVISLSLWHAHINNHYGRYLKLLLRYYEEHPLKEVDEKCIELANIL
GWEHLSRHINTISEACTLICLLVAQRISQTGLLIYNIEKSPQFIAIIAEAMIEGNNIHAWIVKKGLVS
HPYLSTEEALKLGGRNLNLLREWTFQVFYERIQNGLYQHINDFLHKWYLAPRSKNLFMLLITCG
RTVLFIFQENMVTFFDSHSHSTIVNPNRGLVIAQTTIDKLEHLCNWYTEDILNECYNTEANQYELA
FLYPFNSQCCGCNPLCNCGSHCREQ

Band 4 - H9KTR7

MSSAVAKASKYTYRSTGGGTADVSIEYSADLSALSRLEDKIRLLQDDLESERELRQRIERERADL
SVQVIQLSERLEEAEGGAESQFEINKKRDTELAKLRKLLEDVHLESEETAHLLRKKHQEVVVDFQ
DQIDQLSKARARADKEKSKFQQEVYELLAQLDNVTKEKLLSIKTVEKLEVHVAELNVKIEELNR
TIIDITNVKTRISQENIELTKEVQDLKVNIENAVYLKTQIAGQLDDARRRLEDEERRRSLVEASLH
QVESELESVRIQLEEESEARLDIERQLVKANGEVQVWRSKYETEANARAEEVEELRRKYSARIQE
QEEQIETLLVKINNLEKQKSRLQSEVEVLIIDLEKANGTARELQKRVEQLEKINVELKARLDESM
AMYEQSQRDLRNKQQELQRCNAELDKTRELKDQLARENKKLGDDLNDAKNQLSDMNRRLHEL
ELELRRLENEREELAAAYKEAEAGRKIEEQRSQRLSAELTQLRHDYERRLTEKDEEIEIIRKQTSIE
IEQLNARVVEAETKLKTEVQRVKKKLQIQITELELSLDVANKNNIDLQKTIKKQSLTLTELQAHY
DEVQRQLQVTLDQLGISQRRLQSLTAELEEVRGNYDSALRAKRTVEQQYEESVSRINELTTINAN
IVTSKAKLEQELSTLAGDYEEVTKELRVSDERYQRVQTELKHTVEILHEEQERIVKIEAIKKSLEIE
VKNLSVRLEEVEANAIVGGKRIISKLEARIRDLELELDEEKRRHSETVKILRKKERNIKEVMIQVE
EDAKNIALLQESLDKASQKVNLYKRQLQEQEGMSQQSVTRVRRFQRELEAAEDRADTAESNLT
LIRAKHRSFVTTSSVPGSQVYLVQETRSDL

Band 4 - H9K1K1

MNDMEAYGDGYMEPEEEWEREGLLDPAWEKQQKKTFTAWCNSHLRKAGTAIESIEEDFRNGL
KLMLLLEVISGETLPRPDRGKMRFHKIANVNKALDYIASKGVKLVSIGAEEIVDGNLKMTLGMI
WTIILRFAIQDISVEEMTAKEGLLLWCQRKTAPYKNVNVQNFHLSFKDGLAFCALIHRHRPDLID
YNKLSKDNPLENLNTAFDVAEKYLDIPRMLDPDDLINTPKPDERAIMTYVSCYYHAFQGAQQVS
VKKCVLFPYFGYKMTYMRNTAMPDERAVMTYVSSYYHCFSGAQKAETAANRICKVLKVNQEN

ERLMEEYERLASDLLEWIRRTMPWLASRQTDNSLAGCQKKLEEYRTYRRKHKPPRVEQKAKLE
TNFNTLQTKLRLSNRPAYMPTEGKMVSDINKAWKGLELAEKSFEEWLLSEMMRLERLEHLAQK
FKHKADATLEYHDSASVNARCQRICDQWDRLGTLTQRRRQALDEAERILEKIDVLHLEFAKRAA
PFNNWLDGTREDLVDMFIVHTMEEIQGLMDAHAAFKATLGEADKEYNAIVGLVREVESIVKQF
QIPGGLENPYTTLTALDLTKKWSDVRQLVPQRDGTLQAELRKQQNNELLRRQFAEKANAVGPW
IERQLDAVTAIGLGLQGTLEDQLHRLKEYEQAVYQYKVHLEELEKIHQAVQEGMIFENRYTQYT
METLRVGWEQLLTSINRNINEVENQILTRDSKGITQEQLNEFRSSFNHFDKNRTGRLAPDEFKSCL
VSLGYSIGKDRQGDIDFQRILAIVDPNNSGYVHFDAFLDFMTRESTDTDTAEQVIDSFRILAGDKP
YILADELRRELPPDQAEYCIQRMPPYKGPNAIPGALDYRSFSTALYGESDL

Band 5 - H9K918

MLNVVSKAAAGALRAVKPSILQNEITKISGALSVNSRDYAKAASSKGGAQGKIVAVIGAVVDVQ
FDDALPPILNALEVQNRTPRLVLEVAQHLGENTVRTIAMDGTEGLVRGQSVLDSGYPIRIPVGAE
TLGRIINVIGEPIDERGPIPTDKLAPIHADAPEFVDMSVEQEILVTGIKVVDLLAPYAKGGKIGLFG
GAGVGKTVLIMELINNVAKAHGGYSVFAGVGERTREGNDLYHEMIESGVISLKDKTSKVALVY
GQMNEPPGARARVALTGLTVAEYFRDQEGQDVLLFIDNIFRFTQAGSEVSALLGRIPSAVGYQPT
LATDMGSMQERITTTKKGSITSVQAIYVPADDLTDPAPATTFAHLDATTVLSRAIAELGIYPAVDP
LDSTSRIMDPNIIGAEHYNVARGVQKILQDYKSLQDIIAILGMDELSEEDKLTVARARKIQRFLSQ
PFQVAEVFTGHAGKLVPLEETIKGFKKILAGDYDHLPEVAFYMVGPIEEVVAKAESLAKQ

Band 5 - H9KC11

MALLSLRLVSSIARQLPNTTIQVKWPLSISSCKYHVSCSRRSAEISSILEERILGASPKANLEETGRV
LSIGDGIARVYGLKNIQADEMVEFSSGLKGMALNLEPDNVGVVVFGNDRHIKEGDIVKRTGAIV
DVPVGEELLGRVVDALGNPIDGKGPLNSKLRFRIGTKAPGIIPRVSVREPMQTGIKAVDSLVPIGR
GQRELIIGDRQTGKTALAIDTIINQKRFNDAGEEKKKLYCIYVAIGQKRSTVAQIVKRLTDSGAM
DYTIIVSATASDAAPLQYLAPYSGCAMGEFFRDNGKHALIIYDDLSKQAVAYRQMSLLLRRPPGR
EAYPGDVFYLHSRLLERAAKMNESLGGGSLTALPVIETQAGDVSAYIPTNVISITDGQIFLETELF
YKGIRPAINVGLSVSRVGSAAQTKAMKQVAGSMKLELAQYREVAAFAQFGSDLDAATQQLLNR
GVRLTELLKQGQYVPMAIEEQVAVIYCGVRGYLDKMEPTKITAFEKEFLAHIRTSQRDLLNTIAK
DNTISEASDAKLKQVVTDFLASFSG

Band 5 - Q3B712

MSDDEEQYSSEEEVVEETKQPEGRKIEGRASQKESGENIEFMKRQEQKRSDLDEQLKEYIAEWR
KQRAKEEEELKRLKEKQAKRKITRADEEKRLAQKKKEEEERRQREIEEKKQRDMEEKRKRLEES
EKKRQAMMQAMKEQASKKGPNFTITRKDLAGNLTSAQLERNKTKEQLEEEKKISLSIRIKPLEID
GFSIEKLRSKANELWDTIVKLETEKYDLEERQKRQDYDLKELKERQKQQLRHKALKKGLDPEAL
TGKYPPKIQVASKYERRVDTRSYDDKKKLFEGGYDTLLAEINEKLWKQKTEQFMKRTKTKLPK
WFGERPGKKPGDPESPEGEEDVKAAAEDEELEEPQFEEEEEEEEEEEEEEEEEGEKKEGEGEGEE
EEEEEEEEEEEEEEEEEEEEEEEE

Band 6 - H9KNB7
MCDDEVAALVVDNGSGMCKAGFAGDDAPRAVFPSIVGRPRHQGVMVGMGQKDSYVGDEAQS KRGILTLKYPIEHGIITNWDDMEKIWHHTFYNELRVAPEEHPVLLTEAPLNPKANREKMTQIMFE TFNSPAMYVAIQAVLSLYASGRTTGIVLDSGDGVSHTVPIYEGYALPHAILRLDLAGRDLTDYLM KILTERGYSFTTTAEREIVRDIKEKLCYVALDFEQEMATAAASTSLEKSYELPDGQVITIGNERFR CPEALFQPSFLGMESCGIHETVYNSIMKCDVDIRKDLYANNVLSGGTTMYPGIADRMQKEITALA PSTIKIKIIAPPERKYSVWIGGSILASLSTFQQMWISKQEYDESGPGIVHRKCF
Band 6 - H9K667
MCDDEVAALVVDNGSGMCKAGFAGDDAPRAVFPSIVGRPRHQGGVMVGMGQKDSYVGDEAQ SKRGILTLKYPIEHGIITNWDDMEKIWHHTFYNELRVAPEEHPVLLTEAPLNPKANREKMTQIMF ETFNSPAMYVAIQAVLSLYASGRTTGIVLDSGDGVSHTVPIYEGYALPHAILRLDLAGRDLTDYL MKILTERGYSFTTTAEREIVRDIKEKLCYVALDFEQEMATAAASTSLEKSYELPDGQVITIGNERF RCPEALFQPSFLGMESCGIHETVYNSIMKCDVDIRKDLYANTVLSGGTTMYPGIADRMQKEITAL APSTIKIKIIAPPERKYSVWIGGSILASLSTFQQMWISKQEYDESGPGIVHRKCF
Band 6 - H9KKW7
MSDEEVAALVVDNGSGMCKAGFAGDDAPRAVFPSIVGRPRHQGVMVGMGQKDSYVGDEAQS KRGILTLKYPIEHGIVTNWDDMEKIWHHTFYNELRVAPEEHPVLLTEAPLNPKANREKMTQIMF ETFNTPAMYVAIQAVLSLYASGRTTGIVLDSGDGVSHTVPIYEGYALPHAILRLDLAGRDLTDYL MKILTERGYSFTTTAEREIVRDIKEKLCYVALDFEQEMATAASSSSLEKSYELPDGQVITIGNERF RCPEALFQPSFLGMEACGIHETTYNSIMKCDVDIRKDLYANTVLSGGTTMYPGIADRMQKEITAL APSTMKIKIIAPPERKYSVWIGGSILASLSTFQQMWISKQEYDESGPSIVHRKCF
Band 6 – H9KTD0
MTRKQTIIVKLKRSSTGKPWGIRIAGGADLGTPIVVTRSENETLQRGDVIKKIDDYDARDVRHVD AQNLLQNSESIRLVIERSEPSKASRINIRTTSSSIFESNTGDRAASQATEITSGITEESCTAAFHRRIQS ALILAGPPLLAARTPRRSSRGESLFPYRTTPLVLPGAKIKKDAPLGECYLRHHPNPMIRAAPHHYE PAHPEVAMKQKVAETVLQRVLGPNEVPKVVHKQFNSPIGLYSEENIADTIKCQASAIPPKKPMK YDPSKSEAYKALQEEALGDTVQEVKQPARTGVFSPQKVNQNRIYHARPKSPAGPYVNILDDDGE KIHQSNSFKRIMYSVLGQTDY
Band 6 - H9K2W8
MTSIFSVRIAKSNSIEYLTRLCKISKNYNITQVAFIKRIAFKEHIPKPAPYPYWKKVCNEITMILDPT SLRYDDNTKLIVVDGPPAVGKTKLCEQIAKDFGFLYMPAPTHDEIFINYYGFDIRDLNPQLPESCR FYDLKDFLRNPYYYRTASIQLGFFNMRFEQYMNALVHILATGQGVVLNRSIFTEYAFMDAMHK AGYLSDLTVKEFEMMRKNSFKFLLRPHLVIYLDASPEIIQEKIKKRGNVDEINSKVFTTKFLTDLE NATKEKCLSWLSSHSHILIYDWSKEGNNIDVIQDIETLDFEEDQYKEKLQDWVFVDTDQLINFLE RYQNKTYIFDYMNRKTEPIIATDMYLINDERDIQQKVLETVNSEKYQPGCNPYYDKIPWITKKQS

PLFCIYRRTPRDFVNCDLFKFI
Band 7 - H9K538
MDARFRSNLDMIGRNEPITRKARFWQSYVRALKGTDDIRAPEHTHRPRSIFRSDYPELHSTSWPF GKSIFENPIHAADRINVPGYRYLPVHREIYGYSPRQIYPHQYKPVERFIPAKPFDPEQAWADHLNR LADIDKLYPSKSPLLARHISPPLSTKRLFDIHGNLVTDYDYLPSFPSLLRKKPLFDLLEPSVMAPISA FTRDPWWYPSYAPYIPSYAAKSTPFYLRDSYLSPVKRSYLWSRHPIRPFGMYPHYFVIRDTLMKI KIILCLRK
Band 7 - H944R2
MAPPSYNDLGKSARDLFSSGYHFGLIKLDVKTKTKSGVEFSSGGVSNQDTGKVFGSLETKYNID DYGLKFSEKWNTDNTLATDITFADKLLKGLTLGYGCTFSPQTGTKTGKLKTAYKHDNVSAAAD FDLSLSTGPLVNASTVVGYQGWLAGYQACFDTQRNKLTKNNFALGYTASDFTLHAAVNNGCDF SGLIYHKVKPELEGAINLEWNSSNNVTQFGIATKYNLDNDASIRAKVNSNLQVGLGYQQKLRDG VTLTLSTNIDGKNFGSGGHKIGLALDLQA
Band 7 - Q6VQ13
MSGLADPVAFAKDFLAGGVAAAISKTTVAPIERVKLLLQVQHISKQISEEQRYKGMIDCFVRIPK EQGFLSYWRGNLANVIRYFPTQALNFAFKDKYKQVFLGGVDKNTQFLRYFVGNLASGGAAGAT SLCFVYPLDFARTRLAADVGKAGGEREFTGLGNCLTKIFKADGITGLYRGFGVSVQGIIIYRAAY FGFYDTARGMLPDPKKTPFLISWGIAQVVTTVAGIVSYPFDTVRRRMMMQSGRAKSEILYKSTL HCWATIYKTEGGNAFFKGAFSNILRGTGGALVLVLYDEIKNLL
Band 7 - H9KDY8
MFSNHMKTLVQLVVQQQQQQRGMATLKAISIRLKSVKNIQKITQSMKMVSAAKYNRAERDLK QARPLGVGTKIFYEQAEIQAPPEDEKKLVVAITSDRGLCGAVHTGVSRNIRDSLLADPKERENTKI ICVGEKSRAILSRLFANNILFVASEVGRKPPTFNDAAKVAIEIMNSGYSFGSGRIVYNRFKSVVSYS VDQLPLFDKNAVVSAPKLSLYDSLDENVIQSYLEFSLASLLFYSMKEGACSEQSSRMTAMDNAS KNAGEMIDKLTLTFNRTRQAVITRELIEIISGAAALD
Band 8 - H9KF77
MADSGIKRNIPIKLGDFSVIDTEFSNIRERFDAEMRKMEDEMSRFRSELMNRESNNFFKSTTSTTT QSTQNSSLSPPHDSAWLDGLNSPLIQDEGDSKCLKLRFDVSQYTPEEIVVKTVDNKLLVHAKHEE KTESKSVYREYNREFLLPKGTNPESIKSSLSKDGVLTVEAPLPAIGTGEKLIPIAHQ
Band 8 - H9KE53
MSSLLKNYWKLMRNLPVTSPKCYPKLLPLTRMNTTETEKTETRPTIRKIQTDLETIKDLGLYIAA CLPKYVQKTQIVAGDELEILVCPEGIIPTLKFLKLHQNTQYTSLSDITAMDVPSRQYRFEIIYNLLSI TFNKRIRVKTYTDELTPVPSAEPIFDAANWYEREIWDMFGILFMGHTDLRRILTDYGFEGHPLRK

DFPLSGFVEVRYDDELKRVVCEPLELAQEFRKFELSAPWEQFPNFRSIPPSDESKEDSTKDKN
Band 9 - H9KPG4
MDPEQNFFFHFMKKLFYLLDTPVEYFREKIVIPNQKKYPCYHQNFRRVPTIDECYESDVICRWEA QKQFERDKMVDDEILSILRQRYEDCGWYYGNDKDKYCNDLYKTYQDASTAWFIKYGDIGVPLS VVDAFMKQKHRMIWERRHGPVGSGITNKRYDI
Band 9 - H9K1P1
MALRVLSLLYINRTFTRYGLTKRFFANTNKETEQDSEIIVRKIKTDLVSKEEKLAREARKEAVIIVS DAEDVGICSGVPEEHIKSRTVRIYCPAKNAMQSGTNNINHWQIDFDTRERWENPLMGWTSTGDP LSNLHVTFATKEEAIAHCNKMRWKYYIQNPNINNPKPRSYGTNFSWNKRTRVSTK